M. E.

JOURNAL OF THE AEROSPACE SCIENCES

VOLUME 28 AUGUST 1961 NUMBER 8

MECHANICAL ENGINEERING
AUG 14 1961
LIBRARY

PURDUE UNIVERSITY
AUG 8 1961
LIBRARY

CONTENTS

Linear Vibration of a Pinned Rotating Blade.....J. L. BOGDANOFF, J. E. GOLDBERG, AND L. MARCUS 593

Influence of Large Amplitudes on Flexural Vibrations of a Thin Circular Cylindrical Shell.....HU-NAN CHU 602

The Stagnation-Point Boundary Layer in the Presence of an Applied Magnetic Field.....WILLIAM B. BUSH 610

Some Effects of Tensor Conductivity of Magnetohydrodynamics.....B. SONNERUP 612

Shimmy of a Nose Gear With Dual Co-Rotating Wheels.....JOHN ERWIN STEVENS 622

Electrode Boundary Layers in Direct-Current Plasma Accelerators.....JACK L. KERREBROCK 631

Foreign-Gas Injection Into a Compressible Turbulent Boundary Layer on a Flat Plate.....NATHAN NESS 645

Readers' Forum..... 655

Published by
INSTITUTE OF THE AEROSPACE SCIENCES, INC.

JOURNAL OF THE AEROSPACE SCIENCES

Editor: W. R. SEARS
Director, Graduate School of Aeronautical Engineering, Cornell University

Associate Editor: ROBERT R. DEXTER *Editorial Production Manager:* VEHIG S. TAVITIAN
Editorial Assistant: CAROL A. SCHAU

IAS Aerospace Technology Panels

Paul J. Burr, Technical Services Director, Coordinator

The members of the IAS Aerospace Technology Panels shown here are to be available, collectively or as individuals, to assist and advise IAS Committees, Sections, and staff members as to currently interesting and important technical topics related to their specialties and as to people most qualified to speak or write on such topics. The panels will also stimulate thought and scientific papers of potential value for the future, and they should be sensitive to technical activity of other professional groups, seeking through joint action the enlightenment of all having professional aerospace interests. Panel chairmen are indicated with an asterisk (*).

Aerodynamics and Fluid Mechanics
Lester Lees*
Seymour M. Bogdonoff
Dean R. Chapman
Antonio Ferri
Paul Germain
Wayland C. Griffith
Hans W. Liepmann
C. C. Lin
Henry T. Nagamatsu
W. R. Sears
John R. Sellars
R. T. Whitcomb
Hideo Yoshihara

Aeroelasticity
R. L. Bisplinghoff*
Y. C. Fung
I. E. Garrick
Martin Goland
Kurt H. Hohenemser
J. C. Houbolt
W. P. Jones
W. J. Mykytow
Robert F. Speaker

Biomedical Sciences
Brig. Gen. D. Flickinger, USAF*
W. Ross Adey
Capt. Wm. Augerson, USA
Hilding Bjurstedt
Stuart Bondurant
A. Scott Crossfield
Cdr. J. H. Ebersole, USN
W. R. Lovelace, II
Capt. Bruce Pinc, USAF
Stanley Roscoe

Communication
P. C. Sandretto*
K. C. Black
James M. Bridges
Harvard L. Hull
Leonard Jaffe
David S. Little
Cdr. D. O. Mann, USN
Paul Rosenberg
William Sen
Arnold Shostack
Teck A. Wilson

Control and Guidance
Robert N. Brown*
R. C. Berendsen
B. Paul Blasingame
S. F. Eyestone
Percy Halpert
B. J. O'Connor
Robert L. Roderick
S. F. Schmidt
O. Hugo Schuck
H. Philip Whitaker

Energy Conversion
David Altman*
Robert Bromberg
M. U. Clauser
J. Preston Layton
Frank Marble
G. H. Markstein
A. M. Rothrock
Milton M. Slawsky
Martin Summerfield
T. Y. Toong

Flight Mechanics
H. J. Kelley*
Malcolm J. Abzug
H. Julian Allen
A. E. Bryson, Jr.
T. N. Edelbaum
William C. House
George Leitmann
Bernard Maggin
Angelo Miele
John D. Nicolaides
Charles B. Westbrook

Instrumentation
R. H. Tripp*
Paul F. Bechberger
J. M. Hungerford
Mac Lowy
Walter McKay
M. David Prince
Charles P. Sonet
George I. Toumanoff
William A. Wildhack

Management
Edward A. Ledeen*
Garrett C. Covington, Jr.
Maj. Gen. Marvin C. Demler, USAF
Richard G. Folsom
Joel M. Jacobson
Boyd C. Myers
Sidney M. Robbins
Lewis A. Rodert
John H. Sidebottom
R. C. Siebold
Paul Torda

Meteorology
Thomas F. Malone*
Robert D. Fletcher
Henry T. Harrison
Joseph Kaplan
Donald T. Perkins
Herbert Riehl
Morris Tepper
Clayton Van Thullenar
Harry Wexler

Nuclear Applications
J. Donald Rauth*
Jack L. Armstrong
Robert W. Bussard
H. M. Dieckamp
Capt. R. L. Duncan, USN
Harold B. Finger
Donald J. Keirn
Frank E. Rom
Raymer E. Schreiber
D. Roy Shoults
T. B. Taylor

Operations
Benjamin S. Kelsey*
Maj. Gen. Otis Benson, USAF (MC)
Ernest A. Cutrell
Capt. E. E. Fawkes, USN
Melvin N. Gough
Franklin W. Kolk
Col. J. L. Marinelli, USA
Richard V. Rhode
W. E. Rhodes
M. B. Spaulding, Jr.
Maj. Gen. D. Yates, USAF

Propulsion Systems
Bruce T. Lundin*
Robert H. Boden
George W. Brady
David Cochran
Elliot Mitchell
Perry W. Pratt
C. C. Ross
John G. Wilder, Jr.
Maurice J. Zucrow

Space Physics
John C. Evvard*
Herbert Friedmann
Leo Goldberg
C. F. Hansen
Arthur Kantrowitz
Bruno Rossi
S. F. Singer
Leo Steg
Fred L. Whipple

Structures and Materials
Nicholas J. Hoff*
Samuel B. Batdorf
Bruno A. Boley
Pol Duwez
R. R. Heldenfels
Samuel Levy
George N. Mangurian
S. S. Manson
Nathan E. Promisel
Ernest E. Sechler

Support
Ernest G. Stout*
Albert D. Brown
Edward I. Brown
Col. Paul T. Cooper, USAF
P. J. Daniel
Paul Hartline
Donald R. Hill
Capt. N. D. Hodson, USN
Lt. Col. George L. Lovett
R. R. Malik
John McKenna
Gilbert Rolan
Richard A. Schmidt
William R. Owens

Vehicle Design
C. E. Pappas*
Ralph Alex
Adolph Burstein
C. H. Christenson
A. J. Eggers, Jr.
E. V. Marshall
Rene H. Miller
John R. Ragazzini
George S. Schairer
George S. Trimble, Jr.

SUBSCRIPTION RATES

JOURNAL OF THE AEROSPACE SCIENCES, Published Monthly. United States and Possessions: 1 Year, $15.00; Single Copies, $1.50. Foreign Countries Including Canada (American Currency Rates): 1 Year, $16.00; Single Copies, $1.50.

AEROSPACE ENGINEERING, Published Monthly. United States and Possessions: 1 Year, $5.00; Single Copies, $0.50. Foreign Countries Including Canada (American Currency Rates): 1 Year, $6.00; Single Copies, $0.50.

Notices of change of address, which should be sent at least 30 days prior to actual change of address, and correspondence regarding subscriptions should be sent to the Circulation Department, JOURNAL OF THE AEROSPACE SCIENCES, 2 East 64th Street, New York 21, N.Y.

Manuscripts for publication, proofs, and all correspondence should be addressed to the Editorial Office of the JOURNAL.

© *Copyright, 1961, by the Institute of the Aerospace Sciences, Inc.*

Publication Office, 20th and Northampton Sts., Easton, Pa. Second-Class Mail Privileges Authorized at Easton, Pa. Acceptance for mailing at a special rate of postage provided for in Section 1103, Act of October 3, 1917, authorized April 29, 1937.

JOURNAL OF THE AEROSPACE SCIENCES

VOLUME 28 AUGUST 1961 NUMBER 8

Linear Vibration of a Pinned Rotating Blade

J. L. BOGDANOFF,* J. E. GOLDBERG,* AND L. MARCUS**

Summary

Equations of motion are presented and boundary conditions are derived for the small vibration of a blade (compressor blade or turbine bucket, for example) which at one end rolls on a pin which in turn rolls in a hole in a rotating disc, and at the other end is free. The rolling is assumed to take place without slipping and the angular velocity of the disc is assumed constant. Numerical results for natural frequencies are given for a typical compressor blade and these are compared with the natural frequencies which are obtained with more conventional methods of attachment.

Symbols

O = center of the disc
O_H = center of the hole in the disc
O_P = center of the rolling pin
O_B = center of the hole in the blade lug
G = c.g. of the blade lug
B = c.g. of the platform cross section
P = c.g. of a typical blade cross section
r_0 = distance between O and O_H
r_1 = radius of the rolling pin
r_2 = distance between O_B and G
r_3 = distance between G and B
x_3 = distance between B and P
R_1 = radius of the hole in the disc
R_2 = radius of the hole in the blade lug
$\mathbf{I},\mathbf{J},\mathbf{K}$ = unit vectors along axes fixed in space, with origin at O and $\mathbf{I}$ along the disc axis
$\mathbf{I}_1,\mathbf{I}_2,\mathbf{I}_3$ = unit vectors along axes fixed in the disc, with origin at O_H and $\mathbf{I}_1$ along the disc axis
$\mathbf{j}_1,\mathbf{j}_2,\mathbf{j}_3$ = unit vectors along axes fixed in the disc, with origin at O_H and $\mathbf{j}_1$ along the axis of the hole in the disc
$\mathbf{k}_1,\mathbf{k}_2,\mathbf{k}_3$ = unit vectors along axes with origin at G, $\mathbf{k}_1$ along the axis of the hole in the blade lug and $\mathbf{k}_3$ along the stacking axis of the blade
$\mathbf{i}_{10},\mathbf{i}_{20},\mathbf{i}_{30}$ = unit vectors along axes with origin at B, $\mathbf{i}_{10}$ and $\mathbf{i}_{20}$ along the principal axes of the blade lug cross section
$\mathbf{i}_1,\mathbf{i}_2,\mathbf{i}_3$ = unit vectors along axes with origin at P, $\mathbf{i}_1$ and $\mathbf{i}_2$ along the principal axes of the blade cross section
$\mathbf{u}_1,\mathbf{u}_2,\mathbf{u}_3$ = unit vectors along axes with origin at deformed P, $\mathbf{u}_1$ and $\mathbf{u}_2$ along the principal axes of the deformed blade cross section
ξ = angular displacement of line O_HO_P with respect to $\mathbf{j}_3$-axis
η = angular displacement of the rolling pin with respect to $\mathbf{j}_3$-axis
χ = angular displacement of line O_PO_B with respect to $\mathbf{j}_3$-axis
ζ = angular displacement of line O_BG with respect to $\mathbf{j}_3$-axis
γ_0 = angle between the disc axis and the axis of the hole in the disc
β_0 = angle between the axis of the platform cross section and the axis of hole in the blade lug
ψ = pretwist angle with respect to the blade base
q_1 = angle between $\mathbf{u}_1$- and $\mathbf{i}_1$-axes
q_2 = angle between $\mathbf{u}_2$- and $\mathbf{i}_2$-axes
Ω = constant angular velocity of the disc about its axis of symmetry
$\boldsymbol{\Omega}_i,\boldsymbol{\Omega}_j,\boldsymbol{\Omega}_k$ = angular velocities of the triads $\mathbf{i}_1$, $\mathbf{i}_2$, $\mathbf{i}_3$, $\mathbf{j}_1$, $\mathbf{j}_2$, $\mathbf{j}_3$, and $\mathbf{k}_1$, $\mathbf{k}_2$, $\mathbf{k}_3$, respectively
A,B,C = principal moments of inertia of the blade lug
$\mathbf{m}_G,\mathbf{r}_G,\mathbf{v}_G,\mathbf{a}_G$ = mass, position vector with respect to O, velocity, and acceleration of point G
$\mathbf{h}_G$ = angular momentum of the blade lug
$\mathbf{r}_P,\mathbf{v}_P,\mathbf{a}_P$ = position vector with respect to O, velocity, and acceleration of point P
v_1,v_2 = components of the displacement of point P along $\mathbf{i}_1$- and $\mathbf{i}_2$-axes
T_1,F_1 = tangential and normal forces exerted on the pin by the disc
T_2,F_2 = tangential and normal forces exerted on the pin by the blade lug
$\mathbf{N}_0,\mathbf{G}_0$ = force and couple exerted on the blade lug by the blade or deformed part of the blade
N_{10},N_{20},N_{30} = components of $\mathbf{N}_0$ along $\mathbf{i}_{10}$-, $\mathbf{i}_{20}$-, and $\mathbf{i}_{30}$-axes
G_{10},G_{20},G_{30} = components of G_0 along $\mathbf{i}_{10}$-, $\mathbf{i}_{20}$-, and $\mathbf{i}_{30}$-axes
N_1,N_2,N_3 = components of N along $\mathbf{u}_1$-, $\mathbf{u}_2$- and $\mathbf{u}_3$-axes
G_1,G_2,G_3 = components of G along $\mathbf{u}_1$-, $\mathbf{u}_2$- and $\mathbf{u}_3$-axes
B_1,B_2 = bending stiffness of the blade about $\mathbf{u}_1$- and $\mathbf{u}_2$-axes

Received April 14, 1960. Revised and received October 10, 1960.

* Midwest Applied Science Corp., and Purdue University, Lafayette, Ind.

** Allison Division of General Motors Corp., Indianapolis, Ind.

(I) Introduction

THE PURPOSE OF THIS REPORT is to derive the linear equations of motion of a blade-lug combination

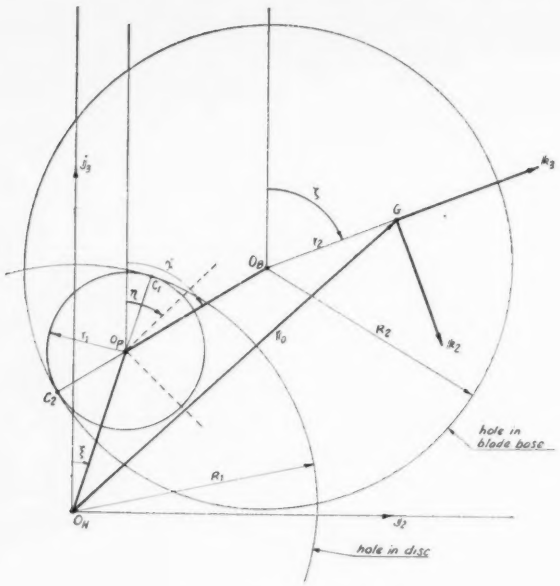

FIG. 1.

supported on a round pin which at one end fits into a hole in the lug and at the other rolls in a hole in a rotating disc. A fairly general disc hole–rolling pin–lug hole geometry is assumed. Both lug and pin are taken to be rigid, the pin having no mass. Rolling of the round pin is postulated to take place without slipping. This assumption appears reasonable in view of the small mass of the pin in comparison to that of the blade-lug, the large radial load coming on the pin at operating speed, and the small motions of the lug with respect to the rotating disc. The blade motion equations are based upon earlier reports; the undeformed blade axis is assumed radial, the Bernoulli-Euler bending theory is assumed, torsional motion is neglected, and the pretwist rate is assumed constant in sections and small. The angular velocity of rotation of the disc is taken as constant. Terms in the radial component of the acceleration of a point which depend upon displacements have been neglected since they are very small in comparison to the constant radial part.

Natural frequencies for one example are presented and these are compared with the corresponding natural frequencies when the blade base is clamped and also simply supported.

(II) Geometry and Kinematics

The geometry of the hole in the disc, the rolling pin, and the hole in the blade lug is shown in Fig. 1. Rolling at C_1 and C_2 is assumed to take place without slipping. Hence, by expressing the velocity of C_1 in terms of the motion of the disc and of the pin and equating these expressions and by expressing the velocity of C_2 in terms of the motion of the pin and of the blade lug and equating, we find that

$$\eta = -(a_1/a_1)\xi \qquad \chi = (a_1/a_2)\xi + (R_2/a_2)\zeta \quad (2.1)$$

where $a_1 = R_1 - r_1, \qquad a_2 = R_2 - r_1$ (2.2)

These formulas are valid for large as well as small angles.

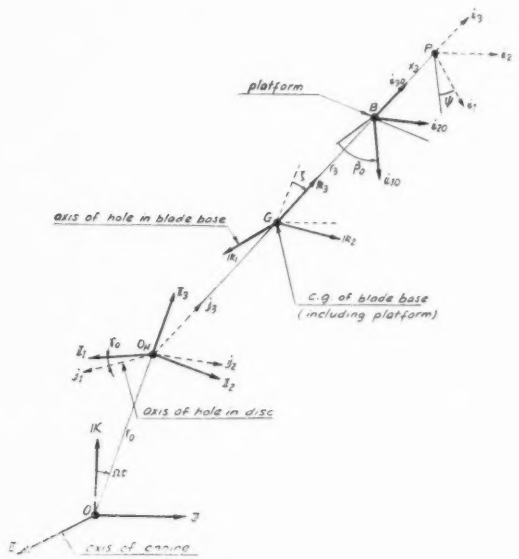

FIG. 2a.

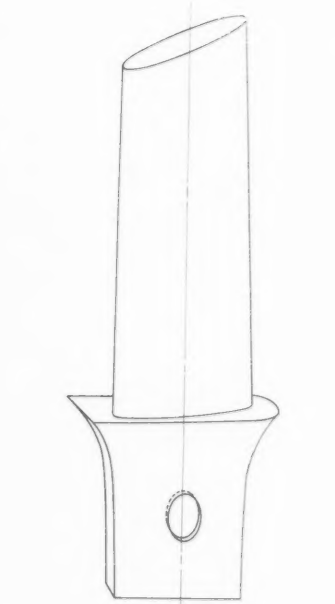

FIG. 2b.

The angular velocity of the unit orthogonal triad $\mathbf{j}_1,\mathbf{j}_2,\mathbf{j}_3$ shown in Fig. 2 is $\Omega\mathbf{I}$; if $\mathbf{I}$ is expressed in terms of $\mathbf{j}_1,\mathbf{j}_2,\mathbf{j}_3$ this angular velocity is given by the equation

$$\boldsymbol{\Omega}_j = \Omega \cos \gamma_0 \mathbf{j}_1 - \Omega \sin \gamma_0 \mathbf{j}_2 \tag{2.3}$$

where Ω is the constant angular velocity of the disc about its axis of symmetry $\mathbf{I}$ $(=\mathbf{I}_1)$ and γ_0 is the angle between the disc axis and the axis of the hole in the disc. The angular velocity of the triad $\mathbf{k}_1,\mathbf{k}_2,\mathbf{k}_3$ differs from $\boldsymbol{\Omega}_j$ by the term $-\dot{\zeta}\mathbf{j}_1$ so that

$$\boldsymbol{\Omega}_k = (\Omega \cos \gamma_0 - \dot{\zeta})\mathbf{j}_1 - \Omega \sin \gamma_0 \, \mathbf{j}_2 \tag{2.4}$$

The point G in Fig. 2 is the c.g. of the blade base or lug—i.e., that part of the blade which is assumed rigid. The position vector of G with respect to O is given by the formula

$$\mathbf{r}_G = (a_1 \sin \xi + a_2 \sin \chi + r_2 \sin \zeta)\mathbf{j}_2 + (r_0 + a_1 \cos \xi + a_2 \cos \chi + r_2 \cos \zeta)\mathbf{j}_3 \tag{2.5}$$

which is valid for all angles.

Using the usual vector methods[1] and linearizing assuming that ξ, χ, ζ are small (see Appendix A for details), we find that the acceleration of G is

$$\mathbf{a}_G = -\Omega^2 \sin \gamma_0 \cos \gamma_0 (a_1\xi + a_2\chi + r_2\zeta)\mathbf{k}_1 + \{a_1\ddot{\xi} + a_2\ddot{\chi} + r_2\ddot{\zeta} - \Omega^2 \cos^2 \gamma_0 (a_1\xi + a_2\chi + r_2\zeta) + \zeta\Omega^2(r_0 + a_1 + a_2 + r_2)\}\mathbf{k}_2 - \{2\Omega(a_1\dot{\xi} + a_2\dot{\chi} + r_2\dot{\zeta}) \cos \gamma_0 + \Omega^2(r_0 + a_1 + a_2 + r_2)\}\mathbf{k}_3 \tag{2.6}$$

We assume that the unit vectors $\mathbf{k}_1$, $\mathbf{k}_2$, $\mathbf{k}_3$ are along the principal axes of inertia of the blade lug. If A, B, C are the principal moments of inertia, the formula for the angular momentum of the lug is (see Appendix A)

$$\mathbf{h}_G = A(\Omega \cos \gamma_0 - \dot{\zeta})\mathbf{k}_1 - B\Omega \sin \gamma_0 \cos \zeta \mathbf{k}_2 - C\Omega \sin \gamma_0 \sin \zeta \, \mathbf{k}_3 \tag{2.7}$$

The linearized form for the rate of change of $\mathbf{h}_G$ becomes (see Appendix A)

$$\dot{\mathbf{h}}_G = \{(C - B)\zeta\Omega^2 \sin^2 \gamma_0 - A\ddot{\xi}\}\mathbf{k}_1 + (C - A)\zeta\Omega^2 \sin \gamma_0 \cos \gamma_0 \mathbf{k}_2 + \{-C\ddot{\zeta}\Omega \sin \gamma_0 + (A - B)(\Omega \cos \gamma_0 - \dot{\zeta}) \sin \gamma_0\}\mathbf{k}_3 \tag{2.8}$$

Let the displacement of a typical blade cross section c.g., P, relative to its undeformed position be

$$v_1\mathbf{i}_1 + v_2\mathbf{i}_2$$

Then, with the abbreviations

$$\left.\begin{aligned} \rho_{10} &= r_0 \sin \zeta + a_1 \sin (\zeta - \xi) + a_2 \sin (\zeta - \chi) \\ \rho_{20} &= r_0 \cos \zeta + a_1 \cos (\zeta - \xi) + a_2 \cos (\zeta - \chi) \\ r_4 &= r_2 + r_3 + x_3, \qquad \beta = \beta_0 + \psi \end{aligned}\right\} \tag{2.9}$$

the position vector of P with respect to O takes the form

$$\mathbf{r}_P = (v_1 - \rho_{10} \sin \beta)\mathbf{i}_1 + (v_2 - \rho_{10} \cos \beta)\mathbf{i}_2 + (r_4 + \rho_{20})\mathbf{i}_3 \tag{2.10}$$

The triad $\mathbf{i}_1,\mathbf{i}_2,\mathbf{i}_3$ differs from $\mathbf{k}_1,\mathbf{k}_2,\mathbf{k}_3$ by a rotation through angle β about $\mathbf{i}_3 = \mathbf{k}_3$. Moreover, β is constant in time, being equal to β (const.) plus the pretwist angle ψ which is assumed small and depends only upon x_3. The angular velocity of $\mathbf{i}_1,\mathbf{i}_2,\mathbf{i}_3$ is thus obtained from $\boldsymbol{\Omega}_k$ on making the coordinate transformation just mentioned:

$$\boldsymbol{\Omega}_i = (\Omega \cos \gamma_0 \cos \beta - \Omega \sin \gamma_0 \cos \zeta \sin \beta - \dot{\zeta} \cos \beta)\mathbf{i}_1 + (-\Omega \cos \gamma_0 \sin \beta - \Omega \sin \gamma_0 \cos \zeta \cos \beta + \dot{\zeta} \sin \beta)\mathbf{i}_2 - \Omega \sin \gamma_0 \sin \zeta \mathbf{i}_3 \tag{2.11}$$

The linearized form of the acceleration of P is found to be (see Appendix A)

$$\begin{aligned} \mathbf{a}_P = {} & [\ddot{v}_1 - \{\ddot{\rho}_{10} - (r_4 + \rho_{20})\ddot{\xi}\} \sin \beta - (r_4 + \rho_{20})\zeta\Omega^2 \sin \gamma_0 \cos (\beta + \gamma_0) - \\ & \{(v_1 - \rho_{10} \sin \beta) \sin^2 (\beta + \gamma_0) + (v_2 - \rho_{10} \cos \beta) \sin (\beta + \gamma_0) \cos (\beta + \gamma_0) + \\ & (r_4 + \rho_{20})q_1\}\Omega^2]\mathbf{u}_1 + [\ddot{v}_2 - \{\ddot{\rho}_{10} - (r_4 + \rho_{20})\ddot{\xi}\} \cos \beta + (r_4 + \rho_{20})\zeta\Omega^2 \sin \gamma_0 \sin (\beta + \gamma_0) - \\ & \{(v_1 - \rho_{10} \sin \beta) \sin (\beta + \gamma_0) \cos (\beta + \gamma_0) + (v_2 - \rho_{10} \cos \beta) \cos^2 (\beta + \gamma_0) - \\ & (r_4 + \rho_{20})q_2\}\Omega^2]\mathbf{u}_2 - (r_4 + \rho_{20})\Omega^2 \mathbf{u}_3 \end{aligned} \tag{2.12}$$

where, since angles are small, we now have

$$\left.\begin{aligned} \rho_{10} &= r_0\zeta + a_1(\zeta - \xi) + a_2(\zeta - \chi) \\ \rho_{20} &= r_0 + a_1 + a_2 \qquad r_4 + \rho_{20} = R + x_3 \end{aligned}\right\} \tag{2.13}$$

from (2.9), and

$$q_1 = \frac{\partial v_1}{\partial x_3} - \frac{\partial \psi}{\partial x_3} v_2 \qquad q_2 = \frac{\partial v_2}{\partial x_3} + \frac{\partial \psi}{\partial x_3} v_1 \tag{2.14}$$

The relationship between the vectors $\mathbf{i}_1,\mathbf{i}_2,\mathbf{i}_3$ and $\mathbf{u}_1$, $\mathbf{u}_2,\mathbf{u}_3$, which are unit vectors in the directions of the deformed cross section principal axes, is shown in Fig. 3. Eqs. (2.14) express the fact that the rotation required to obtain $\mathbf{u}_1,\mathbf{u}_2,\mathbf{u}_3$ from $\mathbf{i}_1,\mathbf{i}_2,\mathbf{i}_3$ depends upon the deformations v_1 and v_2 and upon the pretwist angle ψ. In what follows, ψ and $\partial\psi/\partial x_3$ will be assumed small, with $\partial^2\psi/\partial x_3^2 = 0$.

(III) Linearized Equations of Motion

Fig. 4 shows the forces acting on the pin, which we have taken to be without inertia. Hence equilibrium considerations lead to

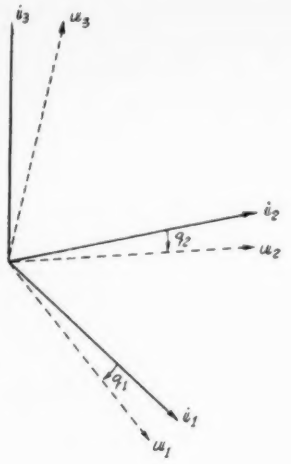

FIG. 3.

$$\left.\begin{aligned} &T_1 + T_2 = 0 \\ &-F_1 \sin \xi + T_1 \cos \xi + \\ &\qquad F_2 \sin \chi - T_2 \cos \chi = 0 \\ &-F_1 \cos \xi - T_1 \sin \xi + \\ &\qquad F_2 \cos \chi + T_2 \sin \chi = 0 \end{aligned}\right\} \quad (3.1)$$

For small angles, these become

$$T_1 = -T_2 \qquad F_1 = F_2 \qquad T_2 = (F_2/2)(\chi - \xi) \quad (3.2)$$

The forces and couples which act upon the blade lug are illustrated in Fig. 5. The force $\mathbf{N}_0$ and couple $\mathbf{G}_0$ which the blade, or deformed part of the blade, exert on the lug are given by the formulas

$$\left.\begin{aligned} \mathbf{N}_0 &= N_{10}\mathbf{i}_{10} + N_{20}\mathbf{i}_{20} + N_{30}\mathbf{i}_{30} \\ \mathbf{G}_0 &= G_{10}\mathbf{i}_{10} + G_{20}\mathbf{i}_{20} + G_{30}\mathbf{i}_{30} \end{aligned}\right\} \quad (3.3)$$

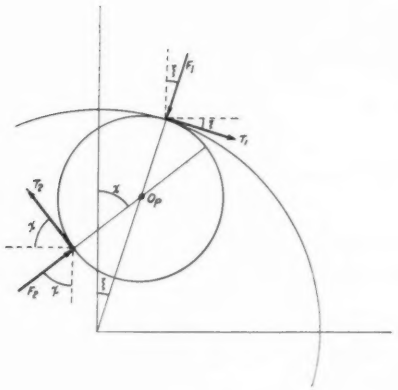

FIG. 4.

or, on changing to the unit vectors $\mathbf{k}_1,\mathbf{k}_2,\mathbf{k}_3$,

$$\left.\begin{aligned} \mathbf{N}_0 &= (N_{10}\cos\beta_0 - N_{20}\sin\beta_0)\mathbf{k}_1 + \\ &\qquad (N_{10}\sin\beta_0 + N_{20}\cos\beta_0)\mathbf{k}_2 + N_{30}\mathbf{k}_3 \\ \mathbf{G}_0 &= (G_{10}\cos\beta_0 - G_{20}\sin\beta_0)\mathbf{k}_1 + \\ &\qquad (G_{10}\sin\beta_0 + G_{20}\cos\beta_0)\mathbf{k}_2 + G_{30}\mathbf{k}_3 \end{aligned}\right\} \quad (3.4)$$

The equations of motion of the blade lug are therefore

$$\left.\begin{aligned} &m_G\{a_1\ddot{\xi} + a_2\ddot{\chi} + r_2\ddot{\xi} - \Omega^2\cos^2\gamma_0(a_1\xi + a_2\chi + r_2\xi) + \zeta\Omega^2(r_0 + a_1 + a_2 + r_2)\} = \\ &\qquad N_{10}\sin\beta_0 + N_{20}\cos\beta_0 + T_2 + F_2(\zeta - \chi), \\ &m_G\{2\Omega\cos\gamma_0(a_1\dot{\xi} + a_2\dot{\chi} + r_2\dot{\xi}) - \Omega^2(r_0 + a_1 + a_2 + r_2)\} = N_{30} + T_2(\zeta - \chi) - F_2 \\ &A\ddot{\xi} - (C - B)\zeta\Omega^2\sin^2\gamma_0 = -G_{10}\cos\beta_0 + G_{20}\sin\beta_0 + r_3(N_{10}\sin\beta_0 + N_{20}\cos\beta_0) + \\ &\qquad R_2F_2(\zeta - \chi) - F_2(R_2 + r_2)(\zeta - \chi) - (R_2 + r_2)T_2 \end{aligned}\right\} \quad (3.5)$$

where m_G is the mass of the lug.

If, in the second of (3.5), we neglect the first-order terms which are small in comparison with the constant terms, we find that F_2 is constant and

$$F_2 = N_{30} + m_G\Omega^2(r_0 + a_1 + a_2 + r_2) \quad (3.6)$$

In what follows, we shall use this equation in place of the second of (3.5).

The elimination of χ and T_2 in the first and third of (3.5) by means of the second of (2.1) and the last of (3.2) provides the two equations

$$\left.\begin{aligned} &2m_Ga_1\dot{\xi} + m_G(R_2 + r_2)\ddot{\xi} + \{(F_2/2)[1 + (a_1/a_2)] - 2m_Ga_1\Omega^2\cos^2\gamma_0\}\xi + \\ &\qquad \{-(F_2/2)[2 - (R_2/a_2)] + m_G(r_0 + a_1 + a_2 + r_2\sin^2\gamma_0 - R_2\cos^2\gamma_0)\}\zeta = N_{10}\sin\beta_0 + N_{20}\cos\beta_0 \\ &A\ddot{\xi} + F_2\left[\frac{R_2 + r_2}{2} - \frac{a_1(R_2 - r_1)}{2a_2}\right]\xi + \left\{F_2\left[r_2 - \frac{R_2(R_2 - r_2)}{2a_2}\right] + (C - B)\Omega^2\sin^2\gamma_0\right\}\zeta = \\ &\qquad -r_3(N_{10}\sin\beta_0 + N_{20}\cos\beta_0) + G_{10}\cos\beta_0 - G_{20}\sin\beta_0 \end{aligned}\right\} \quad (3.7)$$

The blade motion equations are based upon Bernoulli-Euler bending theory with pretwist. A classical reference for the derivation of such equations is Love's text on elasticity.[2] We employ the sign convention of that reference which we have summarized in Fig. 6. The blade axis is initially straight; the mass and elastic axes are assumed to coincide, and torsional deformation is neglected. The pretwist rate $\partial\psi/\partial x_3$ is assumed constant and sufficiently small that powers of it above the first, and itself when multiplied by small quantities, can be neglected. The curvatures are

$$\kappa_1 = -(\partial^2 v_2/\partial x_3^2) + 2(\partial\psi/\partial x_3)(\partial v_1/\partial x_3) \qquad \kappa_2 = \partial^2 v_1/\partial x_3^2 - 2(\partial\psi/\partial x_3)(\partial v_2/\partial x_3) \qquad \tau = \partial\psi/\partial x_3$$

On employing these curvatures, neglecting products and powers of small quantities, and using the basic equations of reference 2, we find that the equations of motion are

$$\left.\begin{aligned}
&\frac{\partial N_1}{\partial x_3} + \left(\frac{\partial^2 v_1}{\partial x_3^2} - 2\frac{\partial\psi}{\partial x_3}\frac{\partial v_2}{\partial x_3}\right)N_3 - \frac{\partial\psi}{\partial x_3}N_2 = m[\ddot{v}_1 - \{\ddot{\rho}_{10} - (r_4 + \rho_{20})\ddot{\xi}\}\sin\beta - \\
&\qquad (r_4 + \rho_{20})\xi\Omega^2 \sin\gamma_0\cos(\beta + \gamma_0) - \{(v_1 - \rho_{10}\sin\beta)\sin^2(\beta + \gamma_0) + \\
&\qquad (v_2 - \rho_{10}\cos\beta)\sin(\beta + \gamma_0)\cos(\beta + \gamma_0) - (r_4 + \rho_{20})q_1\}\Omega^2] \\
&\frac{\partial N_2}{\partial x_3} + \frac{\partial\psi}{\partial x_3}N_1 + \left(\frac{\partial^2 v_2}{\partial x_3^2} + 2\frac{\partial\psi}{\partial x_3}\frac{\partial v_1}{\partial x_3}\right)N_3 = m[\ddot{v}_2 - \{\ddot{\rho}_{10} - (r_4 + \rho_{20})\ddot{\xi}\}\cos\beta + \\
&\qquad (r_4 + \rho_{20})\xi\Omega^2 \sin\gamma_0\sin(\beta + \gamma_0) - \{(v_1 - \rho_{10}\sin\beta)\sin(\beta + \gamma_0)\cos(\beta + \gamma_0) + \\
&\qquad (v_2 - \rho_{10}\cos\beta)\cos^2(\beta + \gamma_0) - (r_4 + \rho_{20})q_2\}\Omega^2]
\end{aligned}\right\} \tag{3.8}$$

$$\left.\begin{aligned}
&\partial N_3/\partial x_3 = -m\Omega^2(r_0 + a_1 + a_2 + r_2 + r_3 + x_3) \\
&\frac{\partial G_1}{\partial x_3} - \frac{\partial\psi}{\partial x_3}G_2 - N_2 = 0 \qquad \frac{\partial G_2}{\partial x_3} + \frac{\partial\psi}{\partial x_3}G_1 + N_1 = 0 \\
&G_1 = -B_1\left(\frac{\partial^2 v_2}{\partial x_3^2} + 2\frac{\partial\psi}{\partial x_3}\frac{\partial v_1}{\partial x_3}\right) \qquad G_2 = B_2\left(\frac{\partial^2 v_1}{\partial x_3^2} - 2\frac{\partial\psi}{\partial x_3}\frac{\partial v_2}{\partial x_3}\right)
\end{aligned}\right\} \tag{3.8}$$

where ρ_{10} and ρ_{20} are given in (2.13), m is the mass per unit length of the blade, B_1 is the bending stiffness about the $\mathbf{u}_1$-axis, and B_2 is the bending stiffness about the $\mathbf{u}_2$-axis. A detailed derivation of (3.8) is given in reference 3. An alternative form of these equations is given in reference 4.

(IV) Illustrative Example and Discussion

The equations of the previous section and the procedure outlined in Appendix C have been used to determine the first two natural frequencies and mode shapes of the blade described in Fig. 7. In the extended position, the outer edge of the platform is located at 3.2 in. from the center of the disc and the length

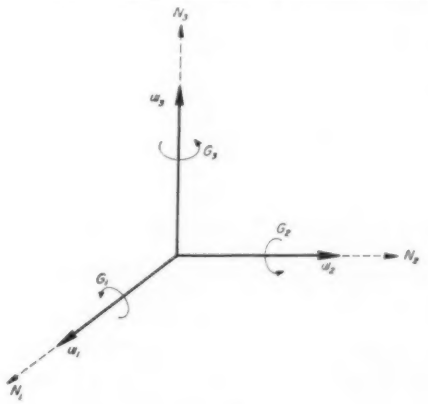

FIG. 6.

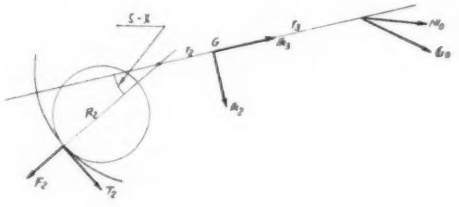

FIG. 5.

of the blade is 5.038 in. The disc is assumed to be rotating at a speed in excess of 12,000 rpm. The results are presented in Fig. 8. The first two natural frequencies were found to be 542 and 2,561 cps, respectively. That is, at these frequencies the determinant which is a measure of the joint magnitude of the set of tip tractions vanishes.

For comparison, the natural frequencies have been computed and are shown for the same blade when clamped at the base and also for the case of the pinned blade when the diameters of the pin and of the holes in disc and lug are equal but the pin is free to roll in these holes. The latter case is designated as "simple

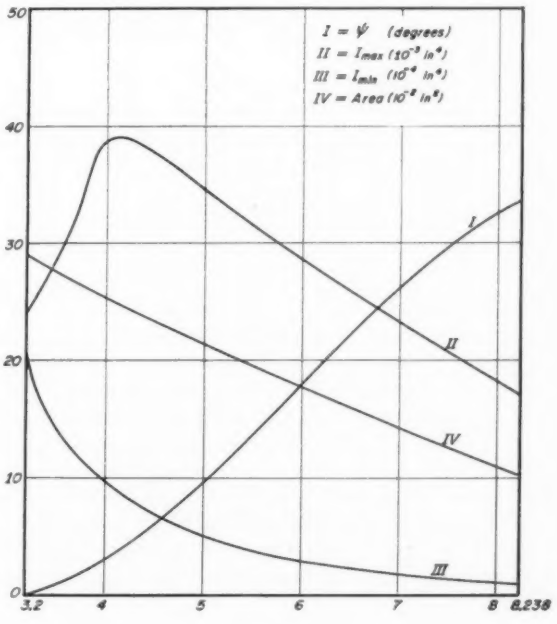

FIG. 7.

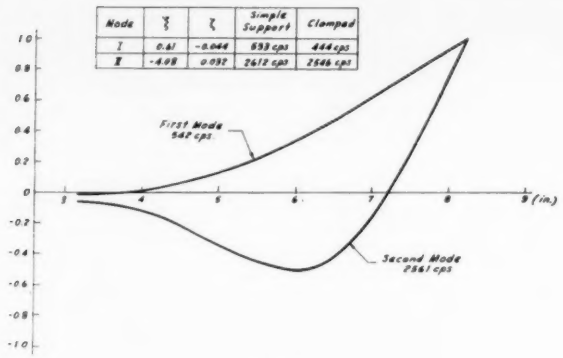

FIG. 8.

support" and it appears that the fundamental frequency for this case is slightly lower than that for the case of the loose pin. This may be explained by the existence of a constraining moment at the center of the pin in the loose pin case while this moment vanishes in the case of the snug pin. It should also be noted that the case in which the blade acts as a physical pendulum has not been included although this might be considered to yield the fundamental mode for the case of the snug pin.

References

[1] Synge, J. L., and Griffith, B., *Principles of Mechanics*, 3rd Ed., McGraw-Hill Book Co., Inc., New York, 1959.

[2] Love, A. E. H., *The Mathematical Theory of Elasticity*, 4th Ed., Ch. 18–20, Cambridge University Press, 1934.

[3] Bogdanoff, J. L., and DeGroff, H. M., *1 × P Forced Motion and Torsional Vibration of Propellers*, Aeroproducts Operations, Inc., November 1954.

[4] Houboult, J. C., and Brooks, G. W., *Differential Equations of Motion for Combined Flapwise Bending, Chordwise Bending and Torsion of Twisted Nonuniform Rotary Blades*, NACA TN 3905, February 1957.

Appendix A

The velocity of G is given by the formula

$$\mathbf{v}_G = \delta\mathbf{r}_G/\delta t + \boldsymbol{\Omega}_k \times \mathbf{r}_G \tag{A.1}$$

where $\mathbf{r}_G$ is given by (2.5) and $\boldsymbol{\Omega}_G$ by (2.4). But

$$\delta\mathbf{r}_G/\delta t = (a_1\dot{\xi}\cos\xi + a_2\dot{\chi}\cos\chi + r_2\dot{\zeta}\cos\zeta)\mathbf{j}_2 + (-a_1\dot{\xi}\sin\xi - a_2\ddot{\chi}\sin\chi - r_2\dot{\zeta}\sin\zeta)\mathbf{j}_3$$

and

$$\boldsymbol{\Omega}_k \times \mathbf{r}_G = \begin{vmatrix} \mathbf{j}_1 & \mathbf{j}_2 & \mathbf{j}_3 \\ \Omega\cos\gamma_0 - \dot{\zeta} & -\Omega\sin\gamma_0 & 0 \\ 0 & a_1\sin\xi + a_2\sin\chi + r_2\sin\zeta & r_0 + a_1\cos\xi + a_2\cos\chi + r_2\cos\zeta \end{vmatrix}$$

$$= -(r_0 + a_1\cos\xi + a_2\cos\chi + r_2\cos\zeta)\Omega\sin\gamma_0\,\mathbf{j}_1 - (r_0 + a_1\cos\xi + a_2\cos\chi + r_2\cos\zeta)(\Omega\cos\gamma - \dot{\zeta})\,\mathbf{j}_2 + (a_1\sin\xi + a_2\sin\chi + r_2\sin\zeta)(\Omega\cos\gamma_0 - \dot{\zeta})\,\mathbf{j}_3$$

so that

$$\mathbf{v}_G = -\{(r_0 + a_1\cos\xi + a_2\cos\chi + r_2\cos\zeta)\Omega\sin\gamma_0\}\mathbf{j}_1 + \{a_1\dot{\xi}\cos\xi + a_2\dot{\chi}\cos\chi + r_2\dot{\zeta}\cos\zeta - (r_0 + a_1\cos\xi + a_2\cos\chi + r_2\cos\zeta)(\Omega\cos\gamma_0 - \dot{\zeta})\}\mathbf{j}_2 + \{-(a_1\dot{\xi}\sin\xi + a_2\dot{\chi}\sin\chi + r_2\dot{\zeta}\sin\zeta) + (a_1\sin\xi + a_2\sin\chi + r_2\sin\zeta)(\Omega\cos\gamma_0 - \dot{\zeta})\}\mathbf{j}_3 \tag{A.2}$$

The acceleration of G follows from the equation

$$\mathbf{a}_G = (\delta\mathbf{v}_G/\delta t) + \boldsymbol{\Omega}_k \times \mathbf{v}_G \tag{A.3}$$

with

$$\delta\mathbf{v}_G/\delta t = \{(a_1\dot{\xi}\sin\xi + a_2\dot{\chi}\sin\chi + r_2\dot{\zeta}\sin\zeta)\Omega\sin\gamma_0\}\mathbf{j}_1 + \{a_1\ddot{\xi}\cos\xi - a_1\dot{\xi}^2\sin\xi + a_2\ddot{\chi}\cos\chi - a_2\dot{\chi}^2\sin\chi + r_2\ddot{\zeta}\cos\zeta - r_2\dot{\zeta}^2\sin\zeta + (r_0 + a_1\cos\xi + a_2\cos\chi + r_2\cos\zeta)\dot{\zeta} + (a_1\dot{\xi}\sin\xi + a_2\dot{\chi}\sin\chi + r_2\dot{\zeta}\sin\zeta)(\Omega\cos\gamma_0 - \dot{\zeta})\}\mathbf{j}_2 + \{-(a_1\ddot{\xi}\sin\xi + a_1\dot{\xi}^2\cos\xi + a_2\ddot{\chi}\sin\chi + a_2\ddot{\chi}^2\cos\chi + r_2\ddot{\zeta}\sin\zeta + r_2\dot{\zeta}^2\cos\zeta) - (a_1\sin\xi + a_2\sin\chi + r_2\sin\zeta)\dot{\zeta} + (a_1\dot{\xi}\cos\xi + a_2\dot{\chi}\cos\chi + r_2\dot{\zeta}\cos\zeta)(\Omega\cos\gamma_0 - \dot{\zeta})\}\mathbf{j}_3 \tag{A.4}$$

$$\boldsymbol{\Omega}_k \times \mathbf{v}_G = \{(a_1\dot{\xi}\sin\xi + a_2\dot{\chi}\sin\chi + r_2\dot{\zeta}\sin\zeta)\Omega\sin\gamma_0 - (a_1\sin\xi + a_2\sin\chi + r_2\sin\zeta) \times (\Omega\cos\gamma_0 - \dot{\zeta})\Omega\sin\gamma_0\}\mathbf{j}_1 + \{(a_1\dot{\xi}\sin\xi + a_2\dot{\chi}\sin\chi + r_2\dot{\zeta}\sin\zeta)(\Omega\cos\gamma_0 - \dot{\zeta}) - (a_1\sin\xi + a_2\sin\chi + r_2\sin\zeta)(\Omega\cos\gamma_0 - \dot{\zeta})^2\}\mathbf{j}_2 + \{(a_1\dot{\xi}\cos\xi + a_2\dot{\chi}\cos\chi + r_2\dot{\zeta}\cos\zeta) \times (\Omega\cos\gamma_0 - \dot{\zeta}) - (r_0 + a_1\cos\xi + a_2\cos\chi + r_2\cos\zeta)(\Omega\cos\gamma_0 - \dot{\zeta})^2 - (r_0 + a_1\cos\xi + a_2\cos\chi + r_2\cos\zeta)\Omega^2\sin^2\gamma_0\}\mathbf{j}_3 \tag{A.5}$$

and the transformation

$$\left.\begin{aligned}\mathbf{j}_1 &= \mathbf{k}_1\\ \mathbf{j}_2 &= \cos\zeta\mathbf{k}_2 + \sin\zeta\mathbf{k}_3\\ \mathbf{j}_3 &= -\sin\zeta\mathbf{k}_2 + \cos\zeta\mathbf{k}_3\end{aligned}\right\} \tag{A.6}$$

The linearized form of $\mathbf{a}_G$ is given by (2.6).

The rate of change of the angular momentum of the blade lug, $\dot{\mathbf{h}}_G$, is computed as follows: We have

$$\boldsymbol{\Omega}_k = (\Omega\cos\gamma_0 - \dot{\zeta})\mathbf{k}_1 - \Omega\sin\gamma_0\cos\zeta\mathbf{k}_2 - \Omega\sin\gamma_0\sin\zeta\mathbf{k}_3 \tag{A.7}$$

and from (2.7)

$$\begin{aligned}\mathbf{h}_G = {} & A(\Omega\cos\gamma_0 - \dot{\zeta})\mathbf{k}_1 - B\Omega\sin\gamma_0\cos\zeta\mathbf{k}_2\\ & - C\Omega\sin\gamma_0\sin\zeta\mathbf{k}_3\end{aligned} \tag{A.8}$$

Since

$$\delta\mathbf{h}_G/\delta t = -A\ddot{\zeta}\mathbf{k}_1 + B\dot{\zeta}\Omega\sin\gamma_0\sin\zeta\mathbf{k}_2 - C\dot{\zeta}\Omega\sin\gamma_0\cos\zeta\mathbf{k}_3$$

and

$$\boldsymbol{\Omega}_k \times \mathbf{h}_G = \begin{vmatrix} \mathbf{k}_1 & \mathbf{k}_2 & \mathbf{k}_3\\ \Omega\cos\gamma_0 - \dot{\zeta} & -\Omega\sin\gamma_0\cos\zeta & -\Omega\sin\gamma_0\sin\zeta\\ A(\Omega\cos\gamma_0 - \dot{\zeta}) & -B\Omega\sin\gamma_0\cos\zeta & -C(\Omega\sin\gamma_0\sin\zeta)\end{vmatrix}$$

we easily find that

$$\begin{aligned}\dot{\mathbf{h}}_G &= (\delta\mathbf{h}_G/\delta t) + \boldsymbol{\Omega}_k \times \mathbf{h}_G\\ &= \{-A\ddot{\zeta} + (C - B)\Omega^2\sin^2\gamma_0\cos\zeta\sin\zeta\}\mathbf{k}_1\\ &+ \{B\dot{\zeta}\Omega\sin\gamma_0\sin\zeta + (C - A)(\Omega\cos\gamma_0 - \dot{\zeta})\sin\gamma_0\sin\zeta\}\mathbf{k}_2\\ &+ \{-C\dot{\zeta}\Omega\sin\gamma_0\cos\zeta + (A - B)(\Omega\cos\gamma_0 - \dot{\zeta})\sin\gamma_0\cos\zeta\}\mathbf{k}_3\end{aligned} \tag{A.9}$$

The linearized form of (A.9) is given in (2.8).

Using (2.10), (2.11), and the formula $\mathbf{v}_P = (\delta\mathbf{r}_P/\delta t) + \boldsymbol{\Omega}_i \times \mathbf{r}_P$ we find that

$$\begin{aligned}\mathbf{v}_P = {} & \{\dot{v}_1 - \dot{\rho}_{10}\sin\beta + (-\Omega\cos\gamma_0\sin\beta - \Omega\sin\gamma_0\cos\zeta\cos\beta + \dot{\zeta}\sin\beta)(r_4 + \rho_{20}) +\\ & (v_2 - \rho_{10}\cos\beta)(\Omega\sin\gamma_0\sin\zeta)\}\mathbf{i}_1 + \{\dot{v}_2 - \dot{\rho}_{10}\cos\beta - (v_1 - \rho_{10}\sin\beta)(\Omega\sin\gamma_0\sin\zeta) -\\ & (\Omega\cos\gamma_0\cos\beta - \Omega\sin\gamma_0\cos\zeta\sin\beta - \dot{\zeta}\cos\beta)(r_4 + \rho_{20})\}\mathbf{i}_2 +\\ & \{(v_2 - \rho_{10}\cos\beta)(\Omega\cos\gamma_0\cos\beta - \Omega\sin\gamma_0\cos\zeta\sin\beta - \dot{\zeta}\cos\beta) -\\ & (v_1 - \rho_{10}\sin\beta)(-\Omega\cos\gamma_0\sin\beta - \Omega\sin\gamma_0\cos\zeta\cos\beta + \dot{\zeta}\sin\beta)\}\mathbf{i}_3\end{aligned} \tag{A.10}$$

The acceleration of P is obtained on combining (A.10) and the formula

$$\mathbf{a}_P = \delta\mathbf{v}_P/\delta t + \boldsymbol{\Omega}_i \times \mathbf{v}_P \tag{A.11}$$

$$\begin{aligned}\mathbf{a}_P = {} & [\{\ddot{v} - \ddot{\rho}_{10}\sin\beta + (\Omega\dot{\zeta}\sin\gamma_0\sin\zeta\cos\beta + \ddot{\zeta}\sin\beta)(r_4 + \rho_{20}) + (\dot{v}_2 - \rho_{10}\cos\beta)(\Omega\sin\gamma_0\sin\zeta) +\\ & (v_2 - \rho_{10}\cos\beta)(\Omega\dot{\zeta}\sin\gamma_0\cos\zeta)\} + (-\Omega\cos\gamma_0\sin\beta - \Omega\sin\gamma_0\cos\zeta\cos\beta + \dot{\zeta}\sin\beta)\times\\ & \{(v_2 - \rho_{10}\cos\beta)(\Omega\cos\gamma_0\cos\beta - \Omega\sin\gamma_0\cos\zeta\sin\beta - \dot{\zeta}\cos\beta) -\\ & (v_1 - \rho_{10}\sin\beta)(-\Omega\cos\gamma_0\sin\beta - \Omega\sin\gamma_0\cos\zeta\cos\beta + \dot{\zeta}\sin\beta)\} +\\ & (\Omega\sin\gamma_0\sin\zeta)\{\dot{v}_2 - \dot{\rho}_{10}\cos\beta - (v_1 - \rho_{10}\sin\beta)(\Omega\sin\gamma_0\sin\zeta) -\\ & (\Omega\cos\gamma_0\cos\beta - \Omega\sin\gamma_0\cos\zeta\sin\beta - \dot{\zeta}\cos\beta)(r_4 + \rho_{20})\}]\mathbf{i}_1 +\\ & [\{\ddot{v}_2 - \ddot{\rho}_{10}\cos\beta - (\dot{v}_1 - \dot{\rho}_{10}\sin\beta)(\Omega\sin\gamma_0\sin\zeta) - (v_1 - \rho_{10}\sin\beta)(\Omega\dot{\zeta}\sin\gamma_0\cos\zeta) +\\ & (\Omega\dot{\zeta}\sin\gamma_0\sin\zeta\sin\beta + \ddot{\zeta}\cos\beta)(r_4 + \rho_{20})\} -\\ & (\Omega\sin\gamma_0\sin\zeta)\{\dot{v}_1 - \dot{\rho}_{10}\sin\beta + (-\Omega\cos\gamma_0\sin\beta - \Omega\sin\gamma_0\cos\zeta\cos\beta + \dot{\zeta}\sin\beta)\times\\ & (r_4 + \rho_{20}) - (v_2 - \rho_{10}\cos\beta)(\Omega\sin\gamma_0\sin\zeta)\} - (\Omega\cos\gamma_0\cos\beta - \Omega\sin\gamma_0\cos\zeta\sin\beta - \dot{\zeta}\cos\beta)\times\\ & \{(v_2 - \rho_{10}\cos\beta)(\Omega\cos\gamma_0\cos\beta - \Omega\sin\gamma_0\cos\zeta\sin\beta - \dot{\zeta}\cos\beta) -\\ & (v_1 - \rho_{10}\sin\beta)(-\Omega\cos\gamma_0\sin\beta - \Omega\sin\gamma_0\cos\zeta\cos\beta + \dot{\zeta}\sin\beta)\}]\mathbf{i}_2 +\\ & [\{(\dot{v}_2 - \dot{\rho}_{10}\cos\beta)(\Omega\cos\gamma_0\cos\beta - \Omega\sin\gamma_0\cos\zeta\sin\beta - \dot{\zeta}\cos\beta) +\\ & (v_2 - \rho_{10}\cos\beta)(\Omega\dot{\zeta}\sin\gamma_0\sin\zeta\beta - \ddot{\zeta}\cos\beta) -\\ & (\dot{v}_1 - \dot{\rho}_{10}\sin\beta)(-\Omega\cos\gamma_0\sin\beta - \Omega\sin\gamma_0\cos\zeta\cos\beta + \dot{\zeta}\sin\beta) -\\ & (v_1 - \rho_{10}\sin\beta)(\Omega\dot{\zeta}\sin\gamma_0\sin\zeta\cos\beta + \ddot{\zeta}\sin\beta)\} +\\ & (\Omega\cos\gamma_0\cos\beta - \Omega\sin\gamma_0\cos\zeta\sin\beta - \dot{\zeta}\cos\beta)\{\dot{v}_2 - \dot{\rho}_{10}\cos\beta - (v_1 - \rho_{10}\sin\beta)(\Omega\sin\gamma_0\sin\zeta) -\\ & (\Omega\cos\gamma_0\cos\beta - \Omega\sin\gamma_0\cos\zeta\sin\beta - \dot{\zeta}\cos\beta)(r_4 + \rho_{20})\} -\\ & (-\Omega\cos\gamma_0\sin\beta - \Omega\sin\gamma_0\cos\zeta\cos\beta + \dot{\zeta}\sin\beta)\{\dot{v}_1 - \dot{\rho}_{10}\sin\beta +\\ & (-\Omega\cos\gamma_0\sin\beta - \Omega\sin\gamma_0\cos\zeta\cos\beta + \dot{\zeta}\sin\beta)(r_4 + \rho_{20}) +\\ & (v_2 - \rho_{10}\cos\beta)(\Omega\sin\gamma_0\sin\zeta)\}]\mathbf{i}_3\end{aligned} \tag{A.12}$$

To transfer to the unit vectors $\mathbf{u}_1,\mathbf{u}_2,\mathbf{u}_3$, we need the equations

$$\mathbf{i}_1 = \mathbf{u}_1 - \theta\,\mathbf{u}_2 + q_1\,\mathbf{u}_3 \qquad \mathbf{i}_2 - \theta\,\mathbf{u}_1 + \mathbf{u}_2 + q_2\,\mathbf{u}_3 \qquad \mathbf{i}_3 = -q_1\,\mathbf{u}_1 - q_2\,\mathbf{u}_2 + \mathbf{u}_3 \tag{A.13}$$

where

$$q_1 = \frac{\partial v_1}{\partial x_3} - \frac{\partial \psi}{\partial x_3}\,v_2 \qquad q_2 = \frac{\partial v_2}{\partial x_3} + \frac{\partial \psi}{\partial x_3}\,v_1 \tag{A.14}$$

Eq. (2.12) is the linearized form of (A.12):

$$\begin{aligned}\mathbf{a}_P = {} & [\ddot{v}_1 - \ddot{\rho}_{10}\sin\beta + (r_4 + \rho_{20})\ddot{\xi}\sin\beta - (v_2 - \rho_{10}\cos\beta)\Omega^2\sin(\beta+\gamma_0)\cos(\beta+\gamma_0) - \\ & (v_1 - \rho_{10}\sin\beta)\Omega^2\sin^2(\beta+\gamma_0) - \Omega^2(r_4+\rho_{20})\zeta\sin\gamma_0\cos(\beta+\gamma_0)]\mathbf{i}_1 + \\ & [\ddot{v}_2 - \ddot{\rho}_{10}\cos\beta + \ddot{\xi}(r_4+\rho_{20})\cos\beta + \Omega^2\zeta(r_4+\rho_{20})\sin\gamma_0\sin(\beta+\gamma_0) - \\ & (v_2 - \rho_{10}\cos\beta)\Omega^2\cos^2(\beta+\gamma_0) - (v_1 - \rho_{10}\sin\beta)\Omega^2\sin(\beta+\gamma_0)\cos(\beta+\gamma_0)]\mathbf{i}_2\end{aligned}$$

Appendix B

To relate blade deflection to axes fixed in the disc, such as the $\mathbf{I}_1$, $\mathbf{I}_2$, $\mathbf{I}_3$ axes, we need a series of transformations. At P of Fig. 2 the displacement is

$$\boldsymbol{\varrho} = v_1\,\mathbf{i}_1 + v_2\,\mathbf{i}_2 \tag{B.1}$$

But

$$\left.\begin{aligned}\mathbf{i}_1 &= \cos(\beta_0+\psi)\,\mathbf{k}_1 + \sin(\beta_0+\psi)\,\mathbf{k}_2 \\ \mathbf{i}_2 &= -\sin(\beta_0+\psi)\,\mathbf{k}_1 + \cos(\beta_0+\psi)\,\mathbf{k}_2\end{aligned}\right\} \tag{B.2}$$

so that

$$\boldsymbol{\varrho} = \{v_1\cos(\beta_0+\psi) - v_2\sin(\beta_0+\psi)\}\,\mathbf{k}_1 + \{v_1\sin(\beta_0+\psi) + v_2\cos(\beta_0+\psi)\}\mathbf{k}_2 \tag{B.3}$$

Eq. (B.3) gives the displacement of P in terms of unit vectors $\mathbf{k}_1,\mathbf{k}_2,\mathbf{k}_3$ at G.

To get to $\mathbf{j}_1,\mathbf{j}_2,\mathbf{j}_3$ axes, we make use of the transformation

$$\mathbf{k}_1 = \mathbf{j}_1 \qquad \mathbf{k}_2 = \cos\zeta\,\mathbf{j}_2 - \sin\zeta\,\mathbf{j}_3 \qquad \mathbf{k}_3 = \sin\zeta\,\mathbf{j}_2 + \cos\zeta\,\mathbf{j}_3 \tag{B.4}$$

and the displacement

$$\begin{aligned}\boldsymbol{\varrho}_G = {} & \{(R_1 - r_1)\sin\xi + (R_2 - r_1)\sin\chi + r_2\sin\zeta\}\,\mathbf{j}_2 + \\ & \{(R_1 - r_1)(1-\cos\xi) + (R_2 - r_1)(1-\cos\chi) + r_2(1-\cos\zeta)\}\,\mathbf{j}_3\end{aligned} \tag{B.5}$$

Then, since the displacement of P with respect to $\mathbf{j}_1,\mathbf{j}_2,\mathbf{j}_3$ is $\boldsymbol{\varrho} + \boldsymbol{\varrho}_G$, we have on combining (B.3) and (B.4)

$$\begin{aligned}\boldsymbol{\varrho}_P = {} & \{v_1\cos(\beta_0+\psi) - v_2\sin(\beta_0+\psi)\}\,\mathbf{j}_1 + \\ & \{v_1\sin(\beta_0+\psi)\cos\zeta + v_2\cos(\beta_0+\psi)\cos\zeta + a_1\sin\xi + a_2\sin\chi + r_2\sin\zeta\}\,\mathbf{j}_2 + \\ & \{-v_1\sin(\beta_0+\psi)\sin\zeta - v_2\cos(\beta_0+\psi)\sin\zeta + a_1(1-\cos\xi) + a_2(1-\cos\chi) + r_2(1-\cos\zeta)\}\,\mathbf{j}_3\end{aligned} \tag{B.6}$$

where (2.2) has been employed also.

Finally, with

$$\mathbf{j}_1 = \cos\gamma_0\mathbf{I}_1 + \sin\gamma_0\mathbf{I}_2 \qquad \mathbf{j}_2 = -\sin\gamma_0\mathbf{I}_1 + \cos\gamma_0\mathbf{I}_2 \qquad \mathbf{j}_3 = \mathbf{I}_3 \tag{B.7}$$

we find

$$\begin{aligned}\boldsymbol{\varrho}_P = {} & \{v_1[\cos(\beta_0+\psi)\cos\gamma_0 - \sin(\beta_0+\psi)\cos\zeta\sin\gamma_0] - \\ & v_2[\sin(\beta_0+\psi)\cos\gamma_0 + \cos(\beta_0+\psi)\cos\zeta\sin\gamma_0] - \\ & (a_1\sin\xi + a_2\sin\chi + r_2\sin\zeta)\sin\gamma_0\}\,\mathbf{I}_1 + \\ & \{v_1[\cos(\beta_0+\psi)\sin\gamma_0 + \sin(\beta_0+\psi)\cos\zeta\cos\gamma_0] - \\ & v_2[\sin(\beta_0+\psi)\sin\gamma_0 - \cos(\beta_0+\psi)\cos\zeta\cos\gamma_0] + \\ & (a_1\sin\xi + a_2\sin\chi + r_2\sin\zeta)\cos\gamma_0\}\,\mathbf{I}_2 + \\ & \{-v_1\sin(\beta_0+\psi)\sin\zeta - v_2\cos(\beta_0+\psi)\sin\zeta + \\ & a_1(1-\cos\xi) + a_2(1-\cos\chi) + r_2(1-\cos\zeta)\}\,\mathbf{I}_3\end{aligned} \tag{B.8}$$

In this equation (B.8), χ is related to ξ and ζ through the second of (2.1).

If ξ, χ, ζ are small, (B.8) simplifies to

$$\begin{aligned}\boldsymbol{\varrho}_P = {} & \{v_1\cos(\beta_0+\psi+\gamma_0) - v_2\sin(\beta_0+\psi+\gamma_0) - (a_1\xi + a_2\chi + r_2\zeta)\sin\gamma_0\}\,\mathbf{I}_1 + \\ & \{v_1\sin(\beta_0+\psi+\gamma_0) + v_2\cos(\beta_0+\psi+\gamma_0) + (a_1\xi + a_2\chi + r_2\zeta)\cos\gamma_0\}\,\mathbf{I}_2\end{aligned}$$

Appendix C

Numerical Analysis

Eqs. (3.8) form a ninth-order system of differential equations which, after appropriate transformations, are best integrated numerically with the aid of an electronic digital computer. The third of (3.8) may be integrated directly using a suitable quadrature formula subject to the boundary condition that the axial traction vanishes at the outer end of the blade to yield the values of N_3 which are needed in the first two of (3.8). The remaining equations form a system of eighth order in the dependent variables v_1, v_2, N_1, N_2, G_1, and G_2.

For steady harmonic oscillation—e.g., free vibration or steady-state forced vibration—this eighth-order system of partial differential equations of motion is readily reduced to an eighth-order system of linear ordinary differential equations by means of the substitutions

$$v_1(x_3,t) = \bar{v}_1 \sin \omega t, \quad \text{etc.} \tag{C.1}$$

where $\bar{v}_1 = \bar{v}_1(x_3)$, etc., representing the local amplitude of the corresponding dependent variable, and ω = circular frequency.

With the introduction of two new variables,

$$\bar{w}_1 = d\bar{v}_1/dx_3 \qquad \bar{w}_2 = d\bar{v}_2/dx_3$$

and some simple algebraic manipulation, the system of equations may be written as a set of eight first-order differential equations of the form

$$\frac{dY_i}{dx_3} = \sum_{j=1}^{8} a_{ij} Y_j, \qquad i = 1, 2, \ldots, 8 \tag{C.2}$$

where Y_i, Y_j represent the eight dependent variables, $\bar{v}_1$, $\bar{v}_2$, $\bar{w}_1$, $\bar{w}_2$, $\bar{N}_1$, $\bar{N}_2$, $\bar{G}_1$, and $\bar{G}_2$, and in which the angular velocity, the frequency of oscillation, the dimension ρ_{20}, and the amplitudes of certain displacements of the attachment (contained in ζ, ρ_{10}) appear as constants.

The equations of motion of the lug (3.7), may be solved for the amplitudes of ξ and ζ in terms of the shears and couples which exist between the root of the blade and the lug. These results, together with (2.1) and (2.13), are now used to eliminate ρ_{20} and the displacements of the attachment from the modified set of equations (C.2).

Recalling that v_1 and v_2 are, in fact, displacements relative to axes attached to the base of the blade, we may take four boundary conditions at the base of the blade as

$$\bar{v}_1 = \bar{v}_2 = \bar{w}_1 = \bar{w}_2 = 0 \tag{C.3}$$

In order to integrate (C.2), we transform the problem from a two-point boundary value problem to an initial problem by means of the replacement of each dependent variable by a linear combination of four new dependent variables:

$$\left.\begin{aligned}
\bar{v}_1 &= \bar{G}_{10}\alpha_1(x_3) + \bar{G}_{20}\beta_1(x_3) + \bar{N}_{10}\gamma_1(x_3) + \bar{N}_{20}\delta_1(x_3)\\
\bar{v}_2 &= \bar{G}_{10}\alpha_2(x_3) + \bar{G}_{20}\beta_2(x_3) + \bar{N}_{10}\gamma_2(x_3) + \bar{N}_{20}\delta_2(x_3)\\
\bar{w}_1 &= \bar{G}_{10}\alpha_3(x_3) + \bar{G}_{20}\beta_3(x_3) + \bar{N}_{10}\gamma_3(x_3) + \bar{N}_{20}\delta_3(x_3)\\
\bar{w}_2 &= \bar{G}_{10}\alpha_4(x_3) + \bar{G}_{20}\beta_4(x_3) + \bar{N}_{10}\gamma_4(x_3) + \bar{N}_{20}\delta_4(x_3)\\
\bar{N}_1 &= \bar{G}_{10}\alpha_5(x_3) + \bar{G}_{20}\beta_5(x_3) + \bar{N}_{10}\gamma_5(x_3) + \bar{N}_{20}\delta_5(x_3)\\
\bar{N}_2 &= \bar{G}_{10}\alpha_6(x_3) + \bar{G}_{20}\beta_6(x_3) + \bar{N}_{10}\gamma_6(x_3) + \bar{N}_{20}\delta_6(x_3)\\
\bar{G}_1 &= \bar{G}_{10}\alpha_7(x_3) + \bar{G}_{20}\beta_7(x_3) + \bar{N}_{10}\gamma_7(x_3) + \bar{N}_{20}\delta_7(x_3)\\
\bar{G}_2 &= \bar{G}_{10}\alpha_8(x_3) + \bar{G}_{20}\beta_8(x_3) + \bar{N}_{10}\gamma_8(x_3) + \bar{N}_{20}\delta_8(x_3)
\end{aligned}\right\} \tag{C.4}$$

in which we have, in fact, taken the weighting functions to be the amplitudes of the tractions at the root of the blade. With the substitution of (C.4) into (C.2), the resulting equations may be integrated for four linearly independent but otherwise arbitrary sets of weighting functions—for example, the following convenient scheme:

Case	$\bar{G}_{10}$	$\bar{G}_{20}$	$\bar{N}_{10}$	$\bar{N}_{20}$
I	1	0	0	0
II	0	1	0	0
III	0	0	1	0
IV	0	0	0	1

Each of the four sets of differential equations is now integrated numerically using an appropriate quadrature formula such as the Runge-Kutta fourth-order process. The values of the resulting solutions at the outer end of the blade yield the values of the amplitudes of the transverse shears and couples at the tip ($x_3 = a$) in the form

$$\left.\begin{aligned}
\bar{N}_{1_\alpha} &= \bar{G}_{10}\alpha_5(a) + \bar{G}_{20}\beta_5(a) + \bar{N}_{10}\gamma_5(a) + \bar{N}_{20}\delta_5(a)\\
\bar{N}_{2_\alpha} &= \bar{G}_{10}\alpha_6(a) + \bar{G}_{20}\beta_6(a) + \bar{N}_{10}\gamma_6(a) + \bar{N}_{20}\delta_6(a)\\
\bar{G}_{1_\alpha} &= \bar{G}_{10}\alpha_7(a) + \bar{G}_{20}\beta_7(a) + \bar{N}_{10}\gamma_7(a) + \bar{N}_{20}\delta_7(a)\\
\bar{G}_{2_\alpha} &= \bar{G}_{10}\alpha_8(a) + \bar{G}_{20}\beta_8(a) + \bar{N}_{10}\gamma_8(a) + \bar{N}_{20}\delta_8(a)
\end{aligned}\right\} \tag{C.5}$$

In the case of free vibration, these tractions will vanish simultaneously and (C.5) will reduce to four homogeneous algebraic equations in the weighting functions as unknowns. These can have a nontrivial solution if, and only if, the determinant formed by the coefficients of these quantities vanishes, or

$$\Delta(\omega) = \begin{vmatrix} \alpha_5(a) & \beta_5(a) & \gamma_5(a) & \delta_5(a) \\ \alpha_6(a) & \beta_6(a) & \gamma_6(a) & \delta_6(a) \\ \alpha_7(a) & \beta_7(a) & \gamma_7(a) & \delta_7(a) \\ \alpha_8(a) & \beta_8(a) & \gamma_8(a) & \delta_8(a) \end{vmatrix} = 0 \tag{C.6}$$

(*Continued on page 609*)

Influence of Large Amplitudes on Flexural Vibrations of a Thin Circular Cylindrical Shell

HU-NAN CHU*
The Martin Company

Summary

In this paper are derived the equations of nonlinear flexural vibrations for a thin circular cylindrical shell. The assumptions employed in the various steps of derivation are clearly set forth. Axial body force terms which may be of practical importance are included in the equations. Nonlinear periods are obtained for the free vibrations case. Numerical examples are given for a shell with a radius thickness ratio of 100 and two numbers of circumferential waves, 8 and 10. The results are plotted and compared with a previous study on flat plates. In these examples, nonlinear effects are found to be considerably less manifest in cylinders than in corresponding flat plates.

Symbols

x,y,z	= axial, circumferential, and radial coordinates, respectively; also used as subscripts to denote quantities in these directions
e,ϵ	= linear and nonlinear strain components, respectively, with appropriate subscripts
ω_x,ω_y	= rotations about x axis and y axis, respectively
R,h	= mean radius and thickness, respectively, of the shell
ρ	= mass density of the shell
σ	= stress components, with appropriate subscripts
N_x,N_y,N_{xy}	= in-plane forces defined by Eq. (6)
M_x,M_y,M_{xy}	= bending moments defined by Eq. (6)
n,s	= normal and tangential coordinates, respectively, of a boundary curve; also used as subscripts; used only before Eq. (17)
f	= components of external traction, with appropriate subscripts
F_x,F_y,m_x $[m_y,q]$	— defined by Eq. (9)
X,Y,Z	= components of body force density
u,v,w	= middle surface displacements defined by Eq. (4)
E,G,D	= Young's modulus, shear modulus, and flexural rigidity, respectively
F	= stress function defined by Eq. (20)
λ_x,λ_y	= axial and circumferential half-wavelengths, respectively
L	= λ_x
r	= λ_y/λ_x
n	= number of circumferential full waves; used only after Eq. (23)
$H(t)$	= time function in nonlinear vibrations
A	= amplitude of flexural vibrations
β	= A/h
$K(k)$	= complete elliptic integral of the first kind
k	— defined by Eq. (32)

(1) Introduction

THE IMPORTANCE of including nonlinear effects in problems regarding strength and stability of modern flight structures has been made clear largely by the works of von Kármán,[1] Tsien,[2] and Donnell.[3] The method advocated by von Kármán and Tsien,[2] for example, has become virtually standard procedure in the solution of stability problems of thin cylinders. Specifically, these nonlinear effects are introduced through the inclusion of the second-order terms in the strain–displacement relations. These second-order terms are quadratic in the rotations of the cross sections. For reference, the reader may turn, for example, to Biot[4,14] and Novozhilov.[5]

Similar effects have been considered in vibration problems by such writers as Carrier,[6] Eringen,[7] Chu and Herrmann,[8] and E. Reissner.[9] One difficulty in problems regarding nonlinear vibrations of elastic bodies appears to be that the meaning of normal modes (which are powerful tools in linear vibration problems) becomes obscure since time and space variables are not separable in most nonlinear vibration problems.

However, since one reason for studying nonlinear vibrations of plates and shells used in flight structures is the solution of problems regarding panel excitations, and since some experiments[10,16] do indicate that the panel behaves like a forced nonlinear system with one or two degrees of freedom, we are therefore guided toward finding these vibrational modes. One approach involves simply the investigation of free vibration problems. The mode shape assumed is the first normal mode shape in the linear theory and is also consistent with the experiments.

These observations would seem to put us in a situation similar to that of the late 1930's regarding stability problems of thin cylinders—that is, the eigenvalue character of the problem becomes lost in changing from the linear to the nonlinear case and we must rely heavily on clues derived from the experiments.

Our approach in this paper is similar in some ways to that of E. Reissner.[9] The differences would be in presentation and interpretation, in various points of emphasis, and in our systematic derivation of equations of motion from a set of consistent assumptions. These equations of motion include terms not included in those derived by Marguerre[11] and used by E. Reissner.[9] The terms in question extend the present work to practical problems under contemplation. However, since the problems regarding the free vibrations must first be solved, these extra terms are merely presented in this paper. Also, examples are worked out with a view to possible application to the flutter and panel excitation

Received May 2, 1960.

* Structures Research Staff, The Martin Company, Denver, Colo.

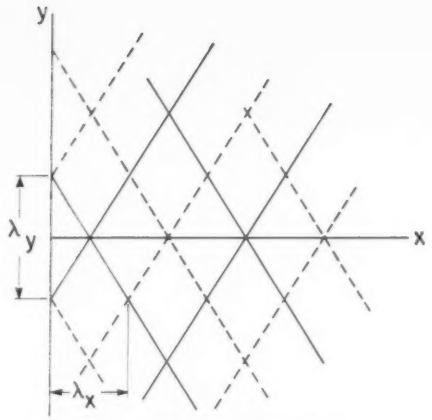

FIG. 1. Pattern of vibration modes.

problems. We start, however, by deriving the differential equations of motion.

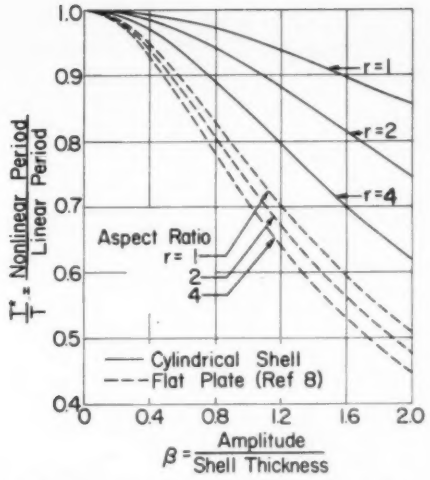

FIG. 2. Influence of large amplitudes on period of vibrations. Number of circumferential waves, $n = 8$.

(2) Stress Equations of Motion

(a) Strains and Displacements

The strain expressions in which the second-order terms are included may be found in a number of references, including, for example, Novozhilov.[5] When applied to cylindrical shells in which the shell thickness is small compared to the radius, they read

$$\left.\begin{aligned} \epsilon_{xx} &= e_{xx} + (1/2)\omega_y^2, \quad \epsilon_{yy} = e_{yy} + (1/2)\omega_x^2, \quad \epsilon_{zz} = e_{zz} + (1/2)(\omega_x^2 + \omega_y^2) \\ \epsilon_{yz} &= e_{yz}, \quad \epsilon_{xy} = e_{xy} - \omega_x\omega_y, \quad \epsilon_{zx} = e_{zx} \end{aligned}\right\} \tag{1}$$

where

$$\left.\begin{aligned} e_{xx} &= \partial u_x/\partial x, \quad e_{yy} = \partial u_y/\partial y + u_z/R, \quad e_{zz} = \partial u_z/\partial z \\ e_{xy} &= \partial u_y/\partial x + \partial u_x/\partial y, \quad e_{zx} = \partial u_x/\partial z + \partial u_z/\partial x, \quad e_{yz} = \partial u_z/\partial y + \partial u_y/\partial z - u_y/R \end{aligned}\right\} \tag{2}$$

are the strain components in the linear theory, and

$$\omega_x = \frac{1}{2}\left(\frac{\partial u_z}{\partial y} - \frac{u_y}{R} - \frac{\partial u_y}{\partial z}\right), \qquad \omega_y = \frac{1}{2}\left(\frac{\partial u_x}{\partial z} - \frac{\partial u_z}{\partial x}\right) \tag{3}$$

are the components of rotation. u_x, u_y, and u_z are the axial, circumferential, and radial displacement components, respectively. x and y are the axial and circumferential coordinates, respectively, measured along the middle surface of the undeformed shell, while z is the radial coordinate measured from this surface. R is the mean radius of the undeformed shell.

Next, we consider only those problems in which the displacements are predominantly flexural. The term u_y/R in Eqs. (2) and (3) can therefore be neglected. In addition, if in these problems the characteristic dimensions involved (the axial and circumferential wavelengths, for example) are large as compared to the shell thickness, we can assume the displacements to be

$$u_x = u(x,y) - z(\partial w/\partial x), \quad u_y = v(x,y) - z(\partial w/\partial y), \quad u_z = w(x,y) \tag{4}$$

where the transverse shear deformation is neglected.

The strain expressions of Eq. (1) can now be calculated by using Eq. (4). The result is

$$\left.\begin{aligned} \epsilon_{xx} &= \frac{\partial u}{\partial x} + \frac{1}{2}\left(\frac{\partial w}{\partial x}\right)^2 - z\frac{\partial^2 w}{\partial x^2}, \quad \epsilon_{yy} = \frac{\partial v}{\partial y} + \frac{w}{R} + \frac{1}{2}\left(\frac{\partial w}{\partial y}\right)^2 - z\frac{\partial^2 w}{\partial y^2} \\ \epsilon_{zz} &= \frac{1}{2}\left(\frac{\partial w}{\partial x}\right)^2 + \frac{1}{2}\left(\frac{\partial w}{\partial y}\right)^2, \quad \epsilon_{xy} = \frac{\partial v}{\partial x} + \frac{\partial u}{\partial y} + \frac{\partial w}{\partial x}\frac{\partial w}{\partial y} - 2z\frac{\partial^2 w}{\partial x \partial y} \end{aligned}\right\} \tag{5}$$

(b) The Strain-Energy Expression

We shall neglect the contribution in strain energy due to σ_{zz}. The discussion will therefore be limited to frequencies below that at which σ_{zz} becomes important—i.e., frequencies of the thickness-stretch vibrations.[12] This is

acceptable since this paper will discuss the effect of large amplitudes on those flexural vibrations whose frequencies are far below those of the thickness-stretch modes.

The strain-energy expression is then

$$W = \frac{1}{2}\iiint (\sigma_{xx}\epsilon_{xx} + \sigma_{yy}\epsilon_{yy} + \sigma_{xy}\epsilon_{xy})dxdydz$$

$$= \frac{1}{2}\iiint \left\{\sigma_{xx}\left[\frac{\partial u}{\partial x} + \frac{1}{2}\left(\frac{\partial w}{\partial x}\right)^2 - z\frac{\partial^2 w}{\partial x^2}\right] + \sigma_{yy}\left[\frac{\partial v}{\partial y} + \frac{w}{R} + \frac{1}{2}\left(\frac{\partial w}{\partial y}\right)^2 - z\frac{\partial^2 w}{\partial y^2}\right] + \sigma_{xy}\left[\frac{\partial v}{\partial x} + \frac{\partial u}{\partial y} + \frac{\partial w}{\partial x}\frac{\partial w}{\partial y} - 2z\frac{\partial^2 w}{\partial x \partial y}\right]\right\} dx\, dy\, dz$$

If we define

$$\left.\begin{aligned} N_x &= \int_{-h/2}^{h/2} \sigma_{xx}\, dz, \quad N_y = \int_{-h/2}^{h/2} \sigma_{yy}\, dz, \quad N_{xy} = \int_{-h/2}^{h/2} \sigma_{xy}\, dz \\ M_x &= \int_{-h/2}^{h/2} \sigma_{xx}\, z\, dz, \quad M_y = \int_{-h/2}^{h/2} \sigma_{yy}\, z\, dz, \quad M_{xy} = \int_{-h/2}^{h/2} \sigma_{xy}\, z\, dz \end{aligned}\right\} \tag{6}$$

where h is the shell thickness, the strain-energy expression can then be written as

$$W = \frac{1}{2}\iint \left\{N_x\left[\frac{\partial u}{\partial x} + \frac{1}{2}\left(\frac{\partial w}{\partial x}\right)^2\right] - M_x\frac{\partial^2 w}{\partial x^2} + N_y\left[\frac{\partial v}{\partial y} + \frac{w}{R} + \frac{1}{2}\left(\frac{\partial w}{\partial y}\right)^2\right] - M_y\frac{\partial^2 w}{\partial y^2} + N_{xy}\left[\frac{\partial v}{\partial x} + \frac{\partial u}{\partial y} + \frac{\partial w}{\partial x}\frac{\partial w}{\partial y}\right] - 2M_{xy}\frac{\partial^2 w}{\partial x \partial y}\right\} dxdy \tag{7}$$

The strain-energy variation becomes

$$\delta W = \iint \left[N_x\left(\frac{\partial \delta u}{\partial x} + \frac{\partial w}{\partial x}\frac{\partial \delta w}{\partial x}\right) - M_x\frac{\partial^2 \delta w}{\partial x^2} + N_y\left(\frac{\partial \delta v}{\partial y} + \frac{\partial w}{\partial y}\frac{\partial \delta w}{\partial y} + \frac{\delta w}{R}\right) - M_y\frac{\partial^2 \delta w}{\partial y^2} + N_{xy}\left(\frac{\partial \delta v}{\partial x} + \frac{\partial \delta u}{\partial y} + \frac{\partial w}{\partial x}\frac{\partial \delta w}{\partial y} + \frac{\partial w}{\partial y}\frac{\partial \delta w}{\partial x}\right) - 2M_{xy}\frac{\partial^2 \delta w}{\partial x \partial y}\right] dxdy$$

which may be integrated by parts to yield

$$\delta W = \oint \left[N_n\, \delta u_n + N_n\frac{\partial w}{\partial n}\delta w + N_{ns}\frac{\partial w}{\partial s}\delta w - M_n\delta\left(\frac{\partial w}{\partial n}\right) + N_{ns}\,\delta u_s + \frac{\partial M_n}{\partial n}\delta w + 2\frac{\partial M_{ns}}{\partial s}\delta w\right] ds - \iint \left\{\left[\frac{\partial N_x}{\partial x} + \frac{\partial N_{xy}}{\partial y}\right]\delta u + \left[\frac{\partial N_{xy}}{\partial x} + \frac{\partial N_y}{\partial y}\right]\delta v + \left[\frac{\partial^2 M_x}{\partial x^2} + \frac{\partial^2 M_y}{\partial y^2} + 2\frac{\partial^2 M_{xy}}{\partial x \partial y} + \frac{\partial}{\partial x}\left(N_x\frac{\partial w}{\partial x}\right) + \frac{\partial}{\partial y}\left(N_y\frac{\partial w}{\partial y}\right) + \frac{\partial}{\partial x}\left(N_{xy}\frac{\partial w}{\partial y}\right) + \frac{\partial}{\partial y}\left(N_{xy}\frac{\partial w}{\partial x}\right) - \frac{N_y}{R}\right]\delta w\right\} dxdy \tag{8}$$

where the line integral is to be taken around the curve bounding the middle surface of the shell element under consideration, and n and s are the normal and tangential coordinates, respectively, to this boundary curve. In setting up Eq. (8), use was made of

$$\iint \left[\frac{\partial}{\partial x}(N_x\delta u) + \frac{\partial}{\partial y}(N_y\delta v)\right] dxdy = \oint N_n\delta u_n\, ds, \qquad \text{etc.,}$$

and

$$-\oint M_{ns}\frac{\partial \delta w}{\partial s}\, ds = \oint \frac{\partial M_{ns}}{\partial s}\delta w\, ds$$

(c) *The External Work*

Let f_x, f_y, and f_z denote the x, y and z components, respectively, of the surface tractions per unit original area. The external work then becomes

$$W_e = \iint_S (f_x u_x + f_y u_y + f_z u_z)\, dS$$

where S indicates the total external surfaces. The external work variation is then

$$\delta W_e = \iint [f_x \delta u_x + f_y \delta u_y + f_z \delta u_z]_{z=-h/2}^{z=h/2} \, dxdy + \oint \int_{-h/2}^{h/2} (f_n \delta u_n + f_s \delta u_s + f_z \delta u_z) \, dzds$$

Hence, by the assumed displacements of Eq. (4), we have

$$\delta W_e = \iint \left[f_x \left(\delta u - z \frac{\partial \delta w}{\partial x} \right) + f_y \left(\delta v - z \frac{\partial \delta w}{\partial y} \right) + f_z \delta w \right]_{z=-h/2}^{z=h/2} dxdy + \oint \int_{-h/2}^{h/2} \left[f_n \left(\delta u_n - z \frac{\partial \delta w}{\partial n} \right) + f_s \left(\delta u_s - z \frac{\partial \delta w}{\partial s} \right) + f_z \delta w \right] dzds$$

Now, if we define

$$\left.\begin{aligned} F_x = f_x]_{z=-h/2}^{z=h/2}, \quad F_y = f_y]_{z=-h/2}^{z=h/2}, \quad q = f_z]_{z=-h/2}^{z=h/2}, \; m_x = z f_x]_{z=-h/2}^{z=h/2} \\ m_y = z f_y]_{z=-h/2}^{z=h/2}, \quad N_n^* = \int_{-h/2}^{h/2} f_n dz, \; N_{ns}^* = \int_{-h/2}^{h/2} f_s dz, \; Q_n = \int_{-h/2}^{h/2} f_z dz \\ M_n^* = \int_{-h/2}^{h/2} f_n z dz, \qquad M_{ns}^* = \int_{-h/2}^{h/2} f_s z dz \end{aligned}\right\} \tag{9}$$

then the external work variation may be written as

$$\left.\begin{aligned} \delta W_e = \iint \left[F_x \delta u + F_y \delta v + \left(\frac{\partial m_x}{\partial x} + \frac{\partial m_y}{\partial y} + q \right) \delta w \right] dxdy + \\ \oint \left[N_n^* \delta u_n + N_{rs}^* \, \delta u_s + \left(Q_n - m_n + \frac{\partial M_{ns}^*}{\partial s} \right) \delta w - M_n^* \delta \left(\frac{\partial w}{\partial n} \right) \right] ds \end{aligned}\right\} \tag{10}$$

where use has been made of

$$\iint \left(m_x \frac{\partial \delta w}{\partial x} + m_y \frac{\partial \delta w}{\partial y} \right) dxdy = \oint m_n \delta w \, ds - \iint \left(\frac{\partial m_x}{\partial x} + \frac{\partial m_y}{\partial y} \right) \delta w \, dxdy$$

and

$$- \oint M_{ns}^* \frac{\partial \delta w}{\partial s} ds = \oint \frac{\partial M_{ns}^*}{\partial s} \delta w \, ds$$

(d) The Kinetic Energy Expression

The kinetic energy is

$$T = \frac{1}{2} \iiint \rho (\dot{u}_x^2 + \dot{u}_y^2 + \dot{u}_z^2) \, dxdydz$$

which by means of Eq. (4) may be written as

$$\begin{aligned} T &= \frac{1}{2} \iiint \rho \left[\left(\dot{u} - z \frac{\partial \dot{w}}{\partial x} \right)^2 + \left(\dot{v} - z \frac{\partial \dot{w}}{\partial y} \right)^2 + \dot{w}^2 \right] dxdydz \\ &= \frac{1}{2} \iint \rho \left[h\dot{u}^2 + h\dot{v}^2 + h\dot{w}^2 + \frac{h^3}{12} \left(\frac{\partial \dot{w}}{\partial x} \right)^2 + \frac{h^3}{12} \left(\frac{\partial \dot{w}}{\partial y} \right)^2 \right] dxdy \end{aligned}$$

where the dot indicates differentiation with respect to time. Hence the kinetic energy variation is

$$\delta T = \iint \left(\rho h \dot{u} \, \delta \dot{u} + \rho h \dot{v} \, \delta \dot{v} - \frac{\rho h^3}{12} \frac{\partial^2 \dot{w}}{\partial x^2} \delta \dot{w} - \frac{\rho h^3}{12} \frac{\partial^2 \dot{w}}{\partial y^2} \delta \dot{w} + \rho h \dot{w} \, \delta \dot{w} \right) dxdy + \oint \frac{\rho h^3}{12} \frac{\partial \dot{w}}{\partial n} \delta \dot{w} \, ds$$

which may be integrated by parts with respect to time to yield

$$\int_{t_1}^{t_2} \delta T \, dt = \int_{t_1}^{t_2} \iint \rho \left[-h\ddot{u} \, \delta u - h\ddot{v} \, \delta v + \frac{h^3}{12} \left(\frac{\partial^2 \ddot{w}}{\partial x^2} + \frac{\partial^2 \ddot{w}}{\partial y^2} \right) \delta w - h\ddot{w} \, \delta w \right] dxdydt - \int_{t_1}^{t_2} \oint \frac{\rho h^3}{12} \frac{\partial \ddot{w}}{\partial n} \delta w \, ds \, dt \tag{11}$$

in which the variations at t_1 and t_2 have been set to zero.

(e) The Work of Body Forces

Let X, Y, and Z be the x, y, and z components, respectively, of the body force per unit original volume. The variation of the work of body forces can then be written as

$$\left.\begin{aligned}\delta W_B &= \iiint (X\,\delta u_x + Y\,\delta u_y + Z\,\delta u_z)\,dxdydz \\ &= \iiint \left[X\left(\delta u - z\frac{\partial \delta w}{\partial x}\right) + Y\left(\delta v - z\frac{\partial w}{\partial y}\right) + Z\,\delta w\right] dxdydz\end{aligned}\right\} \tag{12}$$

If we define

$$\bar{X} = \int_{-h/2}^{h/2} X\,dz, \qquad \bar{Y} = \int_{-h/2}^{h/2} Y\,dz, \qquad \bar{Z} = \int_{-h/2}^{h/2} Z\,dz \tag{13}$$

then Eq. (12) may be written as

$$\delta W_B = \iint [X\,\delta u + Y\,\delta v + Z\,\delta w]\,dxdy - \iiint \left[X\,\delta\left(\frac{\partial w}{\partial x}\right) + Y\,\delta\left(\frac{\partial w}{\partial y}\right)\right] z\,dzdxdy$$

If we limit ourselves to those problems in which

$$\int_{-h/2}^{h/2} (X + Y)z\,dz = 0$$

we will then have

$$\delta W_B = \iint (X\,\delta u + Y\,\delta v + Z\,\delta w)\,dxdy \tag{14}$$

(*f*) *The Shell-Stress Equations of Motion*

The variational principle states that among all the admissible states of stress the actual one is that which satisfies

$$\delta \int_{t_1}^{t_2} L\,dt = 0$$

where $L = T - U = T - W + W_e + W_B$. Therefore, from Eqs. (8), (10), (11), and (14), we obtain the following set of shell-stress equations of motion:

$$\left.\begin{aligned}&\frac{\partial N_x}{\partial x} + \frac{\partial N_{xy}}{\partial y} + F_x + \bar{X} = \rho h\ddot{u} \qquad \frac{\partial N_{xy}}{\partial x} + \frac{\partial N_y}{\partial y} + F_y + \bar{Y} = \rho h\ddot{v} \\ &\frac{\partial^2 M_x}{\partial x^2} + \frac{\partial^2 M_y}{\partial y^2} + 2\frac{\partial^2 M_{xy}}{\partial x \partial y} + \frac{\partial}{\partial x}\left(N_x\frac{\partial w}{\partial x} + N_{xy}\frac{\partial w}{\partial y}\right) + \frac{\partial}{\partial y}\left(N_y\frac{\partial w}{\partial y} + N_{xy}\frac{\partial w}{\partial x}\right) - \\ &\qquad \frac{N_y}{R} + q + \frac{\partial m_x}{\partial x} + \frac{\partial m_y}{\partial y} + \bar{Z} = \rho h\ddot{w} - \frac{\rho h^3}{12}\left(\frac{\partial^2}{\partial x^2} + \frac{\partial^2}{\partial y^2}\right)\ddot{w}\end{aligned}\right\} \tag{15}$$

In addition, at the boundary, we have

$$\left.\begin{aligned}&N_n = N_n^*, \quad N_{ns} = N_{ns}^*, \quad M_n = M_n^*, \quad \text{and} \\ &Q_n = m_n + \frac{\rho h^3}{12}\frac{\partial \ddot{w}}{\partial n} + N_n\frac{\partial w}{\partial n} + N_{ns}\frac{\partial w}{\partial s} + \frac{\partial M_n}{\partial n} + \frac{\partial M_{ns}}{\partial s}\end{aligned}\right\} \tag{16}$$

Since the superposition principle no longer holds in nonlinear problems, a uniqueness theorem similar to that of F. Neumann for the linear case cannot be formulated in our case.

Eqs. (15) (with the exception of the body force terms $\bar{X}$, $\bar{Y}$, and $\bar{Z}$) reduce to those equations derived by L. Donnell[3] when $\ddot{u}$, $\ddot{v}$, and $\ddot{w}$ terms are put to zero, and to that equation derived by G. Herrmann[13] when R tends to infinity.

As mentioned earlier, the axial and circumferential wavelengths considered in this paper are large compared to the shell thickness. Therefore, the term $(\rho h^3/12)(\partial^2/\partial x^2 + \partial^2/\partial y^2)\ddot{w}$ in Eq. (15) can be neglected.

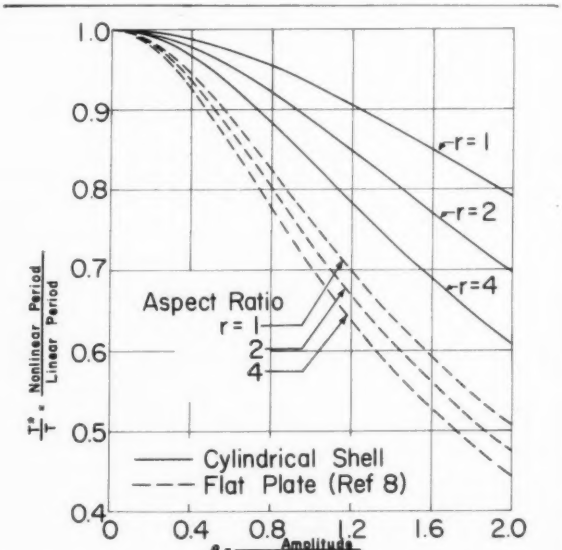

FIG. 3. Influence of large amplitudes on period of vibrations. Number of circumferential waves $n = 10$.

(3) Displacement Equations of Motion

(a) Stress–Displacement Relations

In general, there are six stress–strain relations for a three-dimensional solid. Since the transverse shear strains ϵ_{yz} and ϵ_{zz} are neglected in our case, only four stress–strain relations remain. Then the strain component ϵ_{zz} is eliminated, and we have the following three stress–strain relations:

$$\left.\begin{aligned} \sigma_{xx} &= \frac{E}{1-\nu^2}(\epsilon_{xx}+\nu\epsilon_{yy})+\frac{\nu}{1-\nu}\sigma_{zz} \\ \sigma_{yy} &= \frac{E}{1-\nu^2}(\epsilon_{yy}+\nu\epsilon_{xx})+\frac{\nu}{1-\nu}\sigma_{zz} \\ \sigma_{xy} &= G\,\epsilon_{xy} \end{aligned}\right\} \tag{17}$$

Hence, by using Eq. (5), we have

$$\left.\begin{aligned} \sigma_{xx} &= \frac{E}{1-\nu^2}\left[\frac{\partial u}{\partial x}-z\frac{\partial^2 w}{\partial x^2}+\frac{1}{2}\left(\frac{\partial w}{\partial x}\right)^2+\nu\frac{\partial v}{\partial y}+\right. \\ &\qquad \left.\nu\frac{w}{R}+\frac{\nu}{2}\left(\frac{\partial w}{\partial y}\right)^2-\nu z\frac{\partial^2 w}{\partial y^2}\right]+\frac{\nu}{1-\nu}\sigma_{zz} \\ \sigma_{yy} &= \frac{E}{1-\nu^2}\left[\frac{\partial v}{\partial y}-z\frac{\partial^2 w}{\partial y^2}+\frac{1}{2}\left(\frac{\partial w}{\partial y}\right)^2+\frac{w}{R}+\right. \\ &\qquad \left.\nu\frac{\partial u}{\partial x}+\frac{\nu}{2}\left(\frac{\partial w}{\partial x}\right)^2-\nu z\frac{\partial^2 w}{\partial x^2}\right]+\frac{\nu}{1-\nu}\sigma_{zz} \\ \sigma_{xy} &= G\left(\frac{\partial v}{\partial x}+\frac{\partial u}{\partial y}+\frac{\partial w}{\partial x}\frac{\partial w}{\partial y}\right)-2zG\frac{\partial^2 w}{\partial x\partial y} \end{aligned}\right\} \tag{18}$$

which can then be integrated across the shell thickness h to yield

$$\left.\begin{aligned} N_x &= \frac{Eh}{1-\nu^2}\left[\frac{\partial u}{\partial x}+\frac{1}{2}\left(\frac{\partial w}{\partial x}\right)^2+\right. \\ &\qquad \left.\nu\frac{\partial v}{\partial y}+\nu\frac{w}{R}+\frac{\nu}{2}\left(\frac{\partial w}{\partial y}\right)^2\right] \\ M_x &= -D\left[\frac{\partial^2 w}{\partial x^2}+\nu\frac{\partial^2 w}{\partial y^2}\right] \\ N_y &= \frac{Eh}{1-\nu^2}\left[\frac{\partial v}{\partial y}+\frac{w}{R}+\frac{1}{2}\left(\frac{\partial w}{\partial y}\right)^2+\right. \\ &\qquad \left.\nu\frac{\partial u}{\partial x}+\frac{\nu}{2}\left(\frac{\partial w}{\partial x}\right)^2\right] \\ M_y &= -D\left[\frac{\partial^2 w}{\partial y^2}+\nu\frac{\partial^2 w}{\partial x^2}\right] \\ N_{xy} &= Gh\left(\frac{\partial v}{\partial x}+\frac{\partial u}{\partial y}+\frac{\partial w}{\partial x}\frac{\partial w}{\partial y}\right), \\ M_{xy} &= -D(1-\nu)\frac{\partial^2 w}{\partial x\partial y} \end{aligned}\right\} \tag{19}$$

in which integrals containing σ_{zz} are neglected according to comments presented earlier in this paper regarding thickness-stretch modes.

(b) The Stress Function and Displacement Equations of Motion

If we substitute Eq. (19) into Eq. (15), we obtain the displacement equations of motion. However, equations obtained in this manner are awkward for use in many practical problems. The following considerations therefore appear in order.

We assume that the shell is free from all external forces but subject to the internal pressure p and one constant axial body force. F_z, F_y, m_x, m_y, $\bar{Y}$, and $\bar{Z}$ are then zero, q is equal to p, and $\bar{X}$ is constant. We can, therefore, define a stress function $F(x,y)$ such that

$$N_x+\bar{X}x=h\frac{\partial^2 F}{\partial y^2},\quad N_y=h\frac{\partial^2 F}{\partial x^2},\quad N_{xy}=-h\frac{\partial^2 F}{\partial x\partial y} \tag{20}$$

Furthermore, if the motion is predominantly flexural (as was assumed at the beginning of this paper) the longitudinal and circumferential inertia terms, $\rho h\ddot{u}$ and $\rho h\ddot{v}$ of Eq. (15), can then be shown negligible according to a perturbation procedure.[8] Therefore, the first two equations of (15) are identically satisfied by the stress function defined by Eq. (20), and the third equation of (15) becomes

$$\left.\begin{aligned} \frac{D}{h}\nabla^4 w &= \frac{\partial^2 F}{\partial y^2}\frac{\partial^2 w}{\partial x^2}-2\frac{\partial^2 F}{\partial x\partial y}\frac{\partial^2 w}{\partial x\partial y}+\frac{\partial^2 F}{\partial x^2}\frac{\partial^2 w}{\partial y^2}- \\ &\qquad \frac{1}{R}\frac{\partial^2 F}{\partial x^2}-\frac{\bar{X}}{h}\left(\frac{\partial w}{\partial x}+x\frac{\partial^2 w}{\partial x^2}\right)+\frac{p}{h}-\rho\ddot{w} \end{aligned}\right\} \tag{21}$$

On the other hand, from Eq. (19) we obtain the following equation of compatibility:

$$\frac{1}{E}\nabla^4 F=\left(\frac{\partial^2 w}{\partial x\partial y}\right)^2-\frac{\partial^2 w}{\partial x^2}\frac{\partial^2 w}{\partial y^2}+\frac{1}{R}\frac{\partial^2 w}{\partial x^2} \tag{22}$$

and in Eqs. (21) and (22)

$$\nabla^4=\nabla^2\nabla^2 \quad\text{and}\quad \nabla^2=\partial^2/\partial x^2+\partial^2/\partial y^2$$

(as is customary).

If we think in terms of an axial force field $\bar{X}x$, then $(\bar{X}/h)(\partial w/\partial x)$ may be referred to as the "buoyancy term" while $(\bar{X}x/h)(\partial^2 w/\partial x^2)$ may be called the "curvature term"—to use a phrase coined by M. A. Biot.[14]

Eqs. (21) and (22) will form the basis of our following discussions.

(4) Solution of Free Vibrations

When the shell is free from the external and body forces, the equations take the form

$$\left.\begin{aligned} \frac{D}{h}\nabla^4 w+\rho\ddot{w} &= \frac{\partial^2 F}{\partial y^2}\frac{\partial^2 w}{\partial x^2}-2\frac{\partial^2 F}{\partial x\partial y}\frac{\partial^2 w}{\partial x\partial y}+ \\ &\qquad \frac{\partial^2 F}{\partial x^2}\frac{\partial^2 w}{\partial y^2}-\frac{1}{R}\frac{\partial^2 F}{\partial x^2} \\ \frac{1}{E}\nabla^4 F &= \left(\frac{\partial^2 w}{\partial x\partial y}\right)^2-\frac{\partial^2 w}{\partial x^2}\frac{\partial^2 w}{\partial y^2}+\frac{1}{R}\frac{\partial^2 w}{\partial x^2} \end{aligned}\right\} \tag{23}$$

Since our purpose at present is to establish the effect of large amplitudes in relation to the corresponding linear vibrations, we assume that the vibration modes form a pattern of equal "lobes" (which is suggested by

solution of the corresponding linear vibrations, as we shall presently see). Each lobe is characterized by a longitudinal and a circumferential half-wavelength, λ_x and λ_y, respectively. Thus, we may consider each lobe individually, and position our coordinates accordingly. In particular, we set

$$0 \leq x \leq L \qquad \text{and} \qquad -\pi R/2n \leq y \leq \pi R/2n$$

as a "representative lobe," while n is the number of the circumferential full waves. Apparently,

$$\lambda_x = L \qquad \text{and} \qquad \lambda_y = \pi R/n$$

In Fig. 1, the intersections of solid lines represent points of maximum positive amplitude, while those of the dotted lines represent points of maximum negative amplitude (or vice versa). Also, a full- and dotted-line intersection represents a point where $w = 0$.

(a) *Solution of Free Linear Vibrations*

If the nonlinear terms of Eq. (23) are dropped, then the corresponding linear equations are obtained. Thus

$$\left.\begin{aligned} \frac{D}{h}\nabla^4 w + \rho \ddot{w} &= -\frac{1}{R}\frac{\partial^2 F}{\partial x^2} \\ \nabla^4 F &= \frac{E}{R}\frac{\partial^2 w}{\partial x^2} \end{aligned}\right\} \tag{24}$$

If we assume

$$\left.\begin{aligned} w &= A \sin (\pi x/L) \cos (ny/R) \sin \omega t \\ F &= B \sin (\pi x/L) \cos (ny/R) \sin \omega t \end{aligned}\right\} \tag{25}$$

we get

$$\omega^2 = \frac{E}{\rho}\left[\frac{n^2\pi^2}{12(1-\nu^2)}\left(\frac{h}{R}\right)^2\left(\frac{1}{\lambda_y}\right)^2 (1+r^2)^2 + \left(\frac{1}{R}\right)^2 r^4 (1+r^2)^{-2}\right] \tag{26}$$

Note that Eq. (25) satisfies the boundary conditions

$$\left.\begin{aligned} w = \partial^2 w/\partial x^2 = F = \partial^2 F/\partial x^2 = 0, \quad &\text{at} \quad x = 0, L \\ w = \partial^2 w/\partial y^2 = F = \partial^2 F/\partial y^2 = 0, \quad &\text{at} \quad y = \pm \pi R/2n \end{aligned}\right\} \tag{27}$$

exactly, which are the same as those used in reference 9. Also, in Eq. (26) and thereafter, $r = \lambda_y/\lambda_x$.

(b) *Solution of Free Nonlinear Vibrations*

We assume that

$$w = AH(t) \sin (\pi x/L) \cos (ny/R) \tag{28}$$

in accordance with our assumption that for slight nonlinearities the effect of large amplitudes lies primarily in the frequency of vibrations. From the second equation of (23), we then find

$$\left.\begin{aligned} F = EAH\Bigg\{ &-\frac{1}{R}\left(\frac{\pi}{L}\right)^2\left[\left(\frac{\pi}{L}\right)^2 + \left(\frac{n}{R}\right)^2\right]^{-2} \times \\ &\sin\frac{\pi x}{L}\cos\frac{ny}{R} + \frac{AH}{32} \times \\ &\left[\left(\frac{n}{R}\right)^2\left(\frac{\pi}{L}\right)^{-2}\cos\frac{2\pi x}{L} - \left(\frac{\pi}{L}\right)^2\left(\frac{n}{R}\right)^{-2}\cos\frac{2ny}{R}\right]\Bigg\} \end{aligned}\right. \tag{29}$$

Solution (28) satisfies boundary conditions (27) exactly while solution (29) does not, although they both satisfy boundary conditions (27) in the limit of vanishing amplitudes—i.e., when they tend to the linear vibrations. However, solution (29) does satisfy the boundary conditions (27) "in the mean"—i.e., when it is integrated over the entire wavelength of the boundary. In other words, solutions (28) and (29) apply to only that portion of the cylinder not near the cylinder ends. In passing, it may be noted that it is possible to impose displacement boundary conditions on u and v in the rectangular plate, while this is not the case for a lobe in a complete cylinder. Hence, the boundary conditions of reference 8 are not used here.

If solutions (28) and (29) are substituted into the first equation of (23), permitting the collection of the first harmonic terms, the following is obtained:

$$\ddot{H} + \omega^2 H + (\pi/2)^4 (E/\rho)(A/\lambda_y)^2 \times (1/\lambda_y)^2 (1+r^4) H^3 = 0 \tag{30}$$

where ω is the linear frequency as defined by Eq. (26).

If we write T^* as the nonlinear period of vibrations, T as the linear period of vibrations, and ω^* the nonlinear frequency of vibrations, then, from Eq. (30), we find that

$$T^*/T = [2K(k)/\pi](\omega/\omega^*) \tag{31}$$

where $K(k)$ is the complete elliptic integral of the first kind; and

$$\left.\begin{aligned} k &= \sqrt{\frac{1}{2}\left[1 + \frac{\omega^2}{(\pi/2)^4 (E/\rho)(A/\lambda_y)^2 (1/\lambda_y)^2 (1+r^4)}\right]^{-1/2}} \\ \text{while} \\ \frac{\omega}{\omega^*} &= \left[1 + \frac{\left(\frac{\pi}{2}\right)^4\left(\frac{A}{\lambda_y}\right)^2 (1+r^4)}{\frac{n^2\pi^2}{12(1-\nu^2)}\left(\frac{h}{R}\right)^2 (1+r^2)^2 + \left(\frac{\lambda_y}{R}\right)^2 r^4 (1+r^2)^{-2}}\right]^{-1/2} \end{aligned}\right\} \tag{32}$$

(5) Numerical Examples and Discussions

Numerical examples are given for $R/h = 100$ and $\nu = 0.318$, which are typical for a thin shell made of an aluminum alloy. In Fig. 2, n is equal to 8 (of special interest in flutter analyses[11]) while in Fig. 3, n is equal to 10 (for comparison). Results from reference 8 are reproduced in both Figs. 2 and 3 to show that the reduction in period of vibrations is much less for a cylinder than for a flat plate. Physically, this is due to the fact that the nonlinearities are introduced through the in-plane forces such as N_x and N_y. In linear vibrations, these in-plane forces are zero for flat plates, while this is not the case for cylinders where N_y is not equal to zero. The effect of N_y can be seen through the last term of (26), which vanishes for flat plates. For $n = 8$, this term varies from 7.5 percent of the total [of Eq. (26)] for $r = 4$, to 60 percent of the total for $r = 1$. Therefore, the additional in-plane forces arising from the nonlinear terms should exert less influence for cylinders. This influence reaches a minimum at $r = 1$.

Another interesting feature is that the results are symmetric with respect to r—that is, Eq. (31) has the same value when r is replaced by $1/r$. This is not as obvious for a cylinder as it is for a flat plate. Consequently, in Figs. 2 and 3, curves for $r < 1$ do not appear explicitly and curve $r = 1$ is highest.

In direct consequence of this last observation, if finite amplitudes are to be considered, the square wave pattern then becomes the most likely mode under the assumptions used in this paper. This would facilitate the study of nonlinear panel excitation problems,[10,16] since a mode shape is often assumed to reduce problems of this nature into a forced nonlinear system of but one or two degrees of freedom. Naturally, the most appropriate modes are those which have the least strain energies.[15] In the case of a cylinder, the square wave pattern has least strain energy under the assumptions used in this paper.

References

[1] Kármán, Th. v., *Festigkeitsprobleme im Maschinenbau*, Encyklopädie der Mathematischen Wissenschaften, Vol. IV, No. 4, pp. 311–385, 1910.

[2] Kármán, Th. v., and Tsien, H. S., *The Buckling of Thin Cylindrical Shells under Axicl Compression*, Journal of the Aeronautical Sciences, Vol. 8, No. 8, pp. 303–312, June 1941.

[3] Donnell, L. H., *A New Theory for the Buckling of Thin Cylinders Under Axial Compression and Bending*, Trans. ASME, Vol. 56, p. 795, 1934.

[4] Biot, M. A., *Theory of Elasticity with Large Displacements and Rotations*, Proc. 5th International Congress of Applied Mechanics, pp. 117–122, 1938.

[5] Novozhilov, V. V., *Foundations of the Nonlinear Theory of Elasticity*, Graylock Press, Rochester, N. Y., 1953.

[6] Carrier, G. F., *On the Nonlinear Vibration Problem of the Elastic String*, Quart. Appl. Math., Vol. 3, p. 157, 1945.

[7] Eringen, A. C., *On the Nonlinear Vibration of Elastic Bars*, Quart. Appl. Math., Vol. 10, pp. 361–369, 1952.

[8] Chu, Hu-Nan, and Herrmann, G., *Influence of Large Amplitudes on Free Flexural Vibrations of Rectangular Elastic Plates*, J. Appl. Mech., Trans. ASME, Vol. 78, pp. A532–A540, December 1956.

[9] Reissner, E., *Nonlinear Effects in Vibrations of Cylindrical Shells*, Ramo-Wooldridge Corporation Report AM5-6, September 1955.

[10] Kirchman, E. J., and Greenspon, J. E., *Nonlinear Response of Aircraft Panels to Acoustic Noise*, J. Acoustical Society of America, Vol. 29, No. 7, pp. 854–857, July 1957 W. R. Strong, unpublished report, The Glenn L. Martin Company, August 1957.

[11] Marguerre, K., *Zur Theorie der Gekrümmten Platte Grosser Formänderung*, Proc. 5th International Congress of Applied Mechanics, pp. 93–101, 1938.

[12] Gazis, D. C. *Three-Dimensional Investigation of the Propagation of Waves in Hollow Circular Cylinders*, J. Acoustical Society of America, Vol. 31, pp. 568–578, 1959.

[13] Herrmann, G., *Influence of Large Amplitudes on Flexural Motions of Elastic Plates*, NACA TN 3578, May 1956.

[14] Biot, M. A., *Nonlinear Theory of Elasticity and the Linearized Case for a Body Under Initial Stress*, Edinburgh Phil. Mag. and Sci., Ser. 7, Vol. 27, No. 183, pp. 468–489, April 1939.

[15] Holt, M., and Strack, S. L., *Supersonic Panel Flutter of a Cylindrical Shell of Finite Length*, Journal of Aerospace Sciences, Vol. 28, No. 3, pp. 197–208, March 1961. In this paper, a result from *The Flexural Vibrations of Thin Cylinders*, by Arnold and Warburton, published in the Proceedings of the Institution of Mechanical Engineers, Vol. 167 (1953), was quoted. This quoted result actually indicates an n between 7 and 8. Since n must be an integer and since our paper is concerned with slight nonlinearities, n is chosen to be 8.

[16] Lassiter, L. W., and Hess, R. W., *Calculated and Measured Stresses in Simple Panels Subject to Intense Random Acoustic Loading Including the Near Noise Field of a Turbojet Engine*, NACA Rept. 1367, 1958.

✦ ✦ ✦

Pinned Rotating Blade Linear Vibration

(*Continued from page 601*)

Thus, to find the natural frequencies, a set of trial values of frequency are chosen and, for each of these, the integrations are performed as indicated above and the determinant of (C.6) evaluated. The zeros of this determinant define the natural frequencies. Having found a natural frequency, the corresponding values of the weighting functions, relative to one of the set, may be found from any three of (C.5). Using these, the corresponding mode shapes can be determined by substitution into the first two of (C.4).

The Stagnation-Point Boundary Layer in the Presence of an Applied Magnetic Field†

WILLIAM B. BUSH*

Space Technology Laboratories, Inc.

THE PURPOSE OF THIS NOTE is to expand upon the results of Meyer[1] and Lykoudis[2] concerning the effect upon the stagnation-point heat transfer produced by the interaction of a magnetic field with an electrically conducting fluid in a boundary layer. In the following analysis, the restriction of the solution to small values of the magnetic parameter[1] and constant electrical conductivity across the boundary layer[2] that limited the previous two analyses is no longer applicable.

As has been previously shown by the author,[3] the boundary-layer equations when a normal magnetic field (but no electric field) is applied are:

$$\partial(\rho u r_0^i)/\partial x + \partial(\rho v r_0^i)/\partial y = 0 \tag{1}$$

$$u\frac{\partial u}{\partial x} + v\frac{\partial u}{\partial y} = \left(\frac{\rho_e}{\rho}\right)u_e\frac{du_e}{dx}\left[1 + Q_v \times \left(1 - \frac{\sigma u}{\sigma_e u_e}\right)\right] + \frac{1}{\rho}\frac{\partial}{\partial y}\left(\mu\frac{\partial u}{\partial y}\right) \tag{2}$$

$$u\frac{\partial H}{\partial x} + v\frac{\partial H}{\partial y} = \frac{1}{\rho}\frac{\partial}{\partial y}\left(\frac{\mu}{Pr}\frac{\partial H}{\partial y}\right) + \frac{1}{\rho}\frac{\partial}{\partial y}\left[\mu\left(\frac{Pr - 1}{Pr}\right)u\frac{\partial u}{\partial y}\right] \tag{3}$$

where H is the total enthalpy, σ is the electrical conductivity, Q_v is the magnetic parameter defined by

$$Q_v = \sigma_e B_0^2(\rho_e\, du_e/dx)^{-1} \tag{4}$$

and where the subscript e denotes quantities evaluated at the outer edge of the boundary layer.

If new independent variables, X and Y, given by

$$X = \int_0^x \left(\frac{r_0}{L}\right)^{2i}\frac{\rho_e\mu_e}{\rho_0\mu_0}\,dx; \qquad Y = \int_0^y \left(\frac{r_0}{L}\right)^{i}\left(\frac{\rho}{\rho_0}\right)dy \tag{5}$$

are introduced and the velocity at the outer edge of the boundary layer has the form

$$u_e = C(X/L)^m \tag{6}$$

as can be shown to be the case for stagnation-point flow, and if the stream function and the total enthalpy are of the form

$$\psi = \sqrt{2\mu_0 u_e X/\rho_0(m + 1)}\, f(\eta) \tag{7}$$

$$H = H_e g(\eta) \tag{8}$$

where

$$\eta = Y\sqrt{(m + 1)\rho_0 u_e/2\mu_0 X}$$

then the equations of motion reduce to:

$$(Nf_{\eta\eta})_\eta + ff_{\eta\eta} + \left(\frac{2m}{m + 1}\right)\times \left\{\left(\frac{\rho_e}{\rho}\right)\left[1 + Q_v\left(1 - \frac{\sigma}{\sigma_e}f_\eta\right)\right] - (f_\eta)^2\right\} = 0 \tag{9}$$

$$\left(\frac{N}{Pr}g_\eta\right)_\eta + fg_\eta = \frac{u_e^2}{2H_e}\left[\frac{2N}{Pr}(1 - Pr)f_\eta f_{\eta\eta}\right]_\eta \tag{10}$$

where

$$N = (\rho\mu/\rho_e\mu_e)$$

For isoenergetic flow outside the boundary layer, Eqs. (9) and (10) reduce to ordinary differential equations with η the independent variable if (a) N, (ρ_e/ρ), and (σ/σ_e) are either constants or functions of η; (b) Pr is either (*i*) one or (*ii*) a constant or a function of η when $(u_e^2/2H_e)$ approaches zero or one; (c) Q_v and the enthalpy at the wall are constants. Conditions (a) and (b) in this analysis are satisfied by having

$$\left.\begin{aligned} N &= Pr = 1 \\ \rho_e/\rho &= g(\eta) \\ \sigma/\sigma_e &= g^n(\eta) \end{aligned}\right\} \tag{11}$$

These representations for the density and conductivity ratios are permissible in the stagnation region if the properties of the gas are such that these ratios can be approximated by

$$\rho_e/\rho = h/h_e; \qquad \sigma/\sigma_e = (h/h_e)^n \tag{12}$$

since in this region, $(u_e^2/2H_e) \to 0$ and $(h/h_e) \to (H/H_e)$. Requiring Q_v to be constant means that the component of the field normal to the wall, B_0, must have the following behavior:

$$B_0 = \pm\sqrt{(\rho_e/\sigma_e)(mu_e/X)(r_0/L)^{2i}(\rho_e\mu_e/\rho_0\mu_0)Q_v} \tag{13}$$

(which reduces to give a constant in the stagnation-point region).

The equations

Received April 14, 1960.

† Prepared for the Air Force Ballistic Missile Division, Headquarters Air Research and Development Command, under Contract AF 04(647)-309, Magnetoaerodynamic Research.

* Formerly, Physical Research Laboratory, Space Technology Labs.; now, Graduate Student, California Institute of Technology.

TABLE 1.
Shear and heat-transfer functions. $\beta = 0.5$; $g_w = 0$.

Q_v	n = 0		n = 3	
	f''_w	g'_w	f''_w	g'_w
0	0.5810	0.4945	0.5810	0.4945
1	0.6651	0.5109	0.7609	0.5329
10	1.083	0.5722	1.809	0.6815
100	2.280	0.6613	6.565	0.9827

$$g'' + fg' = 0 \tag{14}$$

$$f''' + ff'' + [2m/(m+1)] \times \{g[1 + Q_v(1 - g^n f')] - (f')^2\} = 0 \tag{15}$$

with the boundary conditions

$$\left.\begin{aligned} f(0) &= f'(0) = 0 \\ g(0) &= g_w \\ f'(\infty) &= 1 \\ g(\infty) &= 1 \end{aligned}\right\} \tag{16}$$

were solved by means of a finite-difference (or line-relaxation) technique,[4] since the method of forward integration failed owing to the serious lack of information available as to what values to assume for the derivatives at the initial boundary. The possibility of a solution using a transformation to the velocity plane was also ruled out when an asymptotic expansion revealed that under certain of the conditions investigated —i.e., $nQ_v > 1$; $g_w < 1$—the phenomenon of velocity "overshoot" occurs. In Tables 1 and 2, f_w'' and g_w' are given for $\beta = [2m/(m+1)] = 0.5$, the value of the parameter for an axisymmetric stagnation point with or without a magnetic field applied; $g_w = 0$ and 0.05 —i.e., a cold wall—and the parameters Q_v and n varying over the ranges 0 to 100 and 0 to 10, respectively.

The heat transfer at the stagnation point in terms of the quantities introduced in this analysis is:

$$(\dot{q}_w)_{sp} = \left(k\frac{\partial T}{\partial y}\right)_{w,\,sp} = (2\rho_e\mu_e)_{sp}^{1/2} H_e \left(\frac{du_e}{dx}\right)_{sp}^{1/2} g'_{w,\,sp} \tag{17}$$

Since the quantities ρ_e, μ_e, and H_e are constant at the stagnation point, the ratio of the heat transfer here with a magnetic field applied to heat transfer without the field applied is

$$\frac{(\dot{q}_w)}{(\dot{q}_w)_{NM}} = \left[\frac{(du_e/dx)_{sp}}{(du_e/dx)_{sp,NM}}\right]^{1/2} \left(\frac{g'_w}{g'_{w,\,NM}}\right)_{\beta=1/2} \tag{18}$$

for the same conditions upstream of the bow shock and the same total enthalpy at the wall. The first component of the right-hand side of the above equation represents the contribution to the heat transfer at the stagnation point due to the modification of the inviscid flow external to the boundary layer. The second component represents the contribution due to the alteration of the total enthalpy profile in the boundary layer.

The data of reference 5 for the inviscid contribution were combined with the boundary-layer solutions obtained to get numerical values for Eq. (18). Fig. 1

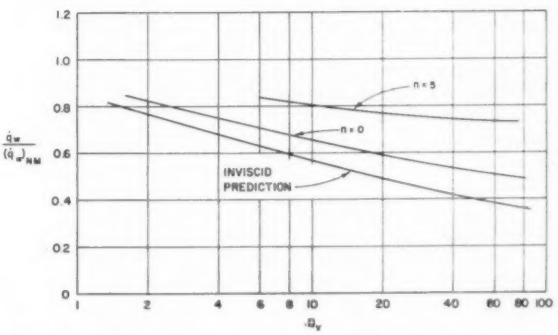

FIG. 1. Heat-transfer ratio versus the magnetic parameter at the stagnation point of an axisymmetric blunt body.

shows $[(\dot{q}_w)/(\dot{q}_w)_{NM}]$ versus Q_v for $g_w = 0.05$. Three curves are shown on the graph. The bottom curve indicates the results predicted assuming that the magnetic field produces no alteration in the boundary-layer profile. The middle curve shows the results when the electrical conductivity is constant across the boundary layer. The top curve shows the ratio when the conductivity in the boundary layer is approximated by $(\sigma/\sigma_e) = g^5$.

From Fig. 1, it can be concluded that the inviscid prediction for the decrease in heat transfer produced by MHD means is a little optimistic. However, if, in the boundary layer, $(\sigma/\sigma_e) \approx 1$, it is clear that substantial reductions in the heat transfer may be obtained. For $n = 5$, the increase due to the alteration in the total-enthalpy profile just about cancels out the decrease due to the MHD reduction of the velocity gradient at the outer edge of the boundary layer.

TABLE 2.
Shear and heat-transfer functions. $\beta = 0.5$; $g_w = 0.05$.

Q_v	n = 0		n = 5		n = 10	
	f''_w	g'_w	f''_w	g'_w	f''_w	g'_w
0	0.5985	0.4723	0.5985	0.4723	0.5985	0.4723
1	0.6909	0.4884	--	--	--	--
5	0.9442	0.5247	1.4576	0.6098	1.5771	0.6304
10	1.1557	0.5485	2.0820	0.6773	2.3045	0.7083
20	1.4501	0.5749	3.0879	0.7613	3.4989	0.8062
50	1.9922	0.6104	5.3699	0.8975	6.2813	0.9682
100	2.5390	0.6356	8.2598	1.0204	9.9036	1.1178

References

[1] Meyer, R. C., *On Reducing Aerodynamic Heat-Transfer Rates by Magnetohydrodynamic Techniques*, Journal of the Aero/Space Sciences, Vol. 25, No. 9, pp. 561–566, 572, September 1958.

(*Continued on page 630*)

Some Effects of Tensor Conductivity in Magnetohydrodynamics†

B. SONNERUP*
Cornell University

Summary

A theoretical investigation concerning some Hall-current effects in inviscid, incompressible magnetohydrodynamics is made. The generalized Ohm's law and the concept of tensor conductivity are discussed. The macroscopic equations governing steady small-perturbation flow of a fully ionized gas are developed for three orientations of an applied magnetic field of infinite extent. These equations are then solved for flow past an insulating sinusoidal wall. The general solutions, pertaining to arbitrary values of magnetic Reynolds number and Hall parameter, are studied in the limits of large and small magnetic Reynolds number, and characteristic Hall-current loops are detected. The pressure distribution on the wavy wall is investigated as a function of magnetic Reynolds number and Hall parameter. For the particular cases investigated here the influence of nonscalar conductivity is found to be much smaller than elementary considerations would indicate.

For completeness, a brief study of transverse hydromagnetic waves is included. The classical plane Alfvén wave is modified to have a slowly rotating plane of polarization in some analogy with the behavior of a plane-polarized light beam in an optically active medium. The modified Alfvén wave is used to explain certain features of the wavy-wall solution for large magnetic Reynolds number and an applied magnetic field perpendicular to the plane of the wall.

Symbols

A = Alfvén speed = $\sqrt{\mu H^2/4\pi\rho}$
A_α, A_β = phase speeds of fast and slow waves, respectively
$\bar{A}$ = phase speed of resultant wave
A_p = complex pressure-influence coefficient
C_a, C_d . . . C_g = complex coefficients
c, c_α, c_β = exponents
$\mathbf{E}$ = electric-field vector
$-e$ = charge of electron
$\mathbf{H}$ = magnetic-field vector
$\mathbf{h}$ = magnetic-field perturbation vector
$\mathbf{j}$ = current-density vector
k_1 = $4\pi\sigma\mu U_0(1 - m^{-2})$
k_2 = $4\pi\sigma\mu U_0$
k, $\bar{k}$, k_α, k_β = wave numbers defined by Eqs. (48) and (50)
$\bar{k}$ — defined by Eq. (50)
$\bar{L}$ = wave length of resultant wave = $(2\pi/\omega_t)\bar{A}$
$\bar{L}_t$ = distance for a full turn of the plane of polarization of the resultant wave
m = Alfvén number = U_0/A_0
m_e, m_i = mass of electron and ion, respectively
n = number of electrons (orions) per unit volume
p = pressure
$\mathbf{q}$ = fluid-velocity vector
R_m = magnetic Reynolds number based on wave length of a wavy wall = $4\pi\sigma\mu U_0\lambda^{-1}$
t = time
U_0 = unperturbed fluid velocity
$\mathbf{u}$ = fluid-velocity perturbation vector
x, y, z = Cartesian coordinates
γ = $\sqrt{1 + \omega_0^2\tau^2}$
ϵ = amplitude of wavy wall
φ_1, φ_2 = harmonic functions defined by Eqs. (23) and (27)
ξ = $\nabla \times \mathbf{H} = \mathbf{j}/4\pi$
λ = $2\pi \times$ (wave length of wavy wall)$^{-1}$
μ = magnetic permeability of free space ($\mu = 1$ in emu)
$\mathbf{\Omega}$ = vorticity vector = $\nabla \times \mathbf{q}$
ω = cyclotron frequency of electrons
ω_i = cyclotron frequency of ions
ω_t = frequency of transverse hydromagnetic wave
ρ = density of fluid
ρ_e = charge density
σ = scalar electric conductivity
τ = collision time of an electron in collisions with ions

Subscripts

x, y, z = components of a vector quantity
0 = unperturbed quantity or referred to unperturbed quantities
1 = parallel fields
2 = crossed fields
e = electron
w = wall

Introduction

In the search for engineering applications of magnetohydrodynamics, considerable effort has been spent obtaining solutions to the combined equations of electro- and aerodynamics for various simple flow cases. These investigations invariably involve a number of simplifying assumptions, and in particular the so-called Hall currents, arising from charged-particle drift across the electric field due to the presence of a magnetic field, are seldom taken into account. At least in some respects the Hall effect can be said to render the electrical conductivity a tensor, and the phenomena involved may be important in many problems concerning flow of a rarefied, ionized gas in the presence of a magnetic field. It is the purpose of the present paper to shed some light on the effects of tensor conductivity in magnetohydrodynamics by reexamination of a few simple flow cases for which scalar-conductivity solutions are already known.

Received April 11, 1960.

† This paper is based on the author's M. Aero. Engr. Thesis,[7] Cornell University, 1960. The author wishes to express his appreciation to Professor W. R. Sears, Director of the Graduate School of Aeronautical Engineering, Cornell University, for supervision and encouragement during the course of this research.

* Avco Mfg. Corp. Fellow in Aeronautical Engineering (a fellowship provided by the Cornell Aeronautical Laboratory, Inc.).

Ohm's Law and Tensor Conductivity

One of the equations needed for the complete description of a magnetohydrodynamic flow is Ohm's law, which relates the current density to the local electric field and the electrical conductivity of the flowing medium. In the absence of a magnetic field the current-density vector $\mathbf{j}$ may be considered proportional to the electric-field vector $\mathbf{E}$, the constant of proportionality being the scalar conductivity σ. If a magnetic field is present conditions are more complicated, as may be realized by considering the motion of a single charged particle in a magnetic field $\mathbf{H}$ where an electric field $\mathbf{E}$ is applied perpendicular to $\mathbf{H}$. Under the influence of the Lorentz force the particle is known to perform a circular motion of frequency ω around the magnetic lines of force with the center of this motion drifting in a direction perpendicular to both $\mathbf{E}$ and $\mathbf{H}$. The frequency ω, called the cyclotron frequency of the particle, is given by

$$\omega = e\mu H/m_e \tag{1}$$

μ being the magnetic permeability (in free space $\mu = 1$ in emu, the units to be used in this paper), e and m_e the particle charge and mass, respectively. This is the so-called Hall effect for a single particle. The macroscopic current density $\mathbf{j}$ set up by particles moving in this fashion will therefore be perpendicular to both $\mathbf{E}$ and $\mathbf{H}$. This current is called a *Hall current*. If, on the other hand, $\mathbf{E}$ and $\mathbf{H}$ are parallel, a single charged particle is found to describe a helical path with the axis of the helix along $\mathbf{E}$ and $\mathbf{H}$, and the current-density vector in this case is parallel to $\mathbf{E}$ and $\mathbf{H}$. From these facts it becomes clear that the magnetic field causes nonisotropic current propagation in an ionized gas composed of ions, electrons, and neutral atoms. Unless the gas is extremely rarefied (or cold), however, the current-carrying particles cannot be considered as noninteracting; they collide with each other and, what is more important, with other kinds of particles. A crude theory for this situation has been given by Cowling[1] and Spitzer.[2] In a fully ionized gas consisting of n electrons of charge $-e$ and mass m_e and n ions of charge $+e$ and mass m_i, the currents are carried entirely by electrons, and assuming that these lose their average momentum in each collision with ions, one obtains the following approximate equation of motion for the electron gas relative to the ion gas:

$$\left.\begin{aligned}\sigma[\mathbf{E} + \mu\mathbf{q} \times \mathbf{H} + (1/ne)\nabla p_e] = \\ \mathbf{j} + \tau(\partial\mathbf{j}/\partial t) + (\omega\tau/H)\mathbf{j} \times \mathbf{H}\end{aligned}\right\} \tag{2}$$
$$\sigma = ne^2\tau/m_e$$

Here $\mathbf{q}$ is the velocity of the mass of the gas, p_e the partial pressure of the electron gas, τ the collision time for an electron in collisions with ions, and ω the electron cyclotron frequency defined by Eq. (1). For stationary currents the term $\tau\partial\mathbf{j}/\partial t$ drops out, and it is of interest to identify the remaining terms one by one: The term $(\mathbf{E} + \mu\mathbf{q}\times\mathbf{H})$ is the electric field experienced by an observer riding with the velocity $\mathbf{q}$ of the gas. The electron-pressure term $(1/ne)\nabla p_e$ takes into account the influence of the pressure distribution in the gas on the conduction of currents, and may be thought of as an additional electrostatic field. Finally, the Hall-current term $(\omega\tau/H)\mathbf{j}\times\mathbf{H}$ takes into account the Hall effect discussed previously. The factor $\omega\tau$ is the ratio of electron cyclotron frequency to electron collision frequency. For dense gases and weak magnetic fields this factor is small—i.e., many collisions take place during the time needed for completion of a full turn of an electron around a magnetic line of force. The entire Hall effect is then negligible, and Eq. (2) essentially reduces to the ordinary Ohm's law describing isotropic current propagation with scalar conductivity σ. Hereafter, Eq. (2) will be called the generalized Ohm's law. For a rarefied gas and/or strong magnetic fields the factor $\omega\tau$ may be large—i.e., the electrons can spiral freely between collisions—and in such a case the Hall effect is predominant and may cause strong anisotropy in the electrical conductivity.

To elucidate this further, it is instructive to solve Eq. (2) for the current components j_x, j_y, and j_z along the axis of a right-hand Cartesian coordinate system (x, y, z). If the square bracket of Eq. (2) is denoted by $\mathbf{E}''$ the solution is

$$\mathbf{j} = \sigma\mathbf{P}\mathbf{E}'' \tag{3}$$

where $\mathbf{P}$ can be written as a matrix and exhibits tensor properties under orthogonal transformations. This explains the term "tensor conductivity." In a coordinate system with x-axis parallel to the magnetic field, the matrix representation for $\mathbf{P}$ simplifies to

$$\mathbf{P} = \frac{1}{1 + \omega^2\tau^2}\begin{pmatrix} 1 + \omega^2\tau^2 & 0 & 0 \\ 0 & 1 & -\omega\tau \\ 0 & \omega\tau & 1 \end{pmatrix} \tag{4}$$

From Eq. (4) it is easy to see that if the net electric field $\mathbf{E}''$ is along the x-axis, the current density is also in this direction and has magnitude $\sigma E''$. This means that the conductivity in this direction is σ, the ordinary scalar value. Transverse to the magnetic field the situation is entirely different, however. If $\mathbf{E}''$ is in the z-direction, Eqs. (3) and (4) give

$$\mathbf{j} = \frac{\sigma E''}{1 + \omega^2\tau^2}\begin{pmatrix} 0 \\ -\omega\tau \\ 1 \end{pmatrix} \tag{5}$$

The conductivity in the z-direction is thus reduced by a factor $(1 + \omega^2\tau^2)$ and a Hall current flows in the y-direction. In the mathematical treatment of tensor-conductivity problems, it is mostly more convenient to use the generalized Ohm's law in vector form, Eq. (2) instead of Eq. (3). We will, however, have occasion to come back to Eqs. (3), (4), and (5) in discussing the results of the subsequent investigation.

Eq. (2) was derived using rather crude physical assumptions. A more refined study[8, 9, 10] may lead to different numerical factors, or additional nonlinear terms, but Eq. 2 is nevertheless believed to give a qualitatively correct description of some essential features

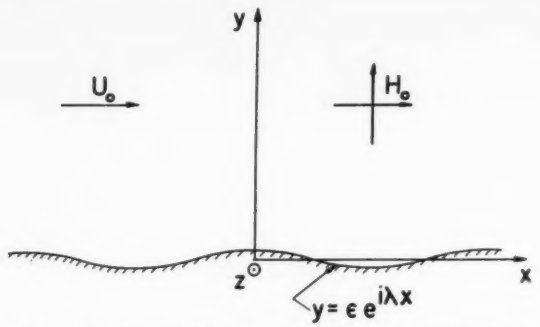

FIG. 1. Notation used in cases of flow past slender two-dimensional bodies—e.g., wavy walls.

of the Hall effect in a fully ionized gas. For a partly ionized gas the motion of the ions relative to the neutral atoms and collisions of electrons and ions with neutral atoms must also be taken into account. In order to avoid the mathematical complications arising from these additional phenomena,[1, 3] our interest will be confined here to fully ionized gases; furthermore, for the sake of simplicity, the flow will be considered inviscid and incompressible. It should also be mentioned that although Eq. (2) was derived for a neutral plasma it can be used without modification if moderate deviations from electrical neutrality occur.[2]

Development of the Equations

Upon neglect of convective currents and the vacuum displacement current, Maxwell's equations for a moving, nonpolarized medium become

$$\nabla \cdot \mathbf{E} = 4\pi c^2 \rho_e \tag{6}$$

$$\nabla \cdot \mathbf{H} = 0 \tag{7}$$

$$\nabla \times \mathbf{E} = -\mu \partial \mathbf{H}/\partial t \tag{8}$$

$$\nabla \times \mathbf{H} = 4\pi \mathbf{j} \tag{9}$$

where c is the speed of light. The medium is further assumed to have the same permeability as empty space—i.e., $\mu = 1$ in emu. Despite this, μ will be retained in the equations in order to facilitate transformation to other units.

The momentum equation for inviscid flow, upon neglect of gravity and the electric force $\rho_e \mathbf{E}$, can be written:

$$(D\mathbf{q}/Dt) + (1/\rho)\nabla p = (\mu/\rho)\mathbf{j} \times \mathbf{H} \tag{10}$$

where D/Dt denotes the convective derivative

$$D/Dt = \partial/\partial t + \mathbf{q} \cdot \nabla$$

Finally, the continuity equation for an incompressible flow can be written:

$$\nabla \cdot \mathbf{q} = 0 \tag{11}$$

The foregoing Eqs. (6) thru (11), plus the generalized Ohm's law, discussed in the previous section [Eq. (2)], will now be simplified and developed to a more convenient form. The first step will be to apply the curl operator to the generalized Ohm's law. Using Maxwell's equations and some elementary vector identities one then obtains:

$$-\frac{\partial \mathbf{H}}{\partial t} + \mathbf{H} \cdot \nabla \mathbf{q} - \mathbf{q} \cdot \nabla \mathbf{H} = -\frac{1}{4\pi\sigma\mu} \nabla^2 \mathbf{H} - \frac{\tau}{4\pi\sigma\mu} \nabla^2 \frac{\partial \mathbf{H}}{\partial t} + \frac{\omega\tau}{4\pi\sigma\mu H} [\mathbf{H} \cdot \nabla(\nabla \times \mathbf{H}) - (\nabla \times \mathbf{H}) \cdot \nabla \mathbf{H}] \tag{12}$$

With the vector identity $(\nabla \times \mathbf{a}) \times \mathbf{a} = \mathbf{a} \cdot \nabla \mathbf{a} - (1/2)\nabla a^2$, where $\mathbf{a}$ is an arbitrary vector function, the momentum equation (10) can be written in two alternative forms:

$$\frac{\partial \mathbf{q}}{\partial t} + \mathbf{q} \cdot \nabla \mathbf{q} - \frac{\mu}{4\pi\rho} \mathbf{H} \cdot \nabla \mathbf{H} = -\nabla \left(\frac{p}{\rho} + \frac{\mu H^2}{8\pi\rho} \right) \tag{13}$$

$$\frac{\partial \mathbf{q}}{\partial t} - \mathbf{q} \times \boldsymbol{\Omega} + \frac{\mu}{4\pi\rho} \mathbf{H} \times \boldsymbol{\xi} = -\nabla \left(\frac{p}{\rho} + \frac{q^2}{2} \right) \tag{14}$$

where the notation $\nabla \times \mathbf{q} \equiv \boldsymbol{\Omega}$ and $\nabla \times \mathbf{H} \equiv \boldsymbol{\xi}$ has been introduced.

The modified expressions for Ohm's law and the momentum equation will now be linearized by introduction of small perturbations in the two vector quantities $\mathbf{H}$ and $\mathbf{q}$, so that

$$\mathbf{H} = \mathbf{H}_0 + \mathbf{h} \qquad \mathbf{q} = \mathbf{U}_0 + \mathbf{u} \tag{15}$$

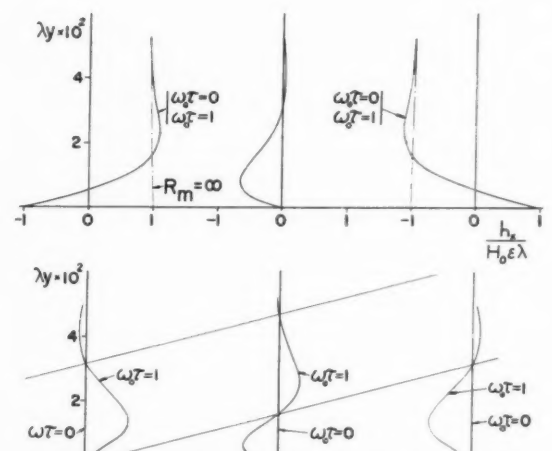

FIG. 2. Wavy wall ($y = \epsilon \cos \lambda x$) in parallel fields and for large magnetic Reynolds number R_m. Magnetic-field perturbation components h_x and h_z [Eqs. (41)], for $k_1/\lambda = R_m(1 - m^{-2}) = 2 \times 10^4$. Current lines for $k_1/\lambda = 2 \times 10^4$, $\omega_0\tau = 1$.

where $|h| \ll |H_0|$ and $|u| \ll |U_0|$.

$\mathbf{H}_0$ and $\mathbf{U}_0$ are now assumed to be constant in space and time. Neglecting higher-order terms, one then obtains the following linearized versions of Ohm's law and the momentum equation for time-independent flow problems:

$$\mathbf{H}_0\cdot\nabla\mathbf{u} - \mathbf{U}_0\cdot\nabla\mathbf{h} = -(1/4\pi\sigma\mu)\nabla^2\mathbf{h} + (\omega_0\tau/4\pi\sigma\mu H_0)\mathbf{H}_0\cdot\nabla(\nabla\times\mathbf{h}) \tag{16}$$

$$\mathbf{U}_0\cdot\nabla\mathbf{u} - \frac{\mu}{4\pi\rho}\mathbf{H}_0\cdot\nabla\mathbf{h} = -\nabla\left(\frac{p}{\rho} + \frac{\mu}{4\pi\rho}\mathbf{H}_0\cdot\mathbf{h}\right) \tag{17}$$

$$\mathbf{U}_0\times\boldsymbol{\Omega} - \frac{\mu}{4\pi\rho}\mathbf{H}_0\times\boldsymbol{\xi} = \nabla\left(\frac{p}{\rho} + \mathbf{U}_0\cdot\mathbf{u}\right) \tag{18}$$

where

$$\omega_0 = \mu e H_0/m_e \tag{19}$$

A useful relation between $\boldsymbol{\xi}$ and $\boldsymbol{\Omega}$ is obtained by applying the curl operator to Eq. (17):

$$\mathbf{U}_0\cdot\nabla\boldsymbol{\Omega} = (\mu/4\pi\rho)\mathbf{H}_0\cdot\nabla\boldsymbol{\xi} \tag{20}$$

The problem has now been reduced to the simultaneous solution of the two vector equations (16) and (20) for a given set of boundary conditions and appropriate auxiliary conditions—e.g., $\nabla\cdot\mathbf{h} = 0$, $\nabla\cdot\mathbf{u} = 0$. One may now adopt a Cartesian coordinate system with x-axis parallel to the $\mathbf{U}_0$ vector and proceed to the study of flow past slender two-dimensional obstacles under conditions such that

$$\partial/\partial z = (\partial/\partial z)_{\text{boundary}} = 0$$

(See, for example, Fig. 1.) This kind of magnetohydrodynamic flow has been considered in references 4 and 5 for scalar conductivity and various orientations of the magnetic-field vector $\mathbf{H}_0$ in the xy-plane. It was also assumed there that $h_z = 0$, $u_z = 0$, an assumption which will clearly not be valid in the tensor-conductivity case where in general currents will flow not only in the z-direction but also in the xy-plane, thus inducing a magnetic-field component h_z and forces in the z-direction.

The following orientations of the unperturbed magnetic-field vector $\mathbf{H}_0$ will now be considered:

$\mathbf{H}_0 = (H_0, 0, 0)$ parallel fields
$\mathbf{H}_0 = (0, H_0, 0)$ crossed fields
$\mathbf{H}_0 = (0, 0, H_0)$ crossed fields, case II

In the case of parallel fields Eq. (20) gives

$$U_0\,\partial\boldsymbol{\Omega}/\partial x = (\mu H_0/4\pi\rho)(\partial\boldsymbol{\xi}/\partial x) \tag{21}$$

which can be integrated to give

$$\boldsymbol{\Omega} = (\mu H_0/4\pi\rho U_0)\boldsymbol{\xi} + \mathbf{f}(y) \tag{22}$$

The arbitrary function $\mathbf{f}(y)$ may be put equal to zero, a choice corresponding, for example, to the existence of an unperturbed flow region far upstream. Eq. (22) can then be integrated once more to give

$$\mathbf{u} = (\mu H_0/4\pi\rho U_0)\mathbf{h} + U_0\nabla\varphi_1 \tag{23}$$

and, since both $\mathbf{u}$ and $\mathbf{h}$ are divergence-free, one finds $\nabla^2\varphi_1 = 0$. If Eqs. (22) and (23) are introduced into the momentum Eq. (17) or Eq. (18), these can be integrated to give the following pressure formula for parallel fields:

$$p - p_0 = -\rho U_0 u_x = -\rho U_0^2(m^{-2}h_x/H_0 + \partial\varphi_1/\partial x) \tag{24}$$

where m is the Alfvén number—i.e., $m = U_0/A_0$, A_0 being the speed of propagation of ordinary Alfvén waves—equal to $\sqrt{\mu H_0^2/4\pi\rho}$. By taking the curl of Ohm's law, Eq. (16), one eliminates the vorticity vector $\boldsymbol{\Omega}$ using Eq. (22), and the following equation emerges:

$$k_1\,\partial\boldsymbol{\xi}/\partial x = \nabla^2\boldsymbol{\xi} - \omega_0\tau\nabla\times\partial\boldsymbol{\xi}/\partial x \tag{25}$$

Here $k_1 \equiv 4\pi\sigma\mu U_0(1 - m^{-2})$ so that negative k_1 corresponds to so-called *subalfvénic* flow, positive k_1 to *superalfvénic* flow. Since $\xi_x = \partial h_z/\partial y$, $\xi_y = -\partial h_z/\partial x$, the vector equation (25) can be reduced to two scalar equations involving as unknowns h_z and ξ_z; viz.,

$$\left.\begin{aligned}\nabla^2 h_z &= k_1\,\partial h_z/\partial x + \omega_0\tau\,\partial\xi_z/\partial x\\ \nabla^2\xi_z &= k_1\,\partial\xi_z/\partial x - \omega_0\tau(\partial/\partial x)\nabla^2 h_z\end{aligned}\right\} \tag{26}$$

The crossed-fields case can be treated in a similar fashion. The resulting equations are

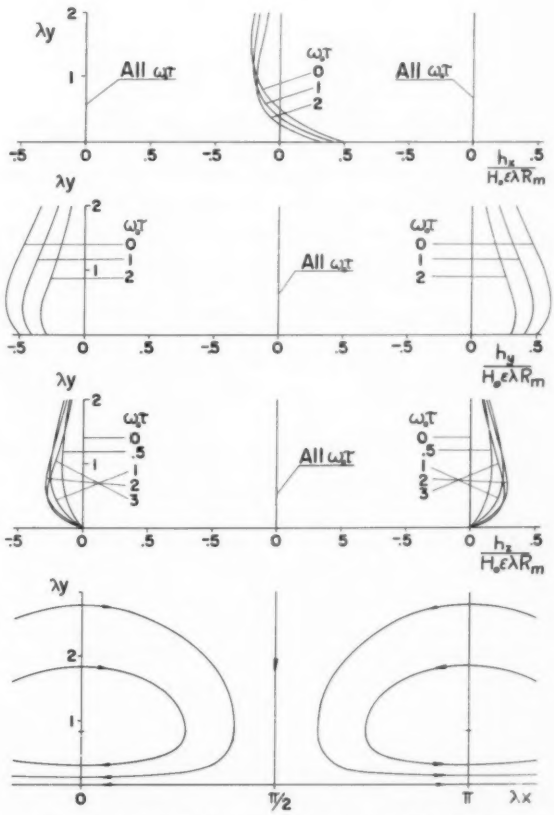

FIG. 3. Wavy wall ($y = \epsilon\cos\lambda x$) in parallel fields and for small magnetic Reynolds number R_m. Magnetic-field perturbation components h_x, h_y, and h_z [Eqs. (43)]. Current lines for $\omega_0\tau = 1$.

$$\partial \mathbf{u}/\partial x = m^{-2}(U_0/H_0)\,\partial \mathbf{h}/\partial y + U_0 \nabla\,\partial\varphi_2/\partial x$$

where
$$\nabla^2\,\partial\varphi_2/\partial x = 0, \tag{27}$$

$$p - p_0 = -\rho U_0^2(m^{-2}h_y/H_0 + \partial\varphi_2/\partial x) \tag{28}$$

$$\left.\begin{aligned}(\partial/\partial x)\nabla^2 h_z &= k_2 W h_z + \omega_0\tau(\partial^2/\partial x\partial y)\xi_z \\ (\partial/\partial x)\nabla^2\xi_z &= k_2 W\xi_z - \omega_0\tau(\partial^2/\partial x\partial y)\nabla^2 h_z\end{aligned}\right\} \tag{29}$$

where

$$k_2 \equiv 4\pi\sigma u U_0 \text{ and } W \equiv (\partial^2/\partial x^2) - m^{-2}(\partial^2/\partial y^2)$$

Finally the second case of crossed fields, where the unperturbed magnetic field is parallel to the boundary but perpendicular to the free-stream velocity vector $\mathbf{U}_0$, gives a particularly simple result. From Eq. (20) one finds $\partial\boldsymbol{\Omega}/\partial x = 0$, which means that the coupling between vorticity and current normally implied by Eq. (20) does not arise. Thus if the flow is irrotational far upstream it will be irrotational everywhere. Ohm's law, Eq. (16), reduces to

$$\nabla^2\mathbf{h} = k_2\,\partial\mathbf{h}/\partial x \tag{30}$$

and it is realized that for appropriate boundary conditions—e.g., flow past an insulating wavy wall—the trivial solution $\mathbf{h} = 0$ is obtained. We therefore leave the crossed-fields case II at this point and continue to study the parallel- and crossed-fields cases further.

Wavy-Wall Problems

The most straightforward method of extracting information from the linear partial differential equations (26) and (29), governing the behavior of ξ_z and h_z in the parallel- and crossed-fields cases, is to study flow past infinite sinusoidal walls. Once we have access to the wavy-wall solutions, it is easy in principle to study flow past infinite two-dimensional walls of arbitrary shape, within the frame of the small-perturbation approach, by the use of Fourier superposition. Suppose that the wall is infinitely thick, nonmagnetic, and insulating, and let the surface (see Fig. 1) be given by

$$y = \epsilon\, e^{i\lambda x}; \qquad \epsilon\lambda \ll 1 \tag{31}$$

Complex notation will be used in what follows, the real part being implied everywhere. The following boundary conditions will be applied:

(1) Vanishing perturbations $\mathbf{u}$ and $\mathbf{h}$ at $y = +\infty$ and vanishing $\mathbf{h}$ at $y = -\infty$.

(2) No flow of fluid or currents through the surface of the wall. These conditions will be satisfied in a linearized fashion in the xz-plane.

(3) Continuous components of $\mathbf{h}$ across the surface—i.e., approximately across the xz-plane.

Inside the insulating wall the magnetic-field perturbation $\mathbf{h}$ must be curl-free and divergence-free, and

$$\left.\begin{aligned}h_x &= H_0 C_a i\, e^{i\lambda x+\lambda y} \\ h_y &= H_0 C_a\, e^{i\lambda x+\lambda y} \\ h_z &= 0\end{aligned}\right\} \tag{32}$$

is easily seen to be the appropriate solution. C_a is a complex constant to be determined later from boundary condition (3). Since $h_z = 0$ everywhere inside the wall, and the components of $\mathbf{h}$ across the boundary have to be continuous, it is seen that $\partial h_z/\partial x$ and thus j_y must vanish in the flow field just outside the wall ($y = 0^+$) for all x. The boundary condition of no current flow across the boundary is therefore automatically satisfied in a linearized fashion.

Outside the wall—i.e., in the flow field—the magnetic field is governed by Eqs. (26) and (29) for parallel and crossed fields, respectively. If a trial solution of the form

$$e^{i\lambda x+cy} \tag{33}$$

is introduced one finds

$$c_{\alpha\beta}/\lambda = -\left(1 + \frac{1}{2}\omega_0^2\tau^2 + \frac{k_1 i}{\lambda} \pm \frac{1}{2}\omega_0^2\tau^2\sqrt{1 + \frac{4k_1 i}{\lambda\omega_0^2\tau^2}}\right)^{1/2} \tag{34}$$

in the parallel-fields case, and

$$c_{\alpha\beta}/\lambda = -\left(\frac{1 + (1/2)\omega_0^2\tau^2 + (k_1 i/\lambda) + (k_2/\lambda m)^2 \pm (1/2)\omega_0^2\tau^2\sqrt{1 - (4/\omega_0^2\tau^2)[(k_2 i/\lambda) + 1](k_2 i/\lambda)\,(1 + m^{-2})}}{\omega_0^2\tau^2 + [(k_2 i/\lambda m^2) - 1]^2}\right)^{1/2} \tag{35}$$

in the crossed-fields case. The square roots (and 1/2 powers) are defined by

$$\sqrt{z} = \sqrt{|z|}\, e^{\frac{1}{2}i\arg z} \qquad -\pi < \arg z < \pi \tag{36}$$

This convention will always be used in what follows. It implies that all square roots have positive real parts, and since all perturbations are required to vanish for large positive y-values, one has to introduce the minus sign in front of the square roots of Eqs. (34) and (35).

As a convention, the index α will be used for the positive and the index β for the negative sign inside the square-roots in Eqs. (34) and (35). Using the basic solutions, Eq. (33), it is now easy to construct expressions for $\mathbf{h}$ and $\mathbf{u}$ which satisfy all boundary conditions, the divergence conditions, and the differential equations (16), (26), and (29). The algebra, however, becomes rather lengthy and will be omitted here.

The parallel- and crossed-fields cases can essentially be treated simultaneously, and the results are:

$$\left.\begin{aligned} h_z &= H_0 C_a i e^{i\lambda x}\{e^{-\lambda y} + C_g[C_d c_\alpha(e^{c_\alpha y} - e^{-\lambda y}) + c_\beta(e^{c_\beta y} - e^{-\lambda y})]\} \\ h_y &= H_0 C_a e^{i\lambda x}\{e^{-\lambda y} + C_g[C_d\lambda(e^{c_\alpha y} - e^{-\lambda y}) + \lambda(e^{c_\beta y} - e^{-\lambda y})]\} \\ h_z &= \pm H_0 C_a C_g \sqrt{c_\beta^2 - \lambda^2}\, e^{i\lambda x}(e^{c_\alpha y} - e^{c_\beta y}) \\ \varphi_1 &= \varphi_2 = C_f e^{i\lambda x - \lambda y} \end{aligned}\right\} \quad (37)$$

The positive sign in front of h_z corresponds to parallel fields, the negative one to crossed fields. Further:

$$C_a = \begin{cases} m^2 i\epsilon\lambda/[1 + (m^2 - 1)C_e] & \text{parallel fields} \\ -m^2\epsilon\lambda/[1 + (m^2 + 1)C_e] & \text{crossed fields} \end{cases} \quad (38)$$

$$C_f = \begin{cases} -(m^2 - 1)i\epsilon C_e/[1 + (m^2 - 1)C_e] & \text{parallel fields} \\ -(m^2 + 1)i\epsilon C_e/[1 + (m^2 + 1)C_e] & \text{crossed fields} \end{cases} \quad (39)$$

$$\left.\begin{aligned} C_e &= [(c_\alpha - \lambda)/(c_\beta + \lambda)]C_d \\ C_d &= \sqrt{(c_\beta^2 - \lambda^2)/(c_\alpha^2 - \lambda^2)} \\ C_g &= 2[(\lambda + c_\beta) + (\lambda + c_\alpha)C_d]^{-1} \end{aligned}\right\} \quad (40)$$

Notice that Eqs. (37) and (40) are valid both for parallel and crossed fields. The exponents c_α and c_β are given by Eq. (34) in the parallel-fields case and by Eq. (35) in the crossed-fields case. By going back to the original form of Ohm's law, Eq. (2), it is finally also possible to determine the electric field $\mathbf{E}$ and then, via Eq. (6), the charge-density distribution. It should be emphasized in this connection that in the parallel-fields case the electric field $\mathbf{E}$ vanishes in the unperturbed flow, while the crossed-fields case must have an unperturbed electric field $\mathbf{E}_0 = -\mu\mathbf{U}_0 \times \mathbf{H}_0$. The solution for the electric field will not be discussed here.

The general solution, Eq. (37), will now be investigated for large and small values of the magnetic Reynolds number $R_m = 4\pi\sigma\mu U_0/\lambda$. In these limits it is possible to simplify the solution considerably by expansion of the square roots of Eqs. (34) and (35), and this is therefore a convenient method for demonstrating some features of the solution.

Parallel Fields—Large Magnetic Reynolds Number

Assuming $|k_1/\lambda| \gg 1$, the solution (for λy at most of order unity) becomes

$$\left.\begin{aligned} h_x &= H_0\epsilon\lambda e^{i\lambda x}\,(e^{-\lambda y} - 2e^{-\lambda y(1\pm i)\sqrt{|k_1/2\lambda|}}\cdot [1 + O(k_1/\lambda)^{-1/2}] \\ h_y &= H_0 i\epsilon\lambda e^{i\lambda x - \lambda y}\,[1 + O(k_1/\lambda)^{-1/2}] \\ h_z &= H_0 i\epsilon\lambda\omega_0\tau\lambda y\, e^{i\lambda x - \lambda y(1\pm i)\sqrt{|k_1/2\lambda|}}\cdot [1 + O(k_1/\lambda)^{-1/2}] \end{aligned}\right\} \quad (41)$$

where it has also been assumed that $\omega_0\tau$ is of the order of unity. The positive sign in the exponent corresponds to $k_1/\lambda > 0$, the negative one to $k_1/\lambda < 0$. Inspection of Eqs. (41) shows that the x- and y-components are independent of $\omega_0\tau$ and in fact agree with the results of reference 4. The z-component, which in the case of scalar conductivity ($\omega_0\tau = 0$) is identically zero, is seen to take on nonzero values when $\omega_0\tau \neq 0$. The component h_z is, however, smaller than h_x and h_y by a factor of order $\sqrt{|k_1|/\lambda}$, and the influence of moderate anisotropy in the conductivity is therefore small in the present case.

The general character of the solution is that the currents are confined to a thin layer, a magnetic boundary layer, close to the wall. The thickness of this layer is

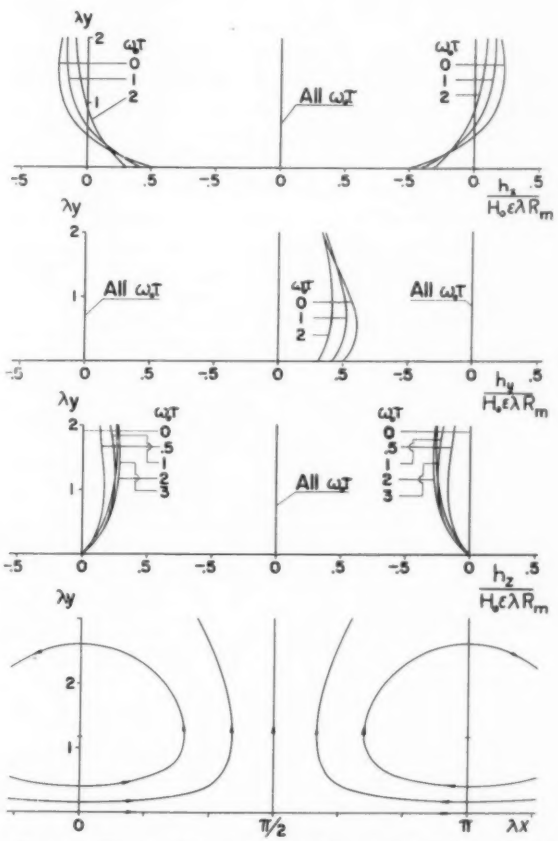

FIG. 4. Wavy wall ($y = \epsilon\cos\lambda x$) in crossed fields and for small magnetic Reynolds number R_m. Magnetic-field perturbation components h_x, h_y and h_z [Eqs. (44)]. Current lines for $\omega_0\tau = 1$.

of the order of $\sqrt{1/|k_1|\lambda}$, and it shrinks to a current sheet of zero thickness in the limit of infinite conductivity. Outside the boundary layer the solution is simply the current-free infinite-conductivity solution, and it is therefore clear that the anisotropy of the electrical conductivity can only play a role inside the current layer. A close examination of the currents in this layer is therefore of interest. In the case of scalar conductivity the currents are purely in the z-direction. For nonzero $\omega_0\tau$ essentially the same current densities exist in this direction but, since $h_z \neq 0$ in the layer, there are also weak currents in the x- and y-directions. These Hall currents form closed loops, as shown in Fig. 2, where current lines defined by

$$dx/j_x = dy/j_y \tag{42}$$

have been plotted for a case $k_1/\lambda = 2 \times 10^4 \cdot \omega_0\tau = 1$. Also shown are the magnetic-field components h_x and h_z. It should be noticed that inside the boundary layer there is a nonzero z-component of the velocity, since u_z, by Eq. (23), is simply proportional to h_z. The projection of a particle path on the xz-plane is thus sinusoidal.

The limiting solution given by Eqs. (41) has two important restrictions due to its boundary-layer character: First, the viscous boundary layer has to be much thinner than the magnetic one, to justify neglecting the viscosity; second, some of the terms which were neglected in the linearization of Ohm's law and the momentum equation become quite important as the boundary-layer thickness decreases with increasing magnetic Reynolds number. In fact, the second restriction is severe enough to make Eqs. (41) useful mostly as a mathematical limit demonstrating some of the properties of the general solution.

Parallel Fields—Small Magnetic Reynolds Number

In order to expand the square roots of Eq. (34) in the case of small R_m, it is necessary to assume $|k_1/\lambda\omega_0{}^2\tau^2| \ll 1$. The following simplified solution is then obtained (for λy at most of the order of unity):

$$\left.\begin{aligned} h_x &= H_0 i\epsilon\lambda(R_m/2\omega_0{}^2\tau^2)e^{i\lambda x} \times \\ &\qquad [(\gamma+1)e^{-\lambda y} - 2\gamma e^{-\gamma\lambda y}]\cdot[1 + O(R_m)] \\ h_y &= -H_0\epsilon\lambda(R_m/2\omega_0{}^2\tau^2)e^{i\lambda x} \times \\ &\qquad [(\gamma+1)e^{-\lambda y} - 2e^{-\gamma\lambda y}]\cdot[1 + O(R_m)] \\ h_z &= -H_0\epsilon\lambda(R_m/\omega_0\tau)e^{i\lambda x} \times \\ &\qquad [e^{-\lambda y} - e^{-\gamma\lambda y}]\cdot[1 + O(R_m)] \end{aligned}\right\} \tag{43}$$

where $R_m = 4\pi\sigma\mu U_0/\lambda$ and $\gamma = \sqrt{1 + \omega_0{}^2\tau^2}$

The magnetic-field components are shown in Fig. 3, together with a plot of current lines defined by Eq. (42). Hall-current loops are obtained again in this case. It should be noted that in the present case the magnetic-field component h_z due to nonzero $\omega_0\tau$ is comparable in magnitude to h_x and h_y, and also that h_x and h_y depend strongly on $\omega_0\tau$. Notice that the scale along the y-axis is very different in Figs. 2 and 3. The solution for small R_m does not have boundary-layer character, so that the restrictions discussed in the previous case do not arise here.

Crossed Fields—Small Magnetic Reynolds Number

Exactly as in the parallel-fields case, one assumes $k_2/\lambda\omega_0{}^2\tau^2 \ll 1$ and obtains the following simplified solution (for λy at most of the order of unity):

$$\left.\begin{aligned} h_x &= H_0\epsilon\lambda(R_m/2\omega_0{}^2\tau^2)e^{i\lambda x} \times \\ &\qquad [(\gamma+1)e^{-\lambda y} - 2e^{-\lambda y/\gamma}]\cdot[1 + O(R_m)] \\ h_y &= H_0 i\epsilon\lambda(R_m/2\omega_0{}^2\tau^2)e^{i\lambda x} \times \\ &\qquad [(\gamma+1)e^{-\lambda y} - 2\gamma e^{-\lambda y/\gamma}]\cdot[1 + O(R_m)] \\ h_z &= -H_0\epsilon\lambda(R_m/\omega_0\tau)e^{i\lambda x} \times \\ &\qquad [e^{-\lambda y} - e^{-\lambda y/\gamma}]\cdot[1 + O(R_m)] \end{aligned}\right\} \tag{44}$$

The magnetic-field components are shown in Fig. 4, together with the now familiar plot of Hall-current loops. The results obtained in this case are very similar to the low R_m, parallel-fields case, and thus need no further discussion.

Crossed Fields—Large Magnetic Reynolds Number

Assuming $R_m = k_2/\lambda \gg 1$, the following solution is obtained in the crossed-fields case (for λy at most of order R_m):

$$\left.\begin{aligned} h_x &= H_0\epsilon\lambda f(m)\left[(m-i)e^{i\lambda x - \lambda y} - 2me^{i\lambda(x-my) - g\lambda y}\cos\left(g\lambda y\,\frac{\omega_0\tau m}{\sqrt{1+m^2}}\right)\right][1 + O(R_m{}^{-1})] \\ h_y &= H_0\epsilon\lambda f(m)\left[i(m-i)e^{i\lambda x - \lambda y} - 2e^{i\lambda(x-my) - g\lambda y}\cos\left(g\lambda y\,\frac{\omega_0\tau m}{\sqrt{1+m^2}}\right)\right][1 + O(R^{-1}{}_m)] \\ h_z &= H_0\epsilon\lambda f(m)2\sqrt{1+m^2}\,e^{i\lambda(x-my) - g\lambda y}\sin\left(g\lambda y\,\frac{\omega_0\tau m}{\sqrt{1+m^2}}\right)[1 + O(R_m{}^{-1})] \end{aligned}\right\} \tag{45}$$

where $f(m) = mi/(m-2i)(m+i)$

and $g = m(1+m^2)\lambda/2k_2$

For $\omega_0\tau = 0$ Eqs. (45) agree with reference 4 and in this limit $h_z = 0$. For nonzero $\omega_0\tau$ the solution still has essentially the same character as far as h_x and h_y are concerned: These two components are given by an irrotational part with damping factor $\exp\{-\lambda y\}$ and a rotational part with an extremely weak damping given by $\exp\{-g\lambda y\}$, where $g \ll 1$ in the present limit. For infinite magnetic Reynolds number this damping vanishes and the rotational part of the solution is then a function of $(x - my)$ only, a fact which can be traced back to the wave operator appearing in Eqs. (29). Only the rotational parts of h_x and h_y are affected by nonzero $\omega_0\tau$; furthermore, close to the wall this influence is negligible for moderate values of $\omega_0\tau$. It can also be seen that close to the wall the component h_z is smaller than h_x and h_y by a factor of order R_m. Far from the wall the situation is different: All three components of the magnetic-field perturbation vector are comparable in size, and h_x and h_y are strongly affected by nonzero $\omega_0\tau$. In Fig. 5 conditions near the wall are examined more closely. Current lines defined by Eq. (42) are shown, and the structure of the Hall-current pattern appears to be quite different from those of the previous cases. In fact, it is easy to see from the expression for h_z that the current lines shown in Fig. 5 all close at large but still finite distance from the wall

and that there will be a whole series of current loops, one outside the other, as indicated schematically in Fig. 6. This peculiar pattern will be discussed later.

Pressures on the Wavy Wall

In the preceding sections the general solution of the wavy-wall problem has been examined in the limiting cases of small and large magnetic Reynolds number. This has provided some information concerning the flow picture, in particular the Hall-current pattern. By study of the pressure on the wall, it is found that the influence of nonscalar conductivity is very small for large R_m, both in the case of parallel and crossed fields. For small R_m, on the other hand, the influence of nonzero $\omega_0\tau$ on the magnetohydrodynamic part of the pressure formula may be shown to be relatively large, but the total magnetohydrodynamic influence on the pressure is of course small in this limit.

In order to estimate the absolute importance of the Hall effect, it is therefore necessary to investigate the general solution for R_m of the order of unity. The pressure distribution on the wall is of particular interest. By use of Eqs. (24) or (28) the following pressure formula is obtained:

$$\left.\begin{aligned} &(p_w - p_0)/\rho U_0^2 = -\epsilon\lambda A_p e^{i\lambda x} \\ &\text{where} \\ &A_p = \frac{[(m^2-1)C_e - 1]}{[(m^2-1)C_e + 1]} \qquad \text{parallel fields} \\ &A_p = \frac{[(m^2+1)C_e - 1]}{[(m^2+1)C_e + 1]} \qquad \text{crossed fields} \end{aligned}\right\} \quad (46)$$

and C_e is given by Eq. (40).

The complex quantity A_p thus describes the total magnetohydrodynamic effect on the pressure distribution, the modulus of A_p giving the amplitude of the pressure perturbation and the argument its phase relative to the wall. The quantities A_p for superalfvénic ($m > 1$) and $1/A_p$ for subalfvénic flow ($m < 1$) have been plotted in Argand diagrams for the parallel- and crossed-fields cases in Figs. 7 and 8, respectively. In these diagrams full lines correspond to $\omega_0\tau = 0$, dashed ones to $\omega_0\tau = 1$. In the parallel-fields case one curve corresponding to $\omega_0\tau = 5$ is also shown. Values of $1/A_p$ inside the shaded areas cannot be obtained. It is interesting to notice that the curves for $m = 1$—i.e., alfvénic flow—and $\omega_0\tau = 0$ are circles of radius unity in both the parallel- and crossed-fields cases. For $m = 1$ and $\omega_0\tau \neq 0$ the same circle is obtained in Fig. 7 but not in Fig. 8. The pressures obtained for infinite magnetic Reynolds number agree with reference 4.

Figs. 7 and 8 indicate a remarkably small influence of the tensor conductivity on the wall pressure. It may be recalled from the introductory discussion of the generalized Ohm's law that the conductivity transverse to the magnetic field may be reduced by as much as a factor $(1 + \omega_0^2\tau^2)$, which would of course lead to much larger effects for $\omega_0\tau = 1$ than Figs. 7 and 8

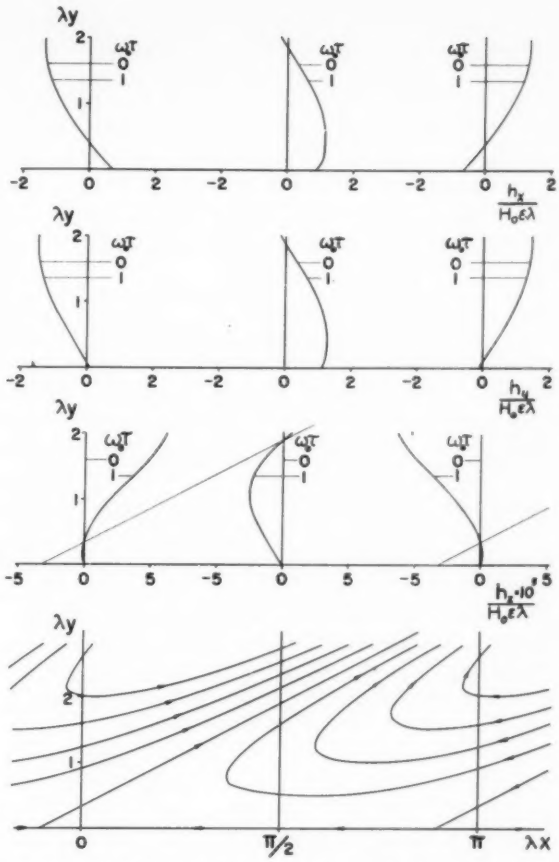

FIG. 5. Wavy wall ($y = \epsilon \cos \lambda x$) in crossed fields and for large magnetic Reynolds number R_m. Magnetic-field perturbation components h_x, h_y and h_z [Eqs. (45)], close to the wall for $R_m = 2 \times 10^4$ and Alfvén number $m = 1$. Current lines for $R_m = 2 \times 10^4$, $m = 1$, $\omega_0\tau = 1$.

indicate. In the parallel-fields case, however, the primary flow direction of the Hall currents would be perpendicular to the wall, and since the wall is an insulator the Hall currents are partly prevented from flowing, in particular for large R_m when the total thickness of the current layer on the wall is small. It may be readily verified from Eqs. (3) and (4) that the conductivity transverse to the magnetic field is restored to its scalar value σ if the Hall currents are prevented from flowing. In the parallel-fields case, the small influence of the tensor conductivity is thus due to the insulating property of the wall, and for a conducting wall the situation may be entirely different.

In the crossed-fields case for moderate and large R_m the complicated current pattern (Fig. 6) extending far out in the flow field makes it difficult to evaluate the true reason for the small influence of the nonscalar conductivity. Mathematically this result can be inferred directly from the generalized Ohm's law, Eq. (2), by letting the conductivity σ become large while at the same time $\omega\tau$ is kept of order unity. The importance of the two current terms in Eq. (2) is then seen to be small for large σ.

Finally, one may notice that the drag on the wavy

wall is proportional to the negative of the imaginary part of A_p. Figs. 7 and 8 can thus be used directly for drag evaluation. The drag is always positive, as it must be, since the energy dissipated by Joule heating is introduced into the flow via the work done on the fluid by the drag force. For parallel fields and infinite R_m the drag is zero, and it is easy to show that no electric energy is released into heat in the infinitely thin current sheet on the wall that characterizes this flow case.

Transverse Hydromagnetic Waves

Since it is recognized that the Alfvén-wave mechanism plays an important role in many magnetohydrodynamic flow problems, it seems appropriate to present a brief discussion of these waves in a plasma with tensor electric conductivity. This problem has been studied in detail in reference 6 and elsewhere, and the discussion given in the present paper will therefore be restricted to a demonstration of some basic features of the modified Alfvén wave when the wave normal is parallel to the unperturbed magnetic field. The problem will be approached by using the macroscopic momentum equation and Ohm's law given by Eqs. (13) and (12), respectively. Let the undisturbed magnetic field be in the x-direction of a right-handed Cartesian coordinate system (x, y, z), and consider transverse wave motion ($q_x \equiv 0$) such that $\partial/\partial y = \partial/\partial z = 0$. Eqs. (7) and (8), combined, then give $H_x = \text{const.} = H_0$, say, and Eqs. (13) and (12) simplify to

$$\left.\begin{aligned} \frac{\partial \mathbf{q}}{\partial t} - \frac{\mu H_0}{4\pi\rho}\frac{\partial \mathbf{H}}{\partial x} &= -\frac{\partial}{\partial x}\left(\frac{p}{\rho} + \frac{\mu H^2}{8\pi\rho}\right) \\ -\frac{\partial \mathbf{H}}{\partial t} + H_0\frac{\partial \mathbf{q}}{\partial x} &= -\frac{1}{4\pi\sigma\mu}\times \\ &\quad \left(\frac{\partial^2 \mathbf{H}}{\partial x^2} + \tau\frac{\partial^3 \mathbf{H}}{\partial x^2 \partial t} - \omega_0\tau\frac{\partial \xi}{\partial x}\right) \end{aligned}\right\} \quad (47)$$

Note that these equations are linear despite the fact that no linearization has been carried out in this section. If the components are written out and trial solutions of the form $\exp\{i(\omega_t t + kx)\}$ substituted for q_y, q_z, H_y, and H_z, the following condition for nontrivial solution emerges:

$$k = \pm \frac{\omega_t}{A_0\left[1 - \left(\frac{\omega_t}{\omega_{i0}}\right)^2\frac{m_e}{m_i} \pm \left(\frac{\omega_t}{\omega_{i0}}\right) + \frac{i}{\omega_0\tau}\left(\frac{\omega_t}{\omega_{i0}}\right)\right]^{1/2}} \quad (48)$$

where the relation $4\pi\sigma\mu A_0^2 = \omega_e\omega_{i0}\tau$, ω_{i0} being the ion cyclotron frequency, has been used. In the limit of infinite collision time, τ, the imaginary term in the square root vanishes and k is seen to be the wave number for

(1) the fast wave, with wave number k_α and phase speed $A_\alpha = \omega_t/k_\alpha$, corresponding to the positive sign inside the square root;

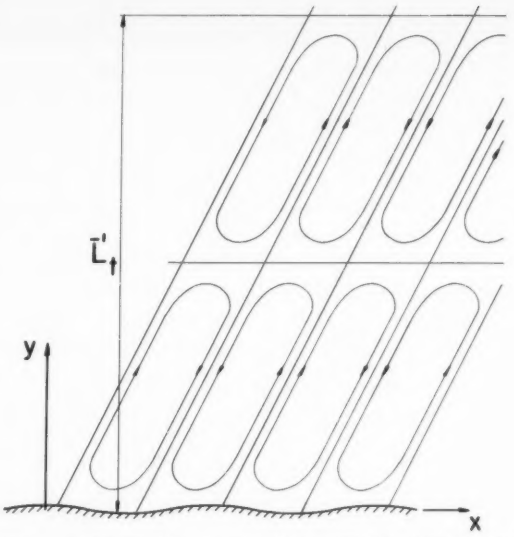

FIG. 6. Wavy wall ($y = \epsilon \cos \lambda x$) in crossed fields and for large magnetic Reynolds number R_m. Schematic configuration of Hall-current loops.

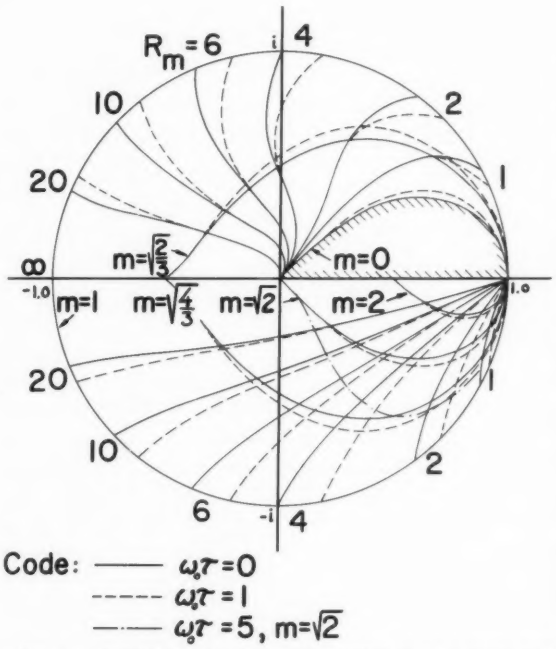

FIG. 7. Parallel fields. Pressure distribution on a wavy wall due to magnetic interaction. The complex pressure-influence coefficient A_p [Eq. (46)], is shown in an Argand diagram for superalfvénic flow ($m > 1$; lower half-plane). For subalfvénic flow ($m < 1$) the inverse quantity $1/A_p$ is given (upper half-plane). Curves of constant magnetic Reynolds number R_m and Alfvén number m are given.

(2) The slow wave, with wave number k_β and phase speed $A_\beta = \omega_t/k_\beta$, corresponding to the negative sign inside the square root.

The phase speeds of these two waves are shown in Fig. 9 as functions of the frequency ω_t. The slow wave

becomes transient for frequencies above ω_{i0}, the ion cyclotron frequency, the fast one for frequencies above ω_0, the electron cyclotron frequency. The ambiguous sign in Eq. (48) corresponds to waves traveling in opposite directions along the x-axis and, finally, the imaginary term in the square root is responsible for the damping.

One can now use these wave solutions to construct a solution satisfying

$$x = 0\text{: } q_y = U_0 e^{i\omega_t t};\ q_z = 0$$

This obviously corresponds to a case where the fluid particles in the yz-plane perform a simultaneous harmonic oscillation in the y-direction. The appropriate solution is:

$$\left.\begin{aligned} q_y &= \frac{1}{2} U_0 e^{i\omega_t t} (e^{ik_\alpha x} + e^{ik_\beta x}) \\ q_z &= -\frac{i}{2} U_0 e^{i\omega_t t} (e^{ik_\alpha x} - e^{ik_\beta x}) \end{aligned}\right\} x > 0 \quad (49)$$

and similar expressions for j_y, j_z and H_y, H_z. For frequencies less than the ion cyclotron frequency and with neglect of damping, Eqs. (49) may be written:

$$\left.\begin{aligned} q_y &= (U_0/2)[\cos(\omega_t t - k_\alpha x) + \cos(\omega_t t - k_\beta x)] = U_0 \cos \bar{k}x \cos(\omega_t t - \bar{k}x) \\ q_z &= (U_0/2)[\sin(\omega_t t - k_\alpha x) - \sin(\omega_t t - k_\beta x)] = U_0 \sin \bar{k}x \cos(\omega_t t - \bar{k}x) \end{aligned}\right\} \quad (50)$$

Fast wave — Slow wave — Resultant wave

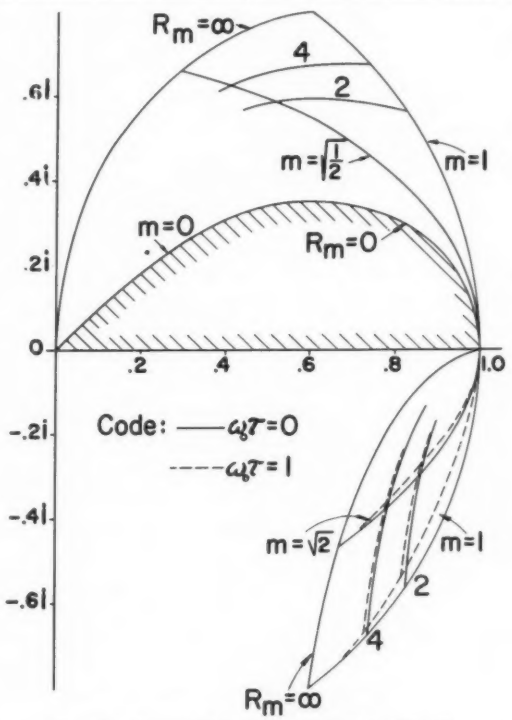

FIG. 8. Crossed fields. See legend for Fig. 7.

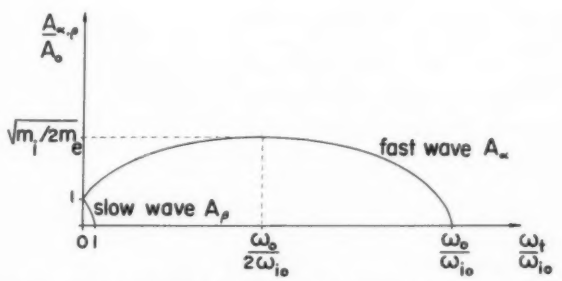

FIG. 9. Phase speeds as functions of frequency ratio, for fast and slow transverse hydromagnetic waves. ω_t = wave frequency; ω_{i0} = ion cyclotron frequency.

where

$$\bar{k} = (1/2)(k_\beta - k_\alpha) \text{ and } \bar{k} = (1/2)(k_\beta + k_\alpha)$$

From these expressions the fast wave is seen to be right-handed, the slow one left-handed circularly polarized. The superposition of these two waves gives a resultant plane-polarized wave having wave number

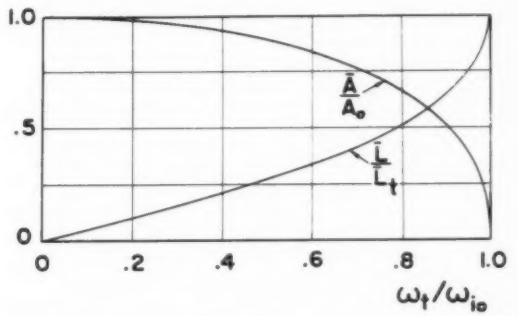

FIG. 10. Phase-speed ratio $\bar{A}/A_0$ and wavelengths ratio $\bar{L}/\bar{L}_t$ as functions of frequency ratio, for resultant transverse hydromagnetic wave. ω_t = wave frequency; ω_{i0} = ion cyclotron frequency.

$\bar{k}$, phase speed $\bar{A}$, and wave length $\bar{L}$, with a clockwise rotating plane of polarization. The distance $\bar{L}_t$ for one complete turn of the plane of polarization is given by

$$\bar{L}_t/\bar{L} = \bar{k}/\bar{k}$$

The quantities $\bar{L}/\bar{L}_t$ and $\bar{A}/A_0$ are shown in Fig. 10. For low frequencies the phase speed $\bar{A}$ is approximately the Alfvén speed A_0, and the twist length $\bar{L}_t$ is large compared to the wave length $\bar{L}$. In this limit the resultant wave may be called a modified Alfvén wave. The resultant wave does not exist above $\omega_t \approx \omega_{i0}$, since the slow wave component is transient for $\omega_t \gtrsim \omega_{i0}$.

In magnetohydrodynamic problems of the type discussed in the previous sections, one is mostly interested

(*Continued on page 643*)

Shimmy of a Nose Gear With Dual Co-Rotating Wheels

JOHN ERWIN STEVENS*

Chance Vought Aircraft, Incorporated

Summary

In the attempt to reduce weight and complexity, many nose gears have been designed with dual co-rotating wheels to prevent shimmy. In some cases these designs have not resulted in shimmy-free landing gears. In this paper equations are developed which describe the behavior of a dual-wheeled landing gear with co-rotating wheels. These equations show that the role of the tire in determining the shimmy characteristics is more important in the dual-wheeled co-rotating system than in more conventional designs. The method is useful for analysis both of conventional landing gears and of landing gears with dual co-rotational wheels.

Symbols

δ	= lateral displacement of the landing gear
δ_F	= lateral displacement of the landing gear at the tire-ground contact area
θ_F	= lateral slope of the landing gear at the axle
α_F	= castor angle of the wheel system
R	= radius of the wheel
ϵ	= trail length
$2s$	= distance between wheels
ϕ	= twist in half the torsion shaft between the wheels
σ	= cornering angle
Δ	= lateral deflection of the tire under side load
V	= forward velocity
ω	= shimmy frequency
Ω	= shimmy frequency parameter $= \omega R/V$
P_S	= side force on the landing gear at the tire-ground contact area
P_{DL}, P_{DR}	= drag forces on the left and right wheels, respectively
P_{VL}, P_{VR}	= vertical forces on the left and right wheels, respectively
M	= moment applied to the landing gear by twisting the tire
$[M_{ij}]$	= mass matrix of the dynamic system
$S_{\alpha j}$	= inertia coupling matrix between strut system and castor degree of freedom (column matrix)
I	= moment of inertia of castoring portion of the landing gear about the castor axis
I_w	= moment of inertia of a wheel about a principal diameter of the wheel, times the number of wheels
I_p	= polar moment of inertia of a wheel about the axle
$[k_{ij}]$	= stiffness matrix for landing gear
$R_m(\omega)$	= real component of shimmy damper coefficient
$I_m(\omega)$	= imaginary component of shimmy damper coefficient
k_ϕ	= twice the torsional spring rate of the shaft connecting the wheels
K_1	= lateral stiffness of a tire
K_2	= torsional stiffness of a tire
K_S	= tire slip coefficient
m_0	= reference mass
k_R	= reference stiffness
$P(\Omega)$, $Q(\Omega)$	= tire parameters
$\{\ \}$	= indicates column matrix
$[\ ]$	= indicates row matrix
$\bar{\delta}$, $\bar{\theta}_F$, $\bar{\alpha}_F$, $\bar{\delta}_F$	= column matricies defining landing gear displacement shapes
$\bar{\delta}'$, $\bar{\theta}_F'$, $\bar{\alpha}_F'$, $\bar{\delta}_F'$	= row matricies defining landing gear displacement shapes
q	= column matrix of generalized coordinates

Introduction

In spite of the problems associated with ground handling, many designers have elected to reduce weight and complexity in nose-gear designs by using a dual-wheeled nose gear with the wheels interconnected by a rigid torsion shaft. It has been assumed that the constraint against turning imposed by the interconnection of the wheels would make shimmy impossible. Many shimmy-free designs have been made with co-rotating dual wheels, but in other designs shimmying still occurs. It is the purpose of this paper to develop a method for analyzing dual-wheeled landing gear with co-rotating wheels which will explain the shimmy behavior of these systems.

In the development of this method extensive use has been made of the test data on tires presented by Smiley and Horne in reference 2, and of the work of this author presented in reference 1. In deriving the equations for the shimmy behavior of the landing-gear system, and in solving the equations of motion, extensive use has been made of flutter-analysis procedures.

The results of the investigation show that the tire plays a much more important part in the shimmy of a dual-wheeled landing gear with co-rotating wheels than would be expected on the basis of Moreland's work on more conventional landing gears. Some of Moreland's work can be found in reference 5.

Shimmy Equations

The equations for the shimmy of a castoring nose gear with two wheels connected by a flexible torsion shaft are derived. Sufficient generality is maintained so that these equations may be limited subsequently to define the shimmy behavior of a single-wheeled nose

Received April 29, 1960. Revised and received July 17, 1960.

* Formerly, Chief of Space Mechanics, Vought Astronautics, a Division of Chance Vought Aircraft, Incorporated; now Assistant to Manager, Engineering, Research and Advanced Development Division, Avco Corp.

gear or a dual-wheeled nose gear without the co-rotational constraint. The equations are derived making use of the following assumptions:

(1) The lateral motions of the landing gear are defined by a linear combination of generalized coordinates. In many problems it is convenient to use the modes of normal vibration of the landing gear and its supporting structure as the generalized displacement function. In this problem it is envisioned that these generalized coordinates are defined assuming that the part of the landing gear which castors is restrained.

(2) The castoring of the landing gear is defined by a single coordinate. In the general case this coordinate will be coupled inertially but not elastically with the lateral degrees of freedom.

(3) The rolling behavior of the tires must be included in the shimmy equations.

(4) The rolling behavior of a tire under the action of a side load can be described by a first-order differential equation as defined in reference 1.

(5) There is no skidding of the wheel or wheels in a direction normal to that defined by the wheel and the tire as it corners. This is the fundamental statement establishing the mechanism for transferring energy from the forward motion of the nose gear to the lateral modes, which makes an instability possible.

(6) The nose gear castors about an axis normal to the ground. When a canted castoring axis is included in the derivation, the generalized forces acting on the dynamic system act on all degrees of freedom. If this derivation is understood, the equations for the more complicated system can be written easily.

(7) The effect of the vertical ground reaction on the lateral stiffness of the strut can be neglected. This effect is negligible for a properly designed gear. If the lateral stiffness reduction due to ground reaction is included, however, in the process the nose gear should be considered to be a column.

(8) Gyroscopic coupling between the castoring of the wheel and the lateral bending of the strut must be included.

(9) For small drag forces, the drag force on a wheel at the ground during braking is proportional to the relative slip velocity of the tire (no skidding occurs). The relative slip velocity is defined as $\Delta V/V$ where ΔV is the apparent change in the forward speed of the wheel which occurs when the drag force is applied, and V is the forward speed of the wheel.

Assumptions (1) through (9) are made in writing the equation of motion. To solve the resulting equations the following will be assumed:

(10) For the critical shimmy situations the motion is simple harmonic. The general practices used in flutter analysis will be followed. First it will be assumed that the solution is simple harmonic; then another parameter will be left as a variable in addition to the frequency, so that both the in-phase and out-of-phase components of the equations can be satisfied independently. This approach has an additional advantage in that most analysts have access to flutter routines which can be used for the solution of this problem.

(11) A frequency parameter Ω similar to the reduced frequency "k" used in flutter analysis can be defined ($\Omega = \omega R/V$ where R is the radius of the wheel, ω is the shimmy frequency and V is the forward velocity of the wheel).

Now, making use of assumptions (1)–(9), we can proceed toward writing the shimmy equations. The lateral displacement of the landing gear with the castoring portion of the gear locked in place can be written as follows, if we assume that the lateral displacement is made up of a linear combination of generalized coordinates:

$$\delta = \sum q_i \bar{\delta}_i(x, z) = \bar{\delta}' q \tag{1}$$

where q is a column matrix and $\bar{\delta}'$ is a row matrix. By use of Eq. (1), the slope of the castor axis due to the lateral deflection of the strut at the wheel axle can be written as

$$\theta_F = \sum q_i \frac{d\bar{\delta}_i}{dz}\,(x = \epsilon, z = R) = \sum q_i \bar{\theta}_{Fi} = \bar{\theta}_F' q \tag{2}$$

The effective castor angle resulting from the lateral deformation of the strut can be written as

$$\alpha_F = \sum q_i \frac{d\bar{\delta}_i}{dx}\,(x = \epsilon, z = 0) = \sum q_i \bar{\alpha}'_{Fi} = \bar{\alpha}_F' q \tag{3}$$

and the lateral displacement of the landing gear due to the lateral flexibility of the strut at the ground can be written as

$$\delta_F = \sum q_i \bar{\delta}_i(x = \epsilon, z = 0) = \bar{\delta}_F' q \tag{4}$$

If we now introduce as another coordinate, the rotation of the castoring portion of the landing gear about the castor axis, δ_F, α_F, and θ_F become

$$\delta_F = [\epsilon, \bar{\delta}_F']\{\alpha, q\} \tag{5}$$

$$\alpha_F = [1, \bar{\alpha}_F']\{\alpha, q\} \tag{6}$$

$$\theta_F = [0, \bar{\theta}_F']\{\alpha, q\} \tag{7}$$

and the lateral displacement of any point on the castoring portion of the strut becomes

$$\delta = [x, \bar{\delta}'(x, z)]\{\alpha, q\} \tag{8}$$

[Because of the definition of the coordinate α, the lateral displacement in the parts of the gear which do not castor are still determined by Eq. (1)].

If now we assume that for any landing gear we will know the mass distribution and the stiffness distribution, we can make use of Lagrange's equations to write the equations of motion, remembering our assumption that gyroscopic terms are necessary, that we assume simple harmonic motion, and that the dynamic system is subjected to a lateral force P_S at the tire

contact with the ground and, if a dual landing-gear arrangement is to be analyzed, a moment M through the tire ground contact area due to twisting of the tire, and drag forces P_{DL} and P_{DR} and vertical forces P_{VL} and P_{VR} on the left and right wheels respectively of the two-wheel system. The general system to be analyzed is shown in Fig. 1.

$$\left(-\omega^2\left\{\begin{bmatrix} M_{ij} & S_{\alpha j} \\ S_{\alpha i} & I \end{bmatrix} - \frac{I_{wi}}{\Omega}\begin{bmatrix} (\bar{\theta}_F\bar{\alpha}_F' - \bar{\alpha}_F\bar{\theta}_F')\,\bar{\theta}_F \\ -\bar{\theta}_F' \end{bmatrix}\right\} + \left\{\begin{bmatrix} k_{ij} & 0 \\ 0 & R_n(\omega) \end{bmatrix} + i\begin{bmatrix} 0 & 0 \\ 0 & I_m(\omega) \end{bmatrix}\right\}\right)\begin{bmatrix} q \\ \alpha \end{bmatrix} =$$

$$P_S\{\bar{\delta}_F, \epsilon\} + M\{\bar{\alpha}_F, 1\} + (P_{DL} - P_{DR})s\{\bar{\alpha}_F, 1\} + (P_{VR} - P_{VL})s\{\bar{\theta}_F, 0\} \quad (9)$$

The inertia matrix in Eq. (9) can be defined as

$$\begin{bmatrix} M_{ij} & S_{\alpha j} \\ S_{\alpha i}' & I \end{bmatrix} = \int_{\text{rigid}} \begin{bmatrix} \bar{\delta}\bar{\delta}' & 0 \\ 0 & 0 \end{bmatrix} dm(x, z) + \int_{\text{castor}} \begin{bmatrix} \bar{\delta}\bar{\delta}' & \bar{\delta}x \\ \bar{\delta}'x & x^2 \end{bmatrix} dm(x, z) \quad (10)$$

where $m(x, z)$ is the mass distribution function for the landing gear. The limit, "rigid" for the first integral of Eq. (10), designates integration over the noncastoring portion of the gear, and the limit "castor" for the second integral indicates integration over the castoring portion of the landing gear. I_w in Eq. (9) is the moment of inertia of the rotating wheel or wheels about a diameter of the wheel through the axle, and Ω is the parameter $\omega R/V$.

The stiffness matrix $[k_{ij}]$ can be calculated from the strain energy in the gear when the gear is deformed in the shapes $\delta(x, z)$. The complex spring torque defined by $[R_m(\omega) + iI_m(\omega)]\alpha$ is the torque supplied to the castoring portion of the landing gear through a shimmy damper when the landing gear castors.

The equations for the lateral motion of the landing gear are expressed in Eq. (9) in terms of the forcing functions P_S, M, $(P_{DL} - P_{DR})$, and $(P_{VR} - P_{VL})$. These forcing functions arise from the motion of the nose gear and are, in fact, variables that can be defined in terms of three new variables as well as the variables q and α already defined.

The generalized force $(P_{VR} - P_{VL})$ is the easiest to define; it comes about as a result of the lateral spacing of the wheels in landing gear with a dual wheel arrangement and the slope of the strut as the landing gear deflects under a side load. We will assume that the vertical spring rate of each tire of a dual-wheeled nose gear is K_v. We can then write

$$P_{VR} = P_V/2 - K_v s[\bar{\theta}_F', 0]\{q, \alpha\}$$

and

$$P_{VL} = (P_V/2) + K_v s[\bar{\theta}_F', 0]\{q, \alpha\}$$

or

$$(P_{VR} - P_{VL}) = -2sK_v[\bar{\theta}_F', 0]\{q, \alpha\} \quad (11)$$

The side load P_S can be defined in terms of the lateral spring rate of the tires on the landing gear and the lateral deflection of the tires under this load:

$$P_S = \bar{K}_1\Delta \quad (12)$$

where $\bar{K}_1 = nK_1$, n being the number of wheels (1 or 2) and K_1 the lateral spring rate of a single tire. Δ is the lateral deflection of the tire under a side load.

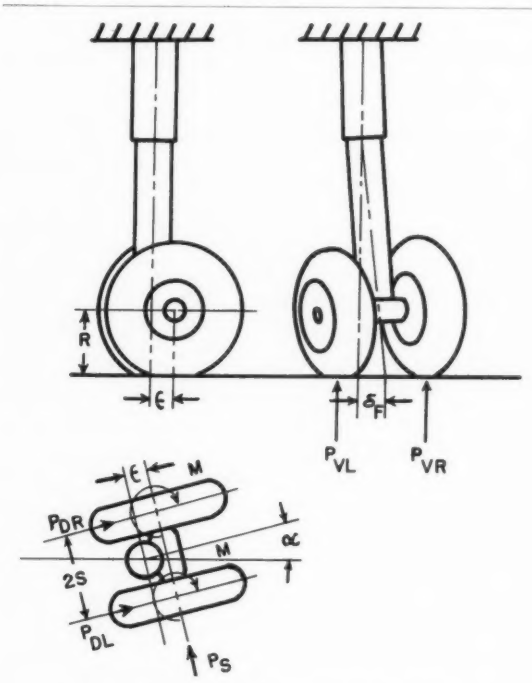

FIG 1. Landing gear with co-rotating wheels.

M is the torque applied to the dynamic system as the tire twists. The twist implies that the tire is cornering as it rolls. We can then write M in terms of the cornering angle:

$$M = \bar{K}_2\sigma \quad (13)$$

where $\bar{K}_2 = nK_2$; n is the number of wheels (1 or 2) and K_2 is the torsional stiffness of a single tire.

Eqs. (12) and (13) have resulted in the introduction of two new variables. Eq. (25) of reference 1 defines a linear differential equation for the straight-line rolling behavior of a pneumatic tire. When this is modified to include the effects due to rolling in a curved path, we obtain the following:

$$(d\sigma/dx) + c_2\sigma = c_1\Delta - (d\alpha/dx)$$

If we assume simple harmonic motion, this equation can be written as

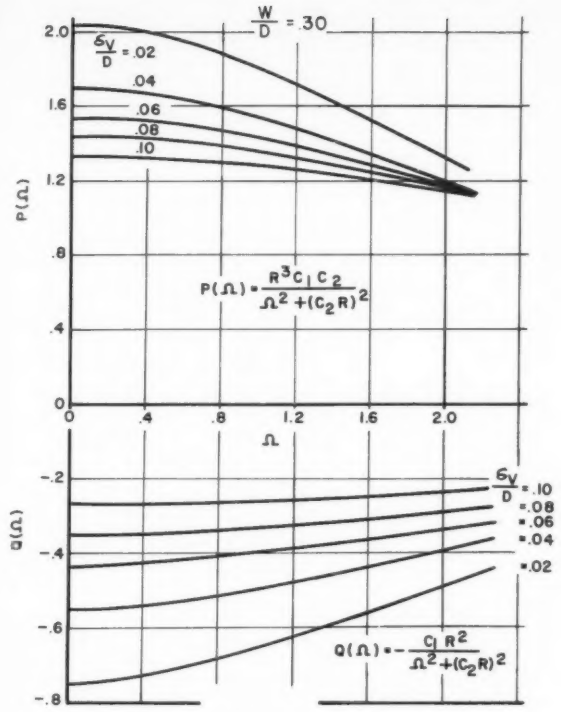

FIG. 2. $P(\Omega)$ and $Q(\Omega)$ vs Ω.

$$\sigma = [P(\Omega) + i\Omega Q(\Omega)](\Delta/R) + \left[\frac{\Omega^2 Q(\Omega)}{c_1 R^2} - \frac{i\Omega P(\Omega)}{c_1 R^2}\right][\bar{\alpha}_F{}', 1]\{q, \alpha\} \quad (14)$$

where

$$P(\Omega) = \frac{R^3 c_1 c_2}{\Omega^2 + (c_2 R)^2}$$

$$Q(\Omega) = -\frac{c_1 R^2}{\Omega^2 + (c_2 R)^2}$$

The functions P and Q may be tabulated for any tire as functions of Ω for any vertical deflection of the tire. Figs. 8 and 9 of reference 1 provide some information that may be used in evaluating P and Q. The value of P and Q for the tire used in an example is given in Fig. 2.

The most fundamental equation, yet to be defined, expresses the condition that there shall be no skidding of the tire normal to the direction of progress of the wheel. This means that the sum of the velocity components of all degrees of freedom at the tire-ground contact area normal to the path of progress defined by the wheel and the cornered tire must be zero:

$$\dot{\delta}_F + \dot{\Delta} + V(\alpha_F + \sigma) = 0$$

or

$$\left[\left(\frac{\bar{\delta}_F{}'}{R} i\Omega + \bar{\alpha}_F{}'\right), \left(\frac{\epsilon}{R} i\Omega + 1\right), i\Omega, 1\right] \times \{q, \alpha, \Delta/R, \sigma\} = 0 \quad (15)$$

Sufficient equations have now been defined so that we could solve for the shimmy of a nose gear, provided the wheels were not co-rotating. We shall now define the equation for the torque $(P_{DL} - P_{DR})s$ which will complete the requirements for solution of the shimmy problem of a nose gear with dual co-rotating wheels. We will consider the general case in which the two wheels are connected by a flexible torsion shaft. This will introduce an additional degree of freedom into our problem. If we consider symmetry and small displacements, then $-P_{DL} = P_{DR}$, and we can consider each half of the shaft between the wheels as a mirror image of the other. If the twist in the shaft relative to its node is ϕ, then

$$I_p \ddot{\phi} + k_\phi \phi = RP_{DR} \quad (16)$$

where I_p is the polar moment of inertia of a wheel about its axle, and k_ϕ is twice the torsional spring rate of the shaft connecting the two wheels. We may now write P_D in terms of the slip coefficient of the tire, K_S:

$$P_{DR} = K_S \frac{\Delta V}{V} = K_S \left(\frac{\dot{\alpha}_F s}{V} - \frac{\dot{\phi} R}{V} - \frac{\theta_F s}{3R}\right)$$

or

$$P_{DR} = K_S \left[\left(i\Omega \frac{s}{R} \bar{\alpha}_F{}' - \frac{\bar{\theta}_F{}' s}{3R}\right), \frac{i\Omega s}{R}, -i\Omega\right] \times \{q, \alpha, \phi\} \quad (17)$$

To obtain K_S use may be made of Eq. (90) of reference 2. In the term $\theta_F s/3R$ of Eq. (17), the factor of $1/3$ results from consideration of the effective rolling radius, as is explained in reference 2. We will now introduce Eq. (17) into Eq. (16):

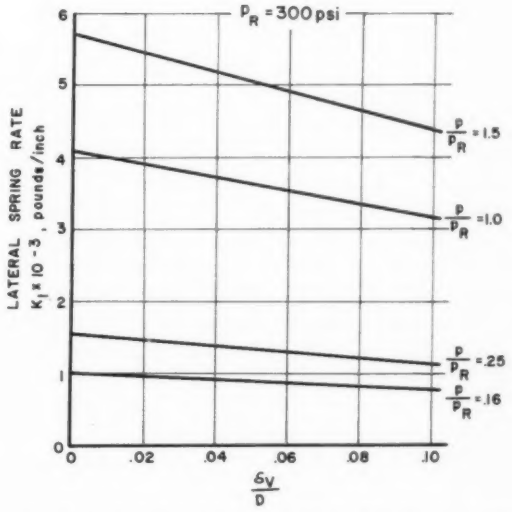

FIG. 3. Lateral spring rate of an 18 × 5.5 tire vs vertical deflection.

$$(-\omega^2 I_p + i\Omega K_S R + k_\phi)\phi = RK_S\left[\left(i\Omega\,\frac{s}{R}\,\bar{\alpha}_F' - \frac{s\bar{\theta}_F'}{3R}\right),\ i\Omega\,\frac{s}{R}\right]\{q,\ \alpha\} \tag{18}$$

and

$$(P_{DL} - P_{DR})s = 2sK_S\left[\left(i\Omega\,\frac{s}{R}\,\bar{\alpha}_F' - \frac{s}{3R}\,\bar{\theta}_F'\right),\ i\Omega\,\frac{s}{R},\ -i\Omega\right]\{q,\ \alpha,\ \phi\} \tag{19}$$

It is now possible to combine Eqs. (9), (11), (12), (13), (14), (15), (18), and (19) to obtain a system of equations for the shimmy of a dual-wheeled co-rotational landing gear. If we define a reference stiffness k_R and a reference mass m_0, these equations can be written in nondimensional form as follows:

$$\left(-\left(\frac{\omega^2 m_0}{k_R}\right)\left\{\begin{bmatrix} \frac{M_{ij}}{m_0} & \frac{S_{\alpha j}}{m_0 R} & 0 & 0 & 0 \\ \frac{S_{\alpha i}}{m_0 R} & \frac{I}{m_0 R^2} & 0 & 0 & 0 \\ 0 & 0 & 0 & 0 & \frac{2I_p}{m_0 R^2} \\ 0 & 0 & 0 & 0 & 0 \\ 0 & 0 & 0 & 0 & 0 \end{bmatrix} - \frac{I_W i}{m_0 R^2 \Omega}\begin{bmatrix} (\bar{\theta}_F\bar{\alpha}_F' - \bar{\alpha}_F\bar{\theta}_F')R^2 & \bar{\theta}_F R & 0 & 0 & 0 \\ -\bar{\theta}_F' R & 0 & 0 & 0 & 0 \\ 0 & 0 & 0 & 0 & 0 \\ 0 & 0 & 0 & 0 & 0 \\ 0 & 0 & 0 & 0 & 0 \end{bmatrix}\right\}\right.$$

$$+\begin{bmatrix} \frac{k_{ij}}{k_R} + 2s^2\left(\frac{K_v}{k_R}\,\bar{\theta}_F\bar{\theta}_F' - \frac{K_S}{Rk_R}\,\bar{\alpha}_F\bar{\theta}_F'\right), & 0, & -\frac{\bar{\delta}_F}{R}, & -\bar{\alpha}_F, & 0 \\ -\frac{2s^2K_S\bar{\theta}_F' R}{3R^3k_R}, & \frac{Rm(\omega)}{k_R R^2}, & -\frac{\epsilon}{R}, & -1, & 0 \\ \frac{2sK_S\bar{\theta}_F' R}{3R^2k_R}, & 0, & 0, & 0, & \frac{2k\phi}{R^2k_R} \\ \bar{\alpha}_F' R, & 1, & 0, & \frac{k_R R^2}{\bar{K}_2}, & 0 \\ \frac{\bar{K}_2\Omega^2 QR\bar{\alpha}_F'}{k_R R^2 c_1 R^2}, & \frac{\bar{K}_2\Omega^2 Q}{k_R R^2 c_1 R^2}, & \frac{\bar{K}_2 P}{\bar{K}_1 R^2}, & -1, & 0 \end{bmatrix}$$

$$\left.+\,i\Omega\begin{bmatrix} \frac{2s^2K_S\bar{\alpha}_F\bar{\alpha}_F' R^2}{R^3k_R}, & \frac{2s^2K_S\bar{\alpha}_F R}{R^3k_R}, & 0, & 0, & \frac{-2sK_S\bar{\alpha}_F R}{R^2k_R} \\ \frac{2s^2K_S\bar{\alpha}_F' R}{R^3k_R}, & \frac{2s^2K_S}{R^3k_R} + \frac{Im(\omega)}{\Omega R^2 k_R}, & 0, & 0, & \frac{-2sK_S}{R^2k_R} \\ -\frac{2sK_S\bar{\alpha}_F' R}{R^2k_R}, & -\frac{2sK_S}{R^2k_R}, & 0, & 0, & \frac{2RK_S}{R^2k_R} \\ \bar{\delta}_F', & \frac{\epsilon}{R}, & \frac{R^2k_R}{R^2\bar{K}_1}, & 0, & 0 \\ -\frac{\bar{K}_2 P\bar{\alpha}_F' R}{k_R R^2 c_1 R^2}, & -\frac{\bar{K}_2 P}{k_R R^2 c_1 R^2}, & \frac{\bar{K}_2 Q}{\bar{K}_1 R^2}, & 0, & 0 \end{bmatrix}\right)\begin{bmatrix} \frac{q}{R} \\ \alpha \\ \frac{RP_S}{k_R R^2} \\ \frac{M}{k_R R^2} \\ \phi \end{bmatrix} = 0 \tag{20}$$

Eqs. (20) are a set of linear homogeneous simultaneous equations in ω, which can be solved if the physical parameters for the landing gear are known and a value of the shimmy parameter Ω is selected. For the landing gear with dual co-rotating wheels, $R_m(\omega) + iI_m(\omega)$ will usually be zero, but the imaginary part may be retained as a variable to be used to make ω real as is required to satisfy our basic assumption of simple harmonic motion. If a co-rotating design is not used, a shimmy damper will usually be required, in this case specific functional relations can be defined for $R_m(\omega) + iI_m(\omega)$. In many cases, however, it will be desirable to solve for $I_m(\omega)$ to determine the damping requirement for shimmy prevention. As one example of the form of $R_m(\omega) + iI_m(\omega)$ which may be used in specific problems, the nose gear is assumed to be restrained against castoring by a linear damper with a damping coefficient C_β in series with a spring of spring constant k_β. $R_m(\omega) + iI_m(\omega)$ can then be expressed as follows, and used directly in Eq. (20):

$$R_m(\omega) + iI_m(\omega) = \frac{\omega^2 C_\beta^2 k_\beta}{\omega^2 C_\beta^2 + k_\beta^2} + \frac{i\omega k_\beta^2 C_\beta}{\omega^2 C_\beta^2 + k_\beta^2} \tag{21}$$

If the approach used in flutter analysis is used for solution, a variable X will be defined for ω^2 such that $X = \omega^2(1 - ig)$, and the complex polynomial in X will be solved for several values of Ω. When $g = 0$ a solution for the shimmy

system will be assumed to exist. Regardless of how the system of equations are solved, certain problems will exist in handling the shimmy damper in the equations. However, these problems can be solved by a number of methods familiar to the flutter analyst.

Stability Criteria

It is sometimes convenient to obtain analytic expressions for the damping required to stabilize the landing gear against shimmy, in order to gain information on how the system can be changed in design to minimize shimmy problems. It turns out that certain simplifying assumptions are required if the resulting analytic expressions are to be simple enough that conclusions may be drawn from them. Two assumptions are often used: (1) The tires are rigid, insofar as lateral rolling behavior is assumed, and (2) The landing gear shock strut is assumed to be rigid against lateral motion. The dual-wheeled co-rotational nose-gear system will be investigated with these two assumptions.

Stability Criteria—Rigid Tires

The basic equations to be investigated are Eqs. (20) which can be simplified by assuming that $\bar{K}_1 = \infty$, $k_\phi = \infty$, $\bar{K}_2 = 0$ and that only one lateral degree of freedom is present. It is assumed that $\bar{\theta}_F = \theta$, $\bar{\alpha}_F = 1.0$, $\bar{\alpha}_F = 0$, and $R_m(\omega) = 0$. Further it is assumed that $I_m(\omega) = \omega C_d$. From this point it is possible to obtain expressions for C_d and ω^2.

$$\frac{\epsilon C_d}{V} = \left(I - S_{\alpha_1}\epsilon - \frac{I_w\theta R}{\Omega^2}\right) - \frac{2s^2K_S\epsilon}{V^2} \qquad \omega^2 = \frac{\epsilon^2(k_{11} + 2s^2k_t\theta^2) + (2s^2K_S/R)(\theta\epsilon/3)}{I - 2\epsilon S_{\alpha_1} + M_{11}\epsilon^2 - (I_w\theta R/\Omega^2)} \qquad (22), (23)$$

$$\Omega = \omega R/V$$

Stability Criteria—Rigid Strut

When the strut is considered rigid, $k_{ij} = \infty$, and the first row and column of Eqs. (20) disappear. We will further assume that $k_\phi = \infty$ and that $I_m(\omega) = \omega C_d$, while $R_m(\omega) = 0$. The type of shimmy described by these simplifications is the tire-type shimmy treated by de Carbon in reference 3 and by Kantrowitz in reference 4.

$$\frac{2s^2K_S + VC_d}{R^3\bar{K}_1} = -\frac{[(\epsilon/R) + (\bar{K}_2/\bar{K}_1R^2)P][P(\epsilon/R) - (1 + Q)] + (\bar{K}_2/\bar{K}_1R^2)Q[P + \Omega^2(\epsilon/R)(Q + 1)]}{P^2 + \Omega^2(Q + 1)^2} + \frac{(\epsilon/R)[P^2 + \Omega^2Q(1 + Q)] - (\bar{K}_2/\bar{K}_1R^2)\Omega^2P}{c_1R^2[P^2 + \Omega^2(Q + 1)^2]} \qquad (24)$$

$$\frac{V^2I}{\bar{K}_1R^4} = \frac{[(\epsilon/R) + (\bar{K}_2/\bar{K}_1R^2)P][P + \Omega^2(1 + Q)(\epsilon/R)] - \Omega^2(Q\bar{K}_2/\bar{K}_1R^2)[(\epsilon/R)P - (Q + 1)]}{\Omega^2[P^2 + \Omega^2(Q + 1)^2} - \frac{(\epsilon/R)P + (\bar{K}_2/\bar{K}_1R^2)[P^2 + \Omega^2Q(1 + Q)]}{c_1R^2[P^2 + \Omega^2(Q + 1)^2]} \qquad (25)$$

where $\Omega = \omega R/V$.

The right-hand sides of Eqs. (24) and (25), except for the nondimensional trail ϵ/R, are functions of tire parameters only. By use of references 1 and 2 it is possible to define the limits of tire-type shimmy without regard to the actual landing gear involved.

Illustrative Example

The method of shimmy analysis developed in this report has been applied to a landing gear with co-rotational wheels which did shimmy. In 1952 it was decided to evaluate a dual-wheeled nose gear with co-rotational wheels without a shimmy damper on the F7U-3 airplane. It was thought that this system could have merit in that it would reduce the weight and complexity of the nose-gear system, and that possibly these factors would more than compensate for the increased problems of ground handling associated with a dual, co-rotating wheel system. At that time it was believed that the constraint associated with the co-rotation of the wheels would preclude the possibility of shimmy. Early in the ground test program this dual-wheeled landing gear with co-rotating wheels shimmied at a frequency of about 13 cps at an airspeed of 60 knots as measured by the airspeed system. All attempts to increase the shimmy speed failed and the design was abandoned. The example used in this paper is based on the F7U-3 nose-gear design.

In the illustrative example the following items will be investigated:

(a) The damping required to prevent shimmy if the tire cornering characteristics are the primary cause of shimmy (strut considered rigid).

(b) The damping required to prevent shimmy if the lateral flexibility of the strut is the primary cause of shimmy (tire considered laterally rigid).

(c) The damping required to prevent shimmy if both the tire and the strut flexibility, in dual-wheeled landing gear with wheels free to rotate independently, are important.

(d) The damping required to prevent shimmy when

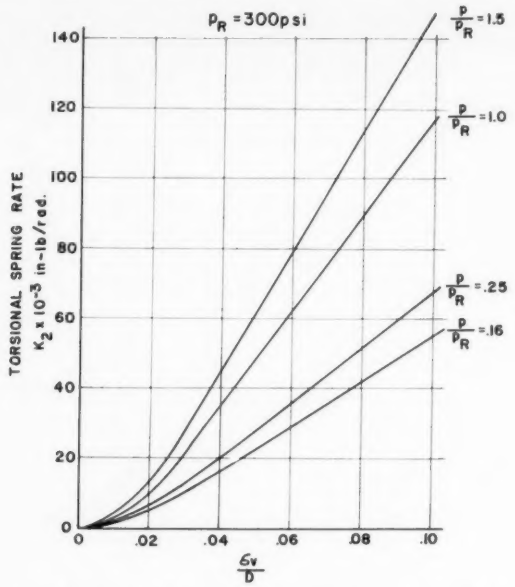

FIG. 4. Torsional spring rate of 18 × 5.5 tire vs vertical deflection.

the wheels are restrained to co-rotate and the lateral tire-flexibility effects are included.

(e) The effects of tire servicing pressure and vertical displacement on the shimmy speed, with tire-cornering effects taken into consideration.

(f) The effect on the shimmy speed of increasing the lateral stiffness of the strut when both lateral stiffness of the strut and cornering of the tire are considered and the wheels are restrained to co-rotate.

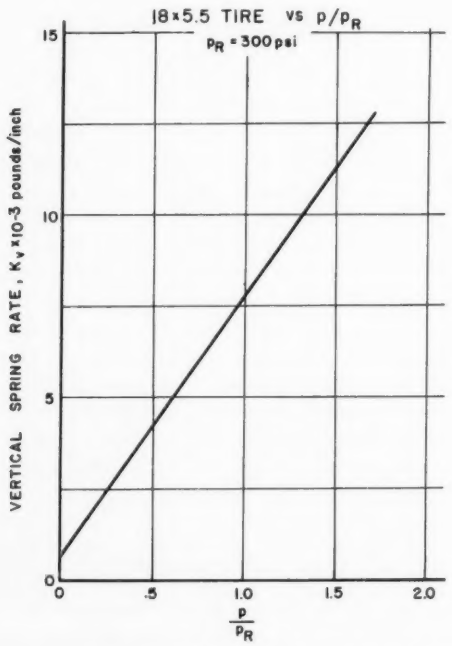

FIG. 5. Vertical spring rate of 18 × 5.5 tire vs p/p_R.

The physical parameters for the landing gear to be analyzed are listed below. It is considered that one lateral degree of freedom is sufficient to define the flexibility of the landing gear.

I_w	= 2.8 lb-in.-sec^2	ϵ	= 3 in.
I	= 14.5 lb-in.-sec^2	k_ϕ	= ∞
M_{11}	= 0.35 lb-sec^2/in.	$R_m(\omega)$	= 0
$S_{\alpha 1}$	= 0.57 lb-sec^2	$I_m(\omega)$	= ωC_d
$\bar{\theta}_F$	= 0.04 1/in.	$P(\Omega)$, $Q(\Omega)$	as in Fig. 2
$\bar{\alpha}_F$	= 0	K_1	as in Fig. 3
k_{11}	= 1,040 lb/in.	K_2	as in Fig. 4
$2s$	= 14 in.	K_v	as in Fig. 5
R	= 9 in.	K_S	as in Fig. 6
$\bar{\delta}_F$	= 1.0		

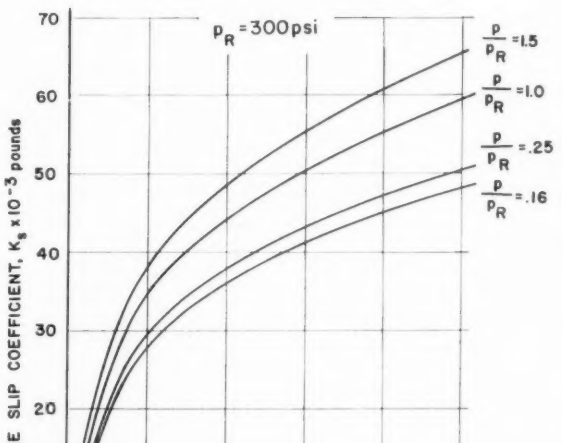

FIG. 6. Tire slip coefficient of 18 × 5.5 tire vs tire vertical deflection.

Tire Shimmy

Tire shimmy was investigated using the values of $P(\Omega)$ and $Q(\Omega)$ from Fig. 2, the curves in which are derived from Eq. (24), and the values of ϵ and R compatible with this example. The damping requirements are shown in nondimensional form in Fig. 7. These results show that the damping required to prevent tire shimmy increases with the vertical deflection of the tire. It also can be shown that for realizable values of the tire-slip coefficient K_S, tire shimmy is unlikely, and that the behavior of the landing gear in the example cannot be explained by consideration of the tire alone.

Flexible Strut Shimmy With the Wheels Free

The damping required to prevent shimmy on the landing gear of the example when the wheels are free

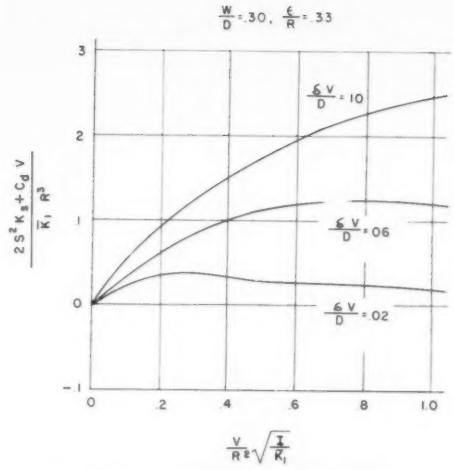

FIG. 7. Damping required to prevent tire shimmy vs speed.

and the strut lateral degree of freedom is included in the analysis, is shown in Fig. 8. When the tires are assumed to be laterally rigid (no cornering) more damping is required to prevent shimmy than when the cornering effects are included. The reduction in damping required to prevent shimmy as the speed increases above about 80 knots is due to gyroscopic coupling effects between the lateral bending of the strut and the castoring of the wheel system. The results found in this study are consistent with those found by other investigators.

Shimmy With Co-Rotating Wheels

When the case of the wheels locked together by a rigid torsion shaft is analyzed, it is found that shimmy is effectively stopped at low speeds but at higher speeds, where shimmy does occur, more damping is required to stabilize the shimmy than would be required if the wheels were not co-rotating. These results are presented in Fig. 9. Furthermore, as can be seen in Fig. 10, the shimmy speed does not change significantly if the load on the tire is increased or the tire servicing pressure is changed. These results are in general agreement with the results found in the test program on the F7U-3 nose gear. It can also be seen from this analysis that tire-cornering effects tend to increase the speed at which shimmy occurs, but that once it occurs more damping is required to contain the shimmy than would be predicted on the basis of an analysis made with the tire assumed to be laterally rigid.

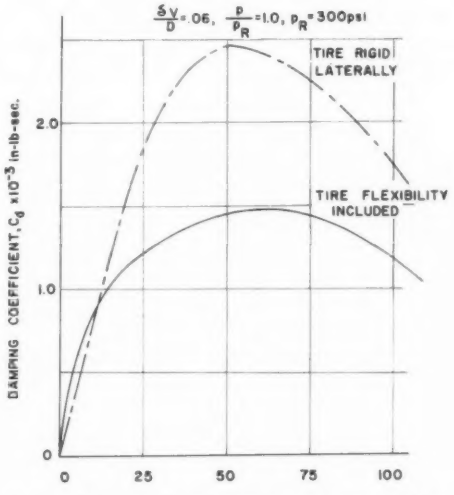

FIG. 8. Damping coefficient required to prevent shimmy on nose gear of example with dual wheels free to rotate independently.

Effect of Strut Stiffness on Shimmy of a Landing Gear With Co-Rotating Wheels

The studies presented in Figs. 9 and 10 show that the shimmy of a landing gear with dual co-rotating wheels is relatively insensitive to changes in tire servicing pressure and vertical deflection of the tire. Fig. 11 shows that when the strut is stiffened the shimmy speed increases rapidly to levels which would make the landing-gear system satisfactory. This result would not be expected if the shimmy were governed by strut stiffness alone; Eq. (22) shows that if the tire is assumed to be laterally rigid (cornering effects neglected) then the strut stiffness has little effect on the shimmy speed. Thus we can conclude that tire-cornering behavior plays a significant role in determining the shimmy speed of a co-rotating wheel system. We can also conclude that a dual, co-rotational

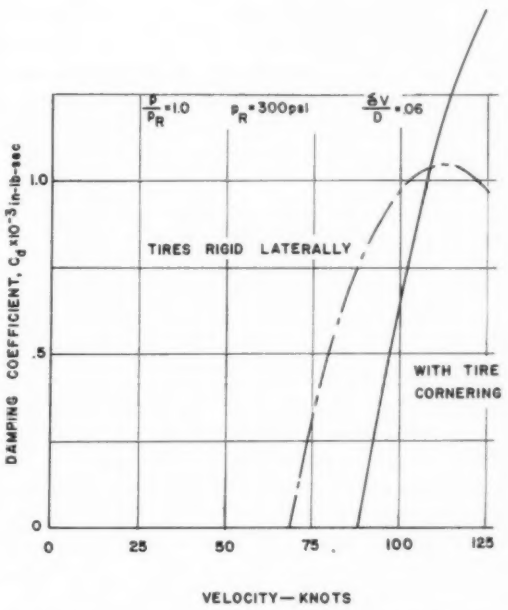

FIG. 9. Damping coefficient required to prevent shimmy on landing gear of example with the wheels co-rotating.

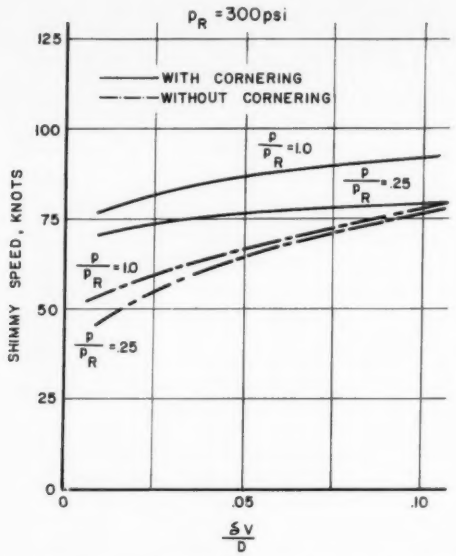

FIG. 10. Shimmy speed vs vertical deflection for landing gear of example with co-rotating wheels.

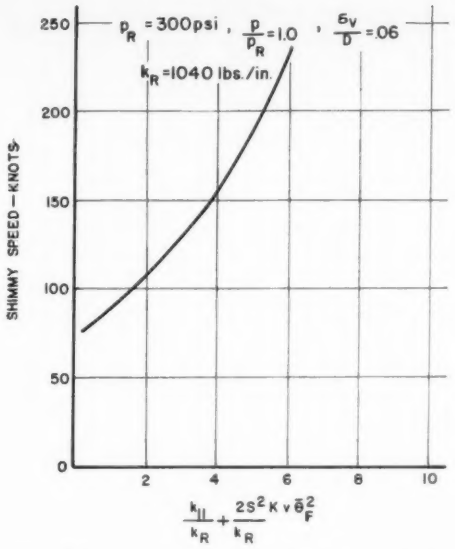

FIG. 11. Shimmy speed vs lateral stiffness of the landing gear strut for the landing gear of example with co-rotating wheels.

wheel system can be designed to be shimmy-free if the strut is sufficiently stiff. The stiffness values required are realizable in most conventional nose gears.

Conclusions

(1) Equations have been developed which explain the shimmy behavior of dual-wheeled landing gear systems with co-rotating wheels.

(2) Solution of the shimmy equations by transformation to the frequency domain in a manner similar to the approach used in flutter analysis is practical and effective.

(3) The cornering behavior of the tire plays a key role in the shimmy analysis of a landing gear with dual co-rotating wheels.

(4) The method of analysis is not restricted to dual-wheeled landing gears or landing gears with co-rotating wheels, and is thus more general than the methods of analysis currently in use.

References

[1] Stevens, J. E., *Relaxation Characteristics of Pneumatic Tires*, Journal of the Aero/Space Sciences, Vol. 26, No. 6, pp. 343–350, June 1959.

[2] Smiley, R. F., and Horne, W. B., *Mechanical Properties of Pneumatic Tires with Special References to Modern Aircraft Tires*, NACA TN 4110, January 1958.

[3] Bourcier de Carbon, Christian, *Analytical Study of Shimmy of Airplane Wheels*, NACA TM 1337, 1952.

[4] Kantrowitz, Arthur, *Stability of Castoring Wheels for Aircraft Landing Gears*, NACA Report 686, 1940.

[5] Moreland, W. J., *The Story of Shimmy*, Journal of the Aeronautical Sciences, Vol. 21, No. 12, pp. 793–808, December 1954.

✦ ✦ ✦

Stagnation-Point Boundary Layer

(*Continued from page 611*)

[2] Lykoudis, P. S., *On a Class of Magnetic Laminar Boundary Layers*, 1958 Heat Transfer and Fluid Mechanics Institute preprint, June 1958.

[3] Bush, W. B., *Compressible Flat-Plate Boundary-Layer Flow with an Applied Magnetic Field*, Journal of the Aero/Space Sciences, Vol. 27, No. 1, pp. 49–58, January 1960.

[4] Bush, W. B., *On the Laminar Compressible Boundary Layer in the Presence of an Applied Magnetic Field*, Space Technology Laboratories TR-59-0000-00668, October 2, 1959.

[5] Bush, W. B., *A Note on Magnetohydrodynamic-Hypersonic Flow Past a Blunt Body*, Journal of the Aero/Space Sciences, Vol. 26, No. 8, pp. 536–537, August 1959.

Microcards for Volumes 1–5 Available

Microcards for Volumes 3–5 of the JOURNAL are now available (Vols. 1 and 2 were republished in this form earlier). All five volumes are priced at $5.50 each, and are obtainable through:

J. S. Canner & Company, Inc.
Boston, Roxbury 20, Mass.

Electrode Boundary Layers in Direct-Current Plasma Accelerators†

JACK L. KERREBROCK*
California Institute of Technology

Summary

One of the problems that must be faced in the development of direct-current plasma accelerators is that of boundary-layer growth on the electrode surfaces. These surfaces must be maintained at a somewhat lower temperature than is desirable in the bulk of the gas flow. The associated reduction in electrical conductivity near the electrode surface, together with the continuous current through the boundary layer, may result in greatly augmented Joule heating near the surface, and increased heat transfer.

This phenomenon is treated within the framework of boundary-layer theory. It is found that similar solutions for the thermal and viscous boundary layers exist for a certain class of accelerated flows in which the velocity varies as a power of the streamwise coordinate. The solutions show that the heat-transfer rate at Mach numbers near unity may be as much as ten times that which would be expected for a normal boundary layer.

At higher Mach numbers, the similarity is not precisely valid; however, the analysis indicates qualitatively that a stagnation enthalpy overshoot may occur in the high-temperature portion of the boundary layer as a result of the electromagnetic acceleration.

Introduction

MANY OF THE DEVICES which have been suggested for the electromagnetic acceleration of ionized gases for propulsive and other purposes require the presence of electrodes in contact with the flowing plasma. In such devices there may exist a type of boundary-layer flow in which there is an electric current normal to the wall and a magnetic field parallel to the wall and normal to the current. In order that it be a satisfactory conductor, the gas must be at a rather high temperature—at least 2,000°K—and if an appreciable current is to pass from the electrode to the gas, there must be intimate contact of the two. Thus a severe heat-transfer problem seems likely to arise. As will be demonstrated, the effect of the electrical interaction with the fluid, particularly the current flow normal to the wall, is to compound this heating problem, which would be severe even for a normal boundary layer.

Received April 20, 1960.

† This research was supported by the United States Air Force through the Air Force Office of Scientific Research of the Air Research and Development Command, under Contract No. AF 49(638)-758.

* Senior Research Fellow, Daniel and Florence Guggenheim Jet Propulsion Center.

The author wishes to express his gratitude to Prof. Frank E. Marble who, through many discussions, contributed a great deal to the formulation and interpretation of this work.

The current and magnetic field influence the boundary layer in three ways. Joule heating acts as a heat source. Energy is transported by the electron current. The crossed current and magnetic field yield a body force which, like that resulting from a longitudinal pressure gradient, is a constant per unit volume. Of these three effects, the Joule heating is the most unusual. The heating rate varies inversely as the electrical conductivity, which in turn may be a strong function of the temperature. Near the electrode surface, where the temperature must be somewhat below that of the gas in the free stream, the conductivity is low, and the Joule-heating rate correspondingly high. The increased heating rate near the wall will lead to a higher temperature gradient at the wall, and increased heat transfer for a given wall temperature.

The objective of the present work is to explore this situation within the framework of boundary-layer theory, with the particular goal of estimating the magnitude of the heat transfer to be expected. Certain limitations of applicability arise from the nature of the boundary-layer theory itself, others from specific assumptions. In the first category, the continuum approximation requires that the mean free path of the electrons be small compared to the boundary-layer thickness, hence that the pressure be high—a requirement which will be stated more precisely later. It is also necessary that the free-stream and boundary-layer flows be separable—i.e., that the former be influenced to only a small extent by the latter. The fluid mechanical implications of this requirement are well known. Electrically, it implies that the current normal to the wall be determined by the free-stream flow, hence that the resistance of the boundary layer be small compared to that of the free stream. The adoption of a model requiring these conditions for its validity is not meant to imply that they are the best operating conditions for a plasma accelerator; certainly it is not possible to define such conditions at the present time. The intent is rather to study some of the problems which are likely to occur for one possible choice of operating conditions.

As to specific assumptions, the most important ones concern the magnitude and behavior of the conductivity. It is assumed that the plasma is in thermal equilibrium at the local temperature and pressure. In view of the requirement for good electrical conductivity at as low a temperature as possible, "seeding" with an alkali metal is postulated; further,

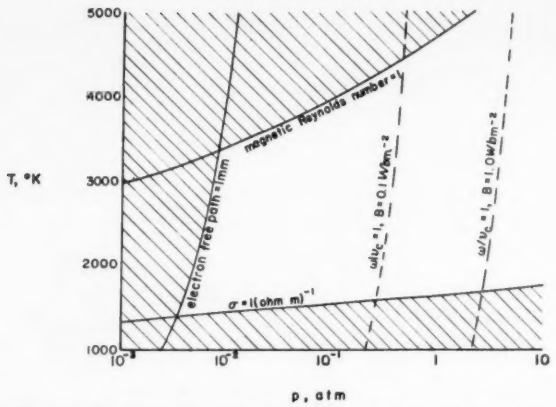

FIG. 1. Region of applicability of the analysis, as determined by the requirements for a small electron mean path, a conductivity greater than 1 (ohm m)$^{-1}$, and a magnetic Reynolds number less than unity. Lines along which the Hall parameter ω/ν_e is unity are also given.

it is assumed that the concentration of seeding material is high enough so that only a small fraction of it is ionized. Under these conditions the electron concentration, and the conductivity, vary exponentially as the negative reciprocal of the temperature. This dependence of the conductivity on the temperature is of course crucial; while the actual variation is probably overestimated by the present model, it is felt that the analysis will at least give an upper limit to the effect of the current on the heat-transfer rate. The conductivity is assumed to be sufficiently low that the magnetic Reynolds number is small. As is well known, a magnetic field may in this case be applied within the fluid by external means, the magnetic field resulting from induced currents being small compared to it. Thus, the fluid mechanical equations are uncoupled from Maxwell's equations.

The conductivity is taken to be scalar—i.e., it is assumed that the collision frequency of the electrons is large compared to their Larmor frequency. This assumption is consistent with the continuum approximation in requiring that the pressure be "high," but may be more restrictive. The existence of Hall currents, in this case currents parallel to the wall, would invalidate the usual boundary-layer assumptions by introducing a body force normal to the wall.

To provide a means for evaluating these various assumptions, and to make the boundary-layer calculations as concrete as possible, the calculations are referred to a particular type of accelerator flow. A channel of rectangular cross section, bounded on two sides by the electrodes and on the other two sides by insulating walls, is envisioned. In view of the severe heat-transfer conditions that are expected to arise, and the sensitivity of the electrical conductivity to temperature, it is assumed that the free-stream static temperature is constant. It is further postulated that the free-stream velocity varies as a power of the streamwise coordinate. In the channel flow approximation, these two conditions lead to simple, closed form solutions for the free-stream flow,[1] in which the interesting physical quantities all vary as powers of the streamwise coordinate. The result is that similar solutions exist for the boundary layer under some conditions.[2] They are in a sense analogous to the "wedge flow" solutions for the incompressible boundary layer. It is hoped that the understanding gained from these relative simple solutions may be carried over to other types of free-stream flow.

Formulation of the Boundary-Layer Problem

The dependence of the electrical conductivity on the magnetic field, electric field, and the state of the gas is of key importance to the present work; therefore, before the equations governing the boundary-layer flow are set down, a brief discussion of the conductivity is appropriate.

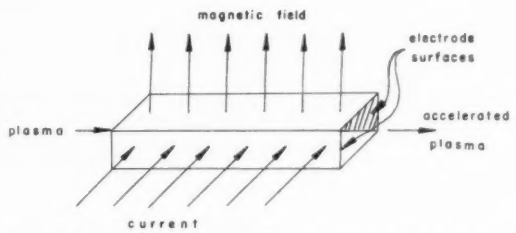

FIG. 2. Schematic diagram of direct-current plasma accelerator.

The Conductivity

An approach by the methods of kinetic theory[3,4] to the problem of diffusion of electrons in an ionized gas in the presence of a magnetic field leads to an expression relating the current $\mathbf{j}$, electric field $\mathbf{E}$, velocity $\mathbf{u}$, and magnetic field $\mathbf{B}$, which may be written as follows:

$$\mathbf{j} = \sigma\left(\mathbf{E} + \mathbf{u} \times \mathbf{B} + \frac{1}{en_e}\,\mathbf{j} \times \mathbf{B}\right) \qquad (1)$$

σ is the usual scalar conductivity, n_e is the electronic concentration, and e the electronic charge. The first two terms on the right will be immediately recognized as the effective electric field which acts on an electron traveling at the fluid velocity $\mathbf{u}$. The last term arises from the tendency for charged particles in the presence of a magnetic field to drift normal to an applied electric field—i.e., the Hall effect. It is the dependence of σ on the gas temperature and pressure that is of principal concern here, though some estimates of the importance of the Hall effect will be made later.

As was mentioned in the Introduction, a gas mixture at a relatively high pressure, such that the electronic mean free path is small compared to other characteristic lengths, is postulated, the mixture comprising a small mole fraction of an alkali metal in some inert gas.

Under such conditions it is consistent to assume that the electrons diffuse under the influence of the electric field, with a velocity which is related to the electric field strength by a proportionality constant, μ, called the mobility. Since the current is the product of the drift velocity, charge, and concentration of the electrons, the conductivity becomes $\sigma = \mu e n_e$.

According to simple mean free path arguments, μ is related to the collision frequency, ν_c, by $\mu = e/m_e\nu_c$.[5] If the collision cross section is constant in electron energy, as it is for helium and hydrogen at low electron energies,[5] then ν_c is directly proportional to the gas density and the electronic thermal speed. Thus if the electrons are in equilibrium with the gas, we may write

$$\mu/\mu_0 = (p_0/p)(T/T_0)^{1/2}$$

where the subscript 0 denotes some reference condition. If the electrons are in equilibrium with the gas, their concentration is given by the Saha equation:

$$n_e = [(2\pi m_e kT)^{3/2}/h^3]^{1/2}(n_a - n_e)^{1/2}e^{-I/2kT}$$

where n_a is the total concentration of the ionizable species, I is the ionization potential, k is Boltzmann's constant, and h is Planck's constant. The fraction n_e/n_a of the seeding material which is ionized thus satisfies an equation of the form

$$(n_e/n_a)^2 = [1 - (n_e/n_a)][f^2(T)/n_a]$$

For $n_e/n_a \ll 1$, $n_e/n_a \approx f(T)/n_a^{1/2}$, while for $f^2(T)/n_a \gg 1$, $n_e/n_a \approx 1$. Thus, n_e/n_a is in general a rather complicated function of T.

It is readily verified that for a given value of T, n_e, and hence σ, increases continuously as n_a increases, to that in view of the probable severity of the heat-transfer problem, and the resulting desirability of obtaining the necessary gas conductivity at as low a temperature as possible, it will be assumed that $n_e/n_a \ll 1$. It should be noted that this assumption results in the greatest possible sensitivity of σ to the temperature.

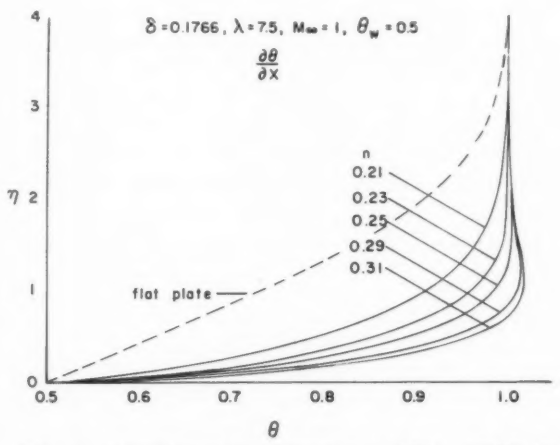

FIG. 3. Dimensionless temperature, $\theta = T/T_\infty$; profiles for $M_\infty = 1$ and several values of the exponent, n in $u_\infty = \alpha \times^n$; $\partial\theta/\partial\bar{x} = 0$.

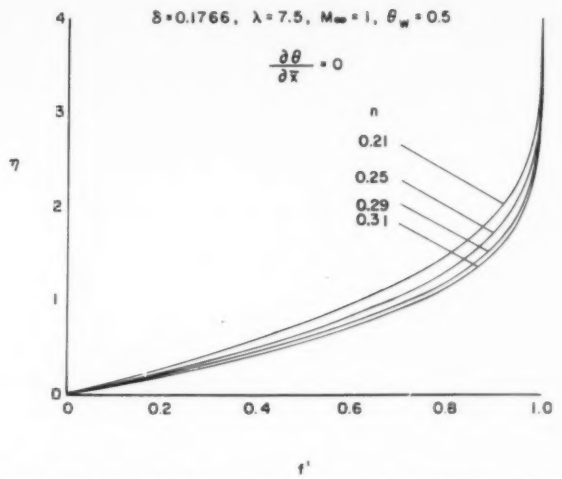

FIG. 4. Dimensionless velocity, $f' = u/u_\infty$; profiles for $M_\infty = 1$ and several values of the exponent n in $u_\infty = \alpha x^n$; $\partial\theta/\partial\bar{x} = 0$.

The resulting expression for the conductivity, again referred to a reference condition, is

$$\frac{\sigma}{\sigma_0} = \left[\frac{n_a/n}{(n_a/n)_0}\frac{p_0}{p}\right]^{1/2}\theta^{3/4}\,e^{-\lambda[(1/\theta)-1]}$$

where $\lambda = I/2kT_0$ and $\theta = T/T_0$. In the present work it will be assumed that the mole fraction of ionizable gas, n_a/n, is constant throughout the flow field, so that the final expression for the scalar conductivity is

$$\sigma/\sigma_0 = (p_0/p)^{1/2}\theta^{3/4}\,e^{-\lambda[(1/\theta)-1]} \qquad (2)$$

The importance of the Hall effect can perhaps best be seen by rewriting Eq. (1) for the case in which there is but one component of **B**, say B_z, and the current is in the x, y plane. In terms of components it then becomes

$$j_x = \frac{\sigma[E_x' - (\omega/\nu_c)E_y']}{1 + (\omega/\nu_c)^2} \qquad j_y = \frac{\sigma[E_y' + (\omega/\nu_c)E_x']}{1 + (\omega/\nu_c)^2}$$

where $\omega = eB_z/m_e$ is the Larmor frequency of the electrons, $E_x' = E_x + vB_z$, and $E_y' = E_y - uB_z$. If there is an electric field in only one direction, these equations state that currents will flow in both directions, the current normal to the electric field being ω/ν_c times as large as that along the field. As an example, in helium at atmospheric pressure and 3,000°K, with a magnetic field of 1 weber/m², ω/ν_c is about 3.6. If a current in, say, the y direction only is desired, the current in the x direction can in principle be suppressed by applying an appropriate field in the x direction;[6] however, this poses some practical difficulties.

Region of Validity of the Analysis

The assumptions of continuum flow, an equilibrium degree of ionization, low magnetic Reynolds number, and a scalar conductivity, prescribe a certain region of

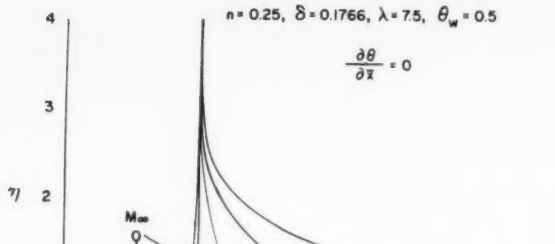

FIG. 5. Dimensionless temperature, $\theta = T/T_\infty$; profiles for $n = 1/4$ (constant flow-area) and several values of Mach number M_∞; $\partial\theta/\partial\bar{x} = 0$.

validity in the pressure-temperature-magnetic field strength space. These limitations are most easily discussed for a particular gas; as an example, helium seeded with one mole per cent of cesium will be considered.

If the continuum approximation is to be valid, the electronic mean free path must be small compared to, for example, the boundary-layer thickness. In Fig. 1, a line is drawn along which the mean free path of a thermal electron is one millimeter. Similarly, lines along which $\omega/\nu_c = 1$ are shown, for two values of magnetic field. The value $B = 1$ weber m^{-2} is about the maximum which is readily obtainable, while $B = 0.1$ is probably about the lowest value which permits significant acceleration of the gas. It seems that the suppression of the Hall effect requires quite high pressures.

A lower limit to the temperature is certainly set by the requirement for significant conductivity. Supposing 1 (ohm m)$^{-1}$ to be a reasonable lower limit for the conductivity, the corresponding line on Fig. 1 describes the lower limiting temperature. On the other hand, an upper limit to the conductivity, and to the temperature, is set by the requirement that the magnetic Reynolds number, $R_m = \mu_0\sigma l u$, be small. A line along which R_m, based on a length of one centimeter and sonic velocity in the gas, is unity, is shown at the top of Fig. 1.

The area within and to the right of the shaded portions is then the region of validity, as determined by all requirements except the suppression of the Hall effect, which requires pressures near or above one atmosphere.

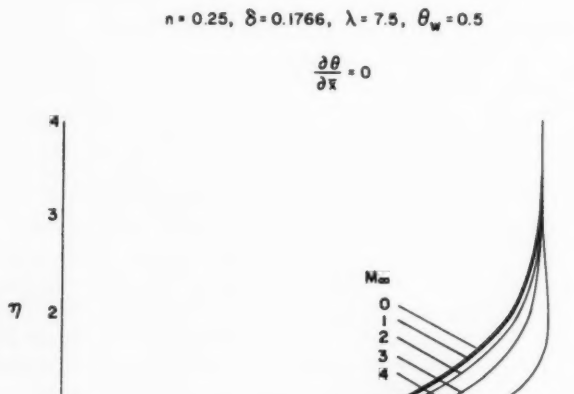

FIG. 6. Dimensionless velocity, $f' = u/u_\infty$; profiles for $n = 1/4$ (constant flow-area) and several values for Mach number M_∞; $\partial\theta/\partial\bar{x} = 0$.

Boundary-Layer Equations

Three modifications of the usual boundary-layer equations are necessary. The electromagnetic body force resulting from the crossed current and the magnetic field must be included in the momentum equation, so that it becomes

$$\rho\left(u\frac{\partial u}{\partial x} + v\frac{\partial u}{\partial y}\right) = \frac{\partial}{\partial y}\left(\mu\frac{\partial u}{\partial y}\right) - \frac{dp}{dx} + jB \quad (3)$$

The other two modifications occur in the energy equation. Energy is transported by the diffusing electrons in a temperature gradient, and the Joule heating effect constitutes a heat source, so that the equation is

$$\rho c_p\left(u\frac{\partial T}{\partial x} + v\frac{\partial T}{\partial y}\right) = \frac{\partial}{\partial y}\left(\kappa\frac{\partial T}{\partial y} + \frac{5kj}{2e}T\right) + \mu\left(\frac{\partial u}{\partial y}\right)^2 + u\frac{dp}{dx} + \frac{j^2}{\sigma} \quad (4)$$

Heat deposition in the boundary layer by ion-electron recombination is neglected on the grounds that the ion and electron concentrations are quite small. It may be argued that large recombination rates are possible because of the large electronic currents; however, it is the ion current which governs the rate of recombination in the boundary layer, and this is much smaller than the electron current, because of the much smaller mobility of the ions as compared to the electrons.

With the assumed scalar conductivity, the current is related to the effective electric field by

$$j = \sigma(E - uB) \quad (5)$$

Since the current is assumed to be determined by the external flow, and the magnetic Reynolds number is low, so that B is determined by outside influences, and is constant across the boundary layer, this equation determines E within the boundary layer, and by integration, the voltage drop across it.

The system of equations is completed by the usual

continuity and state equations

$$(\partial/\partial x)(\rho u) + (\partial/\partial y)(\rho v) = 0 \qquad (6)$$

and

$$p = \rho RT \qquad (7)$$

It is convenient to modify these equations slightly, using approximate results for the free-stream behavior to relate the terms involving the free-stream pressure gradient to other free-stream variables. We make the approximation of one-dimensional, or channel, flow in the free stream, in which case Eqs. (3) and (4) apply to the free stream if derivatives with respect to y are dropped. Thus, with values in the free stream denoted by the subscript ∞, Eq. (3) yields

$$\rho_\infty u_\infty (du_\infty/dx) = -dp/dx + jB$$

and the boundary-layer momentum equation becomes

$$\rho\left(u\frac{\partial u}{\partial x} + v\frac{\partial u}{\partial y}\right) = \frac{\partial}{\partial y}\left(\mu\frac{\partial u}{\partial y}\right) + \rho_\infty u_\infty \frac{du_\infty}{dx} \qquad (8)$$

Similarly, from Eq. (4),

$$\rho_\infty u_\infty c_p (dT_\infty/dx) = u_\infty (dp/dx) + j^2/\sigma_\infty$$

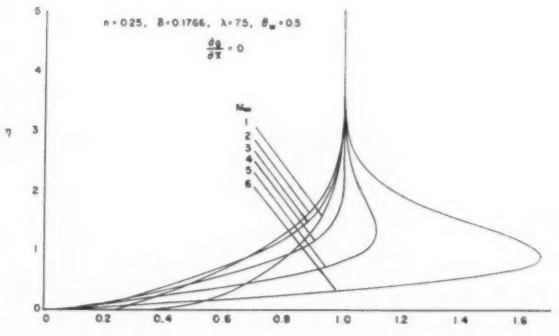

FIG. 7. Total enthalpy ratio, $g = H/H_\infty$; profiles for $n = 1/4$ (constant flow-area) and several values of Mach number M_∞; $\partial g/\partial \bar{x} = 0$.

and the boundary-layer energy equation becomes

$$\rho c_p\left(u\frac{\partial T}{\partial x} + v\frac{\partial T}{\partial y}\right) = \frac{\partial}{\partial y}\left(\kappa\frac{\partial T}{\partial y} + \frac{5kj}{2e}T\right) + \mu\left(\frac{\partial u}{\partial y}\right)^2 + \rho_\infty u_\infty c_p\left(\frac{dT_\infty}{dx}\right)\left(\frac{u}{u_\infty}\right) + \frac{j^2}{\sigma_\infty}\left(\frac{\sigma_\infty}{\sigma} - \frac{u}{u_\infty}\right) \qquad (9)$$

From Eq. (8) it is clear that, for a given free-stream velocity variation, the velocity boundary layer differs from a normal boundary layer only to the extent that it is influenced by the thermal boundary layer, through variation of ρ. However, the energy equation is qualitatively different from the usual boundary-layer energy equation in that it contains the heat source term, j^2/σ.

For low Mach number flow, this term is of dominant importance, outweighing the viscous dissipation and electronic conduction; however, at Mach numbers in excess of unity, the viscous dissipation becomes very important, and the energy equation is then best expressed in terms of the total enthalpy, $H = c_pT + u^2/2$. It becomes

$$\rho\left(u\frac{\partial H}{\partial x} + v\frac{\partial H}{\partial y}\right) = \frac{\partial}{\partial y}\left(\frac{\kappa}{c_p}\frac{\partial H}{\partial y} + \frac{5kj}{2e}T\right) + \left(1 - \frac{1}{Pr}\right)\frac{\partial}{\partial y}\left[\mu\frac{\partial}{\partial y}\left(\frac{u^2}{2}\right)\right] + \frac{j^2}{\sigma} + jBu \qquad (10)$$

where $Pr = c_p\mu/\kappa$ is the Prandtl number.

In addition to the term due to Joule heating, there is a term, jBu, which represents the energy addition to the fluid by the Lorentz force. The work done on the fluid by this force is reversible, in contrast to the energy addition by Joule heating.

Again dropping the derivatives with respect to y from Eq. (10), we find that

$$\rho_\infty u_\infty (dH_\infty/dx) = j^2/\sigma_\infty + jBu_\infty$$

and Eq. (10) becomes

$$\rho\left(u\frac{\partial H}{\partial x} + v\frac{\partial H}{\partial y}\right) = \frac{\partial}{\partial y}\left(\frac{\kappa}{c_p}\frac{\partial H}{\partial y} + \frac{5kj}{2e}T\right) + \left(1 - \frac{1}{Pr}\right)\frac{\partial}{\partial y}\left[\mu\frac{\partial}{\partial y}\left(\frac{u^2}{2}\right)\right] + \frac{j^2}{\sigma_\infty}\left(\frac{\sigma_\infty}{\sigma} - \frac{u}{u_\infty}\right) + \rho_\infty\frac{dH_\infty}{dx}(u) \qquad (11)$$

From this form of the equation it is clear that the reversible work will have a large effect on the boundary layer where dH_∞/dx and ρ_∞/ρ are large, as in the high temperature portion of the boundary layer at high Mach numbers.

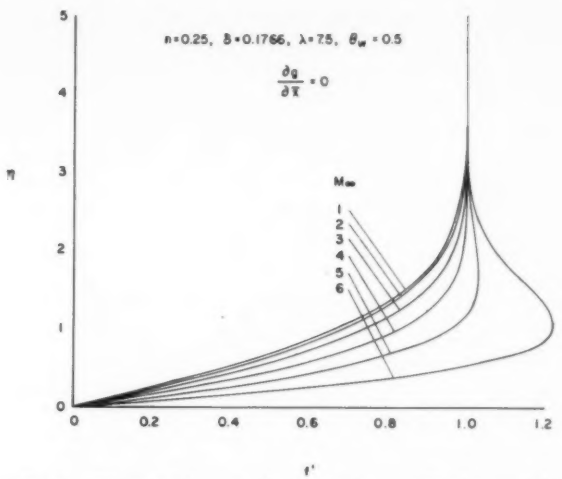

FIG. 8. Dimensionless velocity, $f' = u/u_\infty$; profiles for $n = 1/4$ (constant flow-area) and several values of Mach number M_∞; $\partial g/\partial \bar{x} = 0$.

The Free-Stream Flow

The addition of electromagnetic effects to the equations of motion leads to such a diversity of possible flow behavior that some rather specific model must be

adopted for the free-stream flow before boundary-layer calculations can be carried out. In the present case, flow in a channel, with crossed current and magnetic field, as shown schematically in Fig. 2, is postulated. Quasi-one-dimensional flow, with constant gas temperature, constant conductivity, and constant electric field, is assumed. It was shown in reference 1 that these assumptions lead to a particularly simple

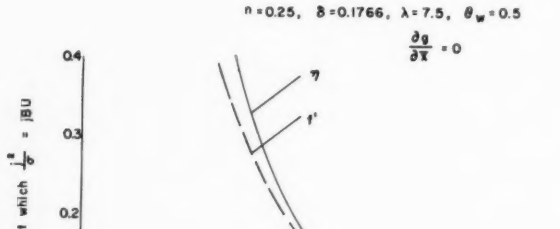

FIG. 9. Values of η and f' at which the rates of energy addition by Joule heating and by the Lorentz force are equal, as functions of Mach number M_∞ for $n = 1/4$ (constant flow-area).

solution of the momentum, energy, continuity, and current equations if the velocity varies as a power of x. Furthermore, the derived flow seems quite reasonable for a plasma accelerator. A constant gas temperature should result in the minimum heat transfer, consistent with adequate gas conductivity. It also insures that the energy added to the gas appears as kinetic, not thermal, energy. The approximation of constant conductivity seems reasonable, since the conductivity depends principally upon the temperature. It is not really necessary; the calculation can also be carried through if the conductivity is proportional to a power of x.

For the sake of completeness, the argument of reference 1 will be repeated here. In the channel flow approximation, for constant gas temperature the equations governing the flow are:

momentum: $$\rho_\infty u_\infty u_\infty' = -p' + jB \tag{12}$$

energy: $$u_\infty p' = -j^2/\sigma_\infty \tag{13}$$

continuity: $$\rho_\infty u_\infty A = \text{constant} \tag{14}$$

state: $$p = \rho_\infty R T_\infty \tag{15}$$

Ohm's law: $$j = \sigma_\infty(E_\infty - u_\infty B) \tag{16}$$

where the prime denotes differentiation with respect to x. Eliminating ρ_∞ from Eq. (12) with Eq. (15), then eliminating p' with Eq. (13) results in an expression for p:

$$p = RT_\infty E_\infty(j/u_\infty^2 u_\infty') \tag{17}$$

Differentiating this expression, and equating the result to the expression for p' obtained from Eq. (13), we find

$$\sigma_\infty R T_\infty E_\infty(j/u_\infty^2 u_\infty')' = -j^2/u_\infty$$

If $\zeta = j/u_\infty^2 u_\infty'$, this equation reduces to

$$\zeta'/\zeta^2 = -u_\infty^3(u_\infty')^2/\sigma_\infty R T_\infty E_\infty$$

and integrating from the origin,

$$\frac{1}{\zeta} - \frac{1}{\zeta(0)} = \frac{1}{\sigma_\infty R T_\infty E_\infty}\int_0^x u_\infty^3(u_\infty')^2\,dx \tag{18}$$

For $u_\infty = \alpha x^n$, this yields

$$\frac{1}{\zeta} = \frac{\alpha^5 n^2}{\sigma_\infty R T_\infty E_\infty}\left(\frac{x^{5n-1}}{5n-1}\right) \qquad n > 1/5$$

and from the definition of ζ,

$$j = (\sigma_\infty R T_\infty E_\infty/\alpha^2 n)(5n-1)x^{-2n} = \sigma_\infty E_\infty(5n-1)/n\gamma M_\infty^2 \tag{19}$$

where $M_\infty = u_\infty/(\gamma R T_\infty)^{1/2}$ is the Mach number. The pressure may now be computed from Eq. (17):

$$p = [\sigma_\infty(R T_\infty E_\infty)^2/\alpha^5][(5n-1)/n^2]x^{1-5n} \tag{20}$$

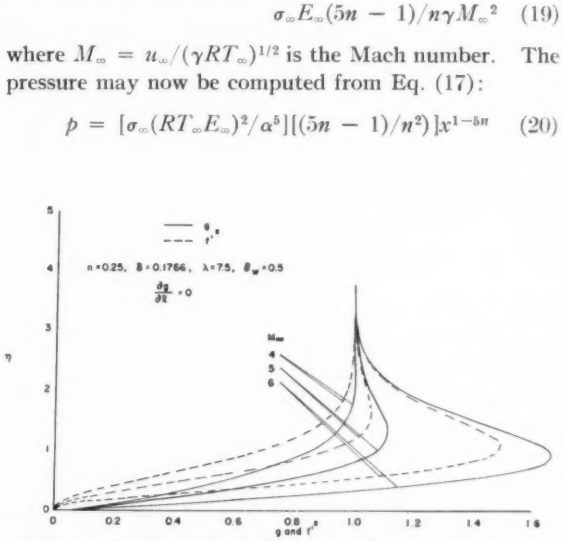

FIG. 10. Comparison of kinetic energy (f'^2) and total enthalpy (g); profiles for large M_∞, indicating that exact similarity does not exist for large M_∞; see Eqs. (31) and (32).

and the flow area from Eq. (14):

$$A = (c\alpha^4 n^2/\sigma_\infty R T_\infty E_\infty^2)[x^{4n-1}/(5n-1)] \tag{21}$$

where c is the constant value of $\rho_\infty u_\infty A$. Finally, from Eq. (16),

$$B = \frac{E_\infty}{u_\infty}\left(1 - \frac{5n-1}{n\gamma M_\infty^2}\right) \tag{22}$$

It is required for the integrability of Eq. (18) that $n \geq 1/5$. In the special case of $n = 1/5$, the above formulas are modified, since then the integral becomes logarithmic. The solutions for $n > 1/5$ describe a class of flows for which acceleration from zero velocity to an arbitrarily high velocity, at constant temperature, is possible. For $1/5 < n < 1/4$, the flow area decreases with increasing velocity, while for $1/4 < n < \infty$, the flow area increases with increasing velocity. Because of the rapid variation of the area with n for n appre-

ciably different from 1/4, values of n near 1/4 seem most interesting for accelerator flows.

For complete consistency, it is of course necessary that **E**, **j**, and **B** satisfy Maxwell's equations, which for the present purposes are:

$$\nabla \cdot \mathbf{E} = \rho_e/\epsilon_0 \qquad \nabla \times \mathbf{E} = 0 \tag{23}$$

and

$$\nabla \times \mathbf{B} = \mu_0 \mathbf{j} \tag{24}$$

where ρ_e is the charge density, ϵ_0 the permittivity, and μ_0 the permeability. In the free stream **E** is constant, and this is consistent with zero charge density; however, in the strictly one-dimensional case Eq. (24) requires $\partial B_z/\partial x = -\mu_0 j_y$. Eqs. (19) and (22) do not satisfy this equation; rather, it is assumed that the magnetic field variation in x consists of two parts, one due to the current distribution, the other to an externally applied field for which $\partial B_z/\partial x - \partial B_x/\partial z = 0$. This field must then have an x component, as well as a z component; however, if the z dimension of the channel is small compared to its length, and B_x is zero on the axis of the channel, then it will be small compared to B_z everywhere. To this approximation, the magnetic field may be regarded as prescribed, and of the form given by Eq. (22).

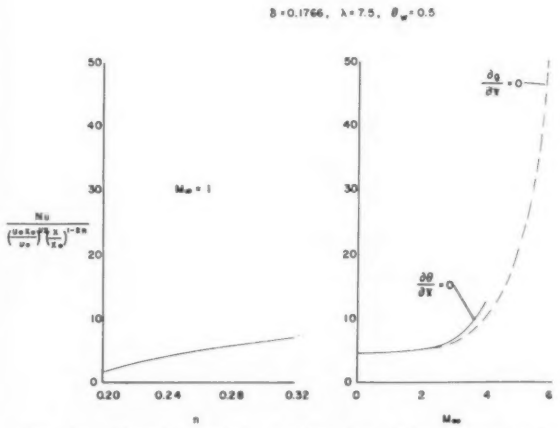

FIG. 11. Nusselt number as a function of the exponent n in $u_\infty = \alpha x^n$, for $M_\infty = 1$ and as a function of M_∞ for $n = 1/4$ (constant flow-area); see Eq. (42).

Similar Solutions

The simple variation of the current and pressure given by Eqs. (19) and (20) suggests the possibility that similar solutions, analogous to the "wedge flow" solutions for the incompressible boundary layer, may exist for the electrode boundary layer in constant temperature flow.

Transformation of the Equations

To investigate this possibility, it is probably most convenient to utilize the transformation given by Levy.[7*] When adapted to the present case of constant temperature flow, it requires that the x and y coordinates be replaced by

$$\bar{x} = \int_0^x \frac{\rho}{\rho_0}\frac{u_0}{u_\infty}\,dx \tag{25}$$

and

$$\eta = \frac{u_\infty}{u_0}\left(\frac{u_0}{2\nu_0}\right)^{1/2}\bar{x}^{-1/2}\int_0^y \frac{\rho}{\rho_0}\,dy \tag{26}$$

where the subscript 0 denotes a reference point in the free stream (not the origin, since ρ is singular there). The continuity equation is satisfied by the definition of the stream function:

$$\frac{\rho}{\rho_0}u = \frac{\partial \psi}{\partial y} \qquad \frac{\rho}{\rho_0}v = -\frac{\partial \psi}{\partial x}$$

If the stream function is taken as

$$\psi = (2\nu_0 u_0)^{1/2}\bar{x}^{1/2}f(\eta)$$

then $\bar{u} = \partial x/\partial \bar{y} = u_0 f'(\eta)$, and if $\mu = \mu_0(T/T_0)$ the momentum equation transforms to:

$$f''' + ff'' + \frac{2\bar{x}}{u_\infty}\frac{du_\infty}{d\bar{x}}\left[\frac{\rho_\infty}{\rho} - (f')^2\right] = 0 \tag{27}$$

In terms of the dimensionless temperature $\theta = T/T_0$, the equation for the temperature, Eq. (9), becomes

$$\frac{1}{Pr}\frac{\partial^2\theta}{\partial\eta^2} + f\frac{\partial\theta}{\partial\eta} = 2f'\bar{x}\frac{\partial\theta}{\partial\bar{x}} - (\gamma-1)M_\infty^2(f'')^2 - \frac{5kj}{e}\left(\frac{u_0}{2\nu_0}\right)^{1/2}\frac{\bar{x}^{1/2}}{c_p\rho_0 u_\infty}\frac{p_0}{p}\frac{\partial\theta}{\partial\eta} - \frac{j^2}{\sigma_0}\frac{2u_0\bar{x}}{c_pT_0\rho_\infty u_\infty^2}\frac{p_0}{p}\theta\left(\frac{\sigma_\infty}{\sigma} - f'\right) \tag{28}$$

* The pair of transformations used in reference (2) are precisely equivalent to the present transformation, after incorporation of the free stream solution of the preceding section.

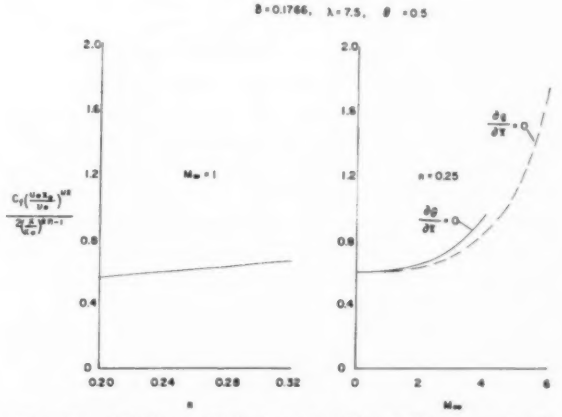

FIG. 12. Friction coefficient as a function of the exponent n in $u_\infty = \alpha x^n$, for $M_\infty = 1$ and as a function of M_∞ for $n = 1/4$ (constant flow-area); see Eq. (43).

where it has been assumed that $\kappa = \kappa_0(T/T_0)$. The $\bar{x}$ dependence of θ has been retained explicitly in Eq. (28), to emphasize the requirements for similarity, which are that the coefficients of θ, f, and their derivatives be independent of $\bar{x}$. Because of the complexity of the coefficients of the electronic conduction and Joule heating terms (the second-to-last and last terms in the equation, respectively), it is difficult to determine the general conditions which will ensure that they are independent of $\bar{x}$. However, it may readily be verified that they are independent of $\bar{x}$ for the free-stream solution obtained in the preceding section. Thus from Eq. (20), $p/p_0 = (x/x_0)^{1-5n}$, and the transformation from x to $\bar{x}$ becomes

$$x/x_0 = [(2 - 4n)(\bar{x}/x_0)]^{1/(2-4n)}$$

for $n < 1/2$. Using this result and Eqs. (19) and (20) to simplify the coefficients, we find:

$$\frac{1}{Pr}\frac{\partial^2\theta}{\partial\eta^2} + f\frac{\partial\theta}{\partial\eta} = 2f'\bar{x}\frac{\partial\theta}{\partial\bar{x}} - (\gamma - 1)M_\infty^2(f'')^2 - \frac{\gamma - 1}{\gamma}\left(\frac{5n - 1}{1 - 2n}\right)^{1/2}\frac{5kT_0}{2e}\left(\frac{\sigma_0}{\mu_0 RT_0}\right)^{1/2}\frac{\partial\theta}{\partial\eta} - \frac{\gamma - 1}{\gamma}\left(\frac{5n - 1}{1 - 2n}\right)\theta\left(\frac{\sigma_\infty}{\sigma} - f'\right) \quad (29)$$

Further, since

$$u_\infty = \alpha x^n = \alpha x_0^n[(2 - 4n)(\bar{x}/x_0)]^{n/(2-4n)}$$

the momentum equation becomes

$$f''' + ff'' + [n/(1 - 2n)][\theta - (f')^2] = 0 \quad (30)$$

$\bar{x}$ does not occur in Eq. (30), and occurs in Eq. (29) only in the Mach number and the term $\bar{x}\,\partial\theta/\partial\bar{x}$. If the Mach number is small, and the boundary conditions are independent of $\bar{x}$, then solutions of Eqs. (29) and (30) will exist such that f and θ are functions of η alone. Thus, similar solutions exist for the thermal and viscous boundary layers if M_∞^2 is small and the wall temperature is constant.

As the free-stream Mach number becomes large, the viscous dissipation term clearly becomes of dominant importance, and there will be no similarity in terms of θ. Under these conditions, a more natural variable is the total enthalpy or, more specifically, the ratio of the total enthalpy to its local free-stream value, since the latter varies in $\bar{x}$.* In terms of this variable, denoted g, Eq. (11) after transformation becomes:

$$\frac{1}{Pr}\frac{\partial^2 g}{\partial\eta^2} + f\frac{\partial g}{\partial\eta} = 2f'\bar{x}\frac{\partial g}{\partial\bar{x}} - \left(1 - \frac{1}{Pr}\right)\frac{[(\gamma - 1)/2]M_\infty^2}{1 + [(\gamma - 1)/2]M_\infty^2}\frac{\partial^2}{\partial\eta^2}(f')^2 - \frac{5kj}{e}\left(\frac{u_0}{2\nu_0}\right)^{1/2}\frac{\bar{x}^{1/2}}{c_p\rho_0 u_\infty}\frac{p_0}{p}\frac{1}{1 + [(\gamma - 1)/2]M_\infty^2}\frac{\partial\theta}{\partial\eta} - \frac{j^2}{\sigma_0}\frac{2u_0\bar{x}}{c_p T_0\rho_\infty u_\infty^2}\frac{p_0}{p}\theta\frac{1}{1 + [(\gamma - 1)/2]M_\infty^2}\left(\frac{\sigma_\infty}{\sigma} - f'\right) - \frac{2\bar{x}}{H_\infty}\frac{dH_\infty}{d\bar{x}}\frac{\gamma - 1}{2}M_\infty^2[g - (f')^2]f' \quad (31)$$

Replacing θ by g in the momentum equation gives

$$f''' + ff'' + [n/(1 - 2n)]\{1 + [(\gamma - 1)/2]M_\infty^2\} \times [g - (f')^2] = 0 \quad (32)$$

The coefficients of the electronic conduction and Joule heating terms (the third and fourth on the right in Eq. 31) are identical with those in the equation for θ, except that they are divided by $1 + (\gamma - 1)M_\infty^2/2$. Thus, for the channel flow solution considered above, they become small as M_∞^2 becomes large. The coefficient of the last term, which represents the work of the Lorentz force, increases as M_∞^2 if H_∞ increases as any power of $\bar{x}$. Furthermore, the last term of Eq. (32) increases as M_∞^2 unless $g - (f')^2 \sim 1/M_\infty^2$. Thus, it appears that if similar solutions exist for large M_∞^2; they must be such that $g - (f')^2 \sim 1/M_\infty^2$. A study of this possibility indicates that the only solution of the equations with such behavior requires $g = f' = 1$. Numerical solutions, which will be described later, support the conclusion that there is no exact similarity at high Mach numbers.

In the next section, solutions of the equations will be described, which were obtained by putting $\partial\theta/\partial\bar{x}$ or $\partial g/\partial\bar{x}$ equal to zero. They are exact similar solutions only for $M_\infty^2 = 0$. For other Mach numbers they are in error to the extent that $\partial\theta/\partial\bar{x}$ or $\partial g/\partial\bar{x}$ varies from zero because of variation of M_∞ with $\bar{x}$. The magnitude of this error may be estimated quite readily by writing the first term on the right of Eq. (31) as

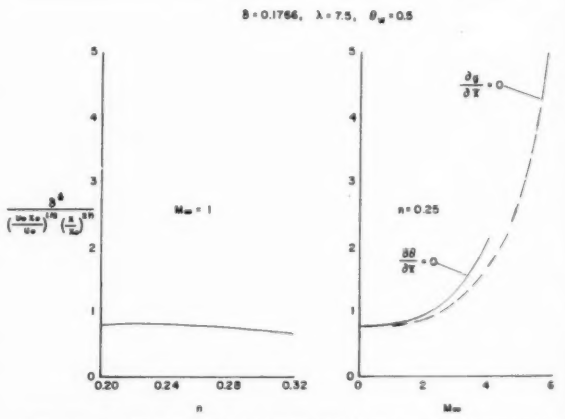

FIG. 13. Displacement thickness as a function of the exponent n in $u_\infty = \alpha x^n$, for $M_\infty = 1$ and as a function of M_∞ for $n = 1/4$ (constant flow-area); see Eq. (43).

* The desirability of investigating high Mach number similarity was suggested to the author and Prof. F. E. Marble by Prof. L. Lees.

$$2f'\bar{x}\left(\frac{\partial g}{\partial \bar{x}}\right) = 2\left(\frac{\partial \log M_\infty}{\partial \log \bar{x}}\right) M_\infty f'\left(\frac{\partial g}{\partial M_\infty}\right)$$

From the channel flow, $\partial \log M_\infty / \partial \log \bar{x} = n/(2-4n)$, and

$$2f'\bar{x}(\partial g/\partial \bar{x}) = [n/(1-2n)]M_\infty f'(\partial g/\partial M_\infty) \quad (33)$$

It would of course be possible to integrate Eqs. (31) and (32) exactly as partial differential equations in the variables η and M_∞. This has not been attempted; however, an estimate of the magnitude of the neglected term will be given.

At low Mach numbers, the solution in terms of θ is probably more accurate than that in terms of g, because the wall boundary condition for the latter is $\bar{x}$-dependent. At high Mach numbers this boundary condition approaches $g(0) = 0$, and g varies more slowly with $\bar{x}$ than does θ, so the solutions in terms of g seem preferable at the higher Mach numbers.

Solution of the Equations

For the sake of simplicity, the Prandtl number is taken to be unity. Then with the assumption of "local similarity"—i.e., that $\partial\theta/\partial\bar{x} = 0$—the equations for f and θ become

$$f''' + ff'' + [n/(1-2n)][\theta - (f')^2] = 0 \quad (34)$$

and

$$\theta'' + \left[f \pm \frac{\gamma-1}{\gamma}\left(\frac{5n-1}{1-2n}\right)^{1/2}\delta\right]\theta' = -(\gamma-1)M_\infty^2(f'')^2 - \frac{\gamma-1}{\gamma}\left(\frac{5n-1}{1-2n}\right)\times\theta\left(\frac{\sigma_0}{\sigma} - f'\right) \quad (35)$$

where

$$\delta = (5kT_0/2e)\,\sigma_0/\mu_0 R T_0^{1/2}$$

σ_0/σ is given by Eq. (2). Because the $\theta^{3/4}$ in Eq. (2) is completely dominated by the exponential factor, we take simply

$$\sigma_0/\sigma = e^{\lambda[(1/\theta)-1]} \quad (36)$$

These equations are to be integrated subject to the boundary conditions

$$\begin{aligned} f(0) &= 0 \qquad \theta(0) = \theta_w = T_w/T_0 \\ f'(0) &= 0 \\ f'(\infty) &= 1 \qquad \theta(\infty) = 1 \end{aligned}$$

In terms of g, the equations are:

$$f''' + ff'' + \frac{n}{1-2n}\left(1 + \frac{\gamma-1}{2}M_\infty^2\right)[g - (f')^2] = 0 \quad (37)$$

and

$$g'' + \left[f \pm \frac{\gamma-1}{\gamma}\left(\frac{5n-1}{1-2n}\right)^{1/2}\delta\right]g' = \frac{\gamma-1}{\gamma}\left(\frac{5n-1}{1-2n}\right)^{1/2}\delta\,\frac{(\gamma-1)M_\infty^2}{1+[(\gamma-1)/2]M_\infty^2}(f'f'') - \frac{\gamma-1}{\gamma}\left(\frac{5n-1}{1-2n}\right)\left[g - \frac{[(\gamma-1)/2]\,M_\infty^2}{1+[(\gamma-1)/2]M_\infty^2}(f')^2\right]\left\{\frac{\sigma_0}{\sigma} - f' + \frac{n\gamma M_\infty^2}{5n-1}\left[\frac{[(\gamma-1)/2]M_\infty^2[g-(f')^2]}{g+[(\gamma-1)/2]M_\infty^2[g-(f')^2]}\right]f'\right\} \quad (38)$$

while the boundary conditions applicable to g are

$$g(0) = \theta_w\{1 + [(\gamma-1)/2]M_\infty^2\}$$

and

$$g(\infty) = 1$$

Since σ/σ_0 is given as a function of θ, we also need

$$\theta = g + [(\gamma-1)/2]\,M_\infty^2[g - (f')^2]$$

There are six parameters in either of these sets of equations, namely, γ, δ, λ, θ_w, n, and M_∞^2. Of these, the first four have been assigned typical values, only n and M_∞^2 being treated parametrically in the calculations. The assigned values are: $\gamma = 5/3$, corresponding to a noble gas; $\delta = 0.1766$, corresponding to helium at 3,000°K; $\lambda = 7.5$, corresponding to cesium at 3,000°K; and $\theta_w = 1/2$. The sign of δ depends on whether the current flows to or from the wall, the plus sign corresponding to the latter case. With the above choice of parameters, the effect of electronic conduction on the boundary layer is negligible. It would be important only if the conductivity, σ_0, were very much higher.

Values of n greater than $1/5$ provide acceptable channel flow solutions; however, the coefficients of the electrical interaction terms in the boundary layer equations are singular at $n = 1/2$. Thus, the range of n which is of interest is $1/5 < \eta < 1/2$. Calculations have been carried out for $M_\infty = 1$, and $0.2 < n < 0.32$; also for $n = 1/4$, (the constant flow-area case) and $0 < M_\infty < 6$.

An iterative method of integration was used, in which at each step the energy equation was solved by repeated quadratures, with the f given by solution of the momentum equation in the previous step. The momentum equation was then solved by repeated quadratures, using the resultant θ, and the process was repeated until f and θ no longer changed. Thus, denoting the number of the quadrature by l, and that of the iteration by k, the equations may be written as

$$\theta^{(l)''} + \left[f^{(k-1)} \pm \frac{\gamma-1}{\gamma}\left(\frac{5n-1}{1-2n}\right)^{1/2}\delta\right]\theta^{(l)'} = -(\gamma-1)M_\infty^2(f^{(k-1)''})^2 - \frac{\gamma-1}{\gamma}\left(\frac{5n-1}{1-2n}\right)\theta^{(l-1)}\,[e^{\lambda(1/\theta^{(l-1)}-1)} - f^{(k-1)'}] \quad (39)$$

and

$$f^{(l)'''} + f^{(l-1)} f^{(l)''} + [n^*/(1 - 2n)][\theta^{(k)} - (f^{(l-1)'})^2 = 0 \tag{40}$$

At the beginning of each quadrature for θ, $\theta^{(l-1)} = \theta^{(k-1)}$, and at the beginning of each quadrature for f, $f^{(l-1)} = f^{(k-1)}$.

Eq. (39) is a first-order linear equation for $\theta^{(l)'}$; if it is written in the form

$$\theta^{(l)''} + a^{(k-1)}\theta^{(l)'} = b^{(l-1)}$$

the solution is

$$\theta^{(l)} = \theta_w + I_4^{(l)}(\eta) + \frac{1 - \theta_w - I_4^{(l)}(\infty)}{I_2^{(k-1)}(\infty)} I_2^{(k-1)}(\eta)$$

where

$$I_1^{(k-1)}(\eta) = \int_0^\eta a^{(k-1)}(\eta)d\eta$$

$$I_2^{(k-1)}(\eta) = \int_0^\eta e^{-I_1^{(k-1)}(\eta)}\, d\eta$$

$$I_3^{(l)}(\eta) = \int_0^\eta b^{(l-1)}(\eta)e^{-I_1^{(k-1)}(\eta)}\, d\eta$$

$$I_4^{(l)}(\eta) = \int_0^\eta e^{-I_1^{(k-1)}(\eta)} I_3^{(l)}(\eta)d\eta$$

The values of $I_2(\infty)$ and $I_4(\infty)$ were approximated by the values of the integrals at the largest value of η to which the integration extended.

Similarly, Eq. (40) is a first-order linear equation for $f^{(l)''}$; thus $f^{(l)}$ can be obtained by integrating three times. The method is completely analogous to that for θ.

In all the calculations, the integration interval was 0.02 for $0 < \eta < 0.2$ and 0.1 for $0.2 < \eta < 5$. The maximum $\eta = 5$ was sufficiently large to ensure that no appreciable errors occurred because of the approximate evaluation of $I_2(\infty)$ and $I_4(\infty)$. For the range of parameters considered, the convergence of the iterative procedure was quite satisfactory; the results are believed to be correct to at least three significant figures.

Results

For given gas composition, free-stream temperature, and wall temperature, two parameters, n and M_∞, determine the characteristics of the boundary layer. Both of these quantities are indicative of the behavior of the free-stream velocity—the Mach number of its magnitude, and the exponent n of its rate of change with x—i.e., of the acceleration. Through the assumed channel flow, the electromagnetic variables are related to these two.

In particular, it may be seen from Eq. (19) that the current j increases as the exponent n increases, and decreases as M_∞ increases. Thus, it may be expected that the largest effects of Joule heating will occur at low Mach numbers and high values of n. The trend with n may be seen in Fig. 3, where the temperature profiles are given for $M_\infty = 1$ and n from 0.21 to 0.31. For comparison, the profile for a uniform free stream ($j = 0$) at $M_\infty = 1$ is shown (dashed line). It is clear that the effect of the Joule heating is to increase the temperature gradient near the wall and hence to thin the thermal boundary layer, and that this effect becomes larger as n increases. In fact, for the larger values of n, a temperature excess actually occurs. This is a result of the heat generated by viscous dissipation being blocked from transfer to the wall by the Joule heating, which occurs very near the wall. From Eq. (35), it can be seen that if f' were unity, θ could have no maximum for $M_\infty = 0$, since then the right side of the equation would be positive for $\theta > 1$. The actual value of f' at the peak of θ ranges from 0.8 to 1.0, so the contribution of Joule heating to the formation of the temperature excess is small.

As n increases, the velocity profile fills out as indicated in Fig. 4, and the wall shear increases, as would be expected for a boundary layer in an accelerated flow. This tendency is somewhat amplified by the thinness of the thermal layer, which results in the low free-stream density being maintained well into the viscous layer.

At higher Mach numbers, a considerable temperature excess occurs as a result of the viscous dissipation, as shown in Fig. 5 for $n = 1/4$. The magnitude of this excess is not greatly different from that for a normal high-speed boundary layer. However, the peak occurs nearer to the wall because, relative to the free stream, the Joule heating rate is lower in the regions of temperature excess, and higher in the low-temperature region near the wall. The corresponding velocity profiles, Fig. 6, show a velocity excess at $M_\infty = 4$, as a result of the low density in the high-temperature region of the boundary layer, and the acceleration of the free stream.

The solutions are of course not strictly valid for any Mach number other than zero, because both θ and f depend on M_∞, which changes with $\bar{x}$. At the higher values of M_∞, θ changes quite rapidly with M_∞ and, as was mentioned before, the total enthalpy becomes a more suitable variable. Solutions in terms of the ratio of total enthalpy to its local free-stream value g, in which it is assumed that $\partial g/\partial \bar{x} = 0$, are shown in Figs. 7 and 8. It will be noted that in this formulation the boundary condition on g depends on $\bar{x}$; hence at the lower Mach numbers, the solution in terms of θ is probably to be preferred. However, at Mach numbers in excess of about 3, g clearly changes less rapidly with M_∞ than does θ, so that for the higher Mach numbers, the formulation in terms of g is definitely more accurate.

At Mach numbers above 4, the combination of free-stream acceleration and temperature excess within the boundary layer produces a large excess in the total enthalpy, a phenomenon which is certainly unusual, and perhaps unique to this type of boundary-layer flow. In terms of the electromagnetic effects, it may be seen to result from the fact that the Lorentz force,

jB, is a constant per unit volume and hence is much more effective in accelerating the gas in the low-density region of the boundary layer than it is in accelerating that in the free stream. Part of the total enthalpy excess is in thermal energy, but a considerable portion is in the form of kinetic energy, as may be seen from the velocity profiles of Fig. 8. The peak value of f' at a Mach number of 6 is 1.222.

As the Mach number increases, the work done by the Lorentz force dominates the Joule heating except in a region very near the wall where the temperature and velocity are low. The values of η and f', at which the rates of energy addition by these two means are equal, are shown in Fig. 9 as functions of M_∞.

There is no doubt that the assumption of local similarity results in a serious overestimate of the rate of change of both g and f' with M_∞ as $M_\infty{}^2$ becomes large. For example, from Eq. (33), at $\eta = 1$ and $M_\infty = 5$, the neglected term is $2f'\bar{x}(\partial g/\partial \bar{x}) = 0.77$, while the last term in Eq. (38)—i.e., the term representing the reversible work—is -1.09. Thus, the right side of Eq. (38) is probably overestimated by about a factor of two at $M_\infty = 5$, and the results derived from the calculations at these high Mach numbers must be interpreted with some caution.

The question naturally arises as to whether similar solutions exist as the Mach number tends to infinity. It was argued above that this could be true only if the quantity $g - (f')^2$, which is multiplied by $M_\infty{}^2$ in both the total enthalpy equation and the momentum equation, were proportional to $1/M_\infty{}^2$. It can be seen from Fig. 10 that this is not the case for Mach numbers up to 6. As the Mach number becomes large, g and $(f')^2$ do tend to the same form except very near the wall, where $(f')^2$, by its quadratic form, must deviate from g, which is necessarily linear. This difference in boundary conditions on g and $(f')^2$ precludes the possibility that they approach each other as M_∞ increases; indeed, from Fig. 10, the difference between them increases slowly with increasing M_∞.

From these solutions, estimates of the heat-transfer rate, wall shear, and boundary-layer thickness may be drawn. In addition, it is possible to estimate the potential drop across the boundary layer and the magnitude of the electric fields which occur within it. The latter quantity is of course of interest for making estimates of the likelihood of electrical breakdown.

Heat Transfer

The rate of heat transfer to the wall, q_w, is given by

$$q_w = -\kappa_w T_0 \left[\frac{\partial \theta}{\partial y}\bigg|_w + \frac{5kj}{2e\kappa_w}\,\theta_w \right]$$

the second term representing the transport of energy by electrons. If we define the Nusselt number in the usual way, as

$$Nu = -q_w x/\kappa_0 T_0(1 - \theta_w)$$

then following the transformation from y to η,

$$\frac{Nu}{(u_0 x_0/\nu_0)^{1/2}\,(x/x_0)^{1-2n}} = (1 - 2n)^{1/2} \left\{ \frac{\dfrac{\partial \theta}{\partial \eta}\bigg|_w + \dfrac{\gamma - 1}{\gamma}\left(\dfrac{5n - 1}{1 - 2n}\right)^{1/2} \delta\theta_w}{1 - \theta_w} \right\} \quad (41)$$

As before, the subscript 0 denotes an arbitrary reference point in the free stream. Thus, if $x = x_0$, we have the usual proportionality between the Nusselt number and the square root of the Reynolds number. The way in which the latter quantity varies with x is indicated by the factor $(x/x_0)^{1-2n}$; however, it must be remembered that the factor in brackets also varies with x. The dependence of the quantity on the right on n and M_∞ is indicated in Fig. 11. At the reference point, $n = 1/4$, $M_\infty = 1$, $Nu/(u_0 x_0/\nu_0)^{1/2} = 4.6$, which is about ten times the value for a comparable boundary layer without electromagnetic effects. For $M_\infty = 1$, the heat-transfer rate increases somewhat with n, but the most striking variations occur with Mach number.

The right half of the figure shows the variation of the Nusselt number with M_∞ obtained with $\partial\theta/\partial\bar{x} = 0$ (solid line) and $\partial g/\partial\bar{x} = 0$ (dashed line). Up to $M_\infty = 2$, these two assumptions give nearly the same result. Either indicates very little change of $Nu/Re^{1/2}$ with the Mach number between $M_\infty = 0$ and $M_\infty = 2$, the range where the temperature profile is dominated by Joule heating. Above $M_\infty = 2$, the Nusselt number increases very rapidly. This rapid increase is a direct result of the stagnation enthalpy overshoot near the wall; since the latter is known to be seriously overestimated, the very rapid increase in heat transfer must be viewed as only a qualitative, and not a quantitative, result.

Wall Shear

The friction coefficient is defined as usual in terms of the wall shear τ, as $C_f = \tau/(\rho_\infty u_\infty{}^2/2)$, whence

$$C_f(u_0 x_0/\nu_0)^{1/2}/2(x/x_0)^{2n-1} = (1 - 2n)^{1/2} f''(0) \quad (42)$$

The results, as shown in Fig. 12, are not greatly different from the usual values except at high M_∞, where the tendency toward a velocity overshoot results, effectively, in a thin viscous boundary layer. Again, these results for large M_∞ can be considered only qualitatively correct.

Displacement Thickness

According to the usual definition, the displacement thickness δ^* is

$$\delta^* = \int_0^\infty \left(1 - \frac{\rho u}{\rho_\infty u_\infty}\right) dy$$

and in terms of η,

$$\frac{\delta^*}{(\nu_0 x_0/u_0)^{1/2}(x/x_0)^{2n}} = (1 - 2n)^{1/2} \int_0^\infty (\theta - f')d\eta \quad (43)$$

Except at the higher Mach numbers, the displacement thickness, as shown in Fig. 13, is only a little larger than

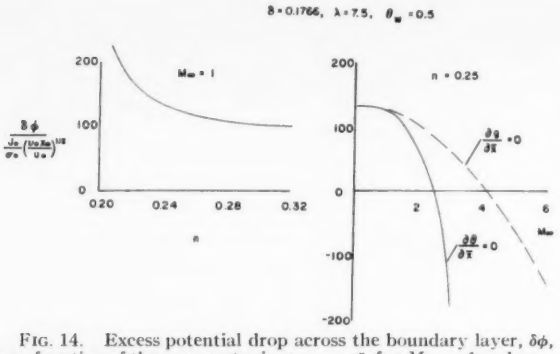

FIG. 14. Excess potential drop across the boundary layer, $\delta\phi$, as a function of the exponent n in $u_\infty = \alpha x^n$, for $M_\infty = 1$ and as a function of M_∞ for $n = 1/4$ (constant flow-area); see Eq. (44).

normal, but at high Mach numbers it becomes very large as a result of the low density in the high-temperature region of the boundary layer. This high-temperature region is actually much thicker than it appears in Figs. 5 and 7, because of the density transformation from y to η.

Voltage Drop and Electric Field

As a result of the variation in electrical conductivity and velocity within the boundary layer, and the continuous current through it, the potential drop through the layer is different from that through an equal distance in the free stream. Denoting this difference as $\delta\phi$, we find from Eq. (5),

$$\delta\phi = \int_0^\infty (E - E_\infty)dy = \int_0^\infty \left[\frac{j}{\sigma} - \frac{j}{\sigma_0} - B(u_\infty - u)\right] dy$$

or in terms of the similarity variable,

$$\frac{\delta\phi}{(j_0/\sigma_0)(\nu_0 x_0/u_0)^{1/2}} = \frac{1}{(1-2n)^{1/2}} \int_0^\infty \theta \left(\frac{\sigma_0}{\sigma} - 1\right) - \left(\frac{\gamma\eta M_\infty^2}{5n-1} - 1\right)(1 - f')\Bigg] d\eta \quad (44)$$

It should be noted that the factor dividing $\delta\phi$, which is the potential drop at the reference point in the free stream over a distance equal to the boundary-layer scale $(\nu_0 x_0/u_0)^{1/2}$, is independent of x, so that all the variation of $\delta\phi$ with x is contained in the right side. It is shown in Fig. 14 as a function of n and M_∞.

At low Mach numbers, $\delta\phi$ is determined principally by the decrease of σ in the low-temperature portion of the boundary layer; it is positive, meaning that the potential drop in the boundary layer exceeds that in an equal distance of the free stream. At higher Mach numbers, the reduction in conductivity is more than offset by the decrease in uB, the "reversed electromotive force" in the low-velocity portions of the boundary layer, and by the increase in conductivity in the high-temperature region, so that $\delta\phi$ becomes negative. In view of the sensitivity of $\delta\phi$ to the temperature and velocity profiles, as exemplified by the large difference between the results for $\partial\theta/\partial\bar{x} = 0$ and $\partial g/\partial\bar{x} = 0$, the negative values of $\delta\phi$ may actually occur at somewhat higher values of M_∞ than the calculations indicate.

In the low-temperature portion of the boundary layer, where the conductivity is low, the continuous current requires the existence of an electric field somewhat larger than that in the free stream; thus, a greater possibility of electrical breakdown exists in these regions. It is the electric field in a coordinate system moving with the fluid that is felt by the electrons, and hence is relevant for this purpose. This field, denoted E', is $E' = E - uB$; therefore, from Eq. (5), $E'/E_\infty' = \sigma_0/\sigma$. Some typical profiles of σ_0/σ are shown in Fig. 15. The large variations are confined to the portion of the boundary layer very close to the wall. For $n = 1/4$, σ_0/σ is 36 at $\eta = 0.1$, and 11 at $\eta = 0.2$.

Numerical Example

A numerical example may be of some help in conveying the magnitudes of the various quantities considered above. For this purpose, consider the acceleration of a gas comprising helium plus one mole per cent of cesium—i.e., the gas described in Fig. 1. Assume that the gas is to be accelerated from $M_\infty = 1$ at a constant temperature of 3,000°K, in a channel of constant area ($n = 1/4$) with a wall temperature of 1,500°K. Let the maximum magnetic field be 1 weber m^{-2}. This maximum value is given by Eq. (22) as $B_m = 2E_\infty/3(3RT_\infty)^{1/2}$, so that $E_\infty = 6{,}500$ volts m^{-1}, or 65 volts cm^{-1}. From Eq. (19), the current density at the initial point of the channel is $j_0 = 3.6 \times 10^6$ amp. m^{-2} = 360 amp. cm^{-2}. Now if the pressure at the initial point ($M_\infty = 1$) is 1 atmosphere, Eq. (20) gives the initial value of x, say x_0, as 0.57 ×

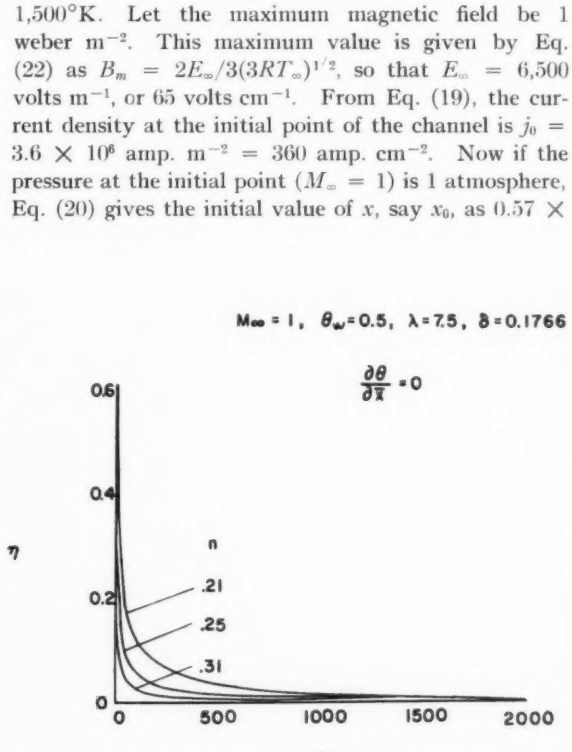

FIG. 15. Ratio of local to free-stream electric field, σ_0/σ, as a function of η for $M_\infty = 1$ and various values of the exponent n in $u_\infty = \alpha x^n$.

10^{-2} m, and in a length of 0.1 m. (10 cm.) a velocity of 6,650 m/sec, or a Mach number of 2.1, would be attained.

The displacement thickness δ^* at x_0 would be 0.74×10^{-4} m or 0.74 mm and, from Eq. (41) and Fig. 11, the heat-transfer rate q_w would be 0.301×10^8 watts m^{-2}. From Eq. (44) and Fig. 14, the excess voltage drop across the boundary layer would be 45 volts.

The difficulty of cooling a wall with a heat-transfer rate of the magnitude given above is quite clear. For example, to pass this heat flux through a tantalum wall would require a temperature drop of 1,000°K in a thickness of about 0.2 cm. Assuming for the moment that such a heat flux can be maintained, one may ask how the power withdrawn by cooling compares with that added by the current and magnetic field. For a channel half-height of 1 cm, the power input based on free-stream conditions, at x_0, would be 2.3×10^8 watts m^{-2}, and with the additional potential drop in the boundary layer included, it would be 3.9×10^8 watts m^{-2}. These power inputs are 7.6 and 13 times the cooling power. Thus, the efficiency of conversion of electrical energy to jet kinetic energy, based on the conditions at $M_\infty = 1$, would be about 0.92.

Concluding Remarks

One of the phenomena that are likely to occur at the surface of a cooled electrode in a hot, flowing plasma has been considered in some detail. As expected, the results show that the current flowing normal to the electrode surface should cause a considerable increase in the heat-transfer rate over that which would exist without the current.

The heat-transfer rates are in fact so high that if operation at high pressures is necessary for suppression of the Hall effect, then some means of cooling the electrode other than simple conduction may be required. Aspiration cooling, either by the gas to be accelerated or by an alkali metal such as lithium, may be a possibility. The latter seems particularly attractive because of the possibility of lowering the work function of the electrode surface. These techniques are susceptible to analysis by the present methods, and seem worthy of study.

At pressure levels below about 0.01 atmosphere, the length of the electron mean free path, as compared to the boundary-layer thickness, invalidates the present treatment. Under these conditions, the departure of the electrons from equilibrium must be explicitly considered. In addition, the Hall effect is likely to have a large influence on the character of the boundary layer.

References

[1] Kerrebrock, Jack L., and Marble, Frank E., *Constant-Temperature Magneto-Gasdynamic Channel Flow*, Readers' Forum, Journal of the Aero/Space Sciences, January 1960.

[2] Kerrebrock, Jack L., *Similar Solutions for Boundary Layers in Constant-Temperature Magneto-Gasdynamic Channel Flow*, Readers' Forum, Journal of the Aero/Space Sciences, February 1960.

[3] Finkelnburg, W., and Maecker, H., "Elektrische Bogen und Thermisches Plasma," *Handbuch der Physik*, Band XXII, p. 325: Springer Verlag, Berlin Göttingen, Heidelberg, 1956.

[4] Chapman, S., and Cowling, T. G., *The Mathematical Theory of Non-Uniform Gases*, Cambridge University Press, 1958.

[5] Brown, Sanborn C., "Conduction of Electricity in Gases," *Handbook of Physics;* McGraw-Hill Book Co., Inc., New York, 1958.

[6] Wood, G. P., and Carter, A. F., *Considerations in the Design of a Steady D.C. Plasma Accelerator*, American Rocket Society—Northwestern Gas Dynamics Symposium, Northwestern University, Evanston, Illinois, August 24–26, 1959.

[7] Levy, S., *Effect of Large Temperature Changes (Including Viscous Heating) Upon Laminar Boundary Layers with Variable Free-Stream Velocity*, Journal of the Aeronautical Sciences, Vol. 21, No. 7, pp. 459–474, July 1954.

✦ ✦ ✦

Magnetohydrodynamics

(*Continued from page 621*)

in low frequencies, in which case the twisting length L_t of the modified Alfvén wave is approximately given by:

$$\bar{L}/L_t \approx (1/2)(\omega_t/\omega_0) \quad \text{with} \quad \bar{L} \approx (2\pi/\omega_t)A_0$$

For example, going back to the wavy-wall problem for crossed fields and large R_m, where the Alfvén mechanism obviously plays an important role, it is realized that the peculiar Hall-current pattern shown in Fig. 6 must be closely related to the twisting of the plane of polarization of the modified Alfvén wave. In fact, it is easily shown that the distance $\bar{L}_t'$, shown in Fig. 6, is given by

$$\bar{L}_t' = \bar{L}_t \cos\psi \quad \text{where} \quad \cos\psi = m/(1 + m^2)^{1/2} \qquad (51)$$

In the wavy-wall problem, it may be noted, the wave normal forms an angle ψ with the magnetic lines of force (see Fig. 6), which gives rise to the factor $\cos\psi$ in Eq. (51).

Finally, it should be mentioned that damping of the waves discussed above can be studied by including the imaginary term in Eq. (48). In the low-frequency limit the damping of the modified Alfvén wave is found to be the same as that of the classical plane Alfvén wave.

Concluding Remarks

The present investigation was carried out as a first step towards a better understanding of Hall-current phenomena in engineering applications of magnetohydrodynamics. Despite the simplifying assumptions of inviscid, incompressible flow and full ionization, the problems treated here are believed to elucidate some important features of real tensor-conductivity gas flow; viz., the formation of Hall-current loops, the

influences of geometry, Alfvén number, and magnetic Reynolds number on the magnitudes of tensor-conductivity effects, and finally Alfvén-wave propagation and the role played by modified Alfvén waves in the creation of certain Hall-current patterns.

References

[1] Cowling, T. G., *Magnetohydrodynamics*, pp. 99–108; Interscience Publishers, Inc., New York, 1957.

[2] Spitzer, L., Jr., *Physics of Fully Ionized Gases*, pp. 18–23; Interscience Publishers, Inc., New York, 1956.

[3] Kemp, N. H., and Petschek, H. E., *Two-dimensional Incompressible Magnetohydrodynamic Flow across an Elliptical Solenoid*, J. Fluid Mech., Vol. 4, Part 6, pp. 553–584, November, 1958.

[4] Sears, W. R., and Resler, E. L., *Theory of Thin Airfoils in Fluids of High Electrical Conductivity*, J. Fluid Mech., Vol. 5, Part 2, pp. 257–273, February 1959.

[5] Resler, E. L., and McCune, J. E., "Electromagnetic Interaction with Aerodynamic Flows," pp. 120–136, *The Magnetodynamics of Conducting Fluids*, D. Bershader, Ed.; Stanford Univ. Press, Stanford, 1959.

[6] Åström, E., *On Waves in an Ionized Gas*, Arkiv för Fysik (Kungl. Svenska Vetenskapsakademien), Vol. 2, No. 5, pp. 443–457, January 1951.

[7] Sonnerup, B., *Some Effects of Tensor Conductivity in Magnetohydrodynamics*, M. Aero. Engr. Thesis, Cornell Univ. Grad. School of Aero. Engrg., Ithaca, N. Y., 1960.

[8] Grad, H., *Notes on Magnetohydrodynamics IV—Ohm's Law*, New York University AEC Research and Development Report NYO 6486, August 20, 1956.

[9] Schlüter, A., *Dynamik des Plasmas—I*, Zeitschrift für Naturforschung, Band 5a, Heft 2, pp. 72–78, 1950.

[10] Lin, S. C., Resler, E. L., and Kantrowitz, A., *Electrical Conductivity of Highly Ionized Argon Produced by Shock Waves*, J. Appl. Phys., Vol. 26, No. 1, January 1955.

✦ ✦ ✦

A Reprint

Journal of the Aeronautical Sciences

Now entitled Journal of the Aerospace Sciences

Available

Volumes 1–5, 1934–1937/1938, paper bound set.....$140.00
Volumes 1–2, 1934–1935, single volumes, paper bound..... 20.00
Volumes 3–5, 1935/1936–1937/1938, single volumes, paper bound..... 35.00

In Preparation

Volumes 6–8, 1938/1939–1940/1941

(Reproduced with the permission of the original publisher, Institute of the Aerospace Sciences, Inc.)

Please address orders and inquiries to:

Johnson Reprint Corporation
111 Fifth Avenue, New York 3, N.Y.

✦ ✦ ✦

Change of Address

Since the Post Office Department does not as a rule forward magazines to forwarding addresses, it is important that the Institute be notified of changes in address 30 days in advance of publishing date to ensure receipt of every issue of the JOURNAL and AEROSPACE ENGINEERING. Notices should be printed legibly and sent to:

Circulation Department
Institute of the Aerospace Sciences, Inc.
2 East 64th Street, New York 21, N.Y.

Foreign-Gas Injection Into a Compressible Turbulent Boundary Layer on a Flat Plate†

NATHAN NESS*

Radio Corporation of America

Summary

The distributed injection of a foreign gas into a compressible, turbulent boundary layer in the absence of a pressure gradient is considered. The analysis is performed within the framework of the binary-mixture concept, that is, the primary fluid flowing over the surface represents one component while the injected species represents the second.

Calculations have been performed for the injection of helium into undissociated air. The results indicate an effect of Mach number on surface shear and energy transfer when distributed light-gas injection normal to the surface exists. A comparison with experimental data indicates reasonable agreement over a range of Mach numbers.

Symbols

a_i = constants defined by Eq. (19) ($i = 0, 1$)
$\tilde{a}$ = parameter defined by Eq. (25)
A = constant in Eq. (23)
b_i = constants defined by Eq. (30) ($i = 0, 1, 2$)
$\tilde{b}$ = parameter defined by Eq. (26)
B = constant in Eq. (23)
c_f = local skin-friction coefficient
c_p = constant-pressure specific heat
C_1 = ρ_1/ρ = mass fraction of injected specie
$\mathfrak{D}_{12}$ = binary-mixture diffusion coefficient
E = constant in Eq. (31)
F = constant in Eq. (31)
h = static enthalpy
k = thermal conductivity
K_1 = constant in Eq. (34)
K_2 = constant in Eq. (44)
$\dot{m}_w$ = $\rho_w v_w$ = mass flux at surface
$\mathfrak{M}$ = molecular weight
M = Mach number
n = exponent in the viscosity–temperature relation for air
p = pressure
Pr = $\mu c_p/k$ = laminar Prandtl number
Pr_t = $\epsilon_t c_p/\epsilon_k$ = turbulent Prandtl number
q_{wc} = thermal-conduction energy transfer at surface; Eq. (51)
q_w = thermal-conduction and mass-diffusion energy transfer at surface; Eq. (48)
Q_w = total energy transfer at surface—i.e., thermal-conduction, mass-diffusion, and enthalpy-flux energy transfer at surface—Eq. (28)
$\Delta q_w/\Delta \dot{m}_w$ = blocking action; Eq. (50)
R = universal gas constant
Re_y = $\rho_e u_e y/\mu_e$ = Reynolds number
Sc = $\mu/\rho\mathfrak{D}_{12}$ = laminar Schmidt number
Sc_t = $\epsilon_t/\overline{\rho}\epsilon d$ = turbulent Schmidt number
T = absolute temperature
u = streamwise velocity component
v = convective normal velocity component
v_i = $V_i + v$ = resultant normal velocity component of species i
V_i = diffusive normal velocity component of species i
x = streamwise coordinate
y = normal coordinate
α_i = constants defined in Eq. (22) ($i = 0, 1, 2$)
δ = boundary-layer thickness
ϵ_d = eddy coefficient of mass diffusion
ϵ_k = eddy coefficient of thermal conductivity
ϵ_ε = eddy coefficient of viscosity
ζ = $\rho_w v_w/\rho_e u_e(c_{f_e}/2)$ = injection parameter
λ_i = exponents in Eq. (31) ($i = 1, 2, 3$)
μ = coefficient of viscosity
π = $\rho_{2w} v_{2w}/\rho_e u_e(c_{f_e}/2)$ = injection parameter
ρ = density
τ = shear stress
ϕ = defined by Eq. (31)
ϕ_t = defined by Eq. (40)
ω_i = exponents in Eq. (23) ($i = 1, 2, 3$)

Subscripts

a = at the interface
$a-$ = at the interface in the laminar sublayer
$a+$ = at the interface in the turbulent region
e = at the outer edge of the boundary layer
i = species i, unless specifically designated otherwise
x = based on streamwise coordinate
x_0 = at the start of the turbulent region
y = based on normal coordinate in sublayer
y_a = based on normal distance to interface
y_t = based on normal coordinate in turbulent region
w = at the wall
1 = species 1; the injected fluid
2 = species 2; the main fluid
δ = based on the boundary-layer thickness
δ^* = based on the displacement thickness
θ = based on the momentum thickness
θ_0 = based on the momentum thickness at the start of the turbulent region
$*$ = nondimensionalized with respect to condition at outer edge of boundary layer

Superscript

$(\bar{\ })$ = time-averaged quantity

Received May 23, 1960. Revised and received November 29, 1960.

† This analysis is based on work performed under the auspices of the U.S. Air Force Ballistic Missiles Division, Contract No. AF 04(647)-269.

* Research Engineer, Missile and Surface Radar Div., Moorestown, N.J. This work was performed while the author was associated with the Missile and Space Vehicle Dept. of the General Electric Company.

The author wishes to acknowledge the capable assistance of Mrs. Gladys Smookler who programed this analysis on the LGP-30 electronic computer and handled the numerical calculations. In addition, the author would like to acknowledge the helpful cooperation of M. E. Long, who contributed in the preparation of the final report.

Introduction

THE DISTRIBUTED INJECTION of a foreign gas into a nonisothermal turbulent boundary layer on a flat plate is considered. The analysis is performed within the framework of the binary-mixture concept—i.e., the primary fluid flowing over the surface represents one component while the injected species represents the second.

The present analysis is based on the Couette-type-flow, Kármán-momentum-integral approach; that is, the defining equations are specialized initially to a Couette-type flow to give relationships between the dependent variables and the coordinate normal to the body surface; the streamwise variations are then introduced by use of the Kármán momentum integral.

Some work has been done previously on the binary-mixture, turbulent-boundary-layer problem. Rubesin and Pappas[1] assumed an isothermal flow (zero Mach number) for the derivation of a skin friction–Reynolds number relation. They considered the Prandtl and Schmidt numbers in the laminar sublayer and in the turbulent region constant, with the turbulent values equal to unity. Energy transfer at the wall was based on thermal conduction only. Their results indicate an increase of energy transfer to the surface at very small injection rates.

Culick[2] considered the nonisothermal case but limited his analysis to the derivation of a Reynolds analogy between skin friction and heat transfer. Fluid properties in the sublayer, entering through the Prandtl, Schmidt, and Lewis numbers, were assumed to vary with concentration, while the turbulent Prandtl and Schmidt numbers were assumed unity. Results are given in terms of the interface velocity as a parameter. Hence, final results in Culick's analysis await experimental data to give the variation of skin friction and interface velocity with injection.

The present paper also considers the concentration dependence of the fluid properties in the sublayer. As in references 1 and 2 quoted above, a helium–air mixture is analyzed subject to the same boundary conditions. It has been shown,[3] by use of the Couette model, that the imposition of concentration-dependent fluid properties in the sublayer makes it impossible to assume arbitrary turbulent Schmidt and Prandtl numbers. In fact, it was shown[3] that assuming a turbulent Schmidt number of unity leads to inconsistent results.

As in all turbulent boundary layer analyses, the present paper depends, to some extent, on experimental data. The present analysis requires an experimental relation between the velocity at the interface and the local skin-friction coefficient. The usual expression for this relation (see references 1 and 4, for example) has been extended, herein, to include the effects of the binary mixture [Eq. (44)]. In addition, the usual initial condition (that the skin-friction coefficient and, consequently, the interface velocity approach infinity at the leading edge of the plate) has been replaced by a more realistic starting condition, namely, that the interface velocity be equal to the edge velocity at the start of the turbulent region.

It is noted that the relationship between the interface velocity and the local skin-friction coefficient [Eq. (44)] contains a constant, K_2. In addition, the Prandtl mixing length introduces a constant K_1 [Eq. (34)]. These constants are determined by analyzing the flow of a constant-property turbulent fluid over an impermeable flat surface. In this special case, a closed-form solution for the skin friction–Reynolds number relation results. The constants K_1 and K_2 are obtained by fitting this relation to low-speed experimental data available in the literature. The details are contained in reference 5.

Analysis

The binary-mixture, turbulent-boundary-layer equations for the steady, frozen flow of a compressible fluid over a two-dimensional surface in the absence of a pressure gradient are as follows:[6]

Continuity:

$$\frac{\partial(\overline{\rho u})}{\partial x} + \frac{\partial(\overline{\rho v})}{\partial y} = 0 \tag{1}$$

Species:

$$\overline{\rho u}\frac{\partial \bar{C}_1}{\partial x} + \overline{\rho v}\frac{\partial \bar{C}_1}{\partial y} = \frac{\partial}{\partial y}\left[\bar{\rho}(\bar{\mathfrak{D}}_{12} + \epsilon_d)\frac{\partial \bar{C}_1}{\partial y}\right] \tag{2}$$

Momentum:

$$\overline{\rho u}\frac{\partial \bar{u}}{\partial x} + \overline{\rho v}\frac{\partial \bar{u}}{\partial y} = \frac{\partial}{\partial y}\left[(\bar{\mu} + \epsilon_v)\frac{\partial \bar{u}}{\partial y}\right] \tag{3}$$

Energy:

$$\begin{aligned}\overline{\rho u}\frac{\partial}{\partial x}\left(\bar{h} + \frac{\bar{u}^2}{2}\right) + \overline{\rho v}\frac{\partial}{\partial y}\left(\bar{h} + \frac{\bar{u}^2}{2}\right) = {}& \\ \frac{\partial}{\partial y}\left[\left(\frac{\bar{\mu}}{\overline{Pr}} + \frac{\epsilon_v}{Pr_t}\right)\frac{\partial}{\partial y}\left(\bar{h} + \frac{\bar{u}^2}{2}\right)\right] + {}& \\ \frac{\partial}{\partial y}\left\{\left[\bar{\mu}\left(1 - \frac{1}{\overline{Pr}}\right) + \epsilon_v\left(1 - \frac{1}{Pr_t}\right)\right]\frac{\partial}{\partial y}\left(\frac{\bar{u}^2}{2}\right)\right\} + {}& \\ \frac{\partial}{\partial y}\left\{\left[\frac{\bar{\mu}}{\overline{Sc}}\left(1 - \frac{\overline{Sc}}{\overline{Pr}}\right) + \frac{\epsilon_v}{Sc_t}\left(1 - \frac{Sc_t}{Pr_t}\right)\right](\bar{h}_1 - \bar{h}_2)\frac{\partial \bar{C}_1}{\partial y}\right\}&\end{aligned} \tag{4}$$

State:

$$\bar{p} = \bar{\rho}R\left[\frac{\mathfrak{M}_1 + (\mathfrak{M}_2 - \mathfrak{M}_1)\bar{C}_1}{\mathfrak{M}_1\mathfrak{M}_2}\right]\bar{T} \tag{5}$$

In the above system of equations, a bar over a symbol represents a time-averaged quantity. The symbols ϵ_v, ϵ_d, and ϵ_k (contained in the turbulent Prandtl and Schmidt numbers Pr_t and Sc_t) are respectively the eddy coefficient of viscosity, the eddy coefficient of binary diffusion, and the eddy coefficient of thermal conductivity.

The boundary conditions are:

$$\begin{aligned} y = 0: &\quad u = 0, \quad T = T_w, \quad C_1 = C_{1w}, \quad v = v_w \\ y = \delta: &\quad u = u_e, \quad T = T_e, \quad C_1 = C_{1e} \end{aligned}$$

At the present time, a rigorous solution of the turbulent boundary-layer equations is unattainable mainly because the functional relationships between the eddy transport coefficients (ϵ_v, ϵ_d, ϵ_k) and the time-averaged dependent variables ($\bar{u}$, $\bar{\rho}$, $\bar{C}_1$, etc.) are unknown. An approximate solution is obtained by considering first a Couette-type flow to relate the dependent variables to the coordinate normal to the body surface; at a later stage, streamwise variations are introduced by the use of the Kármán momentum integral.

To perform the Couette-type analysis, the flow is divided into two regions—i.e., a laminar sublayer and a fully turbulent outer region. The laminar-sublayer conservation equations are obtained from Eqs. (1)–(4) by dropping the bar denoting a time-averaging process, and by neglecting the eddy transport coefficients with respect to the molecular transport coefficients. In a similar manner, the turbulent conservation equations result from Eqs. (1)–(4) when the molecular transport coefficients ($\bar{\mu}$, $\bar{\mathfrak{D}}_{12}$, $\bar{k}$) are neglected with respect to the eddy coefficients. For Couette-type flow—i.e., $\partial/\partial x = 0$—the resulting equations in the laminar sublayer and in the turbulent region are respectively as follows:

Laminar Sublayer

Continuity:

$$(d/dy)(\rho v) = 0 \tag{6}$$

Species:

$$\rho v \frac{dC_1}{dy} = \frac{d}{dy}\left(\rho \mathfrak{D}_{12} \frac{dC_1}{dy}\right) \tag{7}$$

Momentum:

$$\rho v \frac{du}{dy} = \frac{d}{dy}\left(\mu \frac{du}{dy}\right) \tag{8}$$

Energy:

$$\rho v \frac{d}{dy}\left(h + \frac{u^2}{2}\right) = \frac{d}{dy}\left[\frac{\mu}{Pr}\frac{d}{dy}\left(h + \frac{u^2}{2}\right) + \mu\left(1 - \frac{1}{Pr}\right)\frac{d}{dy}\left(\frac{u^2}{2}\right) + \frac{\mu}{Sc}\left(1 - \frac{Sc}{Pr}\right)(h_1 - h_2)\frac{dC_1}{dy}\right] \tag{9}$$

Turbulent Region

Continuity:

$$(d/dy)(\bar{\rho}\bar{v}) = 0 \tag{10}$$

Species:

$$\bar{\rho}\bar{v}\frac{d\bar{C}_1}{dy} = \frac{d}{dy}\left(\bar{\rho}\epsilon_d \frac{d\bar{C}_1}{dy}\right) \tag{11}$$

Momentum:

$$\bar{\rho}\bar{v}\frac{d\bar{u}}{dy} = \frac{d}{dy}\left(\epsilon_v \frac{d\bar{u}}{dy}\right) \tag{12}$$

Energy:

$$\bar{\rho}\bar{v}\frac{d}{dy}\left(\bar{h} + \frac{\bar{u}^2}{2}\right) = \frac{d}{dy}\left[\frac{\epsilon_v}{Pr_t}\frac{d}{dy}\left(\bar{h} + \frac{\bar{u}^2}{2}\right) + \epsilon_v\left(1 - \frac{1}{Pr_t}\right)\frac{d}{dy}\left(\frac{\bar{u}^2}{2}\right) + \frac{\epsilon_v}{Sc_t}\left(1 - \frac{Sc_t}{Pr_t}\right)(\bar{h}_1 - \bar{h}_2)\frac{d\bar{C}_1}{dy}\right] \tag{13}$$

The laminar-sublayer equations satisfy the boundary conditions at the wall; the turbulent equations satisfy the boundary conditions at the edge of the boundary layer. In addition, at the interface between the laminar sublayer and the turbulent region (designated by the subscript a) the following conditions are satisfied:

$$(u)_{a-} = (\bar{u})_{a+}, \quad (T)_{a-} = (\bar{T})_{a+}, \quad \text{etc.} \tag{14}$$

$$(\rho \mathfrak{D}_{12}\, dC_1/dy)_{a-} = (\bar{\rho}\epsilon_d\, d\bar{C}_1/dy)_{a+} \tag{15}$$

$$(\mu\, du/dy)_{a-} = (\epsilon_v\, d\bar{u}/dy)_{a+} \tag{16}$$

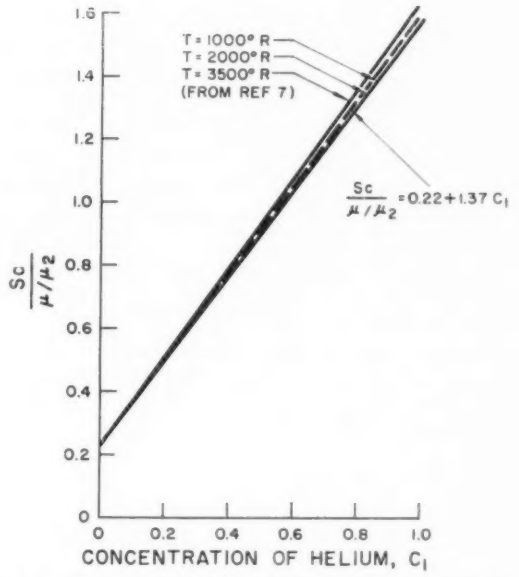

FIG. 1. Property of helium–air mixture as a function of concentration.

$$\left[-k\frac{dT}{dy} + \rho v h - \rho \mathfrak{D}_{12}(h_1 - h_2)\frac{dC_1}{dy}\right]_{a-} = \left[-\epsilon_k \frac{d\bar{T}}{dy} + \bar{\rho}\bar{v}\,\bar{h} - \bar{\rho}\epsilon_d(\bar{h}_1 - \bar{h}_2)\frac{d\bar{C}_1}{dy}\right]_{a+} \tag{17}$$

Eqs. (14) impose continuity of the dependent variables at the interface; in addition, Eqs. (15), (16), and (17) impose, respectively, continuity of diffusion mass transfer, continuity of shear, and continuity of energy transfer. The latter includes the energy transfer by thermal conduction, by enthalpy flux, and by mass diffusion.

Solution of the Laminar Sublayer Equations

The Couette-type laminar-sublayer Eqs. (6)–(9) are solved satisfying the boundary conditions at the wall. Since $\rho v = \rho_w v_w$ [Eq. (6)], the species Eq. (7) may be integrated twice to yield

$$\zeta \frac{c_{f_e}}{2} Re_y = \int_{C_{1w}}^{C_1} \frac{\mu_* dC_1}{Sc[C_1 + (\pi/\zeta) - 1]} \qquad (18)$$

where the symbols are as defined at the beginning of the article.

The quadrature is evaluated in closed form uncoupled from the momentum and energy equations as follows. Initially, the nondimensional viscosity μ_* is replaced by the three equivalent ratios $(\mu_2/\mu_{2e})(\mu_{2e}/\mu_e)(\mu/\mu_2)$. The term μ_2/μ_{2e} is the ratio between the viscosity of the air in the sublayer and the viscosity of the air at the edge of the boundary layer. It is assumed, for calculating this ratio only, that the temperature does not vary much through the sublayer, and that the viscosity of the air may be represented by an exponential function of temperature—i.e., that

$$(\mu_2/\mu_{2e}) = (T_w/T_e)^n$$

where n is a constant. The term μ_{2e}/μ_e is the ratio between the viscosity of the air at the edge of the boundary layer and the viscosity of the mixture at the same point. It is shown in Fig. 4 of reference 7 that this ratio, over the temperature range $810°R < T < 3{,}600°R$, may be considered a function of C_{1e} only, that is, of the concentration of the injected species at the edge of the boundary layer. Consequently, the only ratio of the three equivalent ratios of μ_* to remain under the integral sign in Eq. (18) is μ/μ_2 which may be combined with the Schmidt number in the form $Sc/(\mu/\mu_2)$. To an excellent approximation, for a helium–air mixture, the results of reference 7 (Figs. 4 and 18) indicate that this term may be represented by a linear function of concentration, namely,

$$Sc/(\mu/\mu_2) = a_0 + a_1 C_1 \qquad (19)$$

where $a_0 = 0.22$ and $a_1 = 1.37$. This relation is shown in Fig. 1 as are the data obtained from reference 7. It is noted that Eq. (19) lies practically coincident with the curve $T = 1{,}000°R$. With the aid of Eq. (19), the quadrature in Eq. (18) may be integrated, giving thereby the relationship between the normal coordinate and the concentration as:

$$\zeta \frac{c_{f_e}}{2} Re_y = \frac{(T_w/T_e)^n(\mu_{2e}/\mu_e)}{a_0 - a_1[(\pi/\zeta) - 1]} \times \ln\left[\frac{C_1 + (\pi/\zeta) - 1}{C_{1w} + (\pi/\zeta) - 1} \cdot \frac{a_0 + a_1 C_{1w}}{a_0 + a_1 C_1}\right] \qquad (20)$$

The velocity is related to the normal coordinate by considering the momentum equation (8) and by deriving a relationship between velocity and concentration. The integration of the momentum equation twice, using the condition $\rho v = \rho_w v_w$, yields

$$\ln(1 + \zeta u_*) = \int_{C_{1w}}^{C_1} \frac{dC_1}{Sc[C_1 + (\pi/\zeta) - 1]} \qquad (21)$$

Integration of the quadrature is performed considering the Schmidt number of the binary mixture a function of concentration only. It has been shown (reference 7, Figs. 17–19) that the Schmidt-number dependence on temperature is negligible. In the present analysis, the $Sc(C_1)$ dependence for a helium–air mixture is represented by the quadratic

$$Sc = \alpha_0 + \alpha_1 C_1 + \alpha_2 C_1^2 \qquad (22)$$

where $\alpha_0 = 0.22$, $\alpha_1 = 1.66$, and $\alpha_2 = -0.20$. (A comparison between this relation and the data of reference 7 is shown in reference 13.) With the aid of Eq. (22), Eq. (21) may be integrated, giving thereby

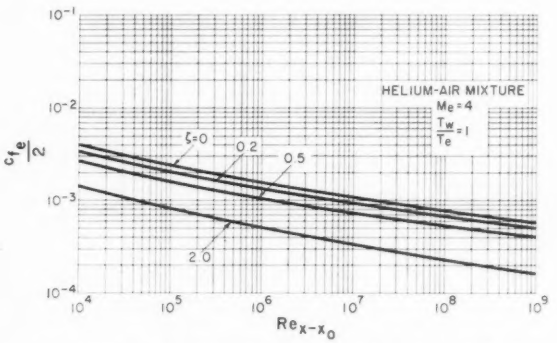

FIG. 2b. Effect of helium injection on local skin-friction coefficient; $M_e = 4$, $(T_w/T_e) = 1$.

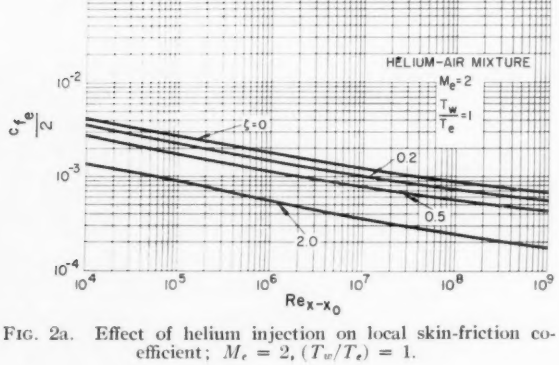

FIG. 2a. Effect of helium injection on local skin-friction coefficient; $M_e = 2$, $(T_w/T_e) = 1$.

the relationship between the velocity and concentration in the sublayer as:

$$1 + \zeta u_* = \left(\frac{C_1 + A}{C_{1w} + A}\right)^{\omega_1}\left(\frac{C_1 + B}{C_{1w} + B}\right)^{\omega_2} \times \left(\frac{C_1 + (\pi/\zeta) - 1}{C_{1w} + (\pi/\zeta) - 1}\right)^{\omega_3} \qquad (23)$$

where

$$A = \frac{\alpha_1 - \sqrt{\alpha_1^2 - 4\alpha_0\alpha_2}}{2\alpha_2}$$

$$B = \frac{\alpha_1 + \sqrt{\alpha_1^2 - 4\alpha_0\alpha_2}}{2\alpha_2}$$

$$\omega_1 = -\frac{1}{\alpha_2(B - A)[A + 1 - (\pi/\zeta)]}$$

$$\omega_2 = \frac{1}{\alpha_2(B - A)[B + 1 - (\pi/\zeta)]}$$

$$\omega_3 = \frac{1}{\alpha_2[A + 1 - (\pi/\zeta)][B + 1 - (\pi/\zeta)]}$$

It is noted that A, B, and $\omega_i (i = 1,2,3)$ are constants dependent only on the coefficients α_i in the $Sc(C_1)$ relation and on the prescribed ratio π/ζ.

The temperature is related to the normal coordinate by considering the energy equation (9) and by deriving a relationship between temperature and velocity (and hence concentration). Since $\rho v = \rho_w v_w$ and the enthalpy h of the mixture in terms of its constituents is $h = h_2 + (h_1 - h_2)C_1$, the energy equation (9) can be integrated once to give

$$\frac{dT_*}{d\phi} + T_* = -\tilde{a} - \tilde{b}u_*\left(1 + \frac{\zeta u_*}{2}\right) \tag{24}$$

where the specific heats of the constituents of the mixture, c_{p_1}, and c_{p_2}, are considered constant. In addition,

$$\tilde{a} = \frac{[Q_w/\rho_e u_e(c_{f_e}/2)h_e\zeta]}{\left[\frac{\pi}{\zeta}\left(\frac{c_{p_1} - c_{p_2}}{c_{p_e}}\right) - \frac{c_{p_1}}{c_{p_e}}\right]} \tag{25}$$

$$\tilde{b} = \frac{(u_e^2/h_e\zeta)}{\left[\frac{\pi}{\zeta}\left(\frac{c_{p_1} - c_{p_2}}{c_{p_e}}\right) - \frac{c_{p_1}}{c_{p_e}}\right]} \tag{26}$$

$$d\phi = \rho_e u_e \frac{c_{f_e}}{2}\zeta\left[\frac{\pi}{\zeta}\left(\frac{c_{p_1} - c_{p_2}}{c_{p_2}}\right) - \frac{c_{p_1}}{c_{p_2}}\right]\frac{c_{p_2}}{c_p} Pr\,\frac{dy}{\mu} \tag{27}$$

$$Q_w = -k_w\left(\frac{dT}{dy}\right)_w + \rho_w v_w h_w - \rho_w \mathfrak{D}_{12w}(h_{1w} - h_{2w})\left(\frac{dC_1}{dy}\right)_w \tag{28}$$

Q_w represents the total energy transfer at the surface resulting from thermal conduction, enthalpy flux, and mass diffusion. Eq. (24) is a first-order, linear, ordinary differential equation. Its solution may be written

$$T_* e^{\phi} - T_{*w} = \tilde{a}(1 - e^{\phi}) - \tilde{b}u_*\left(1 + \frac{\zeta u_*}{2}\right)e^{\phi} + \tilde{b}\int_0^{u_*}(1 + \zeta u_*)e^{\phi}\,du_* \tag{29}$$

The relation between the new independent variable ϕ and the concentration results from Eqs. (18) and (27). With the aid of the former (after differentiation) to eliminate dy/μ, Eq. (27) may be written

$$\phi = \left[\frac{\pi}{\zeta}\left(\frac{c_{p_1} - c_{p_2}}{c_{p_2}}\right) - \frac{c_{p_1}}{c_{p_2}}\right] \times \int_{C_{1w}}^{C_1} \frac{dC_1}{\frac{Sc}{Pr}\cdot\frac{c_p}{c_{p_2}}[C_1 + (\pi/\zeta) - 1]}$$

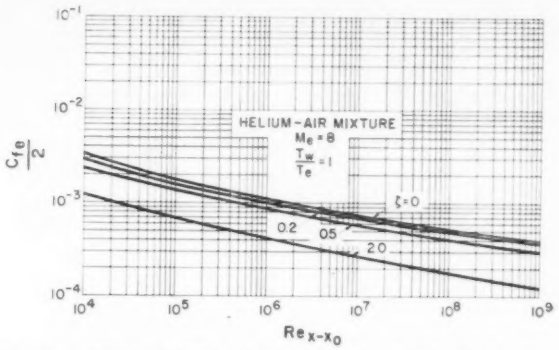

FIG. 2c. Effect of helium injection on local skin-friction coefficient; $M_e = 8$, $(T_w/T_e) = 1$.

The group of terms $(Sc/Pr)(c_p/c_{p_2})$ is considered dependent on concentration only. It is approximated, for a helium–air mixture, by the quadratic relation

$$\frac{Sc}{Pr}\cdot\frac{c_p}{c_{p_2}} = b_0 + b_1 C_1 + b_2 C_1^2 \tag{30}$$

where $b_0 = 0.306$, $b_1 = 8.974$, and $b_2 = 2.490$. (A comparison of Eq. (30) with the data of reference 7 is shown in reference 13.)

Hence the equation for ϕ integrates to

$$\phi = \left[\frac{\pi}{\zeta}\left(\frac{c_{p_1} - c_{p_2}}{c_{p_2}}\right) - \frac{c_{p_1}}{c_{p_2}}\right] \times \ln\left(\frac{C_1 + E}{C_{1w} + E}\right)^{\lambda_1}\left(\frac{C_1 + F}{C_{1w} + F}\right)^{\lambda_2}\left(\frac{C_1 + (\pi/\zeta) - 1}{C_{1w} + (\pi/\zeta) - 1}\right)^{\lambda_3} \tag{31}$$

where E, F, and λ_i $(i = 1,2,3)$ are constants dependent only on the coefficients b_i and the ratio π/ζ. They are defined by

$$E = \frac{b_1 - \sqrt{b_1^2 - 4b_0b_2}}{2b_2}$$

$$F = \frac{b_1 + \sqrt{b_1^2 - 4b_0b_2}}{2b_2}$$

$$\lambda_1 = -\frac{1}{b_2(F - E)[E + 1 - (\pi/\zeta)]}$$

$$\lambda_2 = \frac{1}{b_2(F - E)[F + 1 - (\pi/\zeta)]}$$

$$\lambda_3 = \frac{1}{b_2[E + 1 - (\pi/\zeta)][F + 1 - (\pi/\zeta)]}$$

The solution of the laminar-sublayer Eqs. (6)–(9) is thereby complete. The turbulent equations are considered below.

Solution of the Turbulent Equations

The Couette-type turbulent Eqs. (10)–(13) are solved satisfying the matching conditions at the interface —i.e., at $a+$. The procedure parallels, in many respects, the laminar-sublayer analysis.

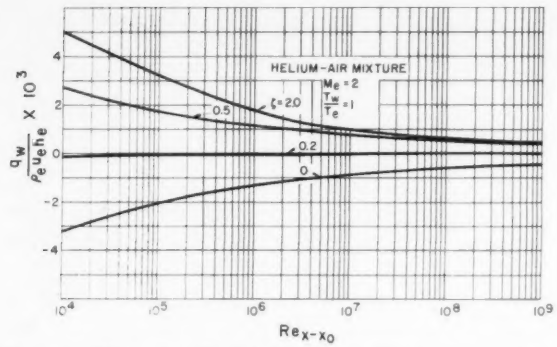

FIG. 3a. Effect of helium injection on local energy transfer; $M_e = 2$, $(T_w/T_e) = 1$.

Integration of the continuity Eq. (10), satisfying continuity of mass flux at the interface, yields $\bar{\rho}\bar{v} = \rho_w v_w$. With the aid of this relation, integration of the species Eq. (11), after satisfying continuity of the concentration and the diffusion mass flux at the interface, yields

$$\zeta \frac{c_{f_e}}{2} dRe_{y_t} = \frac{(\epsilon_v/\mu_e)d\bar{C}_1}{Sc_t[\bar{C}_1 + (\pi/\zeta) - 1]} \tag{32}$$

where the subscript t on the normal coordinate signifies the turbulent region. Eq. (32) cannot be integrated to yield a relationship between the normal coordinate and the concentration (as in the sublayer analysis), as it contains the eddy viscosity coefficient ϵ_v which is related to the density and the velocity through the Prandtl mixing-length concept. Instead, to derive an expression for the normal coordinate the momentum Eq. (12) is considered. With the aid of the relation $\bar{\rho}\bar{v} = \rho_w v_w$, the latter, after one integration and satisfaction of continuity of shear at the interface, gives

$$\frac{c_{f_e}}{2} dRe_{y_t} = \frac{(\epsilon_v/\mu_e)\, d\bar{u}_*}{1 + \zeta\bar{u}_*} \tag{33}$$

The Prandtl mixing length is employed to relate the eddy viscosity coefficient to the density and velocity by[8]

$$\epsilon_v = \bar{\rho}K_1^2 y_t^2 \frac{d\bar{u}}{dy_t} \tag{34}$$

where K_1 is a constant whose value is obtained from experiments. Elimination of ϵ_v from Eqs. (33) and (34) enables the former to be integrated to

$$Re_{y_t} = Re_{y_a} \exp\left[\frac{K_1}{\sqrt{c_{f_e}/2}} \int_{u_{*a}}^{\bar{u}_*} \left(\frac{\bar{\rho}_*}{1 + \zeta\bar{u}_*}\right)^{1/2} d\bar{u}_*\right] \tag{35}$$

This expression relates the local velocity to the normal coordinate provided that $\bar{\rho}_*(\bar{u}_*)$ is known. The equation of state (5) gives the functional relation $\bar{\rho}_* = \bar{\rho}_*(\bar{C}_1, \bar{T}_*)$; it is shown below, from a consideration of the species and momentum equations, that $\bar{C}_1 = \bar{C}_1(\bar{u}_*)$, and from the energy, species, and momentum equations, that $\bar{T}_* = \bar{T}_*(\bar{u}_*)$. Hence, $\bar{\rho}_*(\bar{u}_*)$ is known and the normal coordinate may be evaluated.

The relationship between concentration and velocity in the turbulent region results from Eqs. (32) and (33). Combining the latter, considering the turbulent Schmidt number constant, and integrating, results in

$$\left(\frac{1 + \zeta\bar{u}_*}{1 + \zeta u_{*a}}\right)^{Sc_t} = \frac{\bar{C}_1 + (\pi/\zeta) - 1}{C_{1a} + (\pi/\zeta) - 1} \tag{36}$$

The relationship between temperature and velocity in the turbulent region is obtained from the energy equation (13). As $\bar{\rho}\bar{v} = \rho_w v_w$, the latter may be integrated once to give

$$\frac{d\bar{T}_*}{d\phi_t} + \bar{T}_* = -\tilde{a} - \tilde{b}\bar{u}_*\left(1 + \frac{\zeta\bar{u}_*}{2}\right) \tag{37}$$

where $\tilde{a}$ and $\tilde{b}$ were defined previously, and

$$d\phi_t = \rho_e u_e \frac{c_{f_e}}{2} \zeta \left[\frac{\pi}{\zeta}\left(\frac{c_{p_1} - c_{p_2}}{c_{p_2}}\right) - \frac{c_{p_1}}{c_{p_2}}\right] \frac{c_{p_2}}{c_p} Pr_t \frac{dy_t}{\epsilon_v} \tag{38}$$

In the derivation of Eq. (37), the continuity conditions at the interface, as given by Eqs. (14), (16), and (17) have been satisfied. Eq. (37) is a first-order, linear, ordinary differential equation whose solution may be written

$$\bar{T}_* e^{\phi_t} - T_{*a} = \tilde{a}(1 - e^{\phi_t}) + \tilde{b}\left[u_{*a}\left(1 + \frac{\zeta u_{*a}}{2}\right) - \bar{u}_*\left(1 + \frac{\zeta\bar{u}_*}{2}\right)e^{\phi_t} + \int_{u_{*a}}^{\bar{u}_*} (1 + \zeta\bar{u}_*)e^{\phi_t} d\bar{u}_*\right] \tag{39}$$

This equation gives the relationship between the temperature and the velocity in the turbulent region. The exponential term e^{ϕ_t} is related to the concentration by considering Eqs. (32) and (38). Eliminating dy_t/ϵ_v from these equations, and integrating, gives

$$\phi_t = \frac{Pr_t}{Sc_t} \ln\left\{\left[\frac{C_{1a} + (\pi/\zeta) - 1}{\bar{C}_1 + (\pi/\zeta) - 1}\right] \times \left[\frac{1 + (c_{p_1}/c_{p_2} - 1)\bar{C}_1}{1 + (c_{p_1}/c_{p_2} - 1)C_{1a}}\right]\right\} \tag{40}$$

where the turbulent Prandtl and Schmidt numbers were assumed constant.

The solution of the turbulent Eqs. (10)–(13) is complete. In the next section, the integrated Couette-sublayer and turbulent equations are combined and their method of solution discussed.

Solution of the Integrated Couette-Type Equations

The solution of the integrated Couette-type equations is initiated by a consideration of the concentration–velocity relations in the sublayer and in the turbulent region. When Eq. (23) is evaluated at the

interface, and Eq. (36) is evaluated at the outer edge of the boundary layer, and u_{*a} is eliminated from the resulting expressions, the relation obtained is:

$$\left(\frac{C_{1a}+A}{C_{1w}+A}\right)^{\omega_1}\left(\frac{C_{1a}+B}{C_{1w}+B}\right)^{\omega_2}\left(\frac{C_{1a}+(\pi/\zeta)-1}{C_{1w}+(\pi/\zeta)-1}\right)^{\omega_3} - (1+\zeta)\left(\frac{C_{1a}+(\pi/\zeta)-1}{C_{1e}+(\pi/\zeta)-1}\right)^{1/Sc_t} = 0 \quad (41)$$

This equation represents the starting point in the calculation procedure. It relates the concentration at the interface to the concentrations at the wall and at the edge of the boundary layer for prescribed values of the turbulent Schmidt number Sc_t, and for prescribed values of the nondimensional injection parameters ζ and π.

The implications of the solution of Eq. (41) were discussed previously in reference 3. It was shown therein that if the laminar Schmidt number is permitted to vary through the sublayer (as permitted in the present analysis), then the magnitude of the turbulent Schmidt number, still considered constant, cannot be arbitrarily assumed. In fact, it was shown that

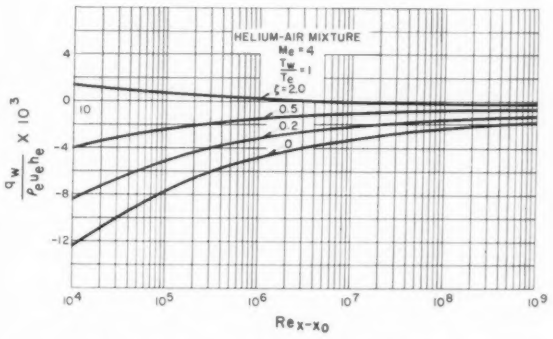

FIG. 3b. Effect of helium injection on local energy transfer; $M_e = 4$, $(T_w/T_e) = 1$.

the (usual) assumption of a turbulent Schmidt number of unity leads to inconsistent results (when the injection parameter ζ is greater than unity). It was concluded that the inconsistent results could be eliminated by either of two methods: (1) by restricting the value of the turbulent Schmidt number outside the range of variation of the laminar Schmidt number [for a helium–air mixture, the laminar Schmidt number varies between 0.22 and 1.68—see Eq. (22)], or (2) by imposing continuity of the Schmidt number at the interface. In the present report, the latter method was applied. It is interesting to note that, as Eq. (41) is uncoupled from the energy equation, its solution is general for all temperature ratios T_w/T_e and for all flow conditions along the outer edge of the boundary layer (provided that $C_{1e} = 0$, as assumed herein).

The next step in the solution requires an expression for the quantity $\tilde{a}$ [defined by Eq. (25)]. For this purpose, the temperature–velocity relations in the sublayer and in the turbulent region are considered. When Eq. (29) is evaluated at the interface, and Eq. (39) is evaluated at the edge of the boundary layer, and T_{*a} is eliminated from the resulting expressions, the equation for $\tilde{a}$ is:

$$\tilde{a} = [e^{\phi_a+\phi_{t_e}} - 1]^{-1}\left[T_{*w} - \left\{1 + \tilde{b}\left(1+\frac{\zeta}{2}\right)\right\}e^{\phi_a+\phi_{t_e}} + \tilde{b}\left\{\int_0^{u_{*a}}(1+\zeta u_*)e^{\phi}\,du_* + e^{\phi_a}\int_{u_{*a}}^{1}(1+\zeta\tilde{u}_*)e^{\phi_t}d\tilde{u}_*\right\}\right] \quad (42)$$

Close examination of Eq. (42) indicates that $\tilde{a}$ is a function of the following parameters:

$$\tilde{a} = \tilde{a}[\pi, \zeta, C_{1e}, C_{1w}\ T_w/T_e, u_e^2/h_e] \quad (43)$$

Hence, in addition to π, ζ, C_{1e}, and C_{1w},* which were required for the solution of Eq. (41), $\tilde{a}$ requires specification of the temperature ratio T_w/T_e and the energy ratio u_e^2/h_e. It should be noted that each set of input data results in a unique value for $\tilde{a}$. The exponential terms e^{ϕ_a} and $e^{\phi_{t_e}}$ are given by Eqs. (31) and (40), respectively, with $C_1 = C_{1a}$ in the former and $\bar{C}_1 = C_{1e}$ in the latter. In Eq. (40), $Sc_t = Sc_a$ and $Pr_t = Pr_a$; the latter value must be consistent with Eq. (30). The local velocity in the sublayer is found from Eq. (23) by assuming $C_{1w} \leq C_1 \leq C_{1a}$, while the local velocity in the turbulent region is found from Eq. (36) by assuming $C_{1a} \leq \bar{C}_1 \leq C_{1e}$; $\tilde{b}$, in Eq. (26), is dependent only on given input data. The integrals in Eq. (42) were evaluated numerically.

With $\tilde{a}$ known, the temperature distributions through the sublayer and the turbulent region follow from Eqs. (29) and (39) respectively. The integrals were evaluated numerically.

It is noted that the calculations to this point have

* Actually, in the solution of Eq. (41), C_{1a} was assumed and C_{1w} was calculated. This is a much simpler procedure than the reverse, as Sc_t is assumed equal to Sc_a and, hence, is a function of the interface concentration [Eq. (22)].

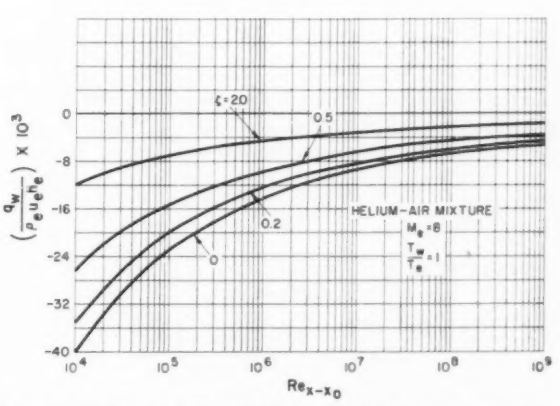

FIG. 3c. Effect of helium injection on local energy transfer; $M_e = 8$, $(T_w/T_e) = 1$.

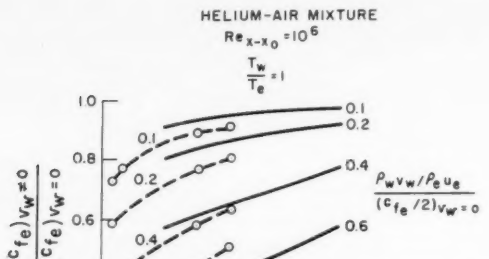

FIG. 4. Effect of Mach number on skin-friction ratio at constant injection rates (comparison with experimental data).

not required specification of the injection ratio $\rho_w v_w/\rho_e u_e$ or the skin-friction coefficient $c_{f_e}/2$ separately; only their ratio, designated by ζ, need be stipulated. However, when the normal coordinate is calculated [Eq. (20) for the sublayer and Eq. (35) for the turbulent region], the local skin-friction coefficient, corresponding to the input data assumed, must be specified.

For this purpose, recourse is made to experimental data, wherein it has been shown (at least for low-speed flow) that the interface velocity is proportional to the square root of the local skin-friction coefficient. For high-speed flow, this experimental relation has been extended to account for compressibility by introducing the density ratio ρ_e/ρ_w as follows:[9]

$$u_{*a} = K_2 \sqrt{c_{f_e}/2} \sqrt{\rho_e/\rho_w}$$

where K_2 is a constant dependent on experimentation. Or, considering the equation of a state (5), the interface velocity is defined by:

$$u_{*a} = K_2 \sqrt{\frac{c_{f_e}}{2}} \sqrt{\frac{T_w}{T_e}} \sqrt{\frac{1 + \left(\frac{\mathfrak{M}_2}{\mathfrak{M}_1} - 1\right) C_{1w}}{1 + \left(\frac{\mathfrak{M}_2}{\mathfrak{M}_1} - 1\right) C_{1e}}} \qquad (44)$$

This expression fixes the local skin-friction coefficient for each set of input data π, ζ, C_{1e}, C_{1w}, and T_w/T_e.

The displacement thickness and the momentum thickness may now be determined. In terms of Reynolds numbers, they are calculated from:

$$\frac{Re_{\delta^*}}{Re_\delta} = \int_0^{Re_{y_a}/Re_\delta} (1 - \rho_* u_*) d\left(\frac{Re_y}{Re_\delta}\right) + \int_{Re_{y_a}/Re_\delta}^1 (1 - \bar{\rho}_* \bar{u}_*) d\left(\frac{Re_{y_t}}{Re_\delta}\right) \qquad (45)$$

$$\frac{Re_\theta}{Re_\delta} = \int_0^{Re_{y_a}/Re_\delta} \rho_* u_* (1 - u_*) d\left(\frac{Re_y}{Re_\delta}\right) + \int_{Re_{y_a}/Re_\delta}^1 \bar{\rho}_* \bar{u}_* (1 - \bar{u}_*) d\left(\frac{Re_{y_t}}{Re_\delta}\right) \qquad (46)$$

The first integral represents the contribution of the laminar sublayer while the second integral represents the contribution of the turbulent region; Re_{y_a} is obtained from Eq. (20) by setting $C_1 = C_{1a}$, and Re_δ (the boundary-layer thickness) is obtained from Eq. (35) by setting the upper limit on the integral equal to unity. The density in the sublayer, ρ_*, is obtained from the equation of state (5). The integrals in Eqs. (45) and (46) are evaluated numerically. A unique displacement and momentum thickness results for each set of input data indicated in Eq. (43).

The energy transfer at the surface may be expressed in several ways. For example, the total energy transfer at the surface, arising from thermal conduction, enthalpy flux, and mass-diffusion flux [Eq. (28)] is:

$$Q_w = \rho_e u_e \frac{c_{f_e}}{2} h_e \zeta \tilde{a} \left[\frac{\pi}{\zeta}\left(\frac{c_{p_1} - c_{p_2}}{c_{p_e}}\right) - \frac{c_{p_1}}{c_{p_e}}\right] \qquad (47)$$

or, if only thermal conduction and mass diffusion are considered, the energy transfer at the surface is:

$$q_w = \rho_e u_e \frac{c_{f_e}}{2} h_e \zeta \left[\tilde{a}\left\{\frac{\pi}{\zeta}\left(\frac{c_{p_1} - c_{p_2}}{c_{p_e}}\right) - \frac{c_{p_1}}{c_{p_e}}\right\} - \frac{T_w}{T_e}\left\{\frac{c_{p_2}}{c_{p_e}} + \left(\frac{c_{p_1} - c_{p_2}}{c_{p_e}}\right) C_{1w}\right\}\right] \qquad (48)$$

It should be noted that the analysis to this point considers only Couette-type flow—i.e., flow without streamwise variations. The streamwise variations are considered in the following section by the use of the Kármán momentum integral which, essentially, relates the local skin-friction coefficient to the local streamwise Reynolds number.

Consideration of Streamwise Variations

For a flow without a pressure gradient over a two-dimensional surface, the Kármán momentum integral, in terms of Reynolds number, may be written

$$(dRe_\theta/dRe_x) = (1 + \zeta)(c_{f_e}/2)$$

which upon integration becomes

$$Re_x - Re_{x_0} = \frac{1}{1 + \zeta} \int_{Re_{\theta_0}}^{Re_\theta} \frac{dRe_\theta}{c_{f_e}/2} \qquad (49)$$

The integral is evaluated numerically. The starting Reynolds number Re_{θ_0} is obtained from the Couette-type analysis by setting $C_{1a} = C_{1e}$. This is analogous to setting u_{*a} equal to unity, and imposes that only laminar flow exist at the starting point for the integration of Eq. (49). As C_{1a} varies and approaches C_{1w} (correspondingly, u_{*a} decreases and approaches zero), Re_θ increases and approaches infinity. It should be noted that the usual starting condition, that when $x \to 0$, $c_{f_e}/2 \to \infty$ and $Re_{\theta_0} \to 0$, is not used in this analysis as this condition imposes an infinite interface velocity at the leading edge [Eq. (44)].

Details of the Numerical Calculations

Numerical calculations were performed for the in-

jection of helium into undissociated air. The properties of the helium–air mixture were obtained from reference 7; they were grouped into certain required combinations and were approximated by linear or quadratic functions of concentration [see Eqs. (19), (22), and (30)].

The following conditions were imposed on the analysis: $C_{1e} = 0$ and $\pi = 0$. The first condition stipulates that the injected helium remain in the boundary layer, while the second condition is identical to the boundary condition $v_{2w} = 0$. Since $v_{2w} = v_w + V_{2w}$, the condition $\pi = 0$ states that the convective velocity of the mixture at the wall v_w is equal in magnitude but opposite in direction to the diffusion velocity of the air at the wall V_{2w}.

The curves for $\zeta = 0$ were obtained by performing a separate analysis for the turbulent flow of undissociated air over an impermeable, flat surface. To be consistent with the helium–air calculations, wherein continuity of the Prandtl number at the interface is imposed, it is necessary when performing the $\zeta = 0$ calculations to assume the laminar Prandtl number equal to the turbulent Prandtl number. From Eqs. (22) and (30), when $C_1 = 0$, $Pr = 0.72$ and represents the value used for the $\zeta = 0$ calculations.

The constants K_1 [Eq. (34)] and K_2 [Eq. (44)] are dependent on experimentation. In the absence of more reliable information, these constants were determined from a constant-property, turbulent air flow analysis over an impermeable, flat surface, which gave $K_1 = 0.392$ and $K_2 = 11.5$. The details are contained in reference 5. These values were used in all the calculations.

For helium, $c_{p_1} = 1.25$ Btu/lbm and $\mathfrak{M}_1 = 4$ lbm/lbm-mole; for air, $c_{p_2} = 0.241$ Btu/lbm and $\mathfrak{M}_2 = 29$ lbm/lbm-mole.

In Eq. (20), the exponent n on the temperature ratio is assigned the value of 3/4, while, in the same equation, since $C_{1e} = 0$, the viscosity ratio μ_{2e}/μ_e is unity.

Discussion of Results

Reported herein are the results of calculations for a temperature ratio T_w/T_e of unity at free-stream Mach numbers of 2, 4, and 8. (Additional results are contained in reference 13.)

Figs. 2a–2c show the effect of helium injection on the local skin-friction coefficient at constant values of the injection parameter ζ. Figs. 3a–3c show the effect of helium injection on the local energy transfer where the energy transfer includes the contributions of thermal conduction and mass diffusion [Eq. (48)].

Fig. 4 shows a comparison between the present results (contained in Figs. 2a–2c) and the experimental data of Pappas.[10] The figure shows the effect of Mach number on the skin-friction coefficient at constant injection rates. The solid curves result from the present analysis and represent local skin-friction coefficients at a local streamwise Reynolds number $Re_{x-x_0} = 10^6$. The test points (encircled) are average skin-friction coefficients resulting from tests on a partially porous pointed cone and are connected by the dashed curves. The test data and the present analysis both indicate a significant dependence of the skin-friction coefficient on the Mach number, especially at the higher injection rates. It is interesting to note that the solid curves have the same trend as the dashed curves. At lower injection rates, the solid and dashed curves are concave downward while at higher injection rates they both become concave upward.

Fig. 5 shows a comparison between the present results (Fig. 3b) and other analyses available in the literature. The figure shows the relative blocking actions of helium and air injection into laminar and turbulent flow. The ordinate is defined by

$$\frac{1}{h_e}\left(\frac{\Delta q_w}{\Delta \dot{m}_w}\right) = \frac{(q_w/\rho_e u_e h_e)_{v_w \neq 0} - (q_w/\rho_e u_e h_e)_{v_w = 0}}{(\rho_w v_w/\rho_e u_e)} \qquad (50)$$

where the ratio $\Delta q_w/\Delta \dot{m}_w$ is termed the blocking action and represents the effectiveness of fluid injection on reducing the energy transfer at the surface. The results of the present analysis (helium-to-air, turbulent) are compared to those of Rubesin (reference 4, air-to-air, turbulent), Baron (reference 11, helium-to-air, laminar), and Low (reference 12, air-to-air, laminar). A comparison between the laminar and turbulent analyses is probably not conclusive, since the former are based on $1/\sqrt{x}$-type injection (similar solutions), while the latter are based on an injection distribution consistent with the ζ = const. assumption. The turbulent analyses may, however, be compared since they are both based on the same surface injection distribution. As would be expected, helium injection exhibits a much greater blocking action than does air injection (compare Rubesin's curves to the present

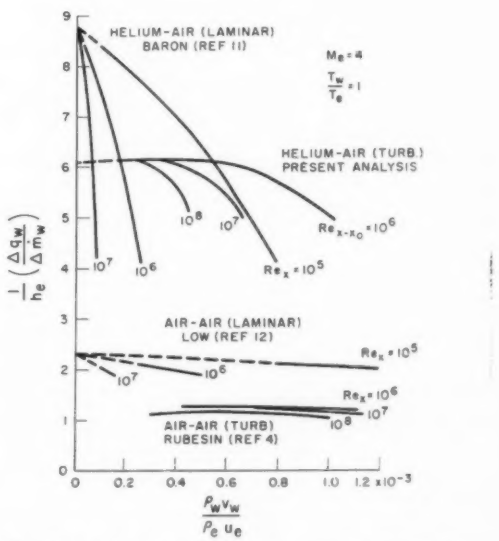

FIG. 5. Blocking action of fluid injection (comparison with other analyses).

analysis). The present analysis, however, exhibits a marked dependence on Reynolds number as the injection ratio increases, whereas Rubesin's analysis does not. It was considered possible that this effect was introduced by the manner of defining the energy transfer q_w. In Rubesin's analysis,[4] since air-to-air injection was considered, q_w was properly defined in terms of thermal conduction only, whereas in the present analysis, as a foreign gas is being added to the main fluid, q_w is defined in terms of thermal conduction and mass diffusion [Eq. (48)]. A calculation was made to determine the thermal-conduction blocking action of helium injection defined by

$$(1/h_e)(\Delta q_{w_c}/\Delta \dot{m}_w)$$

where q_{w_c} is the thermal-conduction energy transfer and is obtained from

$$q_{w_c} = \rho_e u_e (c_{f_e}/2) h_e \zeta [\tilde{a} + (T_w/T_e)] \times \left[\frac{\pi}{\zeta}\left(\frac{c_{p_1} - c_{p_2}}{c_{p_e}}\right) - \frac{c_{p_1}}{c_{p_e}}\right] \quad (51)$$

The results (not shown in Fig. 5) indicate that the thermal-conduction blocking action from the present analysis is Reynolds-number dependent, becoming more so as the injection rate $\rho_w v_w/\rho_e u_e$ increases. At $Re_{x-x_0} = 10^6$, the thermal-conduction blocking action varies between 2.23, at an injection rate of 0.000260, to 2.98 at an injection rate of 0.001036; at $Re_{x-x_0} = 10^8$ the thermal-conduction blocking action varies between 2.35, at an injection rate of 0.000132, to 3.51 at an injection rate of 0.000444.

It is concluded, therefore, that the present analysis indicates a Reynolds-number dependence for both the thermal-conduction blocking action and the thermal-conduction-plus-mass-diffusion blocking action (shown in Fig. 5). Furthermore, the results indicate that the blocking action arising from mass diffusion is of the same order of magnitude as the blocking action arising from thermal conduction.

It should be noted that the present analysis is based on considering the injection parameter ζ constant. Consistent with this assumption, the solution imposes a pointwise variation of the helium surface concentration along the plate which can be determined from Eq. (14). For example, at the start of the turbulent region, where $C_{1a} = C_{1c}$, Eq. (41) gives $C_{1w} = 0.1177$ for $\zeta = 0.5$ and $C_{1w} = 0.4378$ for $\zeta = 2$; at an infinite distance downstream, where $C_{1a} = C_{1w}$, Eq. (41) gives $C_{1w} = 0.197$ for $\zeta = 0.5$ and $C_{1w} = 0.785$ for $\zeta = 2$. Eq. (41) is shown plotted in reference 3.

Concluding Remarks

An analysis has been presented for the distributed injection of a foreign gas into a compressible, turbulent boundary layer on a flat plate. Calculations have been performed for the injection of helium into undissociated air, and show the effect of Mach number and Reynolds number on local shear and energy transfer.

The results indicate a significant dependence of the skin-friction coefficient on Mach number, consistent with the experimental data of Pappas.[10] Furthermore, the analysis exhibits the superior blocking action of helium injection when compared to the air injection of Rubesin.[4] However, the present analysis indicates, as the injection ratio increases, a marked dependence on the Reynolds number, whereas Rubesin's analysis does not.

References

[1] Rubesin, M. W., and Pappas, C. C., *An Analysis of the Turbulent Boundary-Layer Characteristics on a Flat Plate with Distributed Light-Gas Injection*, NACA TN 4149, February 1958.

[2] Culick, F. E. C., *Turbulent Diffusion Boundary Layer*, MIT Naval Supersonic Laboratory TR 279, April 1958.

[3] Ness, N., *On the Continuity of the Schmidt Number at the Interface Between the Laminar Sublayer and the Outer Turbulent Region*, Journal of the Aero/Space Sciences, Vol. 26, No. 6, pp. 396–397, June 1959.

[4] Rubesin, M. W., *An Analytical Estimation of the Effect of Transpiration Cooling on the Heat-Transfer and Skin-Friction Characteristics of a Compressible Turbulent Boundary Layer*, NACA TN 3341, December 1954.

[5] Ness, N., *Distributed Injection of Air Into a High-Temperature, Equilibrium Air, Turbulent Boundary Layer*, General Electric Co. Missile and Space Vehicle Dept., Aerophysics Operation TM 141, August 18, 1959.

[6] Ness, N., and Lew, H. G., *Turbulent Boundary Layer Equations with Binary Diffusion*, General Electric Co., TIS R 59SD310, January 1959.

[7] Carlson, W. O., *Engineering Relationships for Binary Gas Mixture Transport Properties*, General Electric Co. Missile and Space Vehicle Dept., Aerophysics Operation TM 64, December 9, 1957.

[8] Schlichting, H., *Boundary Layer Theory*, McGraw-Hill, New York, 1955, p. 395.

[9] Frankl, F., and Voishel, V., *Turbulent Friction in a Boundary Layer of a Flat Plate in a Two-Dimensional Compressible Flow at High Speeds*, NACA TM 1053, 1943.

[10] Pappas, C. C., *Effect of Injection of Foreign Gases on the Skin Friction and Heat Transfer of the Turbulent Boundary Layer*, IAS Report No. 59-78, Presented at the IAS 27th Annual Meeting, New York, January 26–27, 1959.

[11] Baron, J. R., *The Binary Mixture Boundary Layer Associated with Mass Transfer Cooling at High Speeds*, MIT NSL TR160, May 1956.

[12] Low, G. M., *The Compressible Laminar Boundary Layer with Fluid Injection*, NACA TN 3404, March 1955.

[13] Ness, N., *Foreign Gas Injection Into a Compressible Turbulent Boundary Layer on a Flat Plate*, General Electric Co. TIS R 60SD320, October 2, 1959.

✦ ✦ ✦

Readers' Forum

BRIEF REPORTS of investigations in the aerospace sciences and discussions of papers published in the JOURNAL are presented in this special department. Entries must be restricted to a maximum of 1,300 words or the equivalent of one JOURNAL page including formulas and illustrations. Publication is completed as soon as possible after receipt of the material. The Editorial Committee does not hold itself responsible for the opinions expressed by the correspondents.

Contents

On the Nonexistence of Finite Critical Times for Generalized Linear Viscoelastic Columns With Arbitrary Initial Curvatures ..... HARRY H. HILTON 655

The Limitations of the Hydraulic Analogy ..... E. V. LAITONE 656

On the Torsion of a Beam of L-Shaped Cross Section ..... HOWARD E. BRANDT 657

Downstream Effects of Transpiration Cooling ..... RICHARD P. BERNICKER 658

Further Comments on "Mach-Line Determination for Air in Dissociation Equilibrium" ..... ANDREW G. HAMMITT 659

Author's Reply ..... ROY J. HEYMAN 660

Author's Reply ..... ELDON L. KNUTH 660

Pressure Drag for a Sphere at Extreme Speeds ..... S. LAMPERT 661

On the Bending of Orthotropic Cylindrical Shells ..... V. C. DAS 661

The Relation Between Wall Temperature and the Effect of Roughness on Boundary-Layer Transition ..... J. LEITH POTTER and JACK D. WHITFIELD 663

Dissociation Relaxation Behind a Plane, Oblique, Shock Wave ..... MELVIN EPSTEIN 664

Solving Structural Redundants in Terms of Quadratic Double Roots ..... LAWRENCE L. MARGOLIN 665

Geometric Derivation of Compatability Equation for Finite Deformation of Rotationally Symmetric Shells ..... B. PAUL 666

Laminar Jet Mixing of an Electrically Conducting Fluid in the Presence of a Magnetic Field ..... KAORU TOBA 667

Determination of the Flow Field Around a Hollow Body of Revolution Using a Ring Source ..... DAVID C. PAULSON 668

Flutter of a Hot-Wire Probe ..... MAX M. MUNK 669

On the Bending of Prismatic Shafts ..... M. I. I. RASHED 669

Characteristics Method for Two-Dimensional Conductive Flow With Crossed Fields ..... CHUL PARK 670

A Note on Two-Point Taylor's Series for Solving Ordinary Differential Equations ..... MAURICE FINE 671

On the Nonexistence of Finite Critical Times for Generalized Linear Viscoelastic Columns With Arbitrary Initial Curvatures

Harry H. Hilton
Professor of Aeronautical Engineering, University of Illinois, Urbana, Ill.

October 24, 1960

IN A PREVIOUS PAPER Kempner and Pohle[1] have shown that a linear viscoelastic column of the Maxwell type does not possess a finite critical time. The present note uses a different approach to examine columns of arbitrary initial curvature obeying generalized, linear, compressible viscoelastic stress-strain laws.

For the sake of simplicity, consider a column at constant temperature, simply supported at both ends, loaded by an axial load P, and with an initial curvature

$$w_0 = w_0(\xi) = \sum_{n=1}^{N} \delta_n \sin n\xi \quad (1 \leq N \leq \infty, \quad 0 \leq \xi \leq \pi) \quad (1)$$

Let the column obey the general one-dimensional, compressible viscoelastic stress-strain law

$$\{R + CQ\}\{\sigma\} = 3G\,Q\{\epsilon\} \quad (2)$$

where $C = G/K$ with K and G, respectively, the bulk and shear moduli and where

$$R + CQ = \sum_{m=0}^{r} a_m(\partial^m/\partial t^m) + C \sum_{m=0}^{s} b_m(\partial^m/\partial t^m) = \sum_{m=0}^{r_1} c_m(\partial^m/\partial/\partial t^m) \quad (3)$$

$$Q = \sum_{m=0}^{s} b_m(\partial^m/\partial t^m) \quad (4)$$

The limit r_1 equals r or s depending on whether r is respectively larger or smaller than s.

In reference 2 it was shown that the solution for the lateral

Contributors Please Note

Readers' Forum contributions that exceed the *Journal's* one-page limit will be returned to author for condensation and rewrite. Avoid inconvenience and delay by adhering to:

(1) Five, double-spaced, typewritten, manuscript pages ($8\frac{1}{2}$ by 11 in)., including wide margins, formulas, and headings, equal one printed page.

(2) For every illustration, deduct at least one-half or as much as one manuscript page, depending on the size of the illustration.

deflection w of a column under the conditions assumed here and for P less than the Euler load P_E can be obtained in the form

$$w = w(\xi,t) = \sum_{n=1}^{N} w_n g_n(t) \sin n\xi \tag{5}$$

where

$$w_n = \delta_n[1 - \alpha_n^{-2}]^{-1} \tag{6}$$

with $\alpha_n^2 = n^2 P_E/P$. The functions $g_n(t)$ are determined from the differential equations

$$\{R - (\alpha_n^2 - C)Q\}\{g_n(t)\} = -b_0\delta_n\alpha_n^2 \qquad (1 \leq n \leq N) \tag{7}$$

with initial conditions (except for the Kelvin body) on the functions $g_n(0) = 1$ and other initial conditions on the time derivatives of g_n depending upon the particular stress-strain relation.

In general the solutions of Eqs. (7) will be in the form

$$g_n(t) = \sum_{p=1}^{r_1} A_{pn}\, e^{\lambda_{pn}t} - \frac{b_0\delta_n\alpha_n^2}{a_0 - (\alpha_n^2 - C)b_0} \tag{8}$$

where λ_{pn} are the roots of Ω_n obtained by substituting Eqs. (8) into (7) which results in

$$\sum_{m=0}^{r} a_m\Omega_n^m - (\alpha_n^2 - C)\sum_{m=0}^{s} b_m\Omega_n^m = 0 \tag{9}$$

(For repeated roots, the coefficients A_{pn} in Eqs. (8) can be suitably modified to contain proper polynomials of t.) The behavior of viscoelastic columns is such that the functions $g_n(t)$ physically represent the amplitude magnifications of the various harmonics over and above the elastic amplitudes w_n.

The condition for creep buckling is defined in the usual manner—i.e., at the critical time, t_{cr}, the lateral deflection w tends to infinity, or

$$\lim_{t \to t_{cr}} w(\xi,t) \to \infty \tag{10}$$

Since w_n are the coefficients of a series solution for an equivalent elastic column and since this series is known to converge for all $P < P_E$, clearly the stability of w depends on the behavior of the functions $g_n(t)$. The limit of Eq. (10) can be reached if either any $g_n(t_{cr})$ increases without bounds or if the series of Eq. (5) fails to converge at $t = t_{cr}$.

An examination of Eqs. (8), or their modified versions in case of repeated roots, shows that for any finite r_1 all $g_n(t)$ are finite for $t < \infty$. This means that a linear viscoelastic column having its initial curvature defined by a finite sum ($N < \infty$) of the type given by Eq. (1) will always possess an infinite critical time for any R and Q operators.

Unfortunately, when $N = \infty$—i.e., when w_0 is such that it must be described by an infinite sine series, the convergence of the series cannot be readily tested for arbitrary values of the operators R and Q, since the coefficients A_{pn} are different functions of n which depend on specific R and Q values. Under these circumstances the series must be examined for each combination of R and Q.

It can be readily shown that for the elementary linear viscoelastic stress-strain laws, such as those of the Maxwell body, standard linear solid, combination Maxwell-Kelvin body, etc., the functions $g_n(t)$ are such that series (5) converges absolutely and uniformly for $t < \infty$ provided that

$$\lim_{n \to \infty} |w_{n+1}/w_n| < 1$$

The latter inequality is always satisfied, since it is the condition for the convergence of the elastic solution which always holds for $P < P_E$. Consequently, in these cases for $N = \infty$, there is also no finite critical times for linear viscoelastic columns.

References

[1] Kempner, J., and Pohle, F. V., *On the Nonexistence of a Finite Critical Time for Linear Viscoelastic Columns*, Journal of the Aeronautical Sciences, Vol. 20, No. 8, pp.572–573, August 1953.

[2] Hilton, H. H., *Creep Collapse of Viscoelastic Columns With Initial Curvatures*, Journal of the Aeronautical Sciences, Vol. 19, No. 12, pp. 844–846, December 1952.

The Limitations of the Hydraulic Analogy

E. V. Laitone
Professor, College of Engineering, University of California, Berkeley

October 24, 1960

EVEN when restricted to very small potential variations, the nonlinear hydraulic analogy to a perfect-gas flow will be shown to be limited to the simple case of a liquid in a rectangular, constant-cross-section channel, corresponding to a fictitious gas having a specific-heat ratio of $\gamma = 2$. For example, it is proved that a triangular cross-section channel does not provide the nonlinear analogy corresponding to a specific-heat ratio of $\gamma = 1.5$, even for the simplest case of unsteady one-dimensional flow.

Finally, it is pointed out that when larger perturbations are involved, the second approximation to shallow-water theory completely invalidates any hydraulic analogy by allowing the formation of finite-amplitude waves that are propagated without a change in shape or form. This is in direct opposition to the equations of gasdynamics, which predict that all finite-amplitude waves must form a discontinuity or shock wave. The simplest of these finite-amplitude, permanent water waves are the solitary wave of Boussinesq and Rayleigh, and the cnoidal waves of Korteweg and de Vries.

Analysis

The equations generally used in deriving the hydraulic analogy to a perfect-gas flow are approximate relations that are satisfactory only for a flat horizontal-bottom channel with nearly vertical side walls. For example, the equations used by Bryant[1] and Loh[2, 3] for unsteady one-dimensional flow may be expressed in the form

$$H_t + (uH)_x = 0 \tag{1}$$

$$u_t + uu_x = -gH_x \tag{2}$$

where $H = h + \eta$ is the total local water depth as shown in Fig. 1. Now we will first prove that Eq. (2) is valid only for a horizontal bottom, and then we will show that both equations are valid only for nearly vertical side walls.

The correct Eulerian equations for assumed one-dimensional flow over a nonhorizontal bottom were derived by Stoker,[4] also by Wehausen and Laitone,[5] in the following form:

$$\eta_t + [u(h + \eta)]_x = 0 \tag{3}$$

$$u_t + uu_x = -p_x/\rho = -g\eta_x \tag{4}$$

where, as shown in Fig. 1, η is the change in height of the free surface and h is the local depth of the rigid bottom below the undisturbed free surface. Since $H = h + \eta$, it is immediately evident that although Eq. (1) is satisfactory for any rigid bottom, Eq. (2) is valid only for a horizontal bottom because it is only the variation in η (the water height above the undisturbed free surface) that produces the unsteady flow variations. That is, we must write the assumed hydrostatic-pressure variation as

$$p(x\,z,t) = \rho g[\eta(x,t) - z]$$

$$p_x/\rho \quad = g\eta_x = gH_x - gh_x \tag{5}$$

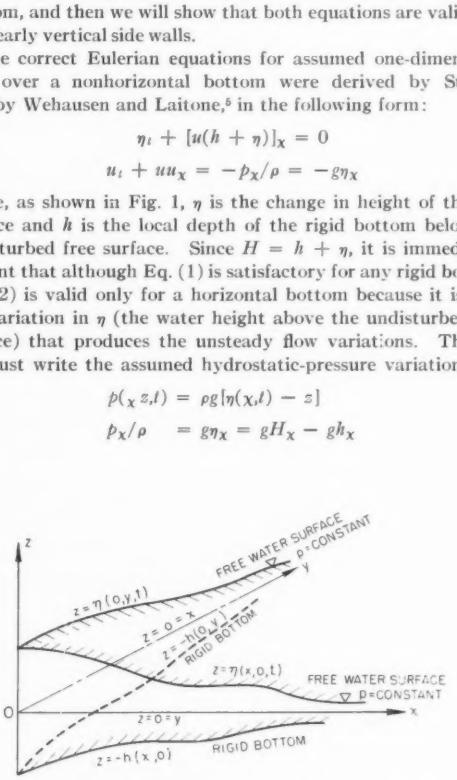

FIG. 1. Surface waves over a general rigid bottom.

The much simpler behavior of Eq. (2), as compared to the correct Eq. (4) for a nonhorizontal bottom, is demonstrated by Stoker,[4] and by Wehausen and Laitone,[5] by introducing the equivalent of the speed of sound, namely,

$$c = \sqrt{gH} = \sqrt{g(h + \eta)} \tag{6}$$

and then showing that although the characteristic curves are given by $(u \pm c)$ for both sets of equations, an important distinction is created by the fact that the Riemann invariants do not even exist for the general case of Eqs. (3) and (4), whereas they are always given by $(u \pm 2c)$, the same as in the nonsteady one-dimensional gasdynamic case, for Eqs. (1) and (2). Stoker,[4] also Wehausen and Laitone,[5] have shown that the Riemann invariants exist for Eqs. (3) and (4) in the form $(u \pm 2c - gh_x t)$ only if the bottom slope h_x is constant. Consequently, the behavior of the correct Eqs. (3) and (4) is much more complicated than the approximate Eqs. (1) and (2) unless the bottom slope is negligible. If the bottom slope is adjusted to balance the frictional drag for uniform flow, the subsequent variation in water depth must remain very small.

More important for most applications is the fact that all of these equations are restricted to channels having nearly vertical side walls. This is explained more readily by inspection of the rigorous first approximation to shallow-water theory,* which shows that the exact continuity equation

$$u_x + v_y + w_z = 0 \tag{7}$$

reduces in the first approximation to

$$\eta_t + [u(h + \eta)]_x + [v(h + \eta)]_y = 0 \tag{8}$$

not because $w = 0$ (as assumed by Bryant[1]), but only because the direct dependence of w on h_x and h_y (through the exact boundary conditions on the rigid bottom) may be used to eliminate w as a variable in Eq. (7). This indicates that v can never be considered to be a negligible quantity unless h_y is negligible and the side walls are vertical. It is also important to note that even though w does not directly appear in the final equations of the shallow-water first approximation, it still has a finite magnitude.

This exact shallow-water result, proving that $w \neq 0$, and that v is not negligible in magnitude unless h_y itself may be considered negligible, is also verified by the classical infinitesimal-wave or small-disturbance approximation. For example, in Lamb[6] (pp. 447–450) the classical infinitesimal-wave solutions are given for small disturbances in two triangular cross-section channels and it is found that the disturbance potential depends directly upon the slope of the sides (h_y) to the order of $(h/\lambda)^2$, where λ is the wavelength of the disturbance, and both v/u and w/u have a finite magnitude of the order of (h/λ). The profiles of the waves have a severe dependence upon y at the sides of the channel and the propagation velocities of all but the longest wavelength disturbances are directly dependent upon the magnitude of h_y. These results are contrary to the assumptions and results of Eqs. (1) and (2), which yield no dependence on y or h_y. For example, Bryan[1] and Loh[2,3] find that any triangular cross section has the same propagation velocity (corresponding to a specific-heat ratio of $\gamma = 1.5$ in the assumed hydraulic analogy), and the wave profiles have a uniform height independent of y, a result that could only be approximately true for nearly vertical side walls and very long wavelength, extremely-small-amplitude disturbances which correspond to linearized theory.

The direct and deleterious effect of finite-amplitude disturbances upon the hydraulic analogy is proved by Wehausen and Laitone[5] (pp. 701–714). The second approximation to shallow-water theory shows that now finite-amplitude waves can be propagated without a change in shape or form. These are the solitary wave of Boussinesq and Rayleigh, and the cnoidal waves of Korteweg and de Vries (also, see Lamb,[6] pp. 423–427). These permanent finite-amplitude waves completely destroy the hydraulic analogy, since the equations of gasdynamics always predict that any finite-amplitude disturbance must degenerate to a finite discontinuity.

The higher approximations of shallow-water theory, which are given by Wehausen and Laitone,[5] show that for a constant-rectangular-cross-section channel

$$w/\sqrt{gh} \sim (\eta/h)^{3/2} \qquad u_{z/h}/\sqrt{gh} \sim (\eta/h)^2 \tag{9}$$

and even more important, it is found that the pressure variation is no longer hydrostatic when terms of the order $(\eta/h)^2$ are considered. Experimentally, it has been shown that these finite-amplitude effects are even more severe for sloping channel walls which produce a strong dependence on y, and may even form large vortices with asymmetrical flow at the sloping walls.

* E.g., see Wehausen and Laitone,[5] pp. 466–468.

References

[1] Bryant, R. A. A., *The Hydraulic Analogy for External Flow*, Journal of the Aero/Space Sciences, Vol. 27, No. 2, pp. 148–149, February 1960.

[2] Loh, W. H. T., *Hydraulic Analogy for Two-Dimensional and One-Dimensional Flows*, Journal of the Aero/Space Sciences, Vol. 26, No. 6, pp. 389–391, June 1959.

[3] Loh, W. H. T., *Hydraulic Analogue for One-Dimensional Unsteady Gas Dynamics*, J. Franklin Inst., Vol. 269, No. 1, pp. 43–55, January 1960.

[4] Stoker, J. J., *The Formation of Breakers and Bores, Communications on Pure and Applied Mathematics*, Vol. 1, No. 1, pp. 1–87, January 1948.

[5] Wehausen, J. V., and Laitone, E. V., *Surface Waves*, Handbuch der Physik, Vol. 9, pp. 446–778, Springer-Verlag, Germany, 1960.

[6] Lamb, H., *Hydrodynamics*, 6th Ed.; Cambridge University Press, 1932; Dover Publications, New York, 1945.

On the Torsion of a Beam of L-Shaped Cross Section

Howard E. Brandt
Massachusetts Institute of Technology, Cambridge, Mass.

October 13, 1960

THE GALERKIN METHOD is here applied to determine the stress field, displacement field, and torsional rigidity for an L-shaped beam subjected to pure torsion. Prismatic bars of various cross section have widespread application in aeronautical engineering. The solutions for several types of beams have been presented in the Journal of Aerospace Sciences.[1–6] This paper is a further contribution to torsional phenomenology.

Mathematical Formulation of the Problem

The Prandtl stress functions will be employed in the solution of this problem:

$$\psi(x, y) = \sum_{m=1}^{n} A_m \eta_m(x, y), \qquad (m = 1, 2, \ldots, n) \tag{1}$$

and the Galerkin form of the problem becomes

$$\iint_S [\nabla^2 \psi(x, y) + 2]\eta_r(x, y) dS = 0, \qquad (r = 1, 2, \ldots, n) \tag{2}$$

A_m are constants satisfying Eq. (2); and η_r are coordinate functions which are to be found such that

$$\psi(\Gamma) = 0 \tag{3}$$

where Γ is the boundary of the beam (Fig. 1), and S is the domain

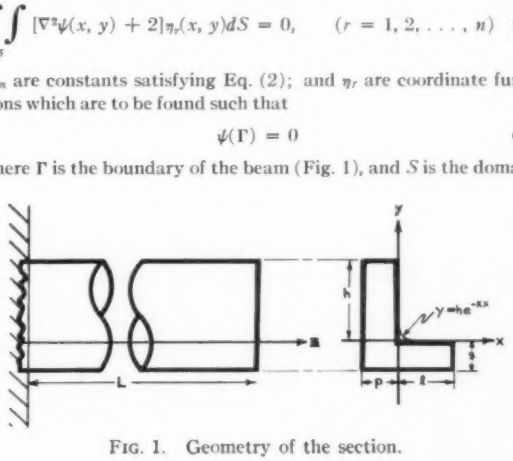

FIG. 1. Geometry of the section.

of integration.

A function, $\psi(x, y)$, must be determined which satisfies Eq. (3). Solving the Dirichlet problem is considerably complicated in the case of nonconvex polygons. The usual approach, when constructing ψ, in order to take into consideration a re-entrant angle, is to introduce moduli, and to assign the function piecewise in different parts of the region.[7] In the present paper this difficulty is circumvented by representing the boundary along the coordinate axis by an exponential function which decays very rapidly and is pragmatically equivalent to the actual L-shaped boundary. This boundary is represented by

$$\phi(x, y) \equiv y - he^{-Kx} = 0 \tag{4}$$

where h is the dimension indicated in Fig. 1, and K is a constant chosen such that

$$he^{-Kx} \approx 0 \text{ for } 0 < x < l \tag{5}$$

The first approximation, which is satisfactory for engineering purposes as illustrated by Stanišić, will be used because of limitation of space.[2] In order that $\psi(x, y)$ vanish along the total boundary, Γ, it must clearly be of the following form:

$$\psi(x, y) = A_1(x - l)(x + P)(y + q)(y - h)(y - he^{-Kx}) \tag{6}$$

where A_1 is a constant of first approximation. Then Eq. (2) becomes

$$\iint_S [A_1\nabla^2\eta_1(x, y) + 2]\eta_1(x, y)dS = 0 \tag{7}$$

where

$$\eta_1(x, y) = (x - l)(x + P)(y + q)(y - h)(y - he^{-Kx})$$

Solving for A_1 yields

$$A_1 = -2\,\frac{\displaystyle\int_0^l\int_{-q}^{he^{-Kx}} \eta_1(x, y)dydx + \int_{-q}^{h}\int_{-p}^{0} \eta_1(x, y)dxdy}{\displaystyle\int_0^l\int_{-q}^{he^{-Kx}} [\nabla^2\eta_1(x, y)]\eta_1(x, y)dydx + \int_{-q}^{h}\int_{-p}^{0} [\nabla^2\eta_1(x, y)]\eta_1(x, y)dxdy} \tag{8}$$

Thus the Prandtl stress function, $\psi(x, y)$, is uniquely determined.

The torsional rigidity is given by

$$D = 2G\left[\int_0^l\int_{-q}^{he^{-Kx}} \psi(x, y)dydx + \int_{-q}^{h}\int_{-p}^{0} \psi(x, y)dxdy\right] \tag{9}$$

where G is the shear modulus.

The stress tensor is given by

$$[\tau_{ij}] = \begin{bmatrix} 0 & 0 & G\alpha\,\dfrac{\partial\psi(x, y)}{\partial y} \\ 0 & 0 & -G\alpha\,\dfrac{\partial\psi(x, y)}{\partial x} \\ G\alpha\,\dfrac{\partial\psi(x, y)}{\partial y} & -G\alpha\,\dfrac{\partial\psi(x, y)}{\partial x} & 0 \end{bmatrix} \tag{10}$$

where α is the twist per unit length.

The displacement field is given by

$$u_i = \begin{bmatrix} -\alpha yz \\ \alpha xz \\ \alpha F(x, y) \end{bmatrix} \tag{11}$$

where

$$F(x, y) = \int_{P_0(x_0,y_0)}^{P(x,y)} \left[\frac{\partial f(x, y)}{\partial y}\,dx - \frac{\partial f(x, y)}{\partial x}\,dy\right] \tag{12}$$

and

$$f(x, y) = \psi(x, y) + \frac{1}{2}(x^2 + y^2) \tag{13}$$

The stress and displacement field are uniquely determined.

References

[1] Brandt, H. E., *On a Generalized Solution to a Torsion Problem in Linear Elasticity*, Journal of the Aerospace Sciences, Readers' Forum, Vol. 28, No. 5, pp. 422–424, May 1961.

[2] Shirely, L. K., and Stanišić, M. M., *On the Torsion of Cylindrical Beam Having a Trapezoidal Cross Section*, Journal of the Aero/Space Sciences Readers' Forum, Vol. 27, pp. 461–463, June 1960.

[3] Stanišić, M. M., Hauck, C. A., and Mathias, R. A., *Concerning the Torsion of Prismatic Bars Having a Hexagonal Cross Section*, Journal of the Aerospace Sciences, Readers' Forum, Vol. 27, No. 8, pp. 631–633, Aug. 1960.

[4] Brandt, H. E., *on the Torsion of a Rectangular Beam with Diametrically Opposite Sides of the Form ax^n*, Journal of the Aerospace Sciences, Readers' Forum, Vol. 28, No. 6, pp. 503–505, June 1961.

[5] Brandt, H. E., *On a Generalized Solution for the Torsion of a Prismatical Beam of any Polygonal Cross Section*, Journal of the Aerospace Sciences, Readers' Forum, to be published.

[6] Stanišić, M. M., and Sherwood, B. A., *Torsion of an Elliptical Shaft with Diametrically Opposite Flat Sides*, Journal of the Aero/Space Sciences, Readers' Forum, Vol. 27, No. 6, pp. 462–463, June 1960.

[7] Kantorovich, L. V., and Krylov, V. I., *Approximate Methods of Higher Analysis*, Interscience Publishers, Inc., New York, 1958.

Downstream Effects of Transpiration Cooling*

Richard P. Bernicker**
Naval Supersonic Laboratory, Massachusetts Institute of Technology, Cambridge, Mass.

November 14, 1960

Symbols

F	=	wall injection parameter, $[(\rho v)_w/(\rho u)_{e,0}]\sqrt{Re_0}$
K_x	=	constant in Eq. (1)
Re	=	Reynolds number $= (\rho_e u_e x)/\mu_e$
T	=	temperature, °R
x	=	distance along nozzle contour surface
x^*	=	distance parameter, $(x - x_i)/(x_0 - x_i)$
θ	=	wall cooling parameter, $(T_w - T_c)/(T_{aw} - T_c)$
$(\overline{\rho v})_w$	=	mean injection mass flow per unit area
(ρu)	=	mainstream mass flow per unit area

Subscripts

$(\,)_0$	=	refers to injection cut-off point
$(\,)_i$	=	refers to start of injection
$(\,)_{aw}$	=	adiabatic local wall conditions under zero injection
$(\,)_c$	=	refers to coolant supply conditions
$(\,)_*$	=	refers to sonic conditions
$(\,)_e$	=	refers to local external free stream conditions

AN EFFECTIVE MEANS for protecting surfaces exposed to high-energy gas streams is to inject small quantities of a relatively cold gas through a porous wall into the boundary layer. This mass-transfer cooling effect manifests itself in two distinct ways. First of all, the injected or coolant gas can absorb a considerable quantity of heat as it passes through the wall and undergoes a temperature rise from the supply temperature to the wall-surface temperature. Secondly, injection from the surface alters the boundary-layer behavior in such a manner as to reduce the heat transfer to the wall. This "blanketing" effect upon the boundary layer continues to protect the downstream areas of the surface whether or not they are porous. Hence transpiration cooling may be applied in the region of severest heating; say the nose of an axisymmetric body or a rocket-nozzle throat, with the residual effect of the cooled boundary layer protecting the solid surface downstream of the porous section. Such upstream transpiration cooling has been investigated[1, 2] for the zero-pressure-gradient case with air and helium as coolants, with major interest centering on the decay of the cooling effect with increasing distance downstream of the injection section.

This note summarizes the findings of an experiment[3] in which the effect of partial porous-wall injection upon the downstream portions of a two-dimensional supersonic nozzle was investigated. Two such nozzles were built, each containing the porous injection strip in a different region of the subsonic portion of the nozzle. The nozzle contour was well insulated and the area downstream

* This research was supported by the USAF under Contract AF49(638)-245, monitored by the Air Force Office of Scientific Research of the ARDC.

** Presently, Stevens Institute of Technology, Hoboken, N. J.

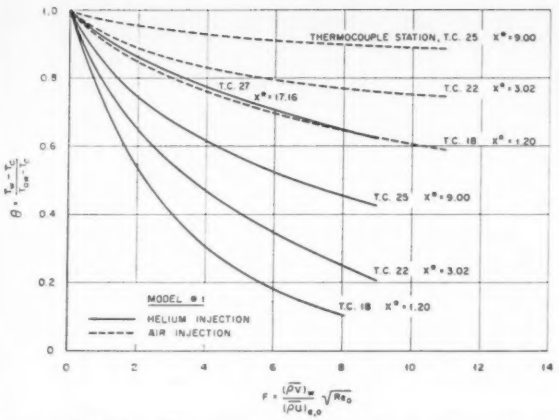

FIG. 1. Injection effect upon downstream surface temperatures.

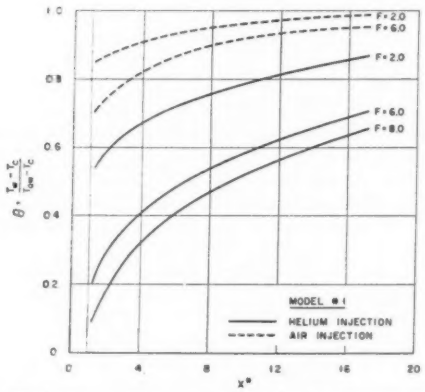

FIG. 2. Surface-temperature distributions for several injection rates.

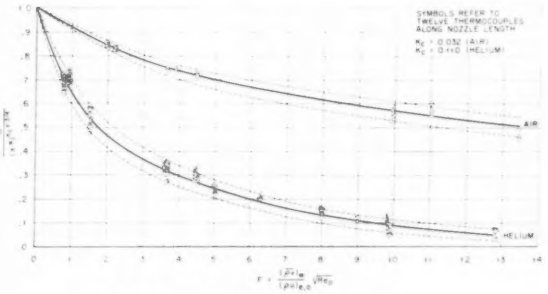

FIG. 3. Correlation of test results.

of the porous section instrumented to determine the effect upon local recovery temperatures. Both air and helium were used as coolants, with the total flow rate of coolant metered and controlled through calibrated sonic orifices and diaphragm valves.

Tests were run with tunnel stagnation temperatures of 600°, 720°, 900°, and 1,200°R, corresponding to coolant supply to tunnel stagnation temperature ratios in the range 0.45–0.90. Coolant specific-mass-flow rates, $(\overline{\rho v})_w$, were set at several levels up to a maximum of 1 percent of the mainstream mass flow at the throat, $(\rho u)_*$.

Fig. 1 illustrates the reduction in recovery temperature from the zero-injection case (normal adiabatic wall conditions). Individual data points have been omitted from Figs. 1 and 2 but are shown in Fig. 3. As the injection rate, F, is increased, the effective amount of cooling diminishes in the downstream direction. The wall cooling parameter, θ, reduces to unity for all stations along the surface when the injection rate vanishes, and corresponds to the local adiabatic wall temperature at each Mach number down the nozzle. For a given fixed value of F, some reduction in wall temperature was noted at the farthest-downstream thermocouple station at the exit plane of the two-dimensional $M = 2.75$ nozzle. The decay of the cooling effectiveness with distance is illustrated in Fig. 2, where the variation in θ with distance for fixed values of F is shown for both air and helium injection. Results from both Figs. 1 and 2 indicate the superiority of helium over air for this mode of cooling, and conform to theoretical predictions.[2]

In attempting to correlate test results for the two nozzles under varying injection conditions, the decay of θ with distance (Fig. 2) was plotted on a logarithmic scale ($ln\ \theta$ versus $ln x^*$) and the resulting slopes were found to be straight lines on a log-log plot against F. The results indicated θ to be proportional to a power of x^*, the exponent itself being separable into a product of coolant and injection-rate contributions. The final correlation is shown in Fig. 3, where test results for both models can be included within a bandwidth of ±15 percent for each coolant used. Thus, for a fixed value of the injection rate,

$$\theta \sim (x^*)^{K_c F^{3/4}} \tag{1}$$

in which the injection-rate exponent is identical for both air and helium injection and both models. The constant K_c differs for each coolant gas.

Analysis[1] has indicated that the expression for θ as a power function of the downstream distance will include a function of the injection rate. The case treated therein is concerned with air injection through a flat plate, and the Prandtl number is taken to be unity. Hence, exact correspondence with the empirical expression determined above cannot be expected. However, the results of Ref. 1 can be correlated approximately by an expression of similar form to that determined for the present experiment, the difference lying in the values of the constant K_b (which must presumably be a function of both coolant and pressure gradient) and the injection-rate exponent (which present results indicate to be solely a function of pressure gradient). Comparison of results for the two coolant mediums at the same injection rate indicated a larger decrease in recovery temperature for helium than for air and, in addition, a persistence of the insulating effect for a greater distance downstream with the helium injection.

REFERENCES

[1] Rubesin, M. W., and Inouye, M., *A Theoretical Study of the Effect of Upstream Transpiration Cooling on the Heat Transfer and Skin-Friction Characteristics of a Compressible, Laminar Boundary Layer*, NACA TN 3969, 1957.

[2] Baron, J. R., *Binary Mixture Boundary Layer Associated with Mass Transfer Cooling at High Speeds*, Massachusetts Inst. of Tech., Naval Supersonic Lab., Tech. Rep. 160, 1956.

[3] Bernicker, R. P., *An Experiment with a Transpiration Cooled Nozzle*, Massachusetts Inst. of Tech., Naval Supersonic Lab., Tech. Rep. 447, 1960.

Further Comments on "Mach-Line Determination for Air in Dissociation Equilibrium"

Andrew G. Hammitt
Head, Aerodynamics Research Section,
Space Technology Laboratories, Inc., Los Angeles, Calif.
November 17, 1960

THE PURPOSE of this note is to correct the misconceptions introduced by Heyman[1] and Knuth[2] concerning the speed of propagation of a shock wave under the limit of zero density change. The impression is given by Heyman that such a shock wave in an imperfect gas travels at a different speed than $\sqrt{(\partial p/\partial \rho)_s}$. Knuth suggests that while a Mach wave travels

at $\sqrt{(\partial p/\partial \rho)_s}$ there may be an additional shock wave with zero density change traveling at a different speed. These conclusions are incorrect. It may be shown by use of the conservation equations alone, for all equations of state, that a weak wave travels with the velocity $\sqrt{(\partial p/\partial \rho)_s}$ and that this is the only zero-density-change wave possible.[3]

The question then arises where the analyses presented[1,2] are in error. The quadratic equation for density[1] is correct:

$$\left(\frac{\rho_1}{\rho_2}\right)^2 - \left[(K_2 + 1)\left(1 + \frac{1}{\gamma M_1^2}\right)\right]\frac{\rho_1}{\rho_2} + K_2\left[1 + \left(1 + \frac{1}{K_1}\right)\frac{1}{\gamma M_1^2}\right] = 0 \quad (1)$$

If this equation is now linearized about conditions at 1, substituting $\rho_2 = \rho_1 + \Delta\rho$ and $K_2 = K_1 + \Delta K$ the following equation is found:

$$\{K_1 - 1 + [(K_1 + 1)/\gamma M_1^2]\}\Delta\rho/\rho_1 + (1/\gamma M_1^2)(\Delta K/K_1) = 0 \quad (2)$$

A relation between $\Delta\rho$ and ΔK is required and the one given[2] for isentropic flow may be used:

$$\Delta K/K_1 = [(\gamma - 1) - K_1(\gamma + 1)]\Delta\rho/\rho_1 \quad (3)$$

Using this relation to eliminate ΔK, the equation becomes

$$(K_1 - 1)(1 - 1/M_1^2)\Delta\rho/\rho_1 = 0 \quad (4)$$

This equation is satisfied for $\Delta\rho = 0$, the case of no change, which can occur at any Mach number: $M_1 = 1$, the case of a wave of near zero strength; or $K = 1$, corresponding to a very unrealistic equation of state.

The error in Heyman's solution[1] is in not expressing K_2 as a function of ρ_2. He effectively assumes K_2 independent of ρ_2 and his result is correct for this case. If K_2 is independent of ρ_2 Eq. (3) shows that $K = (\gamma - 1)/(\gamma + 1)$, which reduces Heyman's result to a wave traveling at a speed of $\sqrt{(\partial p/\partial \rho)_s}$. However, this result cannot be used for air under the conditions shown in Fig. 2.[1]

Knuth's error[2] is more complex. He has linearized the solution to Eq. (1), found without expressing K_2 as a function of ρ_2, and retained only first-order terms. It can be shown that solutions found in this way cannot be used to recover the original equation to the order of $\Delta\rho/\rho_1$.

However, this whole analysis is needlessly complicated, since the classical derivation using only the conservation equations is sufficient.

REFERENCES

[1] Heyman, R. J., *Mach-Line Determination for Air in Dissociation Equilibrium*, Journal of the Aero/Space Sciences, Readers' Forum, Vol. 27, No. 4, pp. 311–312, April 1960.

[2] Knuth, E. L., *Comments on "Mach-Line Determination for Air in Dissociation Equilibrium,"* Journal of the Aerospace Sciences, Readers' Forum, Vol. 27, No. 10, pp. 796–797, Oct. 1960.

[3] Shapiro, A. H., *The Dynamics and Thermodynamics of Compressible Fluid Flow*, The Royal Press Co., New York, 1953.

Author's Reply

Roy J. Heyman
Research Dept., The Martin Company, Denver, Col.

December 5, 1960

AFTER REVIEWING Dr. Hammitt's note I must conclude that he is correct. As he states, merely from conservation of mass and momentum one may derive

$$v^2 = (\partial p/\partial \rho)_s$$

or

$$M_1^2 = 1$$

while if we consider an oblique wave we arrive at

$$\sin \alpha = 1/M_1$$

independent of the state of the gas.

The same result may be obtained in a much more cumbersome fashion, as Hammitt notes. Linearizing the quadratic equation for the density ratio, we may derive Hammitt's Eq. (2); solving for M_1 we obtain:

$$M_1^2 = (K_1 + 1)/\gamma(1 - K_1) + [1/\gamma(1 - K_1)](\Delta K/K_1)(\rho_1/\Delta\rho)$$

From the isentropic relation between $\Delta\rho$ and ΔK as given by Knuth

$$(\Delta K/K_1)(\rho_1/\Delta\rho) = (\gamma - 1) - K_1(\gamma + 1)$$

or $$M_1^2 = (K_1 + 1)/\gamma(1 - K_1) + [(\gamma - 1) - K_1(\gamma + 1)]/\gamma(1 - K_1)$$

which reduces to $M_1^2 = 1$.

I believe that the error has resulted from an improper limit process, performed by both Knuth and myself upon the solution to the quadratic with the failure to retain terms of the order of $(\Delta\rho)^2$, $(\Delta K)^2$, $(\Delta\rho\Delta K)$, etc., under the radical. The correct results may be obtained if the terms are properly retained, but as Hammitt has observed, the analysis is needlessly complicated.

Author's Reply

Eldon L. Knuth*
Associate Professor of Engineering,
University of California, Los Angeles, Calif.

January 26, 1961

THE AUTHOR agrees with Hammitt[1] that, for all equations of state, the only zero-density-change wave possible is a Mach wave. The author feels obligated to the reader, however, to discuss more completely the source of the error introduced by Heyman[2] and retained by Knuth,[3] and to provide a correct expression for the density change across a weak disturbance in a real gas.

If one applies the quadratic formula to a "quadratic" equation with coefficients which are functions of the variable, then one obtains, in general, four values of the variable, two of which do not satisfy the "quadratic" equation. (If the coefficients are functions of the variable, then, since the variable may have one of two values, the coefficients may have one of two sets of values. If the coefficients may have one of two sets of values, then, since the quadratic formula includes a $\pm$ sign, one calculates four values of the variable. The two extraneous values may be identified by substituting into the original "quadratic" equation.) For real gases, the coefficients in the "quadratic" equation for density ratio given by Heyman are functions of the density ratio, and the density ratios found using the negative sign in Heyman's Eq. (5) are found to be extraneous. Consequently, all conclusions regarding real gases reached by Heyman and Knuth using the negative signs are invalid.

For perfect gases, $K = (\gamma - 1)/(\gamma + 1)$, the coefficients appearing in the quadratic equation are constants, and the two density ratios found using the quadratic formula are both roots of the quadratic equation. This situation accounts for the fact that the extraneous density ratio retained by Heyman and Knuth reduced (unfortunately, perhaps) to an expression valid for the case of perfect gases when K was set equal to $(\gamma - 1)/(\gamma + 1)$.

If one chooses to analyze the propagation of small disturbances in real gases using the integrated equations given by Heyman, then one may substitute expressions for ρ_2/ρ_1, p_2/p_1, and K_2/K_1 into (a) the expression obtained using the quadratic formula and the positive sign, or (b) the "quadratic" equation, or (c) the normal-shock relation—i.e., Heyman's Eq. (4). Terms up to and including second-order terms in $\Delta\rho/\rho_1$ must be retained, however, in order to extract both roots. The author finds it most direct to substitute into the normal-shock relation—i.e., to substitute into

$$(p_2 - p_1)/p_1 = \gamma_1 M_1^2(\rho_2 - \rho_1)/\rho_2$$

from

$$\rho_2 = \rho_1 + \Delta\rho$$

* The author appreciates the valuable technical discussions with Dr. A. G. Hammitt during the preparation of this reply to his comments.

$$p_2 \approx p_1 + \left.\frac{\partial p}{\partial \rho}\right|_s \Delta\rho + \frac{1}{2}\left.\frac{\partial^2 p}{\partial \rho^2}\right|_s (\Delta\rho)^2$$

$$\left.\frac{\partial p}{\partial \rho}\right|_s = \frac{\gamma_1 p_1}{\rho_1}$$

$$\left.\frac{\partial^2 p}{\partial \rho^2}\right|_s = \frac{\gamma_1 p_1}{\rho_1^2}\left(\left.\frac{\partial \ln \gamma}{\partial \ln \rho}\right|_s + \gamma_1 - 1\right)$$

to obtain

$$2(M_1^2 - 1)\frac{\Delta\rho}{\rho_1} = \left(\gamma_1 + 1 + \left.\frac{\partial \ln \gamma}{\partial \ln \rho}\right|_s\right)\left(\frac{\Delta\rho}{\rho_1}\right)^2$$

One root

$$\Delta\rho/\rho_1 = 0 \qquad (1)$$

corresponds to the case of no disturbance. The other root

$$\Delta\rho/\rho_1 = 2(M_1^2 - 1)/[\gamma_1 + 1 + (\partial \ln \gamma/\partial \ln \rho)_s] \qquad (2)$$

describes the density change across weak disturbances in real gases. It indicates that a zero-density-change wave is a Mach wave. For perfect gases, γ is constant, and the latter equation reduces to

$$\Delta\rho/\rho_1 = 2(M_1^2 - 1)/(\gamma + 1) \qquad (2')$$

in agreement with results found in gasdynamics texts.

REFERENCES

[1] Hammitt, A. G., *Further Comments on "Mach-line Determination for Air in Dissociation Equilibrium,"* Journal of the Aerospace Sciences, Readers' Forum, Vol. 28, No. 8, pp. 659–660, Aug. 1961.

[2] Heyman, R. J., *Mach-line Determination for Air in Dissociation Equilibrium*, Journal of the Aero/Space Sciences, Readers' Forum, Vol. 27, No. 4, pp. 311–312, April 1960.

[3] Knuth, E. L., *Comments on "Mach-line Determination for Air in Dissociation Equilibrium,"* Journal of the Aerospace Sciences, Readers' Forum, Vol. 27, No. 4, pp. 796–797, Oct. 1960.

Pressure Drag for a Sphere at Extreme Speeds

S. Lampert
Manager, Aeromechanics, Dept.,
Aeronutronic, A Division of Ford Motor Company,
Newport Beach, Calif.

November 1, 1960

IT WAS SHOWN in V. C. Liu's article[1] that the drag coefficient of a sphere traveling at Mach numbers for which the vibrational and dissociative degrees of freedom are activated could be approximated as

$$C_D = 2/(\gamma_e + 1) - 4/[(\gamma_e + 1)M_1^2] + 2/(\gamma_1 M_1^2) \qquad (1)$$

In general, the isentropic exponent is a function of both the local entropy and pressure as shown in Fig. 1 and, therefore, will vary with Mach number. For sea-level conditions the static pressure P_2 behind a normal shock is proportional to M_1^2, or for $M_1 > 8$ it is roughly established that P_2 varies from order 10^2 atmospheres at $\Theta = 0$ to 1 atmosphere as $\Theta \to \pi$. For the range $8 < M_1 < 20$ it may be shown that $30 < S/R < 40$.[2, 3] Hence, from Fig. 1 it appears that for a given S/R in the range indicated, $1.16 < \gamma_e < 1.24$, and a more appropriate value for $\bar{\gamma}_e$ might be 1.2 rather than 1.15.[1] Further, if the equations given in Ref. 1 are integrated, the sign of the second term in Eq. (1) is positive. Using the average value $\bar{\gamma}_e = 1.2$ and correcting Eq. (1), one obtains $C_D \approx 0.95$.

If tables of gas properties which exist for air[3] are used and the modified Newtonian flow introduced[4]

$$(P - P_1)/P_{t_2} = [1 - (P_1/P_{t_2})]\cos^2\Theta \qquad (2)$$

where $P_{t_2} \sim$ total pressure behind shock and $P_1 \sim$ free-stream static pressure, then to first order for $M_1 > 10$

$$(P - P_1)/q_1 = 2\{[1 - (1/2K)] - 1/(\gamma_1 M_1^2)\}\cos^2\Theta \qquad (3)$$

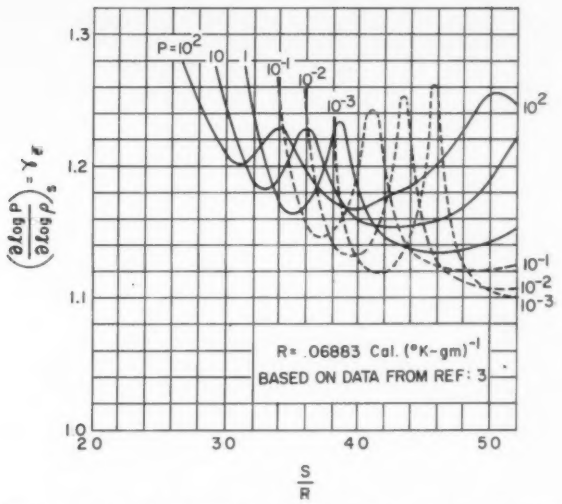

FIG. 1. Isentropic coefficient vs entropy for various values of pressure in atmospheres.

Here, K is proportional to the density increase across the normal shock. If the streamwise component of Eq. (3) is integrated over the streamwise hemisphere of the sphere,[1] and the base drag added,

$$C_D = [1 - (1/2K)] + 1(\gamma_1 M_1^2) \qquad (4)$$

for $M_1 = 10$, $K \sim 9$, and $C_D = 0.952$. It can be shown[2] that over the range $10 < M_1 < 20$ at sea level $9 < K < 12$. If $1/(\gamma_1 M_1^2)$ is neglected, then

$$0.945 < C_D < 0.958 \qquad (5)$$

REFERENCES

[1] Liu, V. C., *On the Drag of a Sphere at Extremely High Speeds*, J. Appl. Phys., Vol. 29, No. 2, pp. 194–195, Feb. 1958.

[2] Lampert, S., *Properties of Dissociated Gas Mixtures and Applications to High Temperature Gas Dynamics*, Aeronutronic Systems Rep. U-293, 1957.

[3] Hilsenrath, J., and Beckett, C. W., *Tables of the Thermodynamic Properties of Argon-Free Air to 15,000°K.*, AEDC TN 56-12, Sept. 1956.

[4] Lees, L., *Recent Developments in Hypersonic Flow*, Jet Prop., Vol. 27, No. 11, pp. 1162–1178, Nov. 1957.

On the Bending of Orthotropic Cylindrical Shells

Y. C. Das
Senior Research Fellow (CSIR),
Dept. of Aeronautical Engineering,
Indian Institute of Science, Bangalore, India

November 7, 1960

THIS NOTE contains a discussion of equations in the Donnell and Vlasov forms, which are applicable to the bending of orthotropic circular cylinders.

A circular cylinder, with radius a, is oriented so that its axial coordinate x and its circumferential coordinate ϕ coincide with the principal directions of orthotropy. In this coordinate system, the relation between stress and strain components can be represented by the following equations:

$$\sigma_x = D_x\epsilon_x + D_1\epsilon_\phi \qquad (1a)$$

$$\sigma_\phi = D_\phi\epsilon_\phi + D_1\epsilon_x \qquad (1b)$$

$$\sigma_{x\phi} = G\epsilon_{x\phi} \qquad (1c)$$

where D_x, D_ϕ, D_1, and G are four constants needed to characterize the elastic properties of an orthotropic material in plane stress.

Let u, v, and w be the displacement components along axial, circumferential, and radial directions, respectively. By the theory of Love's first approximation[1,2] the relations between strains and displacement components for a circular-cylindrical shell are given by

$$\epsilon_x = (\partial u/\partial x) - z(\partial^2 w/\partial x^2) \tag{2a}$$

$$\epsilon_\phi = \frac{1}{a}\left(\frac{\partial v}{\partial \phi} - w\right) - \frac{z}{a^2}\left(\frac{\partial v}{\partial \phi} + \frac{\partial^2 w}{\partial \phi^2}\right) \tag{2b}$$

$$\epsilon_{x\phi} = \frac{1}{a}\frac{\partial u}{\partial \phi} + \frac{\partial v}{\partial x} - \frac{2z}{a}\left(\frac{\partial v}{\partial x} + \frac{\partial^2 w}{\partial x \partial \phi}\right) \tag{2c}$$

By substituting Eqs. (2) into Eqs. (1), stress components can be expressed in terms of displacements, and they are integrated through the thickness of the shell to obtain the following stress resultants (membrane forces) and stress couples (bending moments) per unit length of the normal sections of the shell:

$$N_x = \int_{-h/2}^{h/2} \sigma_x\, dz = h\left[D_x \frac{\partial u}{\partial x} + \frac{D_1}{a}\left(\frac{\partial v}{\partial \phi} - w\right)\right] \tag{3a}$$

$$N_\phi = \int_{-h/2}^{h/2} \sigma_\phi\, dz = h\left[\frac{D_\phi}{a}\left(\frac{\partial v}{\partial \phi} - w\right) + D_1 \frac{\partial u}{\partial x}\right] \tag{3b}$$

$$N_{x\phi} = \int_{-h/2}^{h/2} \sigma_{x\phi}\, dz = h\left[G\left(\frac{1}{a}\frac{\partial u}{\partial \phi} + \frac{\partial v}{\partial x}\right)\right] \tag{3c}$$

$$M_x = \int_{-h/2}^{h/2} \sigma_x\, z dz = -\frac{h^3}{12}\left[D_x \frac{\partial^2 w}{\partial x^2} + \frac{D_1}{a^2}\left(\frac{\partial v}{\partial \phi} + \frac{\partial^2 w}{\partial \phi^2}\right)\right] \tag{3d}$$

$$M_\phi = \int_{-h/2}^{h/2} \sigma_\phi\, z dz = -\frac{h^3}{12}\left[\frac{D_\phi}{a^2}\left(\frac{\partial v}{\partial \phi} + \frac{\partial^2 w}{\partial \phi^2}\right) + D_1 \frac{\partial^2 w}{\partial x^2}\right] \tag{3e}$$

$$M_{x\phi} = -M_{\phi x} = \int_{-h/2}^{h/2} \sigma_{x\phi}\, z dz = \frac{h^3}{12} \times \left[\frac{2G}{a}\left(\frac{\partial v}{\partial x} + \frac{\partial^2 w}{\partial x \partial \phi}\right)\right] \tag{3f}$$

where h is the thickness of the shell.

Substitution of Eqs. (3) into force- and moment-equilibrium equations[3] gives the equilibrium equations in terms of displacements for circular cylinders in the form

$$\frac{\partial^2 u}{\partial \xi^2} + \frac{G}{D_x}\frac{\partial^2 u}{\partial \phi^2} + \frac{D_1 + G}{D_x}\frac{\partial^2 v}{\partial \xi\, \partial \phi} - \frac{D_1}{D_x}\frac{\partial w}{\partial \xi} = 0 \tag{4a}$$

$$\frac{D_1 + G}{D_x}\frac{\partial^2 u}{\partial \xi \partial \phi} + \frac{G}{D_x}\frac{\partial^2 v}{\partial \xi^2} + \frac{D_\phi}{D_x}\frac{\partial^2 v}{\partial \phi^2} - \frac{D_\phi}{D_x}\frac{\partial w}{\partial \phi} = 0 \tag{4b}$$

$$\frac{D_1}{D_x}\frac{\partial u}{\partial \xi} + \frac{D_\phi}{D_x}\frac{\partial v}{\partial \phi} - \frac{D_\phi}{D_x} w - \frac{h^2}{12a^2}(\nabla_0^4 w) = -\frac{qa^2}{hD_x} \tag{4c}$$

where $\xi = x/a$, $q = q(\xi, \phi)$ is the load intensity in radial direction and

$$\nabla_0^4 = \frac{\partial^4}{\partial \xi^4} + \frac{2(D_1 + 2G)}{D_x}\frac{\partial^4}{\partial \xi^2 \partial \phi^2} + \frac{D_\phi}{D_x}\frac{\partial^4}{\partial \phi^4} \tag{5}$$

Uncoupled equations for u and v can be obtained in terms of w from Eqs. (4a) and (4b) in the form,

$$\nabla_1^4 u = \frac{D_1}{D_x}\frac{\partial^3 w}{\partial \xi^3} - \frac{D_\phi}{D_x}\frac{\partial^3 w}{\partial \xi \partial \phi^2} \tag{6a}$$

$$\nabla_1^4 v = \frac{D_\phi}{D_x}\frac{\partial^3 w}{\partial \phi^3} + \frac{D_x D_\phi - D_1^2 - D_1 G}{D_x G}\frac{\partial^3 w}{\partial \xi^2 \partial \phi} \tag{6b}$$

where

$$\nabla_1^4 = \frac{\partial^4}{\partial \xi^4} + \frac{D_x D_\phi - D_1^2 - 2D_1 G}{D_x G}\frac{\partial^4}{\partial \xi^2 \partial \phi^2} + \frac{D_\phi}{D_x}\frac{\partial^4}{\partial \phi^4} \tag{7}$$

Now, operating with ∇_1^4 on Eq. (4c) with $q = 0$, and using Eqs. (6), the following equation is obtained:

$$\frac{h^2}{12a^2}[\nabla_0^4 \nabla_1^4 w] + \frac{(D_x D_\phi - D_1^2)}{D_x^2}\frac{\partial^4 w}{\partial \xi^4} = 0 \tag{8}$$

Eqs. (6) and (8) are similar to Donnell's equations[4] in isotropic cylindrical shells. A displacement function F can be selected such that displacements u, v, and w are obtained as

$$u = \frac{D_\phi}{D_x}\frac{\partial^3 F}{\partial \xi \partial \phi^2} - \frac{D_1}{D_x}\frac{\partial^3 F}{\partial \xi^3} \tag{9a}$$

$$v = -\frac{D_\phi}{D_x}\frac{\partial^3 F}{\partial \phi^3} - \frac{D_x D_\phi - D_1^2 - D_1 G}{D_x G}\frac{\partial^3 F}{\partial \xi^2 \partial \phi} \tag{9b}$$

$$w = -\nabla_1^4 F \tag{9c}$$

With this type of function F, it can be seen that Eqs. (4a) and (4b) are satisfied automatically and Eq. (4c) gives

$$\frac{h^2}{12a^2}[\nabla_0^4 \nabla_1^4 F] + \frac{(\phi_x D_\phi - D_1^2)}{D_x^2}\frac{\partial^4 F}{\partial \xi^4} = -\frac{qa^2}{hDx} \tag{10}$$

This equation is similar to Vlasov's equation[5] in isotropic cylindrical shells. By using Eqs. (9), stress resultants and stress couples, given by Eqs. (3), can be put in terms of displacement function F. If

$$D_x = D_\phi = \frac{E}{(1 - v^2)},\ D_1 = \frac{Ev}{(1 - v^2)},\ \text{and } G = \frac{E(1 - v)}{2(1 - v^2)}$$

Donnell's and Vlasov's equations are obtained from Eqs. (6), (8), and (10), respectively.

As a first example, a portion of a circular cylinder, bounded by $\xi = 0$, $\xi = \xi_1$, $\phi = 0$ and $\phi = \phi_1$ is considered with radial load distribution q and boundary conditions

$$v = w = N_x = M_x = 0 \quad \text{along } \xi = 0 \text{ and } \xi_1 \tag{11a}$$

$$u = w = N_\phi = M_\phi = 0 \quad \text{along } \phi = 0 \text{ and } \phi_1 \tag{11b}$$

Conditions (11) imply that the function F has to satisfy the conditions

$$F = \frac{\partial^2 F}{\partial \xi^2} = \frac{\partial^4 F}{\partial \xi^4} = \frac{\partial^6 F}{\partial \xi^6} = 0 \text{ along } \xi = 0 \text{ and } \xi_1 \tag{12a}$$

$$F = \frac{\partial^2 F}{\partial \phi^2} = \frac{\partial^4 F}{\partial \phi^4} = \frac{\partial^6 F}{\partial \phi^6} = 0 \text{ along } \phi = 0 \text{ and } \phi_1 \tag{12b}$$

The function F is taken in the double trigonometric-series form

$$F = \sum_{m=1}^{\infty}\sum_{n=1}^{\infty} A_{mn} \sin\frac{m\pi\xi}{\xi_1} \sin\frac{n\pi\phi}{\phi_1} \tag{13}$$

which satisfies conditions (12) and the homogeneous part of Eq. (10). The constants A_{mn} are given by

$$A_{mn} = \frac{4}{\xi_1 \phi_1}\frac{a^2}{hD_x} \times \frac{\displaystyle\int_0^{\xi_1}\int_0^{\phi_1} q(\xi,\phi) \sin\frac{m\pi\xi}{\xi_1} \sin\frac{n\pi\phi}{\phi_1}\, d\xi d\phi}{\left\{\frac{h^2\pi^4}{12a^2}\left[\frac{m^4}{\xi_1^4} + \frac{2(D_1 + 2G)}{D_x}\frac{m^2 n^2}{\xi_1^2 \phi_1^2} + \frac{D_\phi}{D_x}\frac{n^4}{\phi_1^4}\right]\left[\frac{m^4}{\xi_1^4} + \frac{(D_x D_\phi - D_1^2 - 2D_1 G)}{D_x G}\frac{m^2 n^2}{\xi_1^2 \phi_1^2} + \frac{D_\phi}{D_x}\frac{n^4}{\phi_1^4}\right] + \frac{(D_x D_x - D_1^2)}{D_x^2}\frac{m^4\pi^4}{\xi_1^4}\right\}} \tag{14}$$

As a second example, a circular cylinder, bounded by $\xi = 0$ and $\xi = \xi_1$ is considered with radial loading q and boundary conditions

$$v = w = N_x = M_x = 0 \text{ along } \xi = 0 \text{ and } \xi_1 \tag{15}$$

Here displacements, forces, etc. must be periodic in ϕ. The function F can be taken as

$$F = \sum_{m=1}^{\infty} \sum_{n=0}^{\infty} \sin \frac{m\pi\xi}{\xi_1} [A_{mn} \cos n\phi + B_{mn} \sin n\phi] \tag{16}$$

where the constants A_{mn} and B_{mn} are given by

$$A_{mn} = \frac{2}{\pi\xi_1} \frac{a^2}{hD_x} \times$$

$$\frac{\int_0^{\xi_1} \int_{-\pi}^{\pi} q(\xi, \phi) \sin \frac{m\pi\xi}{\xi_1} \cos n\phi d\xi d\phi}{\left\{ \frac{h^2}{12a^2} \left[\frac{m^4\pi^4}{\xi_1^4} + \frac{2(D_1 + 2G)}{D_x} \frac{m^2\pi^2}{\xi_1^2} n^2 + \frac{D_\phi}{D_x} n^4 \right] \left[\frac{m^4\pi^4}{\xi_1^4} + \frac{(D_xD_\phi - D_1^2 - 2D_1G)}{D_xG} \frac{m^2\pi^2}{\xi_1^2} n^2 + \frac{D_\phi}{D_x} n^4 \right] + \frac{(D_xD_\phi - D_1^2)}{D_x^2} \frac{m^4\pi^4}{\xi_1^4} \right\}} \tag{17a}$$

$$B_{mn} = \frac{2}{\pi\xi_1} \frac{a^2}{hD_x} \times$$

$$\frac{\int_0^{\xi_1} \int_{-\pi}^{\pi} q(\xi, \phi) \sin \frac{m\pi\xi}{\xi_1} \sin n\phi d\xi d\phi}{\left\{ \frac{h^2}{12a^2} \left[\frac{m^4\pi^4}{\xi_1^4} + \frac{2(D_1 + 2G)}{D_x} \frac{m^2\pi^2}{\xi_1^2} n^2 + \frac{D_\phi}{D_x} n^4 \right] \left[\frac{m^4\pi^4}{\xi_1^4} + \frac{(D_xD_\phi - D_1^2 - 2D_1G)}{D_xG} \frac{m^2\pi^2}{\xi_1^2} n^2 + \frac{D_\phi}{D_x} n^4 \right] + \frac{(D_xD_\phi - D_1^2)}{D_x^2} \frac{m^4\pi^4}{\xi_1^4} \right\}} \tag{17b}$$

References

[1] Naghdi, P. M., *A Survey of Recent Progress in The Theory of Elastic Shells*, Applied Mechanics Reviews, 365, Vol. 19, No. 9, Sept. 1950.

[2] Love, A. E. H., *A Treatise on The Mathematical Theory of Elasticity*, 4th. Ed., p. 543; Dover Publications, New York, 1944.

[3] Timoshenko, S. P., and Woinowsky-Krienger, S., *Theory of Plates and Shells*, 2nd. Ed., p. 514; McGraw-Hill Book Co., Inc., New York, 1959.

[4] Donnell, L. H., *Stability of Thin Walled Tubes Under Torsion*, NACA TR 479, 1933.

[5] Vlasov, W. S., *Allgemeine Schalentheorie Und ihre Anwendung in der Technik*, p. 257; Akademie-Verlag, (German trans. by A. Krom), Berlin, 1958.

The Relation Between Wall Temperature and the Effect of Roughness on Boundary-Layer Transition*

J. Leith Potter and Jack D. Whitfield
von Kármán Gas Dynamics Facility, ARO, Inc., Tullahoma, Tenn.

November 14, 1960

THE EXPERIMENTALLY DEMONSTRATED[1-3] rise and subsequent fall of transition Reynolds number with decreasing wall-to-ambient temperature ratio has been the subject of two recent notes.[4,5] In both cases it was argued that the increased effectiveness of roughness due to wall cooling was not sufficient to explain the transition-reversal phenomenon on nominally smooth bodies. In one case, the criterion for transition reversal was taken to be $Re_k > 600$, and in the other values of Re_k as low as 100 were considered in an effort to be conservative. The parameter Re_k is a Reynolds number formed from velocity and kinematic viscosity based on calculated conditions at the height of roughness element k in the undisturbed, laminar boundary layer at the station of roughness location. The present note is submitted to show that another method for evaluating the effect of roughness on transition leads to an opposite conclusion.

The present authors' method for estimating transition location under the influence of roughness was described in a recent report.[6] Results of further study are being incorporated in a paper soon to be offered for publication. The parameter used to represent the relative disturbance due to roughness was Re'_k, and it was defined as

$$Re'_k \backsimeq Re_k(T_k/T_w)^{0.5+\omega}$$

where T_k = static temperature at height k, corresponding to Re_k

T_w = wall temperature

ω = exponent in viscosity-temperature formula

It is this parameter which is significant in the discussion to follow.

The procedure referred to[6] correlates a variety of data from bodies with walls near adiabatic recovery temperatures. To support an extension to highly-cooled-wall cases, it is necessary to offer further evidence. One example of this appears in Fig. 1, where the Reynolds number of transition, Re_t, calculated on the basis of Ref. 6 with the further refinement referred to above, is compared to typical experimental data from Ref. 2.

To arrive at specific numerical results in Fig. 1, it was necessary to extrapolate the experimental curve arbitrarily for $k = 0$ to wall-to-ambient temperature ratios T_w/T_δ somewhat below those tested with roughness elements. Obviously this cannot be done with even crude accuracy, but the effect of erroneous extrapolation would be quantitative, not qualitative, and it would not change the T_w/T_δ ratio for which transition is estimated effectively at the roughness element.

It should be noted that only single, two-dimensional roughness elements are considered in Fig. 1. For very low temperature ratios, the small but finite roughness due to manufacturing limitations, handling mishaps, and frost formation would become significant near the stagnation region where boundary-layer thickness is small. This cannot be accurately accounted for, but undoubtedly would encourage the reversal phenomenon.

Attention is directed to Table 1, which is based on Fig. 1.

TABLE 1

Roughness k (in.)	Re_k at Reversal		Re_k for Trans. at Roughness,
	Calcd.	Exp.	Calculated
0.0005	30	—	140
0.0010	85	60	206
0.0020	210	200	416

It appears that the criterion $Re_k > 600$, or even 100, is not valid in this case and presumably even less valid for very small, natural roughness.

Referring to the computed Re_t on Fig. 1, it appears that the present empirical theory yields results in general agreement with experiment. Agreement is good where the experimental data for $k = 0$, needed in the present method, are available. Estimated T_w/T_δ at reversal and for transition near the roughness element also are reasonably near experimental values. After acceptance of the computational method, it follows that Re'_k

* Sponsored by Arnold Engineering Development Center, Air Research and Development Command, USAF, under Contract No. AF 40 (600)-800.

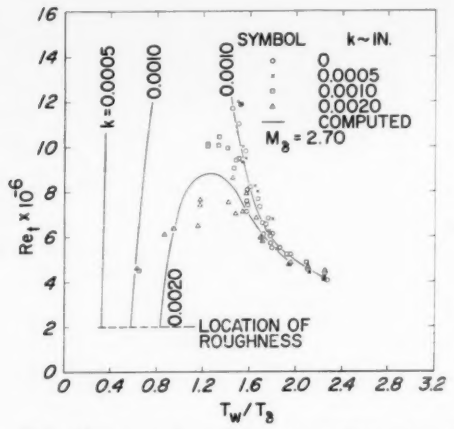

FIG. 1. Transition reversal on 10 deg. cone with local roughness. Data from Ref. 2. Computed curves from Ref. 6 (extended).

always can be made large enough to cause transition reversal if sufficiently low wall temperatures can be applied. Furthermore, and more importantly, wall temperature need not be nearly as low as would be required if $Re_k > 600$ were considered necessary. Indeed, the present method for evaluating the effect of roughness will predict reversal on highly-cooled bodies with Re_k much less than 100, particularly when local Mach numbers are low—e.g., near the noses of blunt bodies. For walls at adiabatic recovery temperature or higher and hypersonic local Mach numbers, it often will predict $Re_k \gg 600$ to bring about transition from laminar to turbulent flow. The value of Re_k needed to bring about transition at the roughness element may fall in the range 10^4–10^5.

REFERENCES

[1] Jack, J. R., Wisniewski, R. J., and Diaconis, N. S., *Effects of Extreme Surface Cooling on Boundary Layer Transition*, NACA TN 4094, Oct. 1957.

[2] Van Driest, E. R., and Boison, J. C., *Experiments on Boundary Layer Transition at Supersonic Speeds*, Journal of the Aeronautical Sciences, Vol. 24, No. 12, pp. 885–899, Dec. 1957.

[3] Stetson, K. F., *Boundary Layer Transition on Blunt Bodies with Highly Cooled Boundary Layers*, Journal of the Aero/Space Sciences, Vol. 27, No. 2, pp. 81–91, Feb. 1960.

[4] Bidwell, J. M., *Use of the Roughness Criterion to Refute Roughness as the Cause of Reported Transition Reversal*, Journal of the Aerospace Sciences, Readers' Forum, Vol. 27, No. 8, pp. 622–623, Aug. 1960.

[5] Cooper, M., Mayo, Ed. E., and Julius, J. D., *The Influence of Low Wall Temperature on Boundary Layer Transition and Local Heat Transfer on 2-Inch-Diameter Hemispheres at a Mach Number of 4.95 and a Reynolds Number Per Foot of 73.2 × 10⁶*, NASA TN D-391, July 1960.

[6] Potter, J. L., and Whitfield, J. D., *Effects of Unit Reynolds Number, Nose Bluntness, and Roughness on Boundary Layer Transition*, Paper presented at AGARD Boundary Layer Research Meeting, London, April 25–29, 1960 (AEDC-TR-60-5).

Dissociation Relaxation Behind a Plane, Oblique, Shock Wave

Melvin Epstein*
Lockheed Aircraft Corporation, Missiles and Space Division, Van Nuys, Calif.

November 15, 1960

THE STREAMLINES downstream of a plane, oblique, shock wave can be shown to be curved if the gas dissociates at a finite rate by means of the following simple argument. Consider the normal AB between any two streamlines in Fig. 1. If the gas is dissociating at a finite rate, then the pressure, velocity, etc., vary along the streamlines. On the other hand, from the geometry of the problem, all quantities must be constant on lines parallel to the shock wave. Since the pressure at A is therefore different from the pressure at B, a pressure gradient exists normal to the streamlines and they must therefore be curved. One concludes that the shock wave generated by a wedge must be curved if the gas is relaxing. This effect may be important in interpreting experimental data such as those presented by Feldman.[1]

The analysis of the flow downstream of the plane shock wave is considerably simplified if one takes advantage of the constancy of all flow variables on lines parallel to the shock wave. Neglecting viscosity, heat conduction, and diffusion, the equations of motion are

$$\text{div}\,(\rho\,\vec{V}) = 0$$

$$\vec{V}\cdot\nabla\vec{V} = -(1/\rho)\text{grad}\,p$$

$$h + \frac{1}{2}|\vec{V}|^2 = H = \text{constant}$$

$$h = 3\mathcal{R}T + (D/2m)\alpha + \frac{p}{\rho}$$

$$p = \rho\mathcal{R}T(1+\alpha)$$

$$D\alpha/Dt = C\rho T^{-s}[(1-\alpha)e^{-D/kT} - \alpha^2(\rho/\rho_D)]$$

where α is the mass fraction of atoms, $\mathcal{R}$ is the molecular gas constant, D is the dissociation energy, and C is the reaction-rate coefficient. The last three equations are obtained by assuming that the gas is the ideal dissociating gas postulated by Lighthill[2] and Freeman.[3] Lines parallel to the shock wave may be described by the equation

$$y = (x - \sigma)\tan\beta$$

where σ is constant on each line and β is the shock-wave angle. Noting that all quantities are functions of σ only, and introducing the nondimensional quantities,

$$R = \rho/\rho_\infty, \qquad U = u/V_\infty, \qquad V = v/V_\infty,$$
$$P = p/\rho_\infty V_\infty^2, \qquad \zeta = (CR^s\rho_\infty)/V_\infty^{2s+1}\sigma$$

the equations of motion reduce to

$$d/d\zeta(RU - RV\,\text{ctn}\,\beta) = 0$$

$$(RU - RV\,\text{ctn}\,\beta)dU/d\zeta = -(dP/d\zeta)$$

$$(RU - RV\,\text{ctn}\,\beta)dV/d\zeta = \text{ctn}\,\beta\,dP/d\zeta$$

$$2[(4+\alpha)/(1+\alpha)]P/R + \mathfrak{D}\alpha + U^2 + V^2 = \mathfrak{C} + 1$$

$$(RU - RV\,\text{ctn}\,\beta)\frac{d\alpha}{d\zeta} = R^2\left[\frac{R(1+\alpha)}{P}\right]^5 \times [(1-\alpha)e^{-\mathfrak{D}R(1+\alpha)/2P} - \alpha^2(R/R_D)]$$

where $\mathfrak{D} = D/m\,V_\infty^2$ and $\mathfrak{C} = (2H/V_\infty^2) - 1$. The first three equations can be integrated directly to give $RU - RV\,\text{ctn}\,\beta = \text{const} = K_1$, $K_1U + P = \text{const} = K_2$, and $K_1V - P\,\text{ctn}\,\beta =$

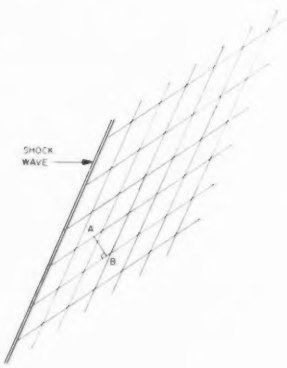

FIG. 1. Flow-field configuration.

* Presently, Head, Theoretical Gasdynamics Section, Aerodynamics and Propulsion Laboratory, Aerospace Corp.

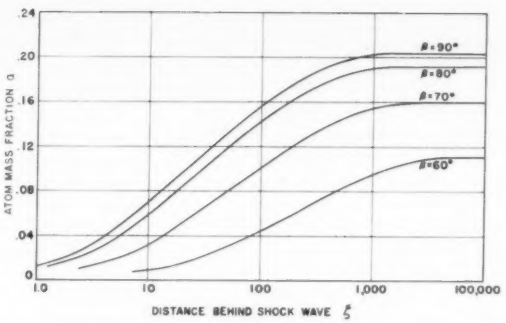

FIG. 2. Variation of atom mass fraction behind an oblique shock wave.

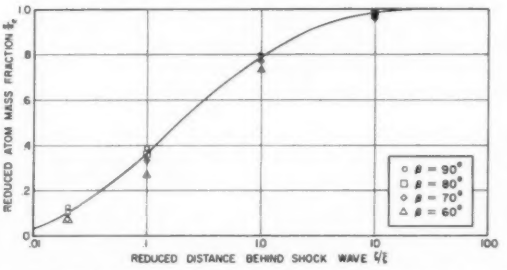

FIG. 3. Correlation of solutions by means of relaxation length.

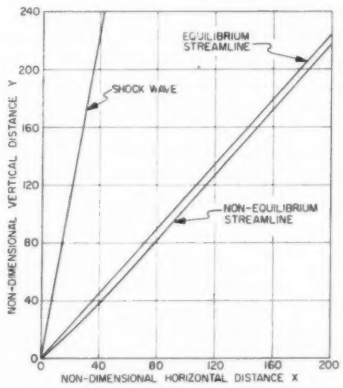

FIG. 4. Effect of relaxation on a typical streamline. $\beta = 80°$.

const $= K_3$. The constants are determined by evaluating these expressions at the shock wave where $\alpha = 0$. Under hypersonic conditions, they are accurately approximated by $K_1 = K_2 = 1$, $K_3 = 0$. The above expressions can then be solved for U, V, and R in terms of P. Using these results in Eq. (4), P can be determined in terms of α. Substituting all of these results into Eq. (5) one obtains

$$d\alpha/d\zeta = F(\alpha) \tag{6}$$

where

$$F(\alpha) = R^2 \left[\frac{R(1+\alpha)}{P}\right]^s [(1-\alpha)e^{-\mathfrak{D}R(1+\alpha)/2P} - \alpha^2(R/R_D)] \tag{7}$$

Noting that $\alpha = 0$ when $\zeta = 0$, Eq. (6) may be integrated to give

$$\zeta = \int_0^\alpha \frac{d\alpha}{F(\alpha)} \tag{8}$$

Eq. (8) can be integrated numerically once $\mathfrak{D}$ and s are specified. Typical results are shown on Fig. 2 for $s = 0$, $\mathfrak{D} = 2$, and various shock-wave angles.

In analogy with displacement, momentum, and energy thicknesses in boundary-layer theory, one may define relaxation distances based on mass, momentum, and energy defects. Another possibility, an atom-deficit relaxation length defined by

$$\alpha_e\zeta = \int_0^\infty (\alpha_e - \alpha)d\zeta \tag{9}$$

where α_e is the equilibrium value, has been found to correlate the numerical solutions quite well (Fig. 3). Using this relaxation length as the unit of length, the deviation of a typical streamline from a straight line is shown in Fig. 4 for $\beta = 80°$. The relaxation effect results in a vertical displacement of the streamline of approximately 10 percent of the relaxation length. Such a calculation may be useful in giving an indication of the order of magnitude of the distortion of the flow pattern due to relaxation effects at a given flight condition.

REFERENCES

[1] Feldman, S., *The Chemical Kinetics of Air at High Temperatures: A Problem in Hypersonic Aerodynamics*, Heat Transfer and Fluid Mechanics Institute, 1957.

[2] Lighthill, M. J., *Dynamics of a Dissociating Gas*, Part I, *Equilibrium Flow*, J. Fluid Mech., Vol. 2, Pt. 1, pp. 1–32, Jan. 1957.

[3] Freeman, N. C., *Non-Equilibrium Flow of an Ideal Dissociating Gas*, J. Fluid Mech., Vol. 4, Pt. 3, July 1958.

Solving Structural Redundants in Terms of Quadratic Double Roots

Lawrence L. Margolin
Senior Structures Engineer
North American Aviation, Inc., Inglewood, California
November 22, 1960

PARABOLAS possess a unique property, in that the point of zero slope can be found without the use of the derivative. The external-work form of the elastic-energy equation is one such case. It is shown here that the solution of redundants can be obtained by the nullification of the discriminant of a quadratic equation, thus expressing the redundants as double roots. This approach is interesting in that regardless of the choice of redundants no use is made of the derivative or simultaneous compatible-deflection equations. In addition, a less abstract interpretation of the minimum-energy principle results.

LIST OF SYMBOLS

U = elastic energy
P_1 = static load
P_2, P_3 = redundant reactions
Δ_{xy} = deflection coefficient, horizontal
δ_{xy} = deflection coefficient, vertical
X = point of deflection considered
Y = load causing the deflection

THEORY

The case depicted in Fig. 1 is representative of a two-redundant problem. Writing the energy equation for this without regard to the final position of point b gives

$$U = {}^1/_2\Delta_{a1}P_1^2 + {}^1/_2\delta_{b2}P_2^2 + {}^1/_2\Delta_{b3}P_3^2 + P_1P_2\delta_{b1} + P_1P_3\Delta_{b1} + P_2P_3\delta_{b3} \tag{1}$$

Rearranging Eq. (1) as a quadratic in P_2 results in the equation

$$({}^1/_2\delta_{b2})P_2^2 + (P_1\delta_{b1} + P_3\delta_{b3})P_2 + ({}^1/_2\Delta_{a1}P_1^2 + {}^1/_2\Delta_{b3}P_3^2 + P_1P_3\Delta_{b1} - U) = 0 \tag{2}$$

Solving for P_2 by the quadratic formula yields the two roots

$$P_2 = -(P_1\delta_{b1} + P_3\delta_{b3})/\delta_{b2} \pm 1/\delta_{b2}[(P_1\delta_{b1} + P_3\delta_{b2})^2 - 2\delta_{b2}({}^1/_2\Delta_{a1}P_1^2 + {}^1/_2\Delta_{a3}P_3^2 + P_1P_3\Delta_{b1} - U)]^{1/2} \tag{3}$$

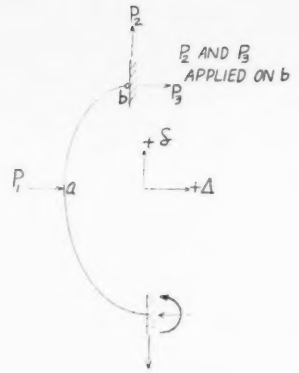

FIG. 1. Redundant problem of sample analysis.

The $\partial U/\partial P_2 = 0$ operation is replaced by setting the discriminant equal to zero, which amounts to imposing uniqueness on P_2 (Fig. 2).

Thus $$P_2 = -(P_1\delta_{b1} + P_3\delta_{b3})/\delta_{b2}$$
or $$P_2\delta_{b2} + P_1\delta_{b1} + P_3\delta_{b3} = 0 \quad (4)$$

and also from under the radical

$$(P_1\delta_{b1} + P_3\delta_{b3})^2 - 2\delta_{b2}(\tfrac{1}{2}\Delta_{a1}P_1^2 + \tfrac{1}{2}\Delta_{b3}P_3^2 + P_1P_3\Delta_{b1} - U) = 0 \quad (5)$$

Eq. (4) is the familiar compatible-deflection equation, $\sum\delta_b = 0$. Eq. (5) is again a second-degree equation, which when put in the form of a quadratic in P_3 is

$$(\delta_{b3}^2 - \Delta_{b3}\delta_{b2})P_3^2 + (2P_1\delta_{b1}\delta_{b3} - 2P_1\Delta_{b1}\delta_{b2})P_3 + (P_1^2\delta_{b1}^2 - P_1^2\Delta_{a1}\delta_{b2} + 2\delta_{b2}U) = 0 \quad (6)$$

Again using the quadratic formula,

$$P_3 = -P_1\frac{(\delta_{b1}\delta_{b3} - \Delta_{b1}\delta_{b2})}{(\delta_{b3}^2 - \Delta_{b3}\delta_{b2})} \pm \frac{P_1}{(\delta_{b3}^2 - \Delta_{b3}\delta_{b2})} \times \left[\left(\delta_{b1}\delta_{b3} - \Delta_{b1}\delta_{b2}\right)^2 - \left(\delta_{b3}^2 - \Delta_{b3}\delta_{b2}\right)\left(\delta_{b1}^2 - \Delta_{a1}\delta_b + 2\delta_{b2}\frac{U}{P_1^2}\right)\right]^{1/2} \quad (7)$$

Nullifying the discriminant gives the final value of P_3 as

$$P_3 = -P_1(\delta_{b1}\delta_{b3} - \Delta_{b1}\delta_{b2})/(\delta_{b3}^2 - \Delta_{b3}\delta_{b2}) \quad (8)$$

This is the same result given by a compatible-deflection analysis. The value of P_2 can be obtained by substitution of Eq. (8) in Eq. (4) or else by solving it as the last redundant in sequence as was P_3. In expressing each redundant consecutively in a quadratic and nullifying the discriminant, the corresponding redundant drops out. Thus for n redundants there would be n discriminants and the last operation would yield the numerical value of the last redundant in sequence and also the numerical value of the stored energy from the last zero discriminant. Each nullification of a discriminant expresses the fact that the corresponding redundant can have only one possible value. In the process this is done for all the redundants. Since the proper energy equation as set up in the beginning is accounted for throughout and the condition of uniqueness is imposed on each redundant, it follows that this method applies to any number of redundants, the two conditions mentioned being the only requirements. As noted in Fig. 2 the energy must be at a point of zero slope for the redundant to have only one value, which it must as a physical quantity. Since the energy has no upper bounds it follows that it is at a minimum.

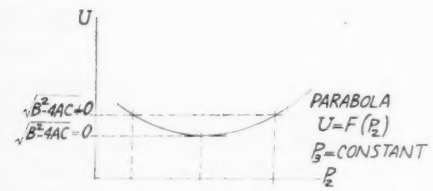

FIG. 2. Defining the equation $\partial U/\partial P_2 = 0$ by forming the double root of P_2.

Although structural redundants can be solved without any of the usual devices, the foregoing procedure does not appear to offer any distinct advantages. Although it is not noted in the example set forth, the process can be made far less cumbersome when dealing with a large number of redundants if the polynomial B in the discriminant $B^2 - 4AC$ is grouped and manipulated as a binomial with one of its terms containing the redundant to be eliminated. Aside from this feature the procedure is clearly analogous to conventional methods in simultaneous equations.

Geometric Derivation of Compatibility Equation for Finite Deformation of Rotationally Symmetric Shells*

B. Paul
Director of Research, Technik Incorporated, Garden City, N. Y.
November 23, 1960

IN THE FORMULATION of the problem of finite symmetrical deflections of shells of revolution it is necessary to establish a compatibility equation involving the principal strains of the middle surface. Reissner[1] has presented a simple analytical derivation of the compatibility equation by expressing each strain in terms of the radial displacement and then eliminating the radial displacement between the two expressions for strain.

Because of the importance of the problem it seems desirable to the author to present a brief geometric derivation which, besides providing insight into the meaning of the compatibility equation, is suitable for teaching purposes at an elementary level.

Fig. 1 illustrates a short segment of the meridian of a surface of revolution in its undeformed position AB. After deformation the element AB will occupy position $A'B'''$ and will have stretched to the length

$$A'B''' = (1 + \epsilon_\phi)ds_0 \quad (1)$$

where ϵ_ϕ represents the finite conventional strain (fractional extension of original length) in the meridional direction. The point A will have moved radially through a distance u so that the circumferential finite strain is given by

$$\epsilon_\theta = u/r_0 \quad (2)$$

where r_0 is the initial radius of point A. The inclination of the line element changes from ϕ_0 to ϕ as shown on Fig. 1 where

$$\cos\phi_0 = dr_0/ds_0 \quad (3)$$

From Fig. 1 it is easily verified that

$$du = (1 + \epsilon_\phi)ds_0\cos\phi - ds_0\cos\phi_0$$

Upon elimination of u and ds_0 by means of Eqs. (2) and (3) one finds

$$\cos\phi_0 d(r_0\epsilon_\theta) = dr_0(\epsilon_\phi\cos\phi + \cos\phi - \cos\phi_0) \quad (4)$$

which is equivalent to Reissner's form [Eq. (20)[1]] of the compatibility equation.

It is perhaps worth noting that the general compatibility equations in the theory of shells are direct consequences of the Gauss-Codazzi integrability conditions of differential geometry.[2] For a symmetrically deformed surface of revolution the only nontrivial integrability condition is equivalent to

$$dr = ds\cos\phi \quad (5)$$

* Results obtained in course of research for Frankford Arsenal under Contract No. DA-30-069-ORD-2971.

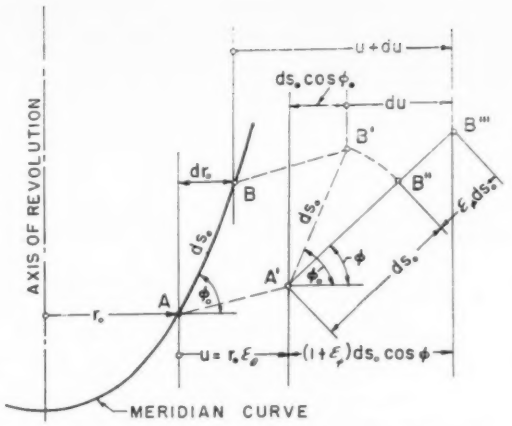

FIG. 1. Element of meridian, before and after deformation.

where r and s represent the deformed values of r_0 and s_0.

Eq. (5) is easily reduced to Eq. (4) by noting that $r = r_0 + u$ and $ds = (1 + \epsilon_\phi)ds_0$. Eq. (5) is then transformed to

$$d(r_0 + u) = (1 + \epsilon_\phi)ds_0 \cos\phi \tag{6}$$

Upon use of Eqs. (2) and (3), Eq. (6) becomes the required compatibility eq. (4).

REFERENCES

[1] Reissner, E., *On The Theory of Thin Elastic Shells*, H. Reissner Anniversary Volume, pp. 231–247; Ann Arbor, Mich., 1949.

[2] Novozhilov, V. V., *The Theory of Thin Shells*, pp. 28, 103; P. Noordhoff, Ltd., Groningen, Netherlands, 1959.

Laminar Jet Mixing of an Electrically Conducting Fluid in the Presence of a Magnetic Field†

Kaoru Toba

Department of Aeronautical Engineering, Rensselaer Polytechnic Institute, Troy, N.Y.

November 1, 1960

RECENTLY there has been discussion about the two-dimensional laminar jet mixing of an incompressible, electrically conducting, viscous fluid under the influence of an applied transverse magnetic field.[1] In this note, a supplementary consideration is offered concerning this type of flow. Let us assume a sufficiently large flow Reynolds number throughout this note, and also that all fluid properties are assumed constant.

The fundamental equations are then

$$\frac{\partial\psi}{\partial y}\frac{\partial^2\psi}{\partial x\partial y} - \frac{\partial\psi}{\partial x}\frac{\partial^2\psi}{\partial y^2} - \frac{\partial^3\psi}{\partial y^3} = -\frac{\partial p}{\partial x} - \beta\frac{\partial A}{\partial x}\nabla^2 A \tag{1}$$

$$0 = -(\partial p/\partial y) + \beta(\partial A/\partial y)\nabla^2 A \tag{2}$$

$$(\partial\psi/\partial y)(\partial A/\partial x) - (\partial\psi/\partial x)(\partial A/\partial y) = (1/\epsilon)\nabla^2 A \tag{3}$$

where ψ is the stream function, A the magnetic vector potential,

$$\beta = (\mu_e H_0^2/\rho U_0^2) \quad \text{and} \quad \epsilon = \nu\sigma\mu_e$$

All quantities involved are nondimensionalized in such a way that

$$x = (U_0/\nu)x^* \qquad y = (U_0/\nu)x^*$$

$$\psi = \psi^*/\nu \qquad H = H^*/H_0 \qquad p = p^*/\rho U_0^2$$

The coordinate system is taken the same as in reference 1.

Now let us assume, as in reference 1, that the magnetic Reynolds number R_m is small. Since ϵ the ratio of the magnetic Reynolds number to the Reynolds number is considered to be small, we may expand ψ and A in power series in ϵ:

$$\left.\begin{aligned}\psi &= \psi_0 + \epsilon\psi_1 + \epsilon^2\psi_2 + \dots\\ A &= A_0 + \epsilon A_1 + \epsilon^2 A_2 + \dots\\ p &= p_0 + \epsilon p_1 + \epsilon^2 p_2 + \dots\ (p_0 = \text{const.})\end{aligned}\right\} \tag{4}$$

Substituting into Eqs. (1)–(3) and comparing the coefficients of the same power of ϵ, we have

$$\frac{\partial\psi_0}{\partial y}\frac{\partial^2\psi_0}{\partial x\partial y} - \frac{\partial\psi_0}{\partial x}\frac{\partial^2\psi_0}{\partial y^2} - \frac{\partial^3\psi_0}{\partial y^3} = 0 \tag{5}$$

$$\left.\begin{aligned}&\frac{\partial\psi_0}{\partial y}\frac{\partial^2\psi_1}{\partial x\partial y} + \frac{\partial\psi_1}{\partial y}\frac{\partial^2\psi_0}{\partial x\partial y} - \frac{\partial\psi_0}{\partial x}\frac{\partial^2\psi_1}{\partial y^2} - \frac{\partial\psi_1}{\partial x}\frac{\partial^2\psi_0}{\partial y^2} - \frac{\partial^3\psi_1}{\partial y^3} = -\frac{\partial p_1}{\partial x} - \beta\frac{\partial A_0}{\partial x}\nabla^2 A_1\\ &0 = -\frac{\partial p_1}{\partial y} + \beta\frac{\partial A_0}{\partial y}\nabla^2 A_1\\ &\frac{\partial\psi_0}{\partial y}\frac{\partial A_0}{\partial x} - \frac{\partial\psi_0}{\partial x}\frac{\partial A_0}{\partial y} = \nabla^2 A_1\end{aligned}\right\} \tag{6}$$

$$\left.\begin{aligned}&\frac{\partial\psi_0}{\partial y}\frac{\partial^2\psi_2}{\partial x\partial y} + \frac{\partial\psi_1}{\partial y}\frac{\partial^2\psi_1}{\partial x\partial y} + \frac{\partial\psi_2}{\partial y}\frac{\partial^2\psi_0}{\partial x\partial y} - \frac{\partial\psi_0}{\partial x}\frac{\partial^2\psi_2}{\partial y^2} - \frac{\partial\psi_1}{\partial x}\frac{\partial^2\psi_1}{\partial y^2} - \frac{\partial\psi_2}{\partial x}\frac{\partial^2\psi_0}{\partial y^2} - \frac{\partial^3\psi_2}{\partial y^3} = -\frac{\partial p_2}{\partial x} - \beta\left(\frac{\partial A_0}{\partial x}\nabla^2 A_2 + \frac{\partial A_1}{\partial x}\nabla^2 A_1\right)\\ &0 = -\frac{\partial p_2}{\partial y} + \beta\left(\frac{\partial A_1}{\partial y}\nabla^2 A_1 + \frac{\partial A_0}{\partial y}\nabla^2 A_2\right)\\ &\frac{\partial\psi_0}{\partial y}\frac{\partial A_1}{\partial x} + \frac{\partial\psi_1}{\partial y}\frac{\partial A_0}{\partial y} - \frac{\partial\psi_0}{\partial x}\frac{\partial A_1}{\partial y} - \frac{\partial\psi_1}{\partial x}\frac{\partial A_0}{\partial y} = \nabla^2 A\end{aligned}\right\} \tag{7}$$

and so on.

It is seen that to the order of ϵ^2, or neglecting $0(\epsilon)$, the flow field can be approximated by the nonmagnetic flow, and that to the order of ϵ, or neglecting $0(\epsilon^2)$, the interaction between the flow and the magnetic field is determined completely by the applied field alone. This is due to the fact that the first-order induced current, $j_1 = \nabla^2 A_1$, is determined completely by ψ_0 and A_0 as shown in the third equation of (6).

For a higher order solution, say to $0(\epsilon^2)$, we should solve the third equation of (7) for A_2 under suitable boundary conditions and then proceed to the first and second equations of (7) to find ψ_2 and p_2, and so forth.

As to the similar solution for the transverse applied field varying proportionately with $x^{-2/3}$, it does not seem to exist. But, as implied in reference 1, it may exist to the order of ϵ—i.e., if the induced filed is neglected. The argument in the same reference starts by neglecting the higher order induced fields and by neglecting the pressure gradient in the x-direction, while the velocity field ψ is expanded in terms of powers in Q. Note that here ψ and Q, as they appear in reference 1, are dimensional. Of course, if these series converge, they constitute the solution of the fundamental equations. However, the fundamental equations are correct to $0(Q)$. Hence it is not quite clear whether or not the higher order terms have any physical significance. Furthermore, the pressure gradient in the x-direction may not be zero in the higher order solution, as seen from the foregoing procedure.

Let us study in more detail the line of approach used in reference 1. By using Eq. (3) to eliminate $\nabla^2 A$ from Eqs. (1) and (2), all expressed in terms of the dimensional quantities, we get

† This research was supported by the United States Air Force through the AFOSR of the ARDC under Contract No. AF 49(638)-23. Reproduction in whole or in part is permitted for any purpose of the United States Government.

$$\left.\begin{aligned} \frac{\partial\psi}{\partial x}\frac{\partial^2\psi}{\partial x\partial y} - \frac{\partial\psi}{\partial x}\frac{\partial^2\psi}{\partial y^2} - \nu\frac{\partial^3\psi}{\partial y^3} &= -\frac{1}{\rho}\frac{\partial p}{\partial x} - \\ Q\frac{\partial A}{\partial x}\left(\frac{\partial\psi}{\partial y}\frac{\partial A}{\partial x} - \frac{\partial\psi}{\partial x}\frac{\partial A}{\partial y}\right) \\ 0 &= -\frac{1}{\rho}\frac{\partial p}{\partial y} + Q\frac{\partial A}{\partial y}\left(\frac{\partial\psi}{\partial y}\frac{\partial A}{\partial x} - \frac{\partial\psi}{\partial x}\frac{\partial A}{\partial y}\right) \end{aligned}\right\} \quad (8)$$

where $Q = (\sigma\mu_e^2 H_1^2/\rho)$. Again, let us expand ψ and A such that

$$\left.\begin{aligned} \psi &= \psi_0 + Q\psi_1 + Q^2\psi_2 + \ldots \\ A &= A_0 + QA_1 + Q^2A_2 + \ldots \\ p &= p_0 + Qp_1 + Q^2p_2 + \ldots \end{aligned}\right\} \quad (9)$$

Substituting these into Eq. (8), and equating the coefficients of the same powers of Q, we get a number of differential equations, as before.

For the transverse applied field $H_0 = H_1x^{-2/3}/3$, we can introduce the similarity parameter $\eta = (1/3\nu^{1/2})(y/x^{2/3})$ and the functions f_i, g_i, and h_i; viz.,

$$\left.\begin{aligned} \psi_i &= \nu^{1/2}x^{1/3}f_i(\eta) \\ A_i &= x^{1/3}g_i(\eta) \\ p_i/\rho &= x^{-2/3}h_i(\eta)/9 \end{aligned}\right\} \quad \left.\begin{aligned} (i = 0,1,2,\ldots) \\ (i = 1,2,\ldots) \end{aligned}\right\} \quad (10)$$

where $g_0 = -1$. Then the equations obtained from (8) reduce to

$$f_0''' + (f_0f_0')' = 0 \quad (11)$$

$$\left.\begin{aligned} f_1''' + 2f_0'f_1' + f_0f_1'' + f_1f_0'' &= -2(h_1 + \eta h_1') + f_0' \\ 0 &= h_1' \end{aligned}\right\} \quad (12)$$

and so on.

The differential equations for f_0 and f_1 or Eqs. (11) and (12) are essentially the same as in reference 1, although (12) is slightly different. If appropriate boundary conditions are given, these equations may be solved completely without knowing the induced field. On the other hand, the higher order solution $f_i (i \geq 2)$ involves the induced field $g_i (i \geq 1)$ and, therefore, cannot be determined according to this scheme.

Let us study the first-order solution f_1 with the boundary conditions

$$\left.\begin{aligned} \eta = 0 \qquad & f_1 = f_1'' = 0 \\ \eta \to \infty \qquad & f_1' \to 0 \end{aligned}\right\} \quad (13)$$

Integrating (12) we get

$$\left.\begin{aligned} f_1'' + f_0f_1' + f_0'f_1 &= -2\eta h_1 + f_0 \\ h_1 &= \text{constant} \end{aligned}\right\} \quad (14)$$

It is readily observed that this equation does not have a solution which satisfies the boundary conditions. Since the shear due to f_1 is proportional to f_1'', this quantity should remain finite as $\eta \to \infty$. But (14) shows that this is not the case unless $h_1 = 0$. Take $h_1 = 0$; then, by integrating Eq. (13) we can easily find that the solution which satisfies the conditions at $\eta = 0$ cannot satisfy that for $\eta \to \infty$.* In reference 1, instead of (14), the equation

$$f''' + ff'' + f'^2 = Qf'$$

is considered. Integrating once we have

$$f'' + ff' = Qf$$

By expanding $f = f_0 + Qf$, we have (14) except for the h_1 term. All in all, our conclusion is that the similar solution does not seem to exist to the order of Q, but it does to the order of Q^0 not only for this prescribed magnetic field but also for any applied field.

* More simply, we should expect $f'' \to 0$ as $\eta \to \infty$, which is not satisfied by (14) even with $h_1 = 0$.

REFERENCE

1 Pai, S. I., *Laminar Jet Mixing of Electrically Conducting Fluid in a Transverse Magnetic Field*, Journal of the Aero/Space Sciences, Vol. 26, No. 4, pp. 254–255, April 1959.

Determination of the Flow Field Around a Hollow Body of Revolution Using a Ring Source

David C. Paulson*

December 1, 1960

AT PRESENT, the streamlines in potential flow about hollow bodies of revolution are most conveniently obtained graphically.[1] This note gives an analytical solution with which the radius of any given streamline may be determined directly.

A ring source of strength m per unit length and radius R is symmetrically placed around the origin of cylindrical coordinates, as shown in Fig. 1.

The potential at any point of coordinates x, r due to the entire ring is

$$\Phi = 2\int_0^\pi \frac{mRd\theta}{\sqrt{x^2 + R^2 + r^2 + 2Rr\cos\theta}}$$

which can be transformed into

$$\Phi = \frac{4mR}{\sqrt{x^2 + R^2 + r^2 + 2Rr}}\int_0^{\pi/2}\frac{d\theta}{\sqrt{1 - k^2\sin^2\theta'}} \quad (1)$$

where $\theta' = \theta/2$

$$k^2 = 4Rr/(x^2 + R^2 + r^2 + 2Rr)$$

and the integral is the tabulated complete elliptic integral of the first kind, $F(k, \pi/2)$.

Applying Prandtl's flow balance to a disk concentric around the axis:[2]

$$\int_0^{r_1} 2\pi r u dr = Q_1 + Q_2 \quad (2)$$

where r_1 = the radius on a streamline
u = $\partial\Phi/\partial x$ = the axial velocity component
Q_1 = the volume of fluid coming with the main stream and equaling $\pi r_0^2 a$, where
a = the velocity of the fluid stream
r_0 = the radius of a given streamline far upstream
Q_2 = the volume of fluid issued by the source if it is upstream from the x-coordinate in question.

Adding the potential $\Phi = ax$ to Eq. (1), differentiating, and substituting in Eq. (2),

$$\pi r_1^2 a + \frac{\pi mx}{\sqrt{R}}\int_0^{r_1}\frac{k^3}{\sqrt{r}}\left[k\frac{dF}{dk} + F(k, \pi/2)\right]dr = Q_1 + Q_2 \quad (3)$$

* Presently at Missiles and Space Systems Dept., Hamilton Standard Div., United Aircraft Corp., Windsor Locks, Conn.

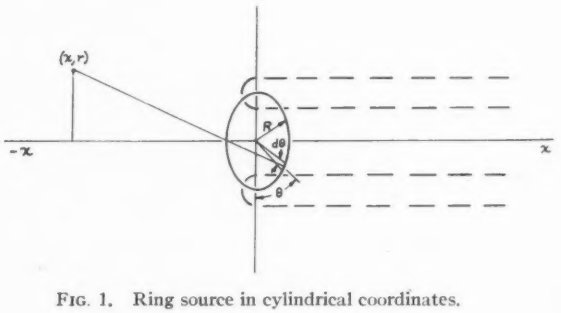

FIG. 1. Ring source in cylindrical coordinates.

which is the relation from which the streamlines can be found.

The integration is not possible in terms of k because of a singularity in dr/dk, but the following method yields a solution for r_1. The function $k^3[k(dF/dk) + F]$ is tabulated as a general function vs k. Then, for any value of x, the integral can be numerically evaluated by successively calculating k for increasing r_1 and adding the increment $(k^3/\sqrt{r})[k(dF/dk) + F]\Delta r$ read from the tabulation. When the left-hand side of Eq. (3) equals the right-hand side, the value of r_1 is on the desired streamline.

This method allows a unique determination of Q_1 for the body surface itself, which is possible only by trial and error in the method of graphical superposition. The integration is carried out at some arbitrary x-value just upstream from the ring source. The left-hand side of Eq. (3) reaches a maximum at r_1, equal to the inner radius of the hollow body at that point. This may be found by differentiating the left-hand side of Eq. (3) with respect to r_1 and setting equal to zero:

$$r_1 = (mx/2a\sqrt{Rr_1})k^3[k(dF/dk) + F]$$

where r_1 is solved by trial and error.

The value of the left-hand side of Eq. (3) at this point is then equal to $Q_1 + Q_2$, and, since the latter is zero upstream from the source, simply equal to $Q_0 = \pi r_0^2 a$. Downstream from the source $Q_2 = 0$ inside the hollow body, and for values of r_1 outside the body of revolution $Q_2 = 2\pi R(4\pi m)$ is added to the right-hand side.

The above method has two distinct advantages over the graphical method of solving the flow field of the hollow body of revolution. First, the radius of any desired streamline can be determined directly at any x-coordinate; and, second, the stagnation streamline can be found directly using the procedure just shown.

This method can also be adapted readily to computer techniques, as can the tabulation of the function $k^3[k(dF/dk) + F]$. A sample flow field has been calculated,[3] and agrees with that solved by the method of graphical superposition.[1]

TABLE 1
Tabulation of the Function $k^3[k(dF/dk) + F(k, \pi/2)]$

Arc sin k	$F(k, \pi/2)$	$k^3[k(dF/dk) + F(k, \pi/2)]$
0	1.5708	0.
5	1.5738	0.001046
10	1.5828	0.006416
15	1.5981	0.02669
20	1.6200	0.06904
25	1.6490	0.1377
30	1.6868	0.2446
35	1.7312	0.4030
40	1.7868	0.6305
45	1.8541	0.9561
50	1.9356	1.4204
55	2.0347	2.1029
60	2.1565	3.1464
65	2.3088	4.8511
70	2.5046	7.9331
75	2.7681	14.483
80	3.1534	32.949
85	3.8317	131.64
86	4.0526	205.86
87	4.3387	365.31
88	4.7427	820.27
89	5.4349	3335.9
90	∞	∞

REFERENCES

[1] Streeter, V. L., "Dynamics of a Non-Viscous, Incompressible Fluid," *Handbook of Engineering Fundamentals*, 2nd. Ed., sec. 6-5, pp. 5–27f.; John Wiley & Sons, Inc., New York, 1952.

[2] Prandtl, L., and Tietjens, O. G., *Fundamentals of Hydro and Aeromechanics*, 1st. Ed. ,pp. 144f.; McGraw-Hill Book Co., Inc., New York, 1934.

[3] Paulson, D. C., *Distortion of a Fluid Lamina Approaching an Aspirating Probe in a Uniform Velocity Fluid Stream with a Section on an Analytical Solution for the Hollow Body of Revolution Using a Ring Source*, Master's Thesis, Univ. of Minnesota, March 1960.

Flutter of a Hot-Wire Probe

Max M. Munk

November 30, 1960

THE HOT-WIRE probe signals indicate the relative motion between the air and the wire. The turbulent air velocity fluctuates. But just as a flag pole shakes in a gusty wind, so will the wire, the prongs, and the prong holder shake in turbulent air. Very small amplitudes of flutter are enough to modify the hot-wire signals. In a typical case, the rms air fluctuation velocity may be 6 in./sec at a frequency of 10,000/sec. This corresponds to a semiamplitude of fluctuation of only about 1/7,000 in. A good fraction of that, say 1/10,000 in., of the wire fluctuation, would cause a noticeable signal distortion.

The resonant frequency of the hot wire itself is within the range of the turbulent frequencies. It is unknown whether the flutter of the wire itself is sometimes significant. The prongs and the prong holder will also flutter. Their dimensions are ordinarily not given in the test reports, nor how firmly the prong holder is held. It is clear that the prong ends move less in the prong direction than at right angles thereto. Hence, if any air-fluctuation measurements show inconsistencies for the components at right angles to the prongs, but not for the component parallel thereto, the finger of suspicion points to significant prong and/or prong-holder flutter.

From all this it seems that experimental turbulence-fluctuation results should not be too readily accepted unless they are accompanied by full data concerning this matter, including actually measured wire fluctuations.

On the Bending of Prismatic Shafts

M. I. I. Rashed
Aeronautical Department, Faculty of Engineering, Cairo University, Giza, Egypt

December 2, 1960

INTRODUCTION

IN STUDYING the problem of bending of prismatic shafts, it is assumed that the normal stress is a linear function of the coordinates (x, y) of the shaft cross section, the axes passing through the center of the area of the section. In the following treatment of the problem, a solution for the case of bending of a circular shaft is given. The bending moment Pz is assumed to be accompanied by a shearing force P. The method of solution can be applied to other sections by the use of conformal mapping. The equilibrium equation and the compatibility equations, together with a transformation of the variables, supply a general form leading to the stress distribution.

FORMULATION OF THE EQUATIONS

Assume that the normal stress σ_z is a linear function of the bending moment Pz. Let τ_{xz}, τ_{yz} be the shearing stresses in the xz, yz, and xy planes. Let all other stresses vanish. Hence we can write

$$\sigma_z = PzF(x, y)$$

The equilibrium and compatibility equations give

$$(\partial\sigma_z/\partial z) + (\partial\tau_{xz}/\partial x) + (\partial\tau_{yz}/\partial y) = 0 \quad (1)$$

$$\nabla^2\tau_{xz} = -[P/(1 + \nu)][\partial F(x, y)/\partial x] \quad (2a)$$

$$\nabla^2\tau_{yz} = -[P/(1 + \nu)][\partial F(x, y)/\partial y] \quad (2b)$$

Introduce the new dependent variables H and G such that

$$\tau_{xz} = (\partial H/\partial y) + (\partial G/\partial x) \quad (3a)$$

$$\tau_{yz} = -(\partial H/\partial x) + (\partial G/\partial y) \quad (3b)$$

Introduce these variables in the equilibrium equation (1) to get

$$PF(x, y) + \frac{\partial^2 H}{\partial x \partial y} + \frac{\partial^2 G}{\partial x^2} - \frac{\partial^2 H}{\partial y \partial x} + \frac{\partial^2 G}{\partial y^2} = 0$$

hence

$$\nabla^2 G = -PF(x, y) \quad (4)$$

Introducing also the new variables in the compatibility Eqs. (2a) and (2b) we find

$$-\frac{P}{1+\nu}\frac{\partial F(x,y)}{\partial x} = \nabla^2\tau_{xz} = \frac{\partial}{\partial y}(\nabla^2 H) + \frac{\partial}{\partial x}(\nabla^2 G) \quad (5a)$$

$$-\frac{P}{1+\nu}\frac{\partial F(x,y)}{\partial y} = \nabla^2\tau_{yz} = -\frac{\partial}{\partial x}(\nabla^2 H) + \frac{\partial}{\partial y}(\nabla^2 G) \quad (5b)$$

Introduce Eq. (4) into Eqs. (5a) and (5b) to get the Cauchy-Riemann equations

$$[\nu/(1+\nu)]P[\partial F(x,y)/\partial x] = (\partial/\partial y)\nabla^2 H \quad (6a)$$

$$[\nu/(1+\nu)]P[\partial F(x,y)/\partial y] = -(\partial/\partial x)\nabla^2 H \quad (6b)$$

Hence we can write

$$\{P[\nu/(1+\nu)]F(x, y) + i\nabla^2 H\} = F(x + iy) \quad (7)$$

With the cross section of the shaft considered as simply connected, and assuming that the stresses and hence the left-hand side of Eq. (7) are everywhere continuous and finite, we can write

$$F(x + iy) = \sum_{n=0}^{\infty} A_n(x + iy)^n \quad (8)$$

—i.e., we get

$$P\frac{\nu}{1+\nu}F(x,y) = \text{real part of } \sum_{n=0}^{\infty} A_n(x + iy)^n \quad (9)$$

Special Case of Circular Cross Sections

Take the axes passing through the center of the area. Assume the shearing force to be parallel to the x axis. Then from the symmetry we can write

$$\sigma_z/Pz = F(x,y) = a_1 x + a_3(x^3 - 3xy^2) + a_5(x^5 - 10x^3y^2 + 10xy^4) + \ldots \quad (10)$$

Eqs. (2a) and (2b) take the form

$$\nabla^2\tau_{xz} = -[P/(1+\nu)][a_1 + a_3(3x^2 - 3y^2) + a_5(5x^4 - 30x^2y^2 - 10y^4) + \ldots] \quad (11)$$

$$\nabla^2\tau_{yz} = -[P/(1+\nu)][-a_3(6xy) + a_5(-20x^3y + 40xy^3) + \ldots] \quad (12)$$

Neglect terms with coefficients a_5, a_7, etc., and evaluate the coefficients as follows.

The bending moment Pz is equal to $\int\int \sigma_z x dx dy$ which yields

$$a_1 = 4/\pi R^4 = 1/I_{yy} \quad (13)$$

where I_{yy} is the second moment of area about the y axis. For the shear components τ_{xz} note that from symmetry we can write

$$\tau_{xz} = c_{00} + c_{20}x^2 + c_{02}y^2 + c_{22}x^2y^2 + c_{40}x^4 + c_{04}y^4 \quad (14)$$

Obtain $\nabla^2\tau_{xz}$ and compare with Eq. (11) to get

$$2c_{20} + 2c_{02} = -[P/(1+\nu)]a_1 \quad (15)$$

$$2c_{22} + 12c_{40} = -[P/(1+\nu)]3a_3 \quad (16)$$

$$2c_{22} + 12c_{04} = [P/(1+\nu)]3a_3 \quad (17)$$

we have but $\int\int \tau_{xz} dx dy = P$, hence we get

$$P = \pi R^2\left[c_{00} + \frac{c_{20} + c_{02}}{4}R^2 + \left(\frac{c_{22}}{24} + \frac{c_{40} + c_{04}}{8}\right)R^4\right] \quad (18)$$

For the shear component τ_{yz} from (skew) symmetry we get

$$\tau_{yz} = b_{11}xy + b_{31}x^3y + b_{13}xy^3 \quad (19)$$

Obtain $\nabla^2\tau_{yz}$ and compare with Eq. (12) to get

$$b_{31} + b_{13} = \frac{P}{1+\nu}a_3 \quad (20)$$

At the boundary—i.e., at $x^2 + y^2 = R^2$—we have

$$\tau_{xzR} = -\tau_{yzR}\tan\theta$$

Transfer Eqs. (14) and (15) to polar coordinates ($x = r\cos\theta$, $y = r\sin\theta$) and insert in the above equations to get

$$c_{00} + c_{02}R^2 + c_{04}R^4 = 0 \quad (21)$$

$$c_{20} - c_{02} - 2c_{04}R^2 = -b_{11} \quad (22)$$

$$c_{04} + c_{40} = -b_{31} \quad (23)$$

$$c_{22} = -b_{13} \quad (24)$$

Solve Eqs. (15) to (18) and (20) to (24) to get the nine coefficients. Introduce these in Eqs. (10), (14), and (19) to get

$$\sigma_z = Pz\left[\frac{1}{I_{yy}}x + a_3(x^3 - 3xy^2)\right] \quad (25)$$

$$\tau_{xz} = \frac{P}{2+2\nu}\left[\left(\frac{3+2\nu}{\pi R^2} - \frac{3+2\nu}{\pi R^4}x^2 - \frac{1-2\nu}{\pi R^4}y^2\right) + a_3(-3x^2y^2 + y^4)\right] \quad (26)$$

$$\tau_{yz} = \frac{P}{2+2\nu}\left[-\frac{2+4\nu}{\pi R^4}xy + a_3(3x^2y - xy^3)\right] \quad (27)$$

Minimization of the Strain Energy

The strain energy of the shaft per unit shaft length is given by

$$V = 1/2E \int\int [\sigma_z^2 + (2+2\nu)(\tau_{xz}^2 + \tau_{yz}^2)]\, dxdy$$

Integration gives

$$V = \frac{1}{2E}\left[P^2z^2(1/I_{yy} + \pi R^8 a_3^2/8) + \frac{P^2}{2+2\nu}\left(\frac{4.667 + 9.333\nu + 5.333\nu^2}{\pi R^2} + 0.054375\,\pi R^{10}a_3^2\right)\right]$$

Minimization gives $a_3 = 0$ with the strain energy per unit shaft length

$$V = \frac{P^2z^2}{2EI} + \frac{P^2}{2GA}\frac{1.1667 + 2.333\nu + 1.333\nu^2}{1 + 2\nu + \nu^2}$$

Use of Conformal Mapping

The region enclosed by the circle in the xy plane can be transformed to another region enclosed by any contour in the $\xi\eta$ plane through a point-to-point transformation. Eq. (7) shows that $\{P[\nu/(1+\nu)]F(x,y) + i\nabla^2 H\}$ or $\{[\nu/(1+\nu)]\sigma_z/z + i\nabla^2 H\}$ is a function of $(x + iy)$. Hence one can retain the same value of $\{[\nu/(1+\nu)]\sigma_z/z + i\nabla^2 H\}$ at the point $(x + iy)$ in the xy plane to the corresponding point $(\xi + i\eta)$ in the $\xi\eta$ plane. Thus the distribution of the normal stresses is obtained. This procedure can be performed analytically by simple or complicated transformations. However, if relaxation methods are used, the shear stress distribution could be obtained as well.

Characteristics Method for Two-Dimensional Conductive Flow With Crossed Fields

Chul Park
Republic of Korea Air Force Academy, Seoul, Korea
November 23, 1960

THE STEADY FLOW of an inviscid electroconductive fluid satisfies the following system of differential equations:[1]

momentum: $\rho\mathbf{q}\cdot\nabla\mathbf{q} + \nabla p = \mathbf{J}\times\mathbf{B}$ (1)

mass: $\nabla\cdot\rho\mathbf{q} = 0$ (2)

energy: $$\sigma\rho T\mathbf{q}\cdot\nabla S = j^2 \quad (3)$$

Ohm's law: $$\mathbf{J} = \sigma(\mathbf{E} + \mathbf{q} \times \mathbf{B}) \quad (4)$$

conduction: $$\mu\mathbf{J} = \nabla \times \mathbf{B} \quad (5)$$

The characteristics method for the two-dimensional flow with crossed electric and magnetic fields of the type $\mathbf{q}(u,v,0)$, $\boldsymbol{\omega} = \nabla \times \mathbf{q} = \boldsymbol{\omega}(0,0,\omega)$, $\mathbf{E}(0,0,E)$, $\mathbf{B}(B_x,B_y,0)$, and $\mathbf{J}(0,0,j)$ can be developed in the following way.

From Eqs. (1), (2), (3), and the relation $\rho T\nabla S = \rho\nabla H - \nabla p$,[2]

$$\rho q(\partial H_0/\partial s) = jE \quad (6)$$

$$q\omega = (\partial H_0/\partial n) - T(\partial S/\partial n) - jB/\rho \quad (7)$$

From Eqs. (1) to (4) and the relation $(\nabla p)/a^2 = \rho\nabla(S/C_p) + \nabla\rho$,

$$(a^2 - u^2)(\partial u/\partial x) - 2uv(\partial v/\partial x) + (a^2 - v^2)(\partial v/\partial y) = uv\omega + (j/\sigma)(\gamma j/\sigma - E) \quad (8)$$

and from Eqs. (4) and (5),

$$q(\partial\chi/\partial s) = r_m\nabla^2\chi - E \quad (9)$$

$$j/\sigma = E + q(\partial\chi/\partial s) \quad (10)$$

where ds and dn are the elements of arc length in the direction of and normal to the streamline, respectively, and $H_0 = H + q^2/2$, $B_y = \partial\chi/\partial x$, $B_x = -\partial\chi/\partial y$, and $\gamma = C_p/C_v$, $r_m = 1/(\sigma\mu)$.

Changing the variables in Eq. (8) by $u = q\cos\theta$, $v = q\sin\theta$ and applying the condition for each of the characteristic curves

$$(dy/dx)_\pm = \tan(\theta \pm \alpha) \quad (11)$$

where α is the Mach angle, there follows,[3]

$$dq \mp q\tan\alpha d\theta = G\cdot D_\pm dx_\pm \quad (12)$$

where

$$\begin{aligned} G &= A\omega + jC(E/\gamma - j/\sigma)/(\rho RT) \quad (13)\\ A &= 1 - (1/2)\sin 2\theta/(\cos^2\theta - \sin^2\alpha)\\ C &= \sin^2\alpha/(\cos^2\theta - \sin^2\alpha)\\ D_\pm &= \cos(\theta \mp \alpha)/\cos\alpha \end{aligned}$$

This problem is not strictly of hyperbolic type because the right-hand side of Eq. (12) contains the unknown factors which can be determined only through solving the elliptic-type equation (9). Therefore, an approximation to the exact solution is possible only through successive approximations incorporating the characteristics method. Say, the distribution of χ is assumed first. The second approximation to χ can be obtained through the completion of the characteristics method once throughout the whole region.

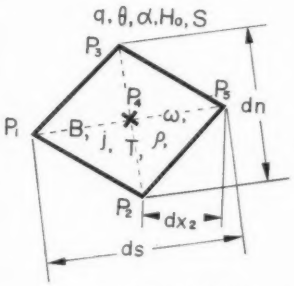

FIG. 1. (Left).

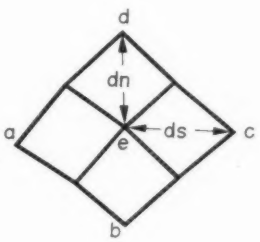

FIG. 2. (Right).

If the quantities q, θ, α, H_0, and S are known at the lattice points P_1, P_2, and P_3 of the equilateral characteristics net (Fig. 1), the quantities at P_5 can be determined as follows. If the net under consideration is not equilateral, it is necessary first to make it so by interpolation.[2]

(1) Assign the value of $B_n = (\partial\chi/\partial s)_4 = (\chi_5 - \chi_1)/ds$ so that it be approximately compatible with the assumed distribution of χ.

(2) Determine j_4 by Eq. (10), using $(\partial\chi/\partial s)_4$, $q_4 = (q_2 + q_3)/2$ and the given value of E_4.

(3) Determine $T_4 = 1/2(T_2 + T_3)$, using $H_0 = C_pT + q^2/2$.

(4) Determine ρ_4, using $\rho_4 = d\psi/(q_4 dn)$. If the spacing of the characteristics net is so chosen at first as to have equal $d\psi$ values between the neighboring streamlines, this can be done easily.

(5) Determine ω_4, using Eq. (7) and quantities at P_4.

(6) Determine G_4, using Eq. (13) and appropriate mean values.

(7) Determine $\theta_5 = \theta_2 + d\theta_2$, using Eq. (12), or

$$d\theta_2 = [G_3D_{+3}(x_2 - x_3) - 2G_4\sin\theta_2\tan\alpha_2 dx_2 + q_2 - q_3 + q_3(\theta_2 - \theta_3)\tan\alpha_3]/(q_2\tan\alpha_2 + q_3\tan\alpha_3)$$

(8) Determine $q_5 = q_2 + dq_2$, using Eq. (12), or

$$dq_2 = q_2\tan\alpha_2 d\theta_2 + G D_{-2} dx_2$$

(9) Determine $H_{05} = H_{01} + dH_{04}$, using Eq. (6), or

$$dH_{04} = (j_4E_4 ds\, dn)/d\psi$$

(10) Determine $S_5 = S_1 + dS_4$, using Eq. (3), or

$$dS_4 = (j_4^2 ds\, dn)/(d\psi\sigma T_4)$$

(11) Determine α_5, using $\tan^2\alpha_5 = q_5^2/(\gamma RT_5) - 1$ and $H_{05} = C_pT_5 + q_5^2/2$.

When the whole region is covered in this way, the second approximation to χ can be obtained through the relaxation method[4] from Eq. (9) which can be written as (Fig. 2)

$$\chi_e = \cos^2\alpha_e[M\chi_a + \chi_b + N\chi_c + \chi_d - E(dn)^2/r_m]/2$$
$$M = \tan\alpha_e[\tan\alpha + (q\, dn)/(2r_m)]_e$$
$$N = \tan\alpha_e[\tan\alpha - (q\, dn)/(2r_m)]_e$$

REFERENCES

[1] Resler, E. L., Jr., and Sears, W. R., *The Prospects for Magneto-Aerodynamics*, Journal of the Aeronautical Sciences, Vol. 25, No. 4, pp. 235–245, April 1958.

[2] Park, C., *The Magneto Gasdynamic Acceleration of Shock Tube Flow* (to be published in J. of Korean Astronautical Soc., Vol. 2, No. 2).

[3] Ferri, A., *Application of the Method of Characteristics to Supersonic Rotational Flow*, NACA Rep. 841, 1946.

[4] Southwell, R. V., *Relaxation Methods in Theoretical Physics*, Oxford Univ. Press, 1946.

A Note on Two-Point Taylor's Series for Solving Ordinary Differential Equations

Maurice Fine
Dowty-Rotol Ltd., Staverton, England
November 4, 1960

TWO-POINT EXPANSIONS, similar to the usual Taylor series, are described; a use in solving ordinary differential equations is indicated.

(1) Let $y_N(x) =$

$$\sum_{n=0}^{N-1}(x - a)^n(x - b)^n[a_n(x - a) + b_n(x - b)] \quad (1)$$

be an approximation to $y(x)$, where y is repeatedly differentiable with respect to x in a suitable interval of x including $a \lessgtr x \lessgtr b$. Let a_n, b_n be determined by the conditions

$$\left.\begin{aligned} &y_N^n(a) = y^n(a), \qquad y_N^n(b) = y^n(b)\\ &\text{where } y_N^n, y^n \text{ denote } \frac{d^n y_N}{dx^n}, \frac{d^n y}{dx^n} \text{ respectively}\\ &\text{and } n = 0, 1, 2, \ldots N - 1 \end{aligned}\right\} \quad (2)$$

Similar series have been known for some time but apparently have not been investigated.

(2) The coefficients a_n, b_n are given by

$$\left.\begin{aligned} 2(b-a)a_n &= (b-a)A_n + 2B_n \\ 2(b-a)b_n &= (b-a)A_n - 2B_n \\ \text{where } (b-a)^{2n+1}A_n &= \sum_{s=0}^{n} \frac{(b-a)^s}{s!}\binom{-n-1}{n-s} \times \\ &\qquad [y^s(b) - (-1)^s y^s(a)] \\ 2(b-a)^{2n}nB_n &= \sum_{s=1}^{n} \frac{(b-a)^s}{(s-1)!}\binom{-n}{n-s} \times \\ &\qquad [y^s(b) + (-1)^s y^s(a)],\ n \neq 0 \\ 2B_0 &= y(b) + y(a) \end{aligned}\right\} \quad (3)$$

and where $\binom{-n}{s}$ is the coefficient of x^s in the expansion of $(1+x)^{-n}$ by the binomial theorem.

The coefficients a_n, b_n are independent of N.

(3) When the derivatives are known y_N is a readily calculable approximation to y. Even though they are not known for an ordinary differential equation with marching conditions, the expansion can be useful. Consider, for example,

$$(dy/dx) - f(x, y) = 0 \quad (4)$$

where y, f are repeatedly differentiable functions of their arguments in the ranges which arise. Suppose $y(a)$ is given and y is required in $a \leqq x \leqq b$. All the derivatives of y at $x = a$, $x = b$ may be expressed in terms of $y(a)$ and an unknown $y(b)$. Hence a_n, b_n may be so expressed. If the series converges to the solution with increase of N then, for the correct value of $y(b)$, $|y_{N+1}(x) - y_N(x)|$ can certainly be made arbitrarily small for sufficiently large N.

It does not follow that making this term small will ensure a good approximation to y. However a few simple first-order equations have been considered and $|y_{N+1}(x) - y_N(x)|$ has been made small by putting $a_N = 0$ and, independently, $b_N = 0$. [Since $y(b)$ is the only parameter, $a_N = 0$, $b_N = 0$ are not usually consistent.] If these equations in $y(b)$ have real roots, they are found, empirically, to tend to the correct value with increase of N if there is no singularity near $x = a$ or $x = b$. Minimizing $a_N^2 + b_N^2$ has given quicker convergence; this may be used if the equations in $y(b)$ have no real roots, or only one.

(4) Two second-order problems have also been considered.

With $\dfrac{d^2y}{dx^2} = -w^2y$, $y(0) = 0$, $y(1) = 1$, $y'(1) = 0$ and an unknown $y'(0)$ then a_n, b_n may be determined, and making $a_N = 0$, $b_N = 0$ gives two equations for the unknowns ω^2, $y'(0)$. They are of the form

$$\left.\begin{aligned} P_N(w^2)y'(0) + Q_N(w^2) &= 0 \\ R_N(w^2)y'(0) + S_N(w^2) &= 0 \end{aligned}\right\} \quad (5)$$

where P_N, Q_N, R_N, S_N, are polynomials in w^2 of degrees non-decreasing with increase of N. Approximations to w^2 corresponding to the first three nontrivial N are given by

$$w^2 - 1.732^2 = 0, \qquad (w^2 - 1.577^2)(w^2 - 5.7^2) = 0,$$
$$(w^2 - 1.5710^2)(w^2 - 4.84^2)(w^2 - 10.4^2) = 0$$

The first three proper values of ω are 1.5708, 4.7124, 7.854 to the number of figures given. Application to this readily soluble problem indicates that the simple form of Eqs. (5) and the introduction of further frequencies with increase of N are advantages of this method in comparison with some other methods.

With the usual dot notation for d/dt and with $\ddot{y} + y + \lambda^2 y^3 = 0$, $y(0) > 0$ given, $\dot{y}(0) = 0$, replace $(x - a)$ in Eq. (1) by $\sin wt$ and $(x - b)$, similarly, by $\cos wt$ where $2\pi/\omega$ is the unknown period; a_n, b_n are still determined by Eq. (2); $y(\pi/2w) = 0$; by conservation of energy, or as a first integral,

$$[\dot{y}(\pi/2w)]^2 = [y(0)]^2\{1 + 0.5\lambda^2[y(0)]^2\} \quad (6)$$

With y_0 replacing $y(0)$ and the use of Eq. (6), real zeros of a_N, b_N give the following successive approximations to w^2:

$$w_0^2 = 1 + 0.5\lambda^2 y_0^2$$
$$3w_1 = w_0 + (w_0^2 + 3 + 3\lambda^2 y_0^2)^{0.5}$$
$$15w_2^3 - 13w_0w_2^2 - 3w_1(3w_1 - 2w_0)w_2 + w_0 = 0$$

For large $\lambda^2 y_0^2$ the values of w_0, w_1, w_2 tend to $0.707\lambda y_0$, $0.859\lambda y_0$, and $0.849\lambda y_0$ respectively; the exact value to three figures is $0.847\ \lambda y_0$ and the error probably decreases with $\lambda^2 y_0^2$. Application to this fairly readily soluble problem indicates that large nonlinearity does not present difficulty and that in some less simple problems good approximations to frequencies may be readily found.

(5) Successive approximations have been worked out mainly to see the rate of convergence. Any approximation may be worked out independently of earlier ones in the examples given.

This work is far from complete; at present it is advisable to check, by substitution in the equation, that an approximation is reasonably accurate—especially at the midpoint of the interval; even so, this account indicates a useful technique. Helpful correspondence and other help has been, and will be, acknowledged elsewhere.

✦ ✦ ✦

An Authorized Binding for
Journal of the Aerospace Sciences

Arrangements have been made by the Institute of the Aerospace Sciences for members and subscribers to have their Journals bound carefully and economically. Simply write for details to:

Publishers' Authorized Bindery Service Ltd., 430 West Erie St., Chicago 10, Ill.

✦ ✦ ✦

REQUIREMENTS *for* CONTRIBUTIONS

to the publications of the

INSTITUTE *of the* AEROSPACE SCIENCES

The Institute of the Aerospace Sciences invites both members and nonmembers from any country to submit papers for publication in the JOURNAL OF THE AEROSPACE SCIENCES and AEROSPACE ENGINEERING. The Institute, following the practice of other societies, does not pay for contributions.

The following directions for the preparation of papers, if followed by authors, will save correspondence, avoid the return of papers for changes, minimize the work of preparation for the printer, and save the expense due to the charges made for "author's corrections."

The author's institutions are requested to pay a publication charge of $30.00 per page which if honored entitles them to 100 free reprints. Instructions will be sent with galley sheets.

MANUSCRIPTS: The original typewritten copy of the paper is desired. **To expedite review, an additional copy of both the manuscript and figures should be submitted.** The manuscript must be double or triple spaced on one side of white paper sheets, consecutively numbered. There should be wide margins to allow for the marking of directions to the printer. Correcting, changing, or adding to papers after they are in type is costly. It is, therefore, imperative that papers submitted be in final form. Typographical errors may be corrected on proofs, but if authors wish to add material, they may do so at their own expense. In mailing, drawings may be rolled, but manuscripts should be sent flat. Send by first-class mail (register if you wish for your own protection) to the Editorial Office, Institute of the Aerospace Sciences, 2 East 64th Street, New York 21, N.Y. All manuscripts will be examined by the Editorial Committee and by the Editor. Authors will be advised as promptly as possible whether the paper is acceptable for publication.

TITLES: The title of the paper should be brief. The name and initials of the author should be written as he prefers. The use of the full name of an author is advocated because of the frequent duplication of initials and surnames which sometimes makes it difficult to establish the identity of the author. This is particularly important for large annual indexing and abstracting services. All titles and degrees or honors are omitted. The name of the organization with which the author is associated should be placed after his name on a separate line. The date on which the paper is received will be inserted by the Editor. The author's title or position should be indicated in a footnote.

SUMMARIES OR ABSTRACTS: An abstract to be printed at the beginning should accompany each article. It should be adequate as an *index* and as a *summary*. It should contain a statement of major conclusions reached, since summaries in many cases constitute the only source of information used in compiling scientific reference indexes. Abstracts printed in other journals, especially foreign, in most cases consist of summaries from printed papers. The summary should explain as adequately as possible the major conclusions to a nonspecialist in the subject and should contain from 100 to 300 words, depending on the length of the paper.

SUBHEADINGS: Subheadings should be inserted by the author at frequent intervals. The work of editorial preparation will be simplified by the author's provision of many subheadings.

MATTER USUALLY DELETED: Photographs or illustrations of little technical interest and not showing advances in general practice. Too detailed tabular matter (general results of such tables may be included in the text). Lengthy descriptions of materials or processes or of preliminary experiments or theories that preceded final results; salient features only are of interest.

REFERENCES: References should be numbered consecutively and grouped together at the end of the manuscript, with only the corresponding number being mentioned in the text. The arrangement should be as follows. For books: [1]Durand, W. F., *Aerodynamic Theory*, 1st Ed., Vol. 1, p. 23; Julius Springer, Berlin, 1934. For magazines: [1]England, C. R., Crawford, A. B., and Mumford, W. W., *Some Results of a Study of Ultra-Short-Wave Transmission Phenomenon*, Proc. IRE, Vol. 20, No. 12, pp. 481–482, March, 1933. Please give author, title, edition, volume number, page, publisher, and place and date of publication as indicated. Omission of one required fact causes much extra editorial work and possible inaccuracies.

ILLUSTRATIONS: Illustrations should accompany manuscripts, and each should always be referred to in the text by number. Drawings or graphs should not be larger than 12 × 16 inches, and must be made with jet black India ink on white paper or tracing cloth, the latter being preferred. *Do not use typewriter for lettering.* The smallest lettering on 8 × 10 inch figures should be no less than $^1/_4$ inch high. Cross-section paper (white with black lines) may be used, but it should not have more than 4 lines per inch. If finer ruled paper is used, the major division lines should be drawn in with black ink, omitting the finer divisions. In the case of finely ruled paper, only blue-lined paper can be accepted. *Tracing paper and blueprints* are not acceptable. Lettering and all markings must be large enough to be readable after reduction to single-column width ($3^1/_{16}$ in.). Mail rolled or flat; never fold. Drawings that cannot be reproduced (including pencil drawings) will be returned to the author for redrawing, thus delaying publication of the paper. Photographs should be distinct and show clear black and white contrasts. They must be on glossy white paper. Avoid round or oval photographs.

CAPTIONS AND LEGENDS: Legends or captions must accompany each drawing or photograph submitted. If written on the drawing or photograph they should be placed below and well outside the part to be reproduced. Each table should have a caption such as Table 1, Table 2, Table 3, etc. Captions should be complete in themselves so as to make the data intelligible to the reader without reference to the text. A duplicate list of captions for figures should be included as the last page of the manuscript. Use "Fig. 1" (not Figure 1), "Figs. 3 and 4," etc., in both the text and the numbering of illustrations. In the text, "Eq. (1)" or "Eqs. (1) and (2)" is used, not "Equation (1)." In captions, legends, and in table headings, write all words in full; do not abbreviate, except for "Fig." and "Eq."

MATHEMATICAL WORK: Formulas may be typewritten or carefully written in pen and ink, the writing to be large enough so that it can be marked for the printer. Considerable space for marking should be allowed above and below all equations. All complicated equations should be repeated on separate sheets with adequate space left for marking. The solidus should be used for simple fractions appearing within the text. Make all expressions clear to the typesetter. Greek letters used in formulas should be clearly designated by name in the margin of the manuscript. The difference between capital and lower-case letters should be clearly distinguished and care taken to avoid confusion between zero (0) and the letter (o), between the numerical (one) and the letter (ell) and the prime (′), between alpha and a, kappa and k, u and mu, v and nu, n and eta. All subscripts and exponents should be clearly distinguished. Avoid complicated exponents and subscripts. Dots and bars over letters or mathematical expressions should also be avoided. When it is necessary to repeat a complicated expression, it should be represented by some convenient symbol.

SYMBOLS AND ABBREVIATIONS: The symbols recommended in the American Standard Association "Letter Symbols for Aeronautical Sciences," ASA Y10.7—1954, should be used wherever practicable. All symbols should be clearly written and carefully checked. Standard abbreviations should be used, and it should be noted that most abbreviations are lower case.

CORPORATE MEMBERS

OF THE

INSTITUTE OF THE AEROSPACE SCIENCES

AC SPARK PLUG DIVISION, GENERAL MOTORS CORPORATION

ACADEMY OF AERONAUTICS

AEROJET-GENERAL CORPORATION

AERONCA MANUFACTURING CORPORATION

AERONUTRONIC, DIVISION OF FORD MOTOR COMPANY

AEROSPACE CORPORATION

AGAWAM AIRCRAFT PRODUCTS, INC.

AIRBORNE INSTRUMENTS LABORATORY, DIVISION OF CUTLER-HAMMER, INC.

ALLIED RESEARCH ASSOCIATES, INC.

ALLISON DIVISION, GENERAL MOTORS CORPORATION

AMERICAN AIRLINES, INC.

AMERICAN BOSCH ARMA CORPORATION

AMERICAN OIL COMPANY

AMOCO CHEMICALS CORPORATION

ARDE ASSOCIATES

ARO, INC.

ASTRO-ELECTRONIC PRODUCTS DIVISION, RADIO CORPORATION OF AMERICA

AVCO-EVERETT RESEARCH LABORATORY

AVCO CORPORATION, RESEARCH AND ADVANCED DEVELOPMENT DIVISION

AVIEN, INC.

BEECH AIRCRAFT CORPORATION

BELL AEROSPACE CORPORATION

THE BENDIX CORPORATION

THE BOEING COMPANY

BOOZ, ALLEN APPLIED RESEARCH, INC.

BULOVA RESEARCH & DEVELOPMENT LABORATORIES, DIVISION OF BULOVA WATCH COMPANY, INC.

CANADAIR, LTD.

CHANCE VOUGHT CORPORATION

THE CHASE MANHATTAN BANK

CHICAGO AERIAL INDUSTRIES, INC.

CONTINENTAL MOTORS CORPORATION

CORNELL AERONAUTICAL LABORATORY INC.

COX & COMPANY, INC.

CURTISS-WRIGHT CORPORATION

DANIEL, MANN, JOHNSON, & MENDENHALL

THE DECKER CORPORATION

DEFENSE ELECTRONIC PRODUCTS DIVISION, RADIO CORPORATION OF AMERICA

DEFENSE SYSTEMS DIVISION, GENERAL MOTORS CORPORATION

DEL MAR ENGINEERING LABORATORIES

DELCO-RADIO DIVISION, GENERAL MOTORS CORPORATION

DELCO-REMY DIVISION, GENERAL MOTORS CORPORATION

DOAK AIRCRAFT COMPANY, INC.

DOUGLAS AIRCRAFT COMPANY, INC.

DZUS FASTENER COMPANY, INC.

EASTERN AIR LINES, INC.

EATON MANUFACTURING COMPANY

EDO CORPORATION

ELASTIC STOP NUT CORPORATION OF AMERICA

ENGINEERING SUPERVISION COMPANY

FAIRCHILD CAMERA AND INSTRUMENT CORPORATION

FAIRCHILD STRATOS CORPORATION

THE GARRETT CORPORATION

GENERAL APPLIED SCIENCE LABORATORIES, INC.

GENERAL DYNAMICS CORPORATION

GENERAL ELECTRIC COMPANY

GENERAL PRECISION, INC.

THE B. F. GOODRICH COMPANY

GOODYEAR AIRCRAFT CORPORATION

GRUMMAN AIRCRAFT ENGINEERING CORPORATION

HOFFMANN AIRCRAFT COMPANY

HUGHES AIRCRAFT COMPANY

INSURANCE COMPANY OF NORTH AMERICA COMPANIES

IBM SPACE GUIDANCE CENTER

THE INTERNATIONAL NICKEL COMPANY, INC.

ITT FEDERAL LABORATORIES, A DIVISION OF INTERNATIONAL TELEPHONE AND TELEGRAPH CORPORATION

JANITROL AIRCRAFT DIVISION, MIDLAND-ROSS CORPORATION

JOHNS-MANVILLE SALES CORPORATION

KOLLSMAN INSTRUMENT CORPORATION

LAVELLE AIRCRAFT CORPORATION

LEAR, INCORPORATED

C. W. LEMMERMAN, INC.

THE LIQUIDOMETER CORPORATION

ARTHUR D. LITTLE, INC.

LOCKHEED AIRCRAFT CORPORATION

THE MARQUARDT CORPORATION

THE MARTIN COMPANY

McDONNELL AIRCRAFT CORPORATION

MELETRON CORPORATION

MINNEAPOLIS-HONEYWELL REGULATOR COMPANY

MOBIL OIL COMPANY

NATIONAL CREDIT OFFICE, INC.

NORTH AMERICAN AVIATION, INC.

NORTHROP CORPORATION

PAN AMERICAN WORLD AIRWAYS, INC.

THE RALPH M. PARSONS COMPANY

PIASECKI AIRCRAFT CORPORATION

POLY INDUSTRIES, INC.

REPUBLIC AVIATION CORPORATION

ROHR AIRCRAFT CORPORATION

RYAN AERONAUTICAL COMPANY

SHELL OIL COMPANY

SIMMONDS PRECISION PRODUCTS, INC.

SOLAR AIRCRAFT COMPANY

SOUTHWEST PRODUCTS COMPANY

SPACE TECHNOLOGY LABORATORIES, INC.

K. DIXON SPEAS ASSOCIATES

SPERRY GYROSCOPE COMPANY, DIVISION OF SPERRY RAND CORPORATION

STANDARD-THOMSON CORPORATION

STANLEY AVIATION CORPORATION

THERM, INCORPORATED

THIOKOL CHEMICAL CORPORATION

THOMPSON RAMO WOOLDRIDGE INC.

TRANS WORLD AIRLINES, INC.

UNION CARBIDE METALS COMPANY, DIVISION OF UNION CARBIDE CORPORATION

UNITED AIR LINES, INC.

UNITED AIRCRAFT CORPORATION

UNITED STATES AVIATION UNDERWRITERS INC.

VEHICLE RESEARCH CORPORATION

WESTERN GEAR CORPORATION

WESTINGHOUSE ELECTRIC CORPORATION